UNIVERSITY OF GLASGOW
SCHOOL OF PHYSICS AND ASTRONOMY
PARTICLE PHYSICS THEORY GROUP

Grand Unification Phenomenology at the LHC and Beyond

António Pestana Morais

Presented as a thesis for the degree of
Doctor of Philosophy

December 2013

Abstract

We investigate models of supersymmetric grand unification based on the gauge groups $SU(5)$, $SO(10)$ and E_6, as well as in a class of orbifolds inspired by four dimensional Strings. We follow a stepwise analysis starting our journey with a revisit to the Standard Model and commenting on major issues that are motivation for new physics. We then introduce supersymmetry and discuss the Minimal Supersymmetric Standard Model (MSSM), with a detailed analysis of its mass spectrum. We study the evolution of the strong and electroweak forces with the energy scale, and interpret the near match of the gauge couplings at the high scale as a clue for the unification of strong and electroweak interactions.

The second half of our journey starts with the introduction of the $SU(5)$, $SO(10)$ and E_6 symmetries. We provide a review of main aspects such as proton stability, split multiplets and Yukawa unification, and show how the MSSM soft parameters may be constrained by these groups. We demonstrate how the measurement of the first and second generation supersymmetric spectrum may be used to probe the underlying grand unification structure and compare our expressions with numerical calculations. We consider $SU(5)$ and $SO(10)$ models with non-universal gaugino masses and confront them with low energy constraints, including the Higgs boson mass and the Dark Matter relic density. We also discuss fine-tuning and show the effect of not including the μ-parameter into fine tuning determinations. With this relaxation, we find viable scenarios with low fine tuning and study some model choices for gaugino mass ratios. We demonstrate that gaugino masses inspired by some orbifold models may provide low fine-tuning and the preferred relic abundance of Dark Matter while evading all experimental constraints. We also determine high scale Yukawa coupling ratios and confront the results with theoretical predictions. We finally consider orbifold models to constrain the full set of soft parameters, and argue that a String inspired framework presents definite theoretical background to relax fine-tuning constraints. We present benchmarks for all our scenarios that should be explored at the LHC and future colliders.

Acknowledgements

I want to thank the University of Glasgow for welcoming me during the last four years and always providing the essential facilities for a healthy student life. I also want to thank to all members of the particle physics theory group for their constant cheer and availability to discuss physics and non-physics related topics, which contributed for a very pleasant working environment. In particular I want to thank Brian, Dan, Gordon, Kate, Liam, Stacey, Bipasha and Ben for the amusing times spent with them, and will never forget the "points game", or the "would you rather game".

I am very grateful to David Miller for his availability in becoming my supervisor, even without knowing me at first. David early understood my working method and gave me all the conditions to consistently grow as a physicist. I will not forget our weekly meetings, as well as the conferences in Bonn, Chicago and Stockholm, which have decisively contributed to my motivation and learning. I would also like to express my sincere and special thanks to David Sutherland, who had an important participation in our weekly meetings, raising crucial questions, providing restless support, criticism and, above all, very fruitful discussions. David Sutherland undoubtedly became a physicist of reference for me that I will not forget. I also want to thank Prof. Christine Davies as head of the PPT group, for welcoming me in the group even before being awarded with my scholarship.

I want to thank the members of the Gr@v group at the Physics Department of the University of Aveiro, particularly Marco Sampaio, Carlos Herdeiro and João Rosa for fruitful discussions and hospitality during visits to Aveiro. I am also very grateful for their availability in supporting my application for a Post-Doc grant, and I am looking forward to become a member of the group as soon as possible.

I acknowledge FCT for the grant SFRH/BD/62203/2009 and partial support by the grants PTDC/FIS/116625/2010 and PTDC/FIS/117951/2010.

I want to thank my parents for being present in all moments of my life and never denying me any help or support. They also supported part of my academic and scientific life, so this thesis is also for them. Without their care, I am sure that I would not be here writing these words.

A very special word for Rita, my girlfriend, who is responsible for one of the best periods of my life and always gave me all the emotional support needed to carry on doing physics and running after my dreams. Thank you Rita for being a special and unique person!! This thesis is also dedicated to you!

Finally, I want to remember my grandmother, and thank her for everything she was for me. She may no longer be around, but I am sure she is very happy about this moment of my life... wherever she is.

Declaration

I declare that the research presented in this thesis is my original work and has not been previously presented for a degree. Furthermore, citations were always included whenever published material was used.

Chapters 2 to 5 provide a general overview of my field of research and serve as theoretical introduction for the remaining chapters. The work presented in chapter 6 was accomplish in collaboration with Prof. Pran Nath Pandita and my supervisor Dr. David Miller. Chapters 7, 8 and 9 contain work that was carried out in close collaboration with Dr. David Miller.

Contents

List of Figures

List of Tables

1. Introduction

The recent launch of operations at the Large Hadron Collider (LHC) as well as various neutrino and astrophysical experiments, have brought into the Particle Physics and Cosmology communities a period of intense activity and enthusiasm. Despite the discovery of a Higgs boson candidate at the LHC [1–4] , thus completing the Standard Model, some other observations suggest that the SM is far from being a complete theory and that our current understanding of the fundamental symmetries of nature is not complete. In particular, the origin of the gauge structure of the SM, $SU(3) \times SU(2) \times U(1)$, is still an unanswered question and one can ask if such a symmetry is a remnant of a lager simple group that is spontaneously broken at a high scale by a Higgs-like mechanism, or if it results from some other framework.

The theoretical problems of the SM and its inability to explain fundamental questions, are strong motivations for the study of physics *Beyond the Standard Model* (BSM). One of the current and most popular proposals is low energy supersymmetry (SUSY) and the Minimal Supersymmetric Standard Model (MSSM). However, supersymmetry breaking in the MSSM, which is essential for a viable phenomenology, is explicit with no underlying model, resulting in 123 extra free parameters. Studies of such a huge parameter space are extremely difficult, which leads the research in this area to be carried out for particular models of supersymmetry breaking such as gravity mediated or gauge mediated supersymmetry breaking, reducing considerably the number of free parameters.

A theory with unification of the strong and electroweak forces, denoted as Grand Unified Theory (GUT), is strongly motivated by the running of gauge couplings, which within supersymmetric models appears to have a common value at a scale of about 10^{16} GeV. The most popular candidates of a unified gauge group are the $SU(5)$, $SO(10)$ and E_6 symmetries, which pose further constraints on the MSSM parameters at the high scale. In particular, different GUT embeddings should leave different signatures in the mass terms of the sfermion and of the gaugino fields, and may have impact on the low energy phenomenology.

The research presented in this thesis focuses on the study of supersymmetric Grand Unification scenarios. We will perform systematic phenomenological analysis of models

based on distinct GUT gauge structures, with emphasis on $SU(5)$ and $SO(10)$. The explicit introduction of free terms to effectively describe some underlying theory, may require unnatural tunings upon the new parameters in order to keep the mass of the Z boson light. This naturalness issue is denoted as *fine-tuning*, and to control it we need to guarantee that small fluctuations upon the free parameters do not cause large fluctuations in M_Z. While fine-tuning can be interpreted as an indicator on how satisfactory a model is, we may alternatively invoke some high scale mechanism capable of fixing such parameters, thus solving the fine-tuning problem. This is, for example, the case of string inspired models, and we also discuss two GUT scenarios based on a class of orbifold constructions.

With the restart of collisions at the LHC scheduled for 2015, it is expected to either uncover new physical phenomena or further constrain the yet allowed regions of the parameter space. It is therefore relevant to study the impact of diverse GUT motivated boundary conditions on the low scale supersymmetric spectrum, confront the results with low energy and fine-tuning constraints, and discriminate whether it is accessible or not for the 14 TeV LHC, or future colliders.

In chapter 2 we introduce the Standard Model of Particle Physics and, in the first part, focus our discussion on its gauge structure and on the electroweak symmetry breaking mechanism. In the second part, we move on to a short overview of renormalization in order to substantiate how perturbative methods can be used to construct the Renormalization Group Equations (RGE). We end the chapter with an overview of motivations for BSM physics, and provide a discussion about the SM hierarchy problem.

In chapter 3 we dedicate our discussion to the study of supersymmetry. We introduce the concept of graded Lie algebras and draw the basic lines towards the construction of a generic supersymmetric theory, with chiral and gauge interactions. We then use the new concepts and explain how the hierarchy problem can be solved. We conclude the chapter with the introduction of soft supersymmetry breaking terms.

It is in chapter 4 where we introduce the minimal supersymmetric extension to the SM. We start with a description of the structure of the MSSM and then focus our attention on the electroweak symmetry breaking, sketching the derivation of the physical masses of the diverse fields in the MSSM. We finish with the running of the gauge couplings, which provide a strong clue towards a Grand Unified Theory.

In chapter 5 we discuss Grand Unification introducing the $SU(5)$, $SO(10)$ and E_6 gauge structures, relevant representations and breaking chains to the gauge group of the SM. We also discuss some common problems the arise in grand unified models such as the proton

decay and the doublet triplet splitting problem.

Chapter 6 contains work carried out in collaboration with Dr. David J. Miller and Prof. P. Nath Pandita, where a systematic analytical analysis of the first and second generation sfermion masses was performed in order to constrain $SU(5)$, $SO(10)$ and E_6 GUT models with low scale observables. We have amended some inconsistencies in a previously published paper and completed the analysis with further studies, including a comparison with numerical calculations.

The research presented in chapter 7 was done in collaboration with Dr. David J. Miller, where we investigate minimal $SU(5)$ models with both universal and non-universal gaugino masses, confronting our results with low energy constraints, including the newly discovered Higgs boson as well as the Dark Matter relic density. We also discuss fine-tuning and the effect of not including the μ-parameter into fine-tuning determinations. With these considerations, we provide predictions for the supersymmetric spectrum for different benchmark models, presenting them in diverse projections of the parameter space. We also construct tables with all the details of relevant examples points.

The work in chapter 8 was also performed in collaboration with Dr. David J. Miller and follows the same philosophy of chapter 7, but for an $SO(10)$ gauge structure. In comparison to $SU(5)$, new relations among the GUT scale parameters are possible, in particular for the gaugino sector. We also provide Yukawa coupling ratios at the GUT scale and confront them with some existing predictions for bottom-tau and top-bottom-tau Yukawa unification conditions.

In chapter 9, we complement the work of the previous two chapters considering a class of orbifold models inspired in four-dimensional strings. We follow once again the same philosophy, but, since we have a more definite theoretical motivation, we allow some relaxation of the fine-tuning constraints. We present further benchmark models and provide predictions for the low scale supersymmetric spectrum.

We summarize and conclude in chapter 10. The work developed in this thesis for chapters 6 and 7 is published in Phys. Rev. D **87** (2013) 015007 and JHEP **1310** (2013) 226 respectively. Two further publications about the work in chapters 8 and 9 are, at the time of writing this thesis, under preparation.

2. The Standard Model

The Standard Model (SM) of Particle Physics is the effective *Relativistic Quantum Field Theory* that describes our current understanding of the Strong and Electroweak forces. It is the framework that depicts all the fundamental particles discovered to date including the recently observed Higgs boson [1–4] at the LHC. The SM is consistent with all current data with the exception of neutrino oscillations [5–9], which requires a mechanism to generate neutrino mass states, not predicted in the model.

The elementary particles of the SM are summarized in Fig. 2.1. While the left column gathers the Fermions, the middle and right columns group the Gauge and the Higgs bosons respectively.

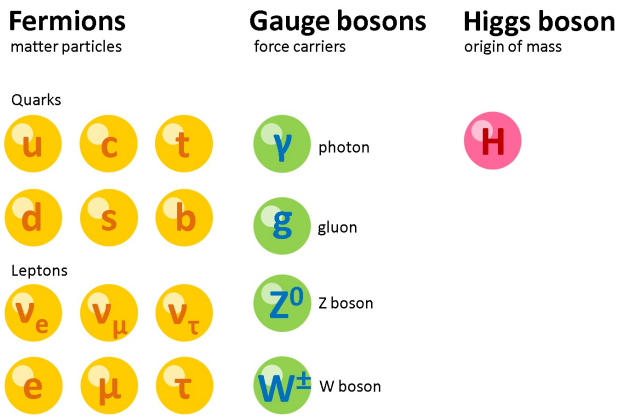

Figure 2.1. *Standard Model particle content. Figure taken from [10]*

.

The Fermions, are spin-1/2 fields and are split up into two sub-groups, the quarks and the leptons, with three generations each. The *up-type* quarks, u, c, t, have positive electric charge, $+2/3e$, whereas the *down-type* ones, d, s, b, carry a negative electric charge equal to $-1/3e$. Here, $e = \left(1.602\,176\,565(35)\times10^{-19}\right)$C [11], is the electron charge magnitude. The quarks interact via both the electromagnetic and weak forces, but are the only known fermions interacting via the strong force. The observed baryons and mesons are bound states of the SM quarks, but only the first generation ones, u and d, form the protons and neutrons, which are the building blocks of the atomic nuclei. In the lepton sector, the up-type ones are the neutrinos, which only interact via the weak force, whereas the down-type ones,

are the charged leptons with electric charge $-e$, which interact via both the electromagnetic and weak forces. The first generation charged lepton is the electron, and, together with the protons and neutrons, make up atoms as electrically neutral bound states.

The force carriers, or gauge bosons, are spin-1 vector-fields responsible for the mediation of the interactions. The photon, γ, is the electromagnetic force messenger, the $W^{\pm}$ and the Z^0 bosons are responsible for the weak interaction and the gluons, g, mediate the strong interaction.

The last piece of the SM is the spin-0 Higgs boson. This is the only fundamental scalar field known to date and plays a crucial role in the Standard Model as it is the particle responsible for mass generation. In the SM, all the fundamental particles that couple to the Higgs field obtain their mass through the Higgs mechanism, which will be explained in section 2.3.

The SM is hard to reconcile with General Relativity (GR), and a theory of *Quantum Gravity* is only possible in extensions to the SM such as String Theory [12,13]. Furthermore, the weakness of the gravitational force in comparison with the remaining ones, makes it very challenging, if they exist, to detect gravitons. These spin-2 fields are not included in the framework of the SM.

2.1. Symmetries in the Standard Model

The Standard Model is a theory designed under the elegant concepts of symmetries of nature. The fundamental object in field theory, either classical or quantum, is the Lagrange density (often referred to as Lagrangian). This is a function of the various fields Φ and their first derivatives with respect to the coordinates, $\partial_\mu \Phi$,

$$\mathcal{L} = \mathcal{L}\left(\Phi, \partial_\mu \Phi\right). \tag{2.1}$$

Theories of interest that describe physical phenomena often have symmetries or formally, invariance of the Lagrangian under transformations of the fields. There are several ways of classifying the different symmetries depending on the transformation parameters. We introduce here two major types of symmetries:

1. *Discrete Symmetries:*
   The parameters take discrete values. In Particle Physics, some of the most relevant types of discrete symmetries are those involving Parity $\hat{\mathbf{P}}$, which reverses the handedness of space, Charge Conjugation $\hat{\mathbf{C}}$, which interchanges particles with anti-particles and Time Reversal $\hat{\mathbf{T}}$, reversing the direction of time. An important result is the **CPT**

Theorem [14, 15], which says that all observables of the SM must be invariant under the total transformation given by $\hat{\mathbf{C}}\hat{\mathbf{P}}\hat{\mathbf{T}}$. In particular, electromagnetic and strong interactions preserve $\hat{\mathbf{P}}$, $\hat{\mathbf{C}}$ and $\hat{\mathbf{T}}$ separately whereas weak interactions violate $\hat{\mathbf{C}}$ and $\hat{\mathbf{P}}$ separately, and for certain rare processes $\hat{\mathbf{C}}\hat{\mathbf{P}}$ [16, 17] and $\hat{\mathbf{T}}$ are also violated.

2. *Continuous Symmetries:*
   The parameters take continuous values. A typical example concerns rotations $\mathcal{R}$ parametrized by a rotation angle θ, $\mathcal{R}(\theta)$, which can take a continuum of values.

Both the discrete and continuous symmetries can be subdivided into two different classes, which, according to *Coleman and Mandula's Theorem* [61], can be regarded separately:

- *Space-Time Symmetries:* Symmetries that act on the space-time coordinates. The Poincaré Group is used to describe such symmetries consisting of proper Lorentz transformations[1] followed by four-dimensional space-time translations. An example of a space-time symmetry is Supersymmetry which will be introduced in the next chapter.

- *Internal Symmetries:* Transformations commute with the Poincaré group, or in other words, they do not mix fields with distinct space-time properties. A popular example of an internal symmetry is the flavour structure of the Standard Model. While we can use parity to convert a left-moving particle into a right-moving one, there is no space-time transformation capable of converting a u-quark into a d-quark, and no matter the reference frame, we always see the same flavour.

We will discuss in chapter 3, that it is possible to extend *Coleman and Mandula's Theorem* in order to relate space-time symmetries with internal symmetries, from where supersymmetry emerges. In addition, we also consider here invariance under *global* and *local* continuous transformations. For the first case, the parameters of the transformation **do not depend** on the space-time coordinates. For instance, if we consider a global symmetry of the Lagrange density (2.1) described by a Lie group G, infinitesimal transformations on the fields

$$\Phi = \begin{pmatrix} \Phi_1 \\ \Phi_2 \\ \vdots \\ \Phi_n \end{pmatrix}, \tag{2.2}$$

given by

$$\Phi \to \Phi' = \Phi + \delta\Phi, \tag{2.3}$$

[1] A Lorentz transformation which can be represented by a matrix whose determinant is +1

will leave the Lagrangian invariant. In particular, the m infinitesimal transformations of G act on Φ as

$$\delta\Phi_i = i\varepsilon^a \Omega^a_{ij}\Phi_j \text{ with } a = 1,2,\ldots,m\,, \tag{2.4}$$

where the ε^a parameters are independent of the coordinates and Ω^a_{ij} are the m group generators represented by $n \times n$ matrices. The Lie algebra of G is defined by the Lie bracket

$$\left[\Omega^a, \Omega^b\right] = if^{abc}\Omega^c, \tag{2.5}$$

where f^{abc} are the structure constants of the group. If $f^{abc} = 0$, G is an **Abelian** global symmetry, otherwise, the group is **non Abelian**.
On the other hand, a local transformation depends on the space-time coordinates and the choice $\varepsilon^a(x)$ is no longer a constant for all space-time. Theories where the Lagrangian is invariant under local transformations,

$$\delta\Phi = i\varepsilon^a(x)\Omega^a\Phi, \tag{2.6}$$

are known as *Gauge Theories* and are central to particle physics. The Standard Model is a framework constructed upon the idea of gauge invariance, which remarkably describes the interactions of the fundamental particles.

2.2. The Gauge Structure of the Standard Model

The requirement that a theory has local invariance is a restrictive condition. It is usually hard to let a theory be locally invariant without adding extra terms to the Lagrangian. In quantum field theory, such terms are associated to the concept of force between interacting particles, and, by promoting a global symmetry G to local, an originally free theory becomes an interacting theory.

2.2.1. Quantum Electrodynamics

Quantum Electrodynamics (QED), is a paradigmatic example of the application of the gauge invariance principle. It is the Relativistic Quantum Field Theory describing the electromagnetic interaction, involving phenomena between electrically charged particles interacting by photon exchange.

A free Dirac spinor[2] is described by the Dirac Lagrangian

$$\mathcal{L} = i\overline{\psi}\gamma^\mu\partial_\mu\psi - m\overline{\psi}\psi, \tag{2.7}$$

[2] A spinor is an element of a complex vector space which, unlike spatial vectors (or more generally tensors), transforms to its negative under a 2π rotation of the orthogonal group.

where γ^μ, with $\mu \in \{0,1,2,3\}$, are the Dirac gamma matrices given as

$$\gamma^0 = \begin{pmatrix} 0 & 1 \\ 1 & 0 \end{pmatrix} \quad \text{and} \quad \gamma^{\mathrm{i}} = \begin{pmatrix} 0 & \sigma^i \\ -\sigma^i & 0 \end{pmatrix}, \tag{2.8}$$

in the Weyl basis, and satisfy the rank-four *Clifford algebra*

$$\{\gamma^\mu, \gamma^\nu\} = 2g^{\mu\nu}. \tag{2.9}$$

Here γ^μ are written in a 2×2 block diagonal form and σ^i are the usual Pauli matrices

$$\sigma^1 = \begin{pmatrix} 0 & 1 \\ 1 & 0 \end{pmatrix}, \quad \sigma^2 = \begin{pmatrix} 0 & -i \\ i & 0 \end{pmatrix} \quad \text{and} \quad \sigma^3 = \begin{pmatrix} 1 & 0 \\ 0 & -1 \end{pmatrix}. \tag{2.10}$$

The adjoint spinor $\overline{\psi} = \psi^\dagger \gamma^0$, is clearly not invariant under the local transformations operated by

$$\delta\psi = i\alpha(x)\psi \quad \text{and} \quad \delta\overline{\psi} = -i\alpha(x)\overline{\psi}. \tag{2.11}$$

Here, $\partial_\mu\psi$ does not transform in the same way as ψ. However, if the covariant derivative is introduced in such a way that the transformation

$$\delta D_\mu\psi = i\alpha(x) D_\mu\psi, \tag{2.12}$$

holds, the Lagrangian (2.7) becomes invariant since now $D_\mu\psi$ gauge-transforms covariantly, i.e., as ψ itself. In a minimal prescription, the covariant derivative is defined as

$$D_\mu = \partial_\mu + ieA_\mu \tag{2.13}$$

where A_μ is the *Gauge Vector Field* which represents the electromagnetic force carrier, or more popularly, the photon. The introduction of the A_μ fields in the Lagrangian, force us to include extra gauge invariant terms with respect to the propagation of the photon and given in terms of the electromagnetic field strength tensor

$$F_{\mu\nu} = \partial_\mu A_\nu - \partial_\nu A_\mu = \Big[D_\mu, D_\nu\Big]. \tag{2.14}$$

In Classical Electromagnetism, it is possible to derive the Maxwell's equations from the Lagrangian

$$\mathcal{L}_{Maxwell} = -\frac{1}{4} F_{\mu\nu}F^{\mu\nu}, \tag{2.15}$$

which is invariant under the gauge transformations $A_\mu \to A_\mu + \delta A_\mu$ where

$$\delta A_\mu = -\frac{1}{e}\partial_\mu \alpha(x). \tag{2.16}$$

The full QED Lagrangian can now be constructed acquiring the form

$$\begin{aligned} \mathcal{L}_{QED} &= -\frac{1}{4}F_{\mu\nu}F^{\mu\nu} + i\overline{\psi}\gamma^\mu D_\mu \psi - m\overline{\psi}\psi \\ &= -\frac{1}{4}F_{\mu\nu}F^{\mu\nu} + i\overline{\psi}\gamma^\mu \partial_\mu \psi - m\overline{\psi}\psi - e\overline{\psi}\gamma^\mu \psi A_\mu. \end{aligned} \tag{2.17}$$

Local gauge invariance has led to the inclusion of a new term, $-e\overline{\psi}\gamma^\mu\psi A_\mu$, which describes the interaction between the electromagnetic field and matter. The transformation parameter $\alpha(x)$ in (2.11) and (2.16) is a phase rotation of a $U(1)$ symmetry. In other words, **QED is a $\mathbf{U(1)_Q}$ gauge theory**, where the subscript Q refers to the electromagnetic charges of the group. Since $U(1)_Q$ is an Abelian group, interactions between photons are not allowed. Furthermore, mass terms of the form $m^2_{photon}A_\mu A^\mu$ are forbidden by gauge invariance in classical field theory, requiring the photon to be massless.

2.2.2. Yang-Mills Theories

The same steps that led us to QED, can be extrapolated to interactions involving the non-Abelian symmetries describing the weak and the strong forces. When a theory with gauge invariance is non-Abelian, it is designated as a *Yang-Mills Theory* [18]. The description given in this section is largely based in [15] and [19], where more detailed calculations can be found.

We consider here a column vector Ψ_i in a vector space of dimension n, under the action of a representation of a non-Abelian group G

$$\delta\Psi_i = i\varepsilon^a(x)\Omega^a_{ij}\Psi_j \quad \text{and} \quad \delta\overline{\Psi}_j = -i\varepsilon^a(x)\Omega^a_{ij}\overline{\Psi}_j, \tag{2.18}$$

where the group generators obey the Lie Algebra (2.5) with non vanishing structure constants. In order to make the free field Lagrangian invariant

$$\mathcal{L}_{free} = \overline{\Psi}_i\left(i(\gamma^\mu)_{ij}\partial_\mu - m\delta_{ij}\right)\Psi_j, \tag{2.19}$$

the covariant derivative is introduced

$$\left(D_\mu\right)_{ij} = \partial_\mu\delta_{ij} + ig(\Omega^a)_{ij}A^a_\mu \tag{2.20}$$

where A^a_μ are m vector fields, $(a = 1,2,\ldots,m)$, playing an analogous role to the photon in QED, g is the gauge coupling constant of G and δ_{ij} is Kronecker-delta symbol. Invariance of the

Lagrangian means that the covariant derivative transforms like the fields Ψ_i taking the form (omitting the representation indexes)

$$\begin{aligned}\delta\left(D_\mu\Psi\right) &= i\varepsilon^a(x)\Omega^a D_\mu\Psi \\ &= i\varepsilon^a(x)\Omega^a\partial_\mu\Psi - g\varepsilon^a(x)\Omega^a A^b_\mu\Omega^b\Psi.\end{aligned} \tag{2.21}$$

If the variation in $D_\mu\Psi$ is explicitly calculated and the results compared, the transformations in the gauge fields A^a_μ are obtained and written as

$$\delta A^a_\mu = -f^{bca}\varepsilon^b(x)A^c_\mu - \frac{1}{g}\partial_\mu\varepsilon^a(x). \tag{2.22}$$

If the group is Abelian, the result (2.22) reduces to the expression of an Abelian theory such as QED. Calculating the commutator of two covariant derivatives, we obtain

$$\left[D_\mu, D_\nu\right] = ig\left(\partial_\mu A^a_\nu\Omega^a - \partial_\nu A^a_\mu\Omega^a + ig\left[\Omega^b,\Omega^c\right]A^b_\mu A^c_\nu\right), \tag{2.23}$$

from where the generalized definition of the Maxwell tensor for a non-Abelian theory can be extracted,

$$F^a_{\mu\nu} \equiv \partial_\mu A^a_\nu - \partial_\nu A^a_\mu - gf^{bca}A^b_\mu A^c_\nu. \tag{2.24}$$

Calculating the variation of the generalized Maxwell tensor, we verify that unlike QED, $F^a_{\mu\nu}$ is not invariant, transforming as a vector in a space of dimension m (the dimension of the group) as

$$\delta F^a_{\mu\nu} = -f^{bca}\varepsilon^b F^c_{\mu\nu}. \tag{2.25}$$

However, with the above infinitesimal transformation of $F^a_{\mu\nu}$, the generalization of the Maxwell Lagrangian is invariant under the gauge transformations (2.22), and, putting all the pieces together, the generalized gauge-invariant Yang-Mills Lagrangian is given by

$$\mathcal{L}_{YM} = \overline{\Psi}_i\left(i\left(\gamma^\mu D_\mu\right)_{ij} - m\delta_{ij}\right)\Psi_j - \frac{1}{4}F^a_{\mu\nu}F^{a\mu\nu} \tag{2.26}$$

Quantum Chromodynamics

If the gauge group is $SU(3)_C$, the (2.26) describes the quantum theory of the strong interaction, or *Quantum Chromodynamics* (QCD), where the label C refers to the color charge. In this framework, the matter fields are quarks, belonging to the fundamental representation, triplets of $SU(3)$, whereas the gauge fields are gluons and are embedded in the 8-dimensional[3]

[3]For $SU(N)$ algebras, the dimension of the group given by N^2-1 is the same as the adjoint representation.

adjoint representation. The QCD Lagrangian is written as

$$\mathcal{L}_{QCD} = \bar{q}_i\Big(i\big(\gamma^\mu D_\mu\big)_{ij} - m\delta_{ij}\Big)q_j - \frac{1}{4}F^a_{\mu\nu}F^{a\mu\nu}, \tag{2.27}$$

where q_i is the quark field and $i = 1,2,3$ is a colour index. As in QED, mass terms of the form $m^2_{gluon}A^a_\mu A^{a\mu}$ do not preserve gauge invariance, which naturally requires that gluons are massless particles. Nonetheless, as a non Abelian theory, interacting terms like $-g_3 f^{abc}\partial_\mu A^a_\nu A^{\mu b}A^{\nu c}$ or even terms with four gauge fields are allowed, predicting that unlike QED, interactions between gauge fields are permitted. The Lagrangian (2.27) also describes quark-gluon interactions through terms of the form $-g_3\bar{q}\gamma^\mu\frac{\lambda^a}{2}A^a_\mu q$, where g_3 is the strong gauge coupling and λ^a are the Gell-Mann matrices.

Finally, the strength of the QCD force increases as the energy scale decreases. As a consequence, strongly interacting objects are believed to be confined to colorless bound states (hadrons) at low energy scales, which makes direct probes of QCD more challenging. However, numerical methods as Lattice Gauge Theory [20], together with perturbative QCD provide testable predictions that have successfully been confirmed by experiments.

Electroweak Interactions

Although the electromagnetic and the weak interactions are significantly different at "everyday" low energy, above a scale of approximately 100 GeV, they merge into a single electroweak force. However, this is not a conventional unification picture and the gauge group that describes the theory is a semi-simple $SU(2)_L \times U(1)_Y$ with two distinct gauge couplings, g and g' respectively. The label L indicates that weakly interacting left-handed quarks and leptons are placed into $SU(2)$ doublets, whereas Y is the weak hypercharge. From the discussion about the electromagnetic interaction, one might have expected to have here the electric charge Q instead of the hypercharge Y. However, as we will see in the next section, QED is obtained when the electroweak symmetry is broken by means of the Higgs mechanism, $SU(2)_L \times U(1)_Y \to U(1)_Q$, where a residual symmetry $U(1)_Q$, with an unbroken generator $\hat{Q}$ survives, corresponding to the electromagnetism.

The Lagrangian of the electroweak theory for the matter fields Ψ has the same structure as the first term in the right-hand-side (rhs) of the generic Yang-Mills Lagrangian (2.26). However, the covariant derivative is a sum over all gauge fields with a coupling constant for each group factor,

$$\big(D_\mu\big)_{ij} = \partial_\mu\delta_{ij} + ig\frac{(\tau^a)_{ij}}{2}A^a_\mu + ig'\frac{Y}{2}B_\mu\delta_{ij}. \tag{2.28}$$

The $SU(2)_L$ gauge fields are represented here by A^a_μ and the generators τ^a are the well known

Pauli matrices. The $U(1)_Y$ gauge field is represented by B_μ. The Lagrangian for the gauge fields is simply the sum of Maxwell-like Lagrangians (2.15) for each group factor. As for QED and QCD, mass terms for the gauge bosons are forbidden in order to preserve local invariance, nonetheless, massive vector bosons for the weak interactions are experimentally observed [21, 22]. Therefore, some mechanism to break the electroweak symmetry and provide mass to the gauge bosons has to be introduced.

The mass terms in the fermion sector will also violate the $SU(2)_L \times U(1)_Y$ gauge invariance. To analyze this point let us consider the free Dirac Lagrangian (2.7) for simplicity. Here, the fermion fields ψ are four-component objects which can be decomposed into left and right-handed chirality states

$$\psi_{L,R} = \frac{1 \mp \gamma^5}{2}\psi, \tag{2.29}$$

where $\gamma^5 = i\gamma^0\gamma^1\gamma^2\gamma^3$. With this decomposition, the mass terms of the Lagrangian take the form

$$\mathcal{L}_{mass} = -m\overline{\psi}\psi = -m\left(\overline{\psi}_L\psi_R + \overline{\psi}_R\psi_L\right). \tag{2.30}$$

For massive fermions, the ψ_L and ψ_R fields are interpreted as different objects which are coupled by the mass. While the left-handed fields are weakly interacting $SU(2)_L$ doublets, the right-handed ones are weak isospin singlets and their infinitesimal transformations are

$$\begin{aligned} \delta\psi_L &= i\varepsilon^a\frac{\tau^a}{2}\psi_L \\ \delta\psi_R &= 0. \end{aligned} \tag{2.31}$$

Transformations under the action of the $U(1)_Y$ group are of the form

$$\delta\psi_{hel} = i\frac{\varepsilon}{2}Y_{hel}\psi_{hel}, \tag{2.32}$$

where ψ_{hel} is any helicity component of the fermions and Y_{hel} its weak hypercharge. The transformation laws above exclude any possibility of the Lagrangian (7.2) being $SU(2)_L$ invariant, and, if the weak hypercharges of the left and right-handed components are different, (2.32) also violates $U(1)_Y$ invariance. As for the gauge sector, a mechanism that provides masses to weak bosons in a gauge invariant way, should also provide invariant mass terms for the quarks and for the leptons.

2.3. Electroweak Symmetry Breaking in the Standard Model

It is to solve the problem of the gauge bosons and fermion masses in the Standard Model that the concept of *Spontaneous Symmetry Breaking* is introduced. The majority of the symmetries observed in nature are not exact. For example, the *Isospin* is such a symmetry since the proton and neutron masses are not equal. A simple way of breaking symmetries is to introduce new mass terms in the Lagrangian that *explicitly* break the symmetry. However, this is not a solution for our problem, since we want to preserve the symmetry of the Lagrangian under the action of the group $SU(2)_L \times U(1)_Y$ but, for the vacuum state (state of least energy), break the symmetry *spontaneously*.

The proposal for a symmetry group unifying the weak and the electromagnetic interactions, $SU(2)_L \times U(1)_Y$ was first introduced by Glashow [23]. It was however Weinberg and Salam [24, 25] who formulated the electroweak theory as it is known nowadays, incorporating the idea of unification proposed by Glashow. The theory is commonly designated as *Glashow-Weinberg-Salam model* and provides the experimentally correct description of the weak interactions. The observed massless gauge bosons of the QCD theory, indicate that the $SU(3)_C$ gauge group of the strong interactions is not broken. On the other hand, although the photon is also massless, it is associated with the residual unbroken $U(1)_Q$ of $SU(2)_L \times U(1)_Y$ and not the weak hypercharge group itself.

The spontaneous breakdown of a continuous symmetry does not in general provide mass terms to the gauge bosons, instead, it introduces new massless degrees of freedom commonly designated as *Nambu-Goldstone bosons*. This results is a consequence of the well known *Goldstone Theorem* that we state below [26–28]:

Goldstone's Theorem. *Let a theory $\mathcal{L}$ be invariant under transformations of a continuous group G with n generators. If there is a spontaneous symmetry breaking such that the vacuum remains invariant under the action of a subgroup of $G' \subset G$ with $m < n$ generators, then, massless spin-0 particles will emerge in equal number to the generators of G that do not leave the vacuum invariant.*

The theorem predicts not only that the theory must contain massless particles as well as provides its number. In particular, we are left with $n - m$ Nambu-Goldstone bosons which, for the case of a $SU(2) \times U(1)$ theory, corresponds to $4 - 1 = 3$ such particles. This result appeared to be an obstacle to realistic theories with spontaneously broken symmetries. However, P. Higgs [29, 30], F. Englert and R. Brout [31], G. Guralnik, C. Hagen and T. Kibble [32, 33], develop a mechanism that solved the problem of massless scalars. It was demonstrated that the combination of local gauge invariance and spontaneous symmetry breaking, leads to a theory where the Nambu-Goldstone degrees of freedom are absorbed into massive vector fields. This is the so called *Higgs Mechanism*.

2.3.1. The Higgs Mechanism

When the Universe is in its minimum energy configuration, commonly denoted as *vacuum*, the Higgs Mechanism postulates a new scalar field, the *Higgs field*, which, in contrast to the fields of the remaining fundamental particles, is expected to have a non-vanishing value. However, when we move from the vacuum to an exited state, the fields of the fundamental particles become non-zero and such particles appear into space which is already populated by many Higgs particles. Therefore, the fundamental particles will interact with the Higgs and see their motion across space disturbed. It is the effect on the motion of the fundamental particles that is perceived as mass.

This idea was recently confirmed at the LHC and its success was awarded this year, 2013, with a *Nobel Prize* for Petter Higgs and François Englert.

Gauge Boson Masses

The Lagrangian of the electroweak interactions for the gauge and scalar sectors of the theory is written as

$$\mathcal{L}_{gs} = \left(D^{\mu}\phi\right)^{\dagger}\left(D_{\mu}\phi\right) - V\left(\phi^{\dagger}\phi\right) - \frac{1}{4}G^{a}_{\mu\nu}G^{a\mu\nu} - \frac{1}{4}F_{\mu\nu}F^{\mu\nu}, \tag{2.33}$$

where a runs over the set $\{1,2,3\}$ and the scalar potential has the form

$$V\left(\phi^{\dagger}\phi\right) = \mu^2\phi^{\dagger}\phi + \lambda\left(\phi^{\dagger}\phi\right)^2. \tag{2.34}$$

The Higgs field is a complex scalar placed into a $SU(2)_L$ doublet

$$\phi = \begin{pmatrix}\phi^{+}\\ \phi^{0}\end{pmatrix} \equiv \frac{1}{\sqrt{2}}\begin{pmatrix}\phi_1 + i\phi_2\\ \phi_3 + i\phi_4\end{pmatrix}. \tag{2.35}$$

and the field strength tensors of the $SU(2)_L$ and $U(1)_Y$ symmetries are respectively

$$G^{a}_{\mu\nu} = \partial_{\mu}A^{a}_{\nu} - \partial_{\nu}A^{a}_{\mu} - g\varepsilon^{abc}A^{b}_{\mu}A^{c}_{\nu}\ , \tag{2.36}$$

$$F_{\mu\nu} = \partial_{\mu}B_{\nu} - \partial_{\nu}B_{\mu}. \tag{2.37}$$

The minimization equations of the scalar potential (2.34) are,

$$\frac{\partial V}{\partial \phi^{\dagger}} = \phi\left(\mu^2 + 2\lambda|\phi|^2\right) = 0 \tag{2.38}$$

$$\frac{\partial V}{\partial \phi} = \phi^{\dagger}\left(\mu^2 + 2\lambda|\phi|^2\right) = 0 \tag{2.39}$$

from where we are left with the following two possibilities for the minimization condition:

1. $\mu^2 > 0$:
   The potential has a minimum at $\phi = 0$ and the gauge symmetry is preserved. The theory describes a complex isodoublet scalar with mass $m = \sqrt{\mu^2}$ and the gauge bosons remain massless.

2. $\mu^2 < 0$:
   The minimum of the potential corresponds to the value

$$|\phi|^2 = -\frac{\mu^2}{2\lambda} \equiv v^2. \tag{2.40}$$

   The vacuum is not invariant under the electroweak symmetry and leads to spontaneous symmetry breaking.

If the scalar field acquires a vacuum expectation value (vev), as in the second scenario, the freedom of $SU(2)$ rotations can be used to choose the isospin axis such that the vev takes the form

$$\langle\phi\rangle = \frac{1}{\sqrt{2}}\begin{pmatrix}0\\ v\end{pmatrix}. \tag{2.41}$$

This particular choice for the isospin axis that breaks the $SU(2)_L \times U(1)_Y$ gauge symmetry, leaves all the initial generators broken. Although the vacuum (2.41) is clearly not invariant for the isospin $\hat{\tau}^{1,2,3}$ and hypercharge $\hat{Y}$ generators, there is a linear combination of the original generators, which is written as

$$\hat{Q} = \frac{\mathbb{1} + \hat{\tau}^3}{2}, \tag{2.42}$$

that leaves the vacuum invariant,

$$\hat{Q}\langle\phi\rangle = \begin{pmatrix}1 & 0\\ 0 & 0\end{pmatrix}\begin{pmatrix}0\\ v\end{pmatrix} = 0. \tag{2.43}$$

The unbroken generator $\hat{Q}$ corresponds to the electric charge and implies the existence of a massless boson which is identified with the photon. The Higgs mechanism is responsible for the breaking of the electroweak symmetry to the electromagnetism,

$$SU(2)_L \times U(1)_Y \longrightarrow U(1)_Q\ . \tag{2.44}$$

The electric charge operator is commonly written in terms of the weak isospin I_3^w and weak hypercharge Y^w generators as

$$Q = \frac{Y^w}{2} + I_3^w. \tag{2.45}$$

To obtain the mass spectrum, one considers radial oscillations $h(x)$ and angular oscillations $\xi(x)$ about the vacuum, and parametrize $\phi(x)$ as

$$\phi(x) = e^{i\frac{\xi(x)}{\sqrt{2}v}} \frac{1}{\sqrt{2}} \begin{pmatrix} 0 \\ v + h(x) \end{pmatrix}. \tag{2.46}$$

However, substituting this into the Lagrangian (2.33), yields crossed terms between the gauge fields $\mathcal{A}_\mu$ and the $\xi(x)$ fields, and it is not easy to read off the mass spectrum. The strategy is to choose a new transformation parameter given as

$$\varepsilon(x) = -\frac{\xi(x)}{\sqrt{2}v} \tag{2.47}$$

such that

$$\phi(x) \quad \rightarrow \quad \phi'(x) = e^{-i\frac{\xi(x)}{\sqrt{2}v}} \phi(x) = \frac{1}{\sqrt{2}} \begin{pmatrix} 0 \\ v + h(x) \end{pmatrix}, \tag{2.48}$$

$$\mathcal{A}_\mu(x) \quad \rightarrow \quad A'_\mu(x) + \frac{1}{g\sqrt{2}v} \partial_\mu \xi(x). \tag{2.49}$$

We can now substitute eq. (2.48) and (2.49) in the Lagrangian (2.33), from were we obtain

$$\begin{aligned} \mathcal{L}_{gs} \quad = \quad & \frac{1}{2}\partial_\mu h \partial^\mu h + \frac{1}{2}\left(-2\mu^2\right)h^2 + \frac{1}{2}\left(\frac{gv}{2}\right)^2 \left(A'^1_\mu A'^{1\mu} + A'^2_\mu A'^{2\mu}\right) \\ & + \frac{1}{2}\frac{v^2}{2}\left(gA'^3_\mu - g'B_\mu\right)\left(gA'^{3\mu} - g'B^\mu\right) + \cdots . \end{aligned} \tag{2.50}$$

We see here that the field $\xi(x)$ was completely removed from the theory. Such fields are responsible for the emergence of massless Nambu-Goldstone bosons but can be easily "gauged away" using the gauge (2.48), which is commonly denoted as *unitary gauge*. It was further demonstrated in [34] that a unitary gauge always exists.

If the last term of (2.50) is diagonalized, the eigenvalues 0 and $\frac{1}{2}v^2\left(g^2 + g'^2\right)$ corresponding to the eigenvectors

$$A_\mu \quad = \quad \frac{1}{\sqrt{g^2 + g'^2}}\left(g'A'^3_\mu + gB_\mu\right) \tag{2.51}$$

$$Z^0_\mu \quad = \quad \frac{1}{\sqrt{g^2 + g'^2}}\left(gA'^3_\mu - g'B_\mu\right) \tag{2.52}$$

respectively, are obtained. Instead of the $A'^{1,2}_{\mu}$ fields, it is usual to introduce the complex vector fields

$$W^{-}_{\mu} = \frac{1}{\sqrt{2}}\left(A'^{1}_{\mu} + iA'^{2}_{\mu}\right) \tag{2.53}$$

$$W^{+}_{\mu} = \frac{1}{\sqrt{2}}\left(A'^{1}_{\mu} - iA'^{2}_{\mu}\right) \tag{2.54}$$

which, as can be read from (2.50) have the same coefficient as the e $A^{1,2}_{\mu}$ fields. We have then verified that in the presence of gauge fields, spontaneous electroweak symmetry breaking does not lead to massless scalar fields as the Goldston's Theorem states. The mass spectrum of the gauge and scalar sector is as follows:

- A scalar boson with mass $m_h = \sqrt{-2\mu^2}$ which is identified with the Higgs boson;
- Two vector gauge bosons with mass $M_W = \sqrt{\frac{1}{2}g^2v^2}$ identified with the $W^{\pm}$ bosons;
- A vector gauge boson with mass $M_Z = \sqrt{\frac{1}{2}v^2(g^2+g'^2)}$ identified with the Z boson;
- A massless gauge fields with is identified with the photon.

Due to both transverse and longitudinal polarizations, the number of degrees of freedom of a massive vector field is 3. On the other hand, a massless one only has 2 transverse polarizations. If we have four massless gauge bosons and three Nambu-Goldstone scalars, the total number of degrees of freedom is $8+3=11$. However, as we showed, we are left with three massive gauge bosons and a massless one leading to a total of $3+3+3+2=11$ degrees of freedom. This counting intuitively explains the removal of the Goldstone bosons degrees of freedom from the theory as being absorbed by the gauge fields that acquired mass.

In the SM Higgs sector, the complex doublet provides 4 degrees of freedom, of which, 3 correspond to the massless Goldstone bosons when the symmetry is broken. We are then left with 1 physical Higgs scalar in the theory. If the model is extended in such a way that the gauge symmetry is the same and an extra complex Higgs doublet is included, there would be 5 physical degrees of freedom. Examples of such modes include the minimal supersymmetric extension of the SM (MSSM) which will be addressed in the next section, or two-Higgs-doublet models 2HDM [35].

Fermion Masses

The interactions between matter and the electroweak fields are described by the fermion-kinetic Lagrangian

$$\begin{aligned}\mathcal{L}_{f-k} &= \sum_{j=1}^{3} \overline{Q}_{Lj}\left(i\gamma^{\mu}D_{\mu}\right)Q_{Lj} + \overline{u}_{Rj}\left(i\gamma^{\mu}D_{\mu}\right)u_{Rj} + \overline{d}_{Rj}\left(i\gamma^{\mu}D_{\mu}\right)d_{Rj} \\ &\quad + \overline{L}_{Lj}\left(i\gamma^{\mu}D_{\mu}\right)L_{Lj} + \overline{e}_{Rj}\left(i\gamma^{\mu}D_{\mu}\right)e_{Rj}\,, \end{aligned} \tag{2.55}$$

where j is a generation index, Q_{Lj} and L_{Lj} are the quark and lepton left-handed chiral fields of the jth generation,

$$Q_{L(1,2,3)} = \begin{pmatrix} u \\ d \end{pmatrix}_L, \begin{pmatrix} c \\ s \end{pmatrix}_L, \begin{pmatrix} t \\ b \end{pmatrix}_L \tag{2.56}$$

$$L_{L(1,2,3)} = \begin{pmatrix} \nu_e \\ e \end{pmatrix}_L, \begin{pmatrix} \nu_\mu \\ \mu \end{pmatrix}_L, \begin{pmatrix} \nu_\tau \\ \tau \end{pmatrix}_L \tag{2.57}$$

and u_{Rj}, d_{Rj} and $\mathrm{e_{Rj}}$ the correspondent right-handed electroweak singlets. Here we are not considering the strong interaction and the covariant derivative is defined as in (2.28), though, terms including the gauge couplings and generators of $SU(3)_C$ for the quark fields as in (2.27) are also present in the total Lagrangian of the SM.

As we discussed above, the $SU(2)_L \times U(1)_Y$ regards the left and right helicities differently. A mass term for the leptons of the form $-m_l\bar{l}l = -m_l\left(\bar{l}_R l_L - \bar{l}_L l_R\right)$ is not an electroweak invariant. The proposal to fix this difficulty is requiring massless leptons before spontaneous symmetry breaking, where the breaking mechanism itself, is responsible for mass generation. To achieve this goal, new interacting terms for the leptons and the Higgs field have to be introduced. Such interaction terms are designated as Yukawa terms where y_l will be the dimensionless Yukawa coupling between the Higgs and the leptons.

To construct a $SU(2)_L \times U(1)_Y$ invariant term, we can build a $SU(2)$ singlet with the doublets L_L and ϕ as $\overline{L}\phi$. This term is however not Lorentz invariant since a right-handed spinor is missing. Adding the $SU(2)$ singlet e_R, and noting that the hypercharges of L_L, ϕ and e_R are -1, $+1$ and -2 respectively, i.e. $Y(\overline{L}_L\phi e_R) = 0$, we can write a Lorentz and $SU(2)_L \times U(1)_Y$ invariant Lagrangian for the lepton sector:

$$\mathcal{L}_l = -(y_l)_{ij}\,\overline{L}_{Li}\phi e_{Rj} + h.c. \tag{2.58}$$

where i, j are generation indexes. The same reasoning can be used to construct the Yukawa

Lagrangian for the down-type quarks:

$$\mathcal{L}_d = -(y_d)_{ij}\,\overline{Q}_{Li}\phi d_{Rj} + h.c. \tag{2.59}$$

For the up-type quarks, we observe that $Y(\overline{Q}_L\phi u_R) = -\frac{1}{3}+1+\frac{4}{3} = 2$, therefore, the $\overline{Q}_L\phi u_R$ term is not invariant for $SU(2)_L \times U(1)_Y$. To solve this problem,consider the Higgs doublet

$$\tilde{\phi} = i\tau^2\phi^* = \begin{pmatrix} 0 & 1 \\ -1 & 0 \end{pmatrix}\begin{pmatrix} \phi^- \\ \phi^0 \end{pmatrix} = \begin{pmatrix} \phi_0 \\ -\phi^- \end{pmatrix} \tag{2.60}$$

where $\left(\phi^+\right)^* \equiv \phi^-$. Now, $Y(\overline{Q}_L\tilde{\phi}u_R) = -\frac{1}{3}-1+\frac{4}{3} = 0$ and we can write an invariant Lagrangian for the up-type quarks:

$$\mathcal{L}_u = -(y_d)_{ij}\,\overline{Q}_{Li}\tilde{\phi}d_{Rj} + h.c. \tag{2.61}$$

Considering a basis where the Yukawa matrices are flavour diagonal, when the Higgs field develops an expectation value

$$\phi \to \langle\phi\rangle = \frac{1}{\sqrt{2}}\begin{pmatrix} 0 \\ v \end{pmatrix} \text{ and } \tilde{\phi} \to \langle\tilde{\phi}\rangle = \frac{1}{\sqrt{2}}\begin{pmatrix} v \\ 0 \end{pmatrix}, \tag{2.62}$$

mass terms for the fermions are generated, and the fermion mass Lagrangian takes the form

$$\mathcal{L}_{fm} = -\frac{v}{\sqrt{2}}\left[(y_u)_{ii}\,\overline{u}_{Li}u_{Ri} - \frac{1}{\sqrt{2}}(y_d)_{ii}\,\overline{d}_{Li}d_{Ri} - \frac{1}{\sqrt{2}}(y_l)_{ii}\,\overline{l}_{Li}l_{Ri}\right] + h.c. \tag{2.63}$$

The fermion masses in the Standard Model are then expressed as

$$m_f = y_f\frac{v}{\sqrt{2}}\,. \tag{2.64}$$

The choice of basis that lead to eq. (2.63), which is the physical one, causes a complication in the gauge-fermion interacting terms of eq. (2.55). To make it clear, consider the unitary transformations

$$u_L^i = \mathcal{U}_u^{ij}u_L'^j \text{ and } \mathrm{d_L^i} = \mathcal{U}_\mathrm{d}^\mathrm{ij}\mathrm{d_L'^j}\,, \tag{2.65}$$

where the primed fields are written the gauge eigenstates basis, whereas the unprimed ones in the mass eigenstates basis. For the later one, if we expand the first term on the right-hand-side (r.h.s) of eq. (2.55), we see that exchange of W-bosons will generate *flavour changing currents* of the form

$$\frac{1}{\sqrt{2}}\overline{u}_L'^i\gamma^\mu d_L'^j = \frac{1}{\sqrt{2}}\overline{u}_L^i\gamma^\mu\left(\mathcal{U}_u^\dagger\mathcal{U}_d\right)_{ij}d_L^j \equiv \frac{1}{\sqrt{2}}\overline{u}_L^i\gamma^\mu(V_{CKM})_{ij}d_L^j\,, \tag{2.66}$$

with V_{CKM} the so called *Cabibbo-Kobayashi-Maskawa* (CKM) matrix.

We conclude this section with tables 2.1 and 2.2 where the massless SM fields are summarized in terms of their representations.

Fermions and Scalars in the SM				
Names		Spin 0	Spin 1/2	$SU(3)_C \times SU(2)_L \times U(1)_Y$
Quarks (3 generations)	Q	$\times$	(u_L, d_L)	**3**, **2**, 1/3
	$\bar{u}$	$\times$	$\bar{u}_L = (u_R)^c$	$\bar{\mathbf{3}}$, **1**, -4/3
	$\bar{d}$	$\times$	$\bar{d}_L = (d_R)^c$	$\bar{\mathbf{3}}$, **1**, 2/3
Leptons (3 generations)	L	$\times$	(ν_{eL}, e_L)	**1**, **2**, -1
	$\bar{e}$	$\times$	$\bar{e}_L = (e_R)^c$	**1**, **1**, 2
Higgs	ϕ	(ϕ^+, ϕ^0)	$\times$	**1**, **2**, 1

Table 2.1. *Fermion and scalar fields in the SM. The leftmost column provides the usual designation for the fundamental particles, the two middle ones the spin and the rightmost the charges under the SM gauge group.*

Gauge Bosons in the SM		
Names	Spin 1	$SU(3)_C \times SU(2)_L \times U(1)_Y$
Gluons	g	**8**, **1**, 0
W Bosons	$W^{\pm}$, W^0	**1**, **3**, 0
B Boson	B	**1**, **1**, 0

Table 2.2. *Gauge bosons in the SM. The left column provides the usual designation for the gauge fields, the middle one the spin and the right one the SM charges.*

2.4. Renormalization and Running of the Gauge Couplings

The description of the Standard Model that we have been so far developing, did not take into account that, as a quantum theory, the SM fields can be Fourier expanded in terms of creation and annihilation operators. It is then possible to create a particle at some point in space x_i, say an electron, and propagate it to a point x_f where it is destroyed. In a free theory, the propagator of the electron is simply given by

$$\frac{i}{\not{p} - m_0} \tag{2.67}$$

where the (bare) mass emerges as a pole in the propagator. In interacting theories like the SM, coupled non-linear equations emerge form the Lagrangian and classical analytical solutions for the physical observables are unattainable. Instead, calculations are realized with the help of perturbation theory as Dyson series [36] expansions in the couplings, g_a, y_f, m,..., pictorially represented by Feynman diagrams [37]. It is not difficult to write down tree-level diagrams once the Feynman rules are established (from the bare

Lagrangian). The perturbative expansion in the couplings, which allows virtual particles to be radiated and reabsorbed, is represented by loop diagrams illustrating formally divergent scale dependent integrals. Such divergences in the intermediate states can however be canceled by divergences in the bare terms, where the leftover finite terms correspond to the observables of the theory. This procedure is called *renormalization* [38, 39]. The resulting expressions for the renormalized parameters should be finite for any energy-scale and when calculating loop diagrams, it is common to define a maximum energy or cut-off scale, say $p = \Lambda$, up to which the theory makes sense.

As a measurable quantity, it is possible to eliminate the Λ dependency from the physical prediction of the electron mass. When higher order terms are included, the pole of the propagator (2.67) is shifted by a divergent amount $\Sigma(\Lambda)$ and the physical measurable mass is now given by

$$m_{ph} = m_0 + \Sigma(\Lambda) \ , \tag{2.68}$$

where the infinities in Σ are cancelled by infinities in the bare mass. When the renormalization process is carried out, certain renormalization rules are applied in order to fix the physical finite values at a particular momentum $Q = Q_0$. These rules are collectively known as *renormalization scheme*, the momentum Q_0 is denoted as *renormalization point* and Q as *renormalization scale*.

After fixing the relation between physical and bare quantities, it is possible to rewrite the Lagrangian in terms of the physical parameters and the leftover bare quantities are collected in counterterms. As an example, consider the electron mass in a QED Lagrangian as (2.17), $-m_0\overline{\psi}_e\psi_e$, where, after switching from bare to physical quantities, one gets $-m_{ph}(1+\delta_m)\overline{\psi}_e\psi_e$, with δ_m the counterterm (see chapter 10 of [15] for details).

The values of the theory parameters are quantities that depend on the choice of the renormalization scale, Q, and its variation is expressed by the *Renormalization Group Equations* (RGE) [40, 41]. To determine the RGEs of a given coupling or mass in a theory with n_B bosons and n_F fermions, we first need to find its β-function, which is obtained from the *Callan-Symanzik equation* (CS) [42–44],

$$\left[Q\frac{\partial}{\partial Q} + \beta_j\frac{\partial}{\partial g_j} + \left(\gamma_{m,b}+1\right)m_b\frac{\partial}{\partial m_b} + n_B(1+\gamma_B) + n_F\left(\frac{3}{2}+\gamma_F\right) - 4\right]G^{n_B,n_F}(Q;g_i,m_a;Q_0) = 0 \tag{2.69}$$

where the renormalization point Q_0 is kept fixed. Here G^{n_B,n_F} is a (n_B+n_F)-point Green function, $\beta_i\left(g_j,m_b;Q\right)$ are the beta-functions, $\gamma_{m,a}\left(g_j,m_b;Q\right)$ RG coefficients for the mass terms and $\gamma_{B,F}$ the boson and fermion anomalous dimensions. Such β and γ functions describe

rescaling upon the couplings , masses and fields, compensating shifts in the renormalization scale in such a way that the theory is invariant for all Q below the cut-off.

To calculate the one-loop β-functions of the SM gauge couplings to some order in perturbation theory, we first need to calculate the counterterms that emerge when we renormalize the theory. In particular, we need to calculate the loop corrections to terms in the Lagrangian involving fermion-fermion-gauge, scalar-scalar-gauge and scalar-scalar-gauge-gauge interactions, pure gauge triple and quartic vertices as well as corrections to the propagators (self-energy diagrams). Terms involving interactions between gauge bosons are only valid for the gauge couplings of the non-Abelian symmetries $SU(2)_L$ and $SU(3)_C$. As an example, corrections to the fermion-fermion-gauge vertex to one-loop order are given by the diagrams of Fig. 2.2. The first term on the rhs is the tree-level diagram and does not contain

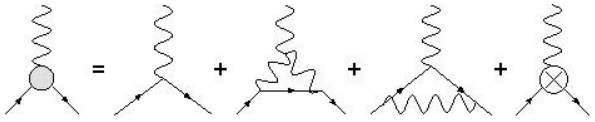

Figure 2.2. *One-loop corrections to the fermion-fermion-gauge vertex*

.

any divergence, the second and third diagrams contain logarithmic divergences which will cancel out against the fourth diagram that corresponds to the counterterm.

In general we will have a CS equation of the type (2.69) with one β_i-function for each gauge coupling g_i, a γ for each field, γ_A, γ_Ψ and γ_ϕ and a γ_m for each mass. Once the counterterms are determined, the β function for gauge theories is

$$\beta(g_i) = \frac{g_i^3}{16\pi^2}\left[-\frac{11}{3}C_2(V) + \frac{4}{3}T_2\left(R_f\right) + \frac{1}{3}T_2(R_s)\right], \tag{2.70}$$

where the $C_2(V)$ and $T_2(R)$ factors are group casimirs defined as $f^{acd}f^{bcd} = C_2(V)\delta^{ab}$ and $tr\left(\Omega^a\Omega^b\right) = T_2(R)\delta^{ab}$. G, R_f and R_s label the adjoint, fermion and scalar group representaions for the corresponding gauge group. The evolution of the gauge couplings is then governed by the evolution equation

$$\beta(g_i) = \frac{dg_i}{dt} = b_i\frac{g_i^3}{16\pi^2}, \tag{2.71}$$

where $t = \log Q/Q_0$, and the b_i coefficients can be read off from equation (2.70).

For convenience, we rewrite equation (2.71) in terms of the structure constants defined

as $\alpha_i = \frac{g_i^2}{4\pi}$, where the running is linear and easier to handle:

$$\frac{d}{dt}\alpha_i^{-1} = -\frac{b_i}{2\pi} \,. \tag{2.72}$$

Here, g_2 and g_3 are the $SU(2)_L$ and $SU(3)_C$ gauge couplings, and $g_1 = \sqrt{\frac{5}{3}}g'$, where the proportionality constant is the canonical Georgi-Glashow $SU(5)$ normalization factor [45–47]. The hypercharge generator, $\frac{Y}{2}$, should also be multiplied by a $\sqrt{\frac{3}{5}}$ factor so that the covariant derivative is kept unchanged.

In order to obtain the RGEs of the three gauge couplings in the SM, all we have to do is to determine the initial conditions and the slopes b_i. From experimental data (see [48]) we know that $\alpha_3(M_Z) = 0.1176 \pm 0.0020$ or $\alpha_3^{-1}(M_Z) \approx 8.50$, where $M_Z = 91.1876 \pm 2.1 \times 10^{-3}$ GeV the Z boson mass. We also know that $\sin^2\theta_W(M_Z) = 0.23119 \pm 1.4 \times 10^{-4}$ and $\alpha_{em}^{-1}(M_Z) \approx 128$, where $\alpha_{em} = \frac{e^2}{4\pi} = \frac{g^2 \sin^2\theta_W}{4\pi} = \alpha_2^2 \sin^2\theta_W$. Hence $\alpha_2^{-1}(M_Z) \approx 29.6$. Finally, from the definition of the structure constants and from $g'^2 = g^2 \tan^2\theta_W$ we have $\alpha_1^{-1}(M_Z) = \frac{3}{5}\alpha'^{-1} = \frac{3}{5}\alpha_2^{-1}(M_Z)\cot^2\theta_W(M_Z) \approx 59.12$. The initial conditions are

$$\alpha_1^{-1}(M_Z) = 59.12 \;\;,\;\; \alpha_2^{-1}(M_Z) = 29.6 \;\;,\;\; \alpha_3^{-1}(M_Z) = 8.40. \tag{2.73}$$

To determine the slopes b_i, we calculate the Casimirs T_2 and C_2. While for $SU(N)$ algebras C_2 is just the dimension of the group, i.e. N, T_2 is a sum over all the fields in the fundamental representation of the corresponding gauge group. To do this, let us start by considering separately the fermion Ψ and the scalar Φ fields.

$$\Psi \in \left\{Q_L, \bar{u}_R, \bar{d}_R, L_L, \bar{e}_R\right\} \;\;,\;\; \Phi \in \left\{\phi\right\} \tag{2.74}$$

Slopes for $SU(3)_C$

To calculate b_3, one must consider the chiral multiplets in the fundamental representation of $SU(3)_C$ and the gauge multiplets in the adjoint representation. An useful formula to calculate this coefficient is

$$b_3 = \frac{1}{3}\sum_{\Psi} A_2^{\Psi} N_{\Psi} + \frac{1}{6}\sum_{\Phi} A_2^{\Phi} N_{\Phi} - 11 \tag{2.75}$$

where $N_{\Psi,\Phi}$ is the number of generations of the corresponding field and

$$A_2^{\Psi,\Phi} = \begin{cases} 1 & \Psi,\Phi \text{ a SU(2) singlet} \\ 2 & \Psi,\Phi \text{ a SU(2) doublet} \end{cases} \tag{2.76}$$

Slopes for $SU(2)_L$

For b_2 the strategy is similar, but now one must consider chiral multiplets in the fundamental representation of $SU(2)_L$.

$$b_2 = \frac{1}{3}\sum_{\Psi} C_3^{\Psi} N_{\Psi} + \frac{1}{6}\sum_{\Phi} C_3^{\Phi} N_{\Phi} - \frac{22}{3} \tag{2.77}$$

where

$$C_3^{\Psi,\Phi} = \begin{cases} 1 & \Psi,\Phi \text{ a SU(3) singlet} \\ 3 & \Psi,\Phi \text{ a SU(3) triplet} \end{cases} \tag{2.78}$$

Slopes for $U(1)_Y$

To determine b_1 recall that the hypercharge is normalized as $\sqrt{\frac{3}{5}}Y$. The corresponding formula is

$$b_1 = \frac{2}{5}\sum_{\Psi}\left(\frac{Y_{\Psi}}{2}\right)^2 C_3^{\Psi} A_2^{\Psi} N_{\Psi} + \frac{1}{5}\sum_{\Phi}\left(\frac{Y_{\Phi}}{2}\right)^2 C_3^{\Phi} A_2^{\Phi} N_{\Phi} \tag{2.79}$$

with the coefficients having the same meaning as in the previous cases.

Computing this formulas for the SM one obtains

$$b_1 = \frac{41}{10} \ , \ b_2 = -\frac{19}{6} \ , \ b_3 = -7. \tag{2.80}$$

The running of the gauge couplings in the SM is represented in Fig. (2.3). In this thesis, we are

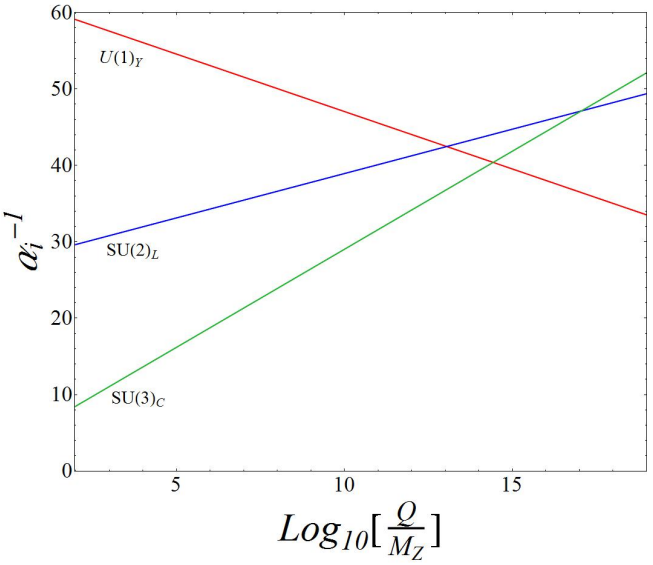

Figure 2.3. *Running of the Gauge Couplings in the Standard Model.*

interested in studying unified descriptions of the strong and electroweak interactions, and as it is evident from Fig: 2.3, using the canonical normalization of $U(1)_Y$, it is not possible to achieve gauge coupling unification in the SM if we do not introduce extra multiplets between the electroweak and the GUT scales. An alternative would be the introduction of different $U(1)_Y$ normalizations inspired by string or orbifold inspired models, see [49] and references therein. The only possibility for a 4D construction with a simple group, is the Georgi-Glashow normalization and Grand Unification can only be attained with the addition of extra matter fields, as we will discuss in the next chapter.

2.5. Motivations for Physics Beyond the Standard Model

Despite the great success of the SM in describing the known particles and their interactions, it is still an incomplete framework with theoretical and experimental disagreements. As we mentioned in the beginning, neutrino oscillations between flavour states were observed. This phenomenon requires the mixing of mass eigenstates, which involves right-handed neutrinos that are not predicted by the Model. However, the SM can be readily adapted in order to include neutrino masses. As an example, it is possible to introduce a $SU(3)\times SU(2)\times U(1)$ singlet containing a right-handed neutrino field N_R, which allows Majorana mass terms[4] of the form $\mathcal{M}_{RR}\overline{N}_R N_R^c$, or Dirac mass terms $m_{LR}\overline{\nu}_L N_R$. It is not yet known whether neutrinos are Dirac or Majorana particles. This question is indeed one of the key subjects of current neutrino experiments.

The Dark Matter component of the Universe, is believed to make up the majority of the matter density. Such dark particles, which only interact via the weak and the gravitational forces, were proposed in order to explain galactic motion. Evidence of Dark Matter is currently very strong, see [50] for an extensive discussion, and its existence is deduced from observing the motion of visible baryonic matter and how it deviates from General Relativity predictions. In the SM, the only candidate particles are the neutrinos. However, current upper limits on their masses require further sources of Dark Matter [51].

The anomalous magnetic moment $a_\mu = (g-2)_\mu/2$ has been determined at BNL [52] to be $a_\mu(exp) = (11\ 659\ 208.9 \pm 6.3)\times 10^{-10}$, which may be compared to the SM prediction [53] $a_\mu(SM) = (11\ 659\ 183.4 \pm 4.9)\times 10^{-10}$. This 3-4$\sigma$ tension of (SM) theory and experiment could be a hint for physics beyond the SM. However it is still possible to be simply a statistical fluctuation.

The gauge structure of the SM is still an unanswered question. One can ask if such a symmetry is a remnant of some larger simple group that is spontaneously broken at a high

[4] A Majorana spinor ψ_M is defined such that $\psi_M^\dagger = \psi_M$ with $\psi_M^\dagger \equiv \gamma_0\psi_M^c$

scale by some Higgs-like mechanism [148], or if it results from some other physics, such as, for example, extra dimensions or higher dimensional operators [55, 56]?

Another reason to exploit new physics is the Hierarchy or fine-tuning problem, which we elaborate below.

2.5.1. The Hierarchy Problem

In section 2.3.1, we discussed the mechanism that provides masses to all SM particles. The only field which is present in the vacuum is the Higgs field, and its expectation value is given by v, a parameter with the dimensions of energy, i.e. a weak scale, with the approximate value of

$$v \approx 246\ GeV\ , \tag{2.81}$$

and where $\left\langle \phi^0 \right\rangle = \sqrt{\frac{2}{\lambda}}\mu = \frac{v}{\sqrt{2}}$. The occurrence of such a vev is a signal of spontaneous symmetry breaking, and, in principle, the scale of all masses in the theory are set by v. The discussion carried out in section 2.3.1 was accomplished at tree-level. We might then ask what happens if we include loops in the discussion? The Standard Model is a renormalizable theory, which means that we can extend the virtual momenta in loop-integrals all the way to infinity obtaining finite results. However, no one believes that the SM is a valid theory for all energy scales. This means that we must have a scale Λ, where new physics appears and where the SM must be modified, being part of a larger theory.

At the very last, new physics must be revealed when quantum gravity becomes important, i.e., at $\Lambda \approx M_p \approx 10^{19} GeV$, but it could also be just few orders of magnitude higher than v. With these ideas in mind, some problems emerge when we go beyond the tree-level. To make this clear, let us consider the self interaction term with quartic coupling[5], $\frac{\lambda_s}{4}\left(\phi^\dagger\phi\right)^2$, which is represented in Fig: 2.4. The Feynman loop integral corresponding to the

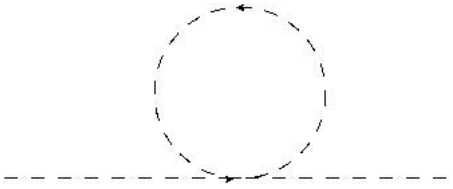

Figure 2.4. *One loop scalar self-energy with quartic coupling*

[5]This example is not unique, and the problem is frequently illustrated with a top quark loop instead, leading to the same conclusions

self interaction $-i\Sigma(k)$, where k is the internal momentum, is of the form

$$-i\Sigma(k) = \lambda_s \int \frac{d^4k}{(2\pi)^4} \frac{1}{k^2 - m_\phi^2} \tag{2.82}$$

If regularized with a cut-off Λ, a leading quadratic divergence is exposed and the self energy produces a correction $\propto \lambda_s \Lambda^2 \phi^\dagger \phi$ to the bare mass term,

$$-\mu^2_{physical} = -\mu^2 + \lambda_s \Lambda^2. \tag{2.83}$$

With the value of v phenomenologically established, we have $\mu_{physical} = \sqrt{\lambda_s}\frac{v}{2}$. Given that λ_s is expected to be of the order of 1, $\mu_{physical}$ can hardly be much greater than few hundred GeV. If we take $\Lambda \sim M_p \sim 10^{19}\ GeV$, a one loop correction will be much greater than $(100\ GeV)^2$ which require a bare μ^2 value also very large, relying on a remarkable cancellation in order to get us from $\sim (10^{19}\ GeV)^2$ to $\sim (100\ GeV)^2$. This fine-tuning problem affects not only the Higgs mass, $m_h = \sqrt{2}\mu_{physical}$, but also the W mass, $M_W = \frac{g\mu_{physical}}{\sqrt{\lambda_s}}$, as well as all the masses in the SM related to $\mu_{physical}$ and v. However, this problem would be less severe if new physics appears at a scale $\Lambda \ll M_p$.

One idea is to eliminate the quadratic dependence on the cut-off scale Λ, equation (2.83), present in theories with elementary scalar fields. To understand how these quadratic divergences can be controlled, let us look at the case of an unbroken gauge theory like QED.

The example of QED

To illustrate what happens in QED, let us consider the vacuum polarization and the electron self-energy, Fig. 2.5. For the vacuum polarization, the loop integral, $\Pi^{\mu\nu}(k)$ can be regularized

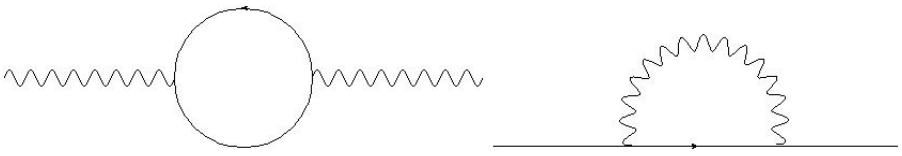

(a) Vacuum polarization (b) Electron self energy

Figure 2.5.

in a gauge invariant way, avoiding quadratic divergences which would imply enormous quantum corrections to the photon mass, breaking the gauge invariance of the theory. For the case of the electron self-energy, $-i\Sigma(\not{p})$, corrections to the fermion mass take the form $\delta m \propto \alpha m \log\Lambda$, where α is the $U(1)_Q$ gauge structure constant. No unpleasant fine-tuning is necessary, and the diagram diverges but only logarithmically. This is a consequence of a symmetry present in the total SM Lagrangian as the masses of the fermions go to zero,

which is called *chiral symmetry*. Formally, the fermion mass terms in the SM Lagrangian are not invariant under transformations of the form

$$\psi(x) \to e^{i\alpha\gamma^5}\psi(x), \tag{2.84}$$

where $\gamma^5 \equiv i\gamma^0\gamma^1\gamma^2\gamma^3\gamma^4$.

We have so far discussed how unbroken gauge symmetries and chiral symmetries remove dangerous quadratic divergences. The idea to solve the hierarchy problem of the SM is to find a framework where scalars and massless fermions are collected in chiral multiplets under the "protection" of chiral symmetry. This is exactly what supersymmetry does, as we will discuss in the next chapter.

3. Supersymmetry

It is not explained in the Standard Model how the electroweak scalars remain almost massless way below the Planck scale without any symmetry to guarantee it. This hierarchy problem is one of the main motivations for supersymmetry (SUSY), where cancellations amongst quadratic divergent terms in Feynman diagrams emerge naturally. This particularity not only stabilizes the SM masses, but also highlights how supersymmetric models have better ultra-violet behaviour than non-supersymmetric ones.

The possibility of embedding the SM into a Grand Unification Theory, would not only provide a powerful explanation for its gauge structure, but also elegantly contribute to reduce the number of free parameters. Despite the attractiveness of this idea, it difficult to attain gauge coupling unification in the SM. This key ingredient for a GUT theory, is easily achieved with the contribution of supersymmetry, which constitutes a tantalizing evidence for a supersymmetric theory of Grand Unification.

The description that follows, is inspired by the references [57–60].

3.1. Supersymmetric Algebra

Originally, supersymmetry was introduced as an extension to *Coleman and Mandula's Theorem* [61], which fundamentally states that given some reasonable physical assumptions, if G is a symmetry group of the S-Matrix containing the Poincaré group, then it cannot be combined with internal symmetries[1] in any but a trivial way. While this no-go theorem implies that there is no symmetry capable of relating particles with different mass and spin, the concept of anti-commuting generators was not taken into account. However, most of the ideas in the theorem crucially apply to SUSY, and an extension to the Coleman-Madula formulation, developed by Haag, Lopuszanski and Sohnius [62], states that some supersymmetries are the only possible non-trivial extensions of the Poincaré algebra.

The concept of a *Graded Lie Algebra* (GLA) has then emerged. A GLA is characterized by a direct sum of two vector spaces, $\mathcal{V}_b \oplus \mathcal{V}_f$, where $\mathcal{V}_b$ is the space of bosonic elements related by commutation relations and $\mathcal{V}_f$ the space of fermionic elements where the operators are

[1] Internal symmetries are those that commute with the Poincaré group.

anti-commuting. Note that $\mathcal{V}_b$ is an ordinary Lie algebra where the Coleman-Mandula theorem is directly applicable.

This is the case of supersymmetry, where the bosonic part $\mathcal{V}_b$ can be identified with the Poincaré group. The generators of $\mathcal{V}_b$ are the four-translations or energy-momentum operator P_μ, and the angular momentum tensor $M_{\mu\nu}$, which generates Lorentz boosts and rotations. The Poincaré algebra is defined by the commutation relations,

$$\begin{aligned}
\left[P_\mu, P_\nu\right] &= 0 && (3.1)\\
\left[M_{\mu\nu}, P_\lambda\right] &= i\left(g_{\nu\lambda}P_\mu - g_{\mu\lambda}P_\nu\right) && (3.2)\\
\left[M_{\mu\nu}, M_{\rho\sigma}\right] &= i\left(g_{\nu\rho}M_{\mu\sigma} + g_{\mu\sigma}M_{\nu\rho} - g_{\mu\rho}M_{\nu\sigma} - g_{\nu\sigma}M_{\mu\rho}\right). && (3.3)
\end{aligned}$$

To close the SUSY algebra we introduce a two-component Weyl spinor generator Q_α, where $\alpha \in \{1,2\}$. This operator changes the spin of a state by $\frac{1}{2}$, transforming fermions into bosons, $Q|F\rangle = |B\rangle$, and bosons into fermions, $Q|B\rangle = |F\rangle$. The supersymmetric algebra is then specified by eq. (3.1 to 3.3) and

$$\begin{aligned}
\left[P_\mu, Q_\alpha\right] &= \left[P_\mu, \overline{Q}^{\dot\alpha}\right] = 0 && (3.4)\\
\left[M_{\mu\nu}, Q_\alpha\right] &= -i\left(\sigma_{\mu\nu}\right)_\alpha^{\ \beta} Q_\beta && (3.5)\\
\left[M_{\mu\nu}, \overline{Q}^{\dot\beta}\right] &= -i\left(\overline{\sigma}_{\mu\nu}\right)^{\dot\beta}_{\ \dot\alpha}\, \overline{Q}^{\dot\alpha} && (3.6)\\
\left\{Q_\alpha, Q_\beta\right\} &= \left\{\overline{Q}_{\dot\alpha}, \overline{Q}_{\dot\beta}\right\} = 0 && (3.7)\\
\left\{Q_\alpha, \overline{Q}_{\dot\beta}\right\} &= 2\sigma^\mu_{\alpha\dot\beta} P_\mu\,. && (3.8)
\end{aligned}$$

Right-handed and left-handed spinors transform differently under Lorentz transformations and should be distinguished. Dotted indices are used to label right-handed spinors. The σ_μ and $\sigma_{\mu\nu}$ objects are defined in terms of the Pauli matrices as

$$\begin{aligned}
\sigma^\mu &\equiv (\mathbb{1}, \sigma^i), && (3.9)\\
\overline{\sigma}^\mu &\equiv (\mathbb{1}, -\sigma^i), && (3.10)\\
\sigma^{\mu\nu} &\equiv \frac{1}{4}(\sigma^\mu\overline{\sigma}^\nu - \sigma^\nu\overline{\sigma}^\mu), && (3.11)\\
\overline{\sigma}^{\mu\nu} &\equiv \frac{1}{4}(\overline{\sigma}^\mu\sigma^\nu - \overline{\sigma}^\nu\sigma^\mu). && (3.12)
\end{aligned}$$

Further copies of the SUSY generators are mathematically allowed. It is of common use to classify a supersymmetry by the number of copies, N, of the generators. However, the only version phenomenologically relevant for low energies is $N = 1$ supersymmetry [63]. The bosonic coordinate system x^μ is also extended in supersymmetry. A fermionic coordinate

θ_α is introduced in order to connect anti-commuting spinor fields with commuting scalar or vector fields. Formally, a superfield $\mathcal{S}$, is a function of both the space-time coordinate as well as of the anti-commuting Grassmann variables,

$$\mathcal{S} = \mathcal{S}\left(x^\mu, \theta_\alpha, \overline{\theta}^{\dot{\alpha}}\right) , \tag{3.13}$$

transforming as

$$\delta\mathcal{S} = i(\epsilon Q + \overline{\epsilon}\overline{Q} - a^\mu P_\mu)\mathcal{S} , \tag{3.14}$$

where ϵ_α is an infinitesimal Weyl spinor and a^μ an infinitesimal space-time translation. The superfield $\mathcal{S}$ can be expanded as a power series in the Grassmann variables, and the coefficients of the various powers (not more than two) of θ and $\overline{\theta}$ are the ordinary fields.

Let us finalize this section with some relevant consequences of the SUSY algebra. The first one emerges from the anti-commuting relation (3.8) where, with the aid of the identity $tr\left(\sigma^\mu\overline{\sigma}^\nu\right) = 2g^{\mu\nu}$, we obtain

$$\left(\overline{\sigma}^\nu\right)^{\dot{\beta}\alpha}\left\{Q_\alpha, \overline{Q}_{\dot{\beta}}\right\} = 4P^\nu , \tag{3.15}$$

with $g^{\mu\nu}$ the Minkowski metric tensor. If we take the matrix element of the zeroth component, $\langle\psi|4P^0|\psi\rangle$, we get the inequality

$$4\langle\psi|Q_\alpha(Q_\alpha)^\dagger + (Q_\alpha)^\dagger Q_\alpha|\psi\rangle \geq 0 . \tag{3.16}$$

This relation shows that in a supersymmetric theory, the Hamiltonian $H = P^0$ is positive semi-definite. The vacuum state of an unbroken supersymmetry has zero energy, and if it is spontaneously broken, the vacuum must have positive energy.

Recalling that Q_α and $\overline{Q}_{\dot{\beta}}$ change the fermion number by one unit, if we introduce $\mathcal{N}_f$, the fermion number generator, such that $(-1)^{\mathcal{N}_f}|F\rangle = -|F\rangle$ and $(-1)^{\mathcal{N}_f}|B\rangle = |B\rangle$, the relation (3.17) is immediate,

$$(-1)^{\mathcal{N}_f} Q_\alpha = -Q_\alpha(-1)^{\mathcal{N}_f} . \tag{3.17}$$

Using (3.17) and the cyclic property of the trace, it is possible to show that

$$tr\left[(-1)^{\mathcal{N}_f}\left\{Q_\alpha, \overline{Q}_{\dot{\beta}}\right\}\right] = tr\left[-Q_\alpha(-1)^{\mathcal{N}_f}\overline{Q}_{\dot{\beta}} + Q_\alpha(-1)^{\mathcal{N}_f}\overline{Q}_{\dot{\beta}}\right] = 0 , \tag{3.18}$$

from where, for non-zero P^μ, we deduce that

$$tr\Big[(-1)^{N_f}\Big] = 0\ . \tag{3.19}$$

This relation provides a rather important property of supersymmetry. If we consider a SUSY representation with an arbitrary number of fermions $n_F(\mathbf{R})$ and an arbitrary number of bosons $n_B(\mathbf{R})$, say $\mathbf{R} = |F_1,\ldots,F_{n_F};B_1,\ldots,B_{n_B}\rangle$, eq. (3.19) implies that

$$n_B(\mathbf{R}) - n_F(\mathbf{R}) = 0\ , \tag{3.20}$$

which guarantees that the number of fermions and bosons in a representation $\mathbf{R}$ of the supersymmetric algebra is the same. Such representations or supermultiplets are organized according to the helicity λ of their states. It is possible to show (see [57] for details) that there are no other states in a supermultiplet besides those with helicities λ and $\lambda - \frac{1}{2}$. The fermion superpartners of the graviton and gauge bosons are commonly denoted as *gravitino* and *gaugino* respectively, whereas the boson superpartners of the chiral fermions are called *sfermions*. A supermultiplet is characterized according to the classification below:

- **Gravity Supermultiplet:** $\lambda = 2$ (graviton) and $\lambda - \frac{1}{2} = \frac{3}{2}$ (gravitino)
- **Gauge Supermultiplet:** $\lambda = 1$ (gauge boson) and $\lambda - \frac{1}{2} = \frac{1}{2}$ (gaugino)
- **Chiral Supermultiplet:** $\lambda = \frac{1}{2}$ (chiral fermion) and $\lambda - \frac{1}{2} = 0$ (chiral sfermion/scalar)

3.2. Lagrangians for Chiral and Gauge Superfields

In this section we introduce a general renormalizable supersymmetric Lagrangian where the propagating and non-propagating degrees of freedom in both chiral and gauge supermultiplets are considered.

3.2.1. Chiral Interactions

We start with a free non-interacting theory for the chiral sector with the Lagrangian

$$\mathcal{L}_{chiral-free} = -\partial^\mu \phi^{*i}\partial_\mu\phi_i + i\psi^{\dagger i}\overline{\sigma}^\mu\partial_\mu\psi_i + F^{*i}F_i\ , \tag{3.21}$$

where ψ is a spinor in the Weyl representation, and the chiral superfields X

$$X_i = \Big(\phi_i, \psi_i, F_i\Big)\ , \tag{3.22}$$

with i a flavour index, may be expanded in terms of the fermionic coordinates as

$$\begin{aligned} X_i\left(x^\mu,\theta,\overline{\theta}\right) &= \phi + \sqrt{2}\theta\psi + \theta\theta F + i\partial_\mu\phi\theta\sigma^\mu\overline{\theta} \\ &- \frac{i}{\sqrt{2}}\theta\theta\partial_\mu\psi\sigma^\mu\overline{\theta} - \frac{1}{4}\partial_\mu\partial^\mu\phi\theta\theta\overline{\theta}\overline{\theta}\,. \end{aligned} \tag{3.23}$$

In the language of superfields, the free Lagrange density (3.21) can be written as

$$\mathcal{L}_{chiral-free} = \int d^4\theta \sum_i X_i^\dagger X_i\,. \tag{3.24}$$

The F fields are auxiliary scalar fields required to guarantee the same degrees of freedom (DOF) on-shell and off-shell. Since the equations of motion (EOM) are satisfied on-shell, ψ describes a field with two spin polarizations whereas ϕ is a complex scalar with two real propagating degrees of freedom. However, when off-shell, the EOM are not necessarily satisfied and the degrees of freedom are those of the configuration space. Since a complex Weyl spinor has four real fermionic DOF, if we want to preserve (3.20), a new complex scalar field F with dimensions of [mass]^2 is introduced. The auxiliary fields are non-propagating and their equations of motion are

$$\frac{\partial\mathcal{L}}{\partial F_i} = 0 \quad \text{and} \quad \frac{\partial\mathcal{L}}{\partial F^{*i}} = 0 \tag{3.25}$$

which guarantees that the equality between the bosonic and fermionic degrees of freedom on-shell is kept unchanged. The free action is invariant under the infinitesimal SUSY transformations

$$\delta\phi_i = \epsilon\psi_i\,, \qquad \delta(\psi_i)_\alpha = -i\left(\sigma^\mu\epsilon^\dagger\right)_\alpha\partial_\mu\phi_i + \epsilon_\alpha F_i\,, \qquad \delta F_i = -i\epsilon^\dagger\overline{\sigma}^\mu\partial_\mu\psi_i \tag{3.26}$$

$$\delta\phi^{*i} = \epsilon^\dagger\psi^{\dagger i}\,, \quad \delta\left(\psi^{\dagger i}\right)_{\dot\alpha} = i(\epsilon\sigma^\mu)_{\dot\alpha}\partial_\mu\phi^{*i} + \epsilon^\dagger_{\dot\alpha}F^{*i}\,, \qquad \delta F^{*i} = i\partial_\mu\psi^{\dagger i}\overline{\sigma}^\mu\epsilon\,. \tag{3.27}$$

The next step is to introduce (non-gauge) interactions into the Lagrangian (3.21) in such a way that the above SUSY transformations are preserved. This was first done by Wess and Zumino [64], and the resulting most general renormalizable interaction terms are

$$\mathcal{L}_{chiral-int} = \left(-\frac{1}{2}W^{ij}\psi_i\psi_j + W^iF_i\right) + h.c.\,, \tag{3.28}$$

where an analytic function $W(\phi_i)$ of the complex scalar fields, called the *superpotential*, is introduced. In order to guarantee that the interaction terms are renormalizable, its mass dimension should not be greater than 4. The most general form of $W(\phi_i)$ that ensures renormalizability of (3.28) [65] is

$$W = L^i\phi_i + \frac{1}{2}\mu^{ij}\phi_i\phi_j + \frac{1}{6}y^{ijk}\phi_i\phi_j\phi_k\,, \tag{3.29}$$

where L^i is a linear term with dimension [mass]^2, μ^{ij} is a bilinear term with dimensions of [mass], and y^{ijk} is a dimensionless coupling totally symmetric under interchange of i, j, k. The W^{ij} and W^i functions in (3.28) are related to the superpotential by

$$W^{ij} = \frac{\partial^2 W}{\partial\phi_i \partial\phi_j} = \mu^{ij} + y^{ijk}\phi_k \tag{3.30}$$

$$W^i = \frac{\partial W}{\partial\phi_i} = L^i + \mu^{ij}\phi_j + \frac{1}{2}y^{ijk}\phi_j\phi_k. \tag{3.31}$$

We can now understand how the auxiliary terms are eliminated. If we apply the equations of motion (3.25) to the total Lagrangian $\mathcal{L} = \mathcal{L}_{chiral-free} + \mathcal{L}_{chiral-int}$, we see that the F-terms can be expressed algebraically in terms of the scalar fields as[2]

$$F^{*i} = -W^i \quad \text{and} \quad F_i = -W_i^* \,. \tag{3.32}$$

The total SUSY preserving Lagrangian involving renormalizable interactions of chiral supermultiplets takes the form

$$\mathcal{L}_{chiral} = -\partial^\mu\phi^{*i}\partial_\mu\phi_i + i\psi^{\dagger i}\bar{\sigma}^\mu\partial_\mu\psi_i - \frac{1}{2}\left(W^{ij}\psi_i\psi_j + h.c.\right) - W^i W_i^* \,, \tag{3.33}$$

where the non-gauge interactions are all specified from the superpotential. The last term in (3.33) is the scalar potential $V(\phi, \phi^*)$ of the chiral sector, which can be read of from eq. (3.31). Furthermore, it is a sum of the squares of the absolute values of W^i, which guarantees boundedness from below. The term $L^i\phi_i$ is only allowed if ϕ is a gauge singlet. Since we are not going to study such scenarios, we will omit it throughout.

3.2.2. Gauge Interactions

A gauge supermultiplet is composed of two propagating fields, the gauge bosons and the gaugino fermions, and a non-propagating auxiliary field. When on-shell, the massless gauge bosons A_μ^a provide two bosonic DOF, whereas the two helicity polarizations of λ^a contribute with two fermionic DOF. However, an off-shell gauge boson can have longitudinal polarizations, which increases to three bosonic DOF, against the four real fermionic DOF of the gauginos. To close the SUSY algebra off-shell, a real scalar auxiliary field with dimensions [mass]^2 is introduced. Such field, commonly designated $\mathcal{D}^a$, is non-propagating and its EOM are

$$\frac{\partial\mathcal{L}}{\partial\mathcal{D}^a} = 0 \,. \tag{3.34}$$

[2]Note that the part of the total Lagrangian that contains F-terms is given by $W^i F_i + W_i^* F^{*i} + F^{*i} F_i$.

The gauge superfields $\mathcal{G}^a$ are expressed as

$$\mathcal{G}^a = \left(A^a_\mu, \lambda^a, \mathcal{D}^a\right) , \tag{3.35}$$

where a runs over the adjoint representation of the gauge group, and may be expanded in terms of the θ coordinates as

$$\mathcal{G}^a\left(x^\mu, \theta, \overline{\theta}\right) = \theta\sigma^\mu\overline{\theta}A^a_\mu(x) + i\theta\theta\overline{\theta}\overline{\lambda}^a(x) - i\overline{\theta}\overline{\theta}\theta\lambda^a + \frac{1}{2}\theta\theta\overline{\theta}\overline{\theta}\mathcal{D}^a(x) . \tag{3.36}$$

The Lagrangian density for the gauge sector has the form

$$\mathcal{L}_{gauge} = -\frac{1}{4}F^a_{\mu\nu}F^{a\mu\nu} + i\lambda^{a\dagger}\overline{\sigma}^\mu D_\mu\lambda^a + \frac{1}{2}\mathcal{D}^a\mathcal{D}^a , \tag{3.37}$$

where $F^a_{\mu\nu}$ is the usual Yang-Mills field strength tensor (2.24), and the covariant derivative acting on the gauginos is defined as

$$D_\mu\lambda^a = \partial_\mu\lambda^a + gf^{abc}A^b_\mu\lambda^c . \tag{3.38}$$

Supersymmetry requires that the Lagrangian (3.37) is invariant under the infinitesimal transformations

$$\delta A^a_\mu = -\frac{1}{\sqrt{2}}\left(\epsilon^\dagger\overline{\sigma}_\mu\lambda^a + \lambda^{a\dagger}\overline{\sigma}_\mu\epsilon\right) , \tag{3.39}$$

$$\delta\lambda^a_\alpha = \frac{i}{2\sqrt{2}}\left(\sigma^\mu\overline{\sigma}^\mu\epsilon\right)_\alpha F^a_{\mu\nu} + \frac{1}{\sqrt{2}}\epsilon_a\mathcal{D}^a , \tag{3.40}$$

$$\delta\mathcal{D}^a = \frac{i}{\sqrt{2}}\left(-\epsilon^\dagger\overline{\sigma}_\mu D_\mu\lambda^a + D_\mu\lambda^{a\dagger}\overline{\sigma}_\mu\epsilon\right) . \tag{3.41}$$

In order to construct the full SUSY Lagrangian, gauge-matter interactions need to be introduced while preserving gauge invariance. Since the scalar, fermion and auxiliary chiral fields are in the same representation of the gauge group, the ordinary derivatives in eq. (3.33) are replaced with covariant derivatives, which are expressed in the usual way as in eq. (2.20).

To have a complete supersymmetric theory, gauge invariant terms with couplings between matter and gaugino fields as well as matter and auxiliary $\mathcal{D}^a$ fields are included. There are three such possibilities describing renormalizable interactions. Therefore, the Lagrangian for the extra terms ought to be

$$\mathcal{L}_{extra} = -\sqrt{2}g\left(\phi^*\Omega^a\psi\right)\lambda^a - \sqrt{2}g\lambda^{a\dagger}\left(\psi^\dagger\Omega^a\phi\right) + g\left(\phi^*\Omega^a\phi\right)\mathcal{D}^a . \tag{3.42}$$

From eq. (3.34) and the terms in the Langrangian involving the auxiliary fields, $\mathcal{L}_{\mathcal{D}} = \frac{1}{2}\mathcal{D}^a\mathcal{D}^a + g\left(\phi^*\Omega^a\phi\right)\mathcal{D}^a$, the equations of motion for the auxiliary fields take the form

$$\mathcal{D}^a = -g\sum_i \left(\phi^{i*}\Omega^a\phi_i\right) , \tag{3.43}$$

where the sum is over flavour indices, and as for the chiral F-fields, it is possible to express $\mathcal{D}^a$ algebraically in terms of the scalar fields.

Combining the gauge and chiral sectors, the Lagrangian density that describes a generic supersymmetic interacting theory is obtained:

$$\begin{aligned}\mathcal{L}_{SUSY} = \; & - D^\mu\phi^{*i}D_\mu\phi_i + i\psi^{\dagger i}\overline{\sigma}^\mu D_\mu\psi_i - \frac{1}{2}\left(W^{ij}\psi_i\psi_j + h.c.\right) - \frac{1}{4}F^a_{\mu\nu}F^{a\mu\nu} + i\lambda^{a\dagger}\overline{\sigma}^\mu D_\mu\lambda^a \\ & - \sqrt{2}g\left(\phi^*\Omega^a\psi\right)\lambda^a - \sqrt{2}g\lambda^{a\dagger}\left(\psi^\dagger\Omega^a\phi\right) + g\left(\phi^*\Omega^a\phi\right)\mathcal{D}^a - V(\phi,\phi^*) ,\end{aligned} \tag{3.44}$$

where the scalar potential is entirely derived from the *F-terms* and *D-terms* contributions taking the form,

$$V(\phi,\phi^*) = F^{i*}F_i + \frac{1}{2}\mathcal{D}^a\mathcal{D}^a = W^iW_i^* + \frac{1}{2}\sum_G\sum_a g_G^2\left(\phi^*\Omega^a\phi\right)^2 , \tag{3.45}$$

where G labels a gauge group with gauge coupling g_G. The potential (3.45) is remarkably completely determined by the interactions of the theory, which is an unique feature of supersymmetries. Furthermore, since it is a sum of squares, it is always non-negative. In addition to the interacting vertices that are predicted in the SM, the Lagrangian (3.44) also contains gaugino-gaugino-gauge boson triple vertexes for non abelian groups, as well as fermion-gaugino-scalar and triple scalar cubic interactions.

3.2.3. Solution to the Hierarchy Problem

As we discussed in section 2.5.1, the scalar sector of the Standard Model suffers from a severe fine-tuning problem when self energy integrals are calculated. Leading contributions to such diagrams depend quadratically on the energy scale (2.83), and the large hierarchy between the electroweak and the Planck scales requires remarkable cancellations between the bare mass terms and the loop corrections.

Let us now consider a fermion loop correction to the $-\mu^2\phi^\dagger\phi$ term in the Higgs scalar potential (2.34) as in Fig. 3.1.

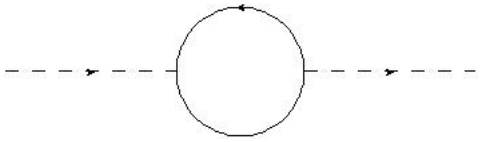

Figure 3.1. *Higgs self-energy with a fermion loop*

At zero external momenta we will have a contribution

$$\Pi(k) \propto -\lambda_f^2 \int d^4k \frac{k^2 + m_f^2}{\left(k^2 - m_f^2\right)^2} \tag{3.46}$$

where from dimensional analysis, the term with k^2 in the numerator is quadratically divergent and the term proportional to m_f^2 is just logarithmically divergent. The minus sign is due to the fermionic loop. Ignoring numerical factors, this contribution together with that of the scalar loop of Fig. 2.4, eq. (2.82), gives a correction to the Higgs mass of the form

$$\left(\lambda_s - \lambda_f^2\right)\Lambda^2 \phi^* \phi \,, \tag{3.47}$$

plus sub-dominant terms proportional to $m_f^2 log\left(\Lambda/m_f\right)$ (diagram of Fig. 3.47) and $m_{\tilde{f}}^2 log\left(\Lambda/m_{\tilde{f}}\right)$ (diagram of Fig. 2.4). If we now consider that the theory is supersymmetric, i.e. described by the Lagrangian (3.44), and if we plug equations (3.30) and (3.31) into $-\frac{1}{2}\left(W^{ij}\psi_i\psi_j + h.c.\right) - W^i W_i^*$, we obtain

$$-\frac{1}{2}\left[(\mu + y\phi)\psi\cdot\psi\right] - \left|\mu\phi + \frac{1}{2}y\phi^2\right|^2 \,, \tag{3.48}$$

from where we extract the quartic scalar and Yukawa type couplings

$$-\frac{1}{4}\left|y\right|^2\phi^2\phi^{*2} \quad \text{and} \quad -\frac{1}{2}y\phi\psi\cdot\psi \tag{3.49}$$

respectively. It is noteworthy that in SUSY, the same coupling y enters both in the quartic and Yukawa interactions (3.49) as well as the scalar cubic interactions of the form

$$-\frac{1}{2}\left(\mu y^*\phi\phi^{*2} + \mu^* y\phi^2\phi^*\right) \,, \tag{3.50}$$

also emerging from (3.48). In particular, the square of the cubic fermion-fermion-scalar coupling is equal to the scalar quartic coupling, so that, $\lambda_s = y^2$ and $\lambda_f^2 = y^2$, implying that

$$\lambda_f^2 = \lambda_s \,. \tag{3.51}$$

Therefore, the quadratic sensitivity to the energy scale Λ in the scalar sector is elegantly

canceled out. The fermion loop can be thought as a top quark whereas the correspondent scalar loop should be a stop, i.e., the top scalar super-partner. The Higgs mass corrections are then logarithmically dependent on the cut-off scale, and the hierarchy is stabilized.

However, it is relevant to consider here a third contribution to the one-loop Higgs mass corrections. A scalar loop, say $\tilde{f}$, of the form of Fig. 3.2, is proportional to $m_f^2 log\left(\Lambda/m_{\tilde{f}}\right)$.

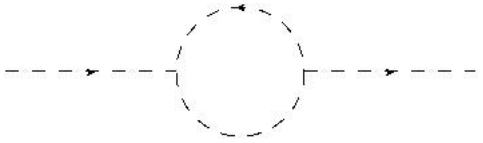

Figure 3.2. *Higgs self-energy with a scalar loop*

Summing up the contributions of the diagrams of Figs. 2.4, 3.1 and 3.2, the leading dependency on the scale is now logarithmic

$$\delta m_h^2 = \frac{\lambda_f^2}{4\pi^2}\left[\left(m_f^2 - m_{\tilde{f}}^2\right) log\left(\frac{\Lambda}{m_{\tilde{f}}}\right) + 3m_f^2 log\left(\frac{m_{\tilde{f}}}{m_f}\right)\right]. \tag{3.52}$$

The quadratic sensitivity to the cut-off scale is converted into a quadratic sensitivity to the *soft supersymmetry breaking* scale $m_{soft} \sim m_{\tilde{f}}$, replacing the hierarchy problem by a *little hierarchy* problem. In particular, the Higgs boson mass is rather sensitive to fluctuations in stop masses. To have an idea, we may define here a tuning measure as

$$\Delta_{m_h^2} \equiv \left|\frac{m_{\tilde{t}}}{m_h^2}\frac{\delta m_h^2}{\delta m_{\tilde{t}}}\right|, \tag{3.53}$$

where $\lambda_f = \lambda_t \sim 1$ is the top Yukawa coupling, $m_h = 125$ GeV the Higgs mass, $m_f = m_t = 174$ GeV the top quark mass and $m_{\tilde{f}} = m_{\tilde{t}} = \sqrt{m_{\tilde{t}_1} m_{\tilde{t}_2}}$ the average stop mass. We estimate the sensitivity as defined in eq. (3.53) for stop masses of 200 GeV, 1 TeV and 5 TeV considering 1% shifts in $m_{\tilde{t}}$, i.e. $\delta m_{\tilde{t}} = 0.01 m_{\tilde{t}}$. We therefore obtain for $\Delta_{m_h^2}$ the values 48, 4.8×10^3 and 1.1×10^5 respectively. We see that small stop masses provide tolerable values for the sensitivity parameter (3.53), however, it is a lot more severe when stops become as heavy as 5 TeV.

3.3. Soft Supersymmetry Breaking

If supersymmetry is unbroken at low energies, the masses of the matter fields are equal for both scalars and fermions when the Higgs develops an expectation value. It is possible to see from the cubic and quadratic terms in the SUSY Lagrangian, and in particular from eqs. (3.48 to 3.50), that a common coupling y imposes such mass symmetry. However, this has

not been observed so a realistic model can contain only a broken supersymmetry. If we want to naturally stabilize the hierarchy of masses, without reintroducing quadratic divergences in the theory [67], we need to introduce terms of positive mass dimensions that *softly* break supersymmetry. This is referred to us as *soft supersymmetry-breaking* (SSB) [66].

The construction of phenomenologically correct models require the introduction of new physical mechanisms. It is common to invoke the existence of a *hidden sector* [68–73] where supersymmetry is spontaneously broken. The communication with the visible sector is accomplished by suppressed interactions which carry information about the breaking mechanism and strongly dictate the high scale structure of the observable scalar masses and couplings.

Similarly to what occurs with the breakdown of the electroweak symmetry, it is possible to make the vacuum of the scalar potential not invariant under the action of the SUSY generators, i.e. $Q_\alpha|0\rangle \neq 0$ and $Q^\dagger_{\dot{\alpha}}|0\rangle \neq 0$. If either an F-term or a D-term develop an expectation value, the vacuum energy as in eq. (3.16) becomes positive and supersymmetry is spontaneously broken. While the former type of SUSY breaking is called O'Raifeartaigh [74], the later one is entitled as Fayet-Iliopoulos [75, 76] SUSY breaking.

The most popular models of mediation between the visible and hidden sectors are gauge mediation [77–82], anomaly mediation [83–85] and Plank-suppressed or gravity mediation [86–92]. However, there is no consensus on which mechanism breaks supersymmetry and how is this information transmitted to the visible sector. Soft supersymmetry-breaking terms ought to be independent of any of such models, providing a parametrization of the unknown. While the research reported in this thesis is based in models inspired by gravity mediation, it is important to point out that the different mediation mechanisms can also impose distinct constraints on the parameter space.

Supersymmetry is introduced as a global symmetry of the Lagrangian, where the transformation parameters ϵ_α and a^μ in (3.14) are not position dependent. However, as for gauge symmetry, it is possible to realize supersymmetry locally. In particular, as we discussed in section 3.1, it is a space-time symmetry that contains the generator of translations P_μ of the Poincaré Algebra. If such translations are allowed to vary from point to point, a theory of general space-time coordinate transformations emerges becoming a theory of gravity. Local supersymmetry is also referred as *supergravity* (SUGRA). Analogously to the spin 1 gauge bosons and spin 1/2 gauginos that are present due to the locality of gauge symmetries, a spin 2 field, the graviton, and its spin 3/2 superpartner, the gravitino, are introduced and together form a gravity supermultiplet. We will usually neglect the gravitino mass as well as SUGRA, except in chapter 9.

3.3.1. Soft Scalar Masses and Bilinear Couplings

Supergravity is a non-renormalizable quantum field theory containing interactions whose couplings are of negative mass dimensions. If we assume mediation through gravitational interactions, we have an effective theory below the Planck scale containing higher dimensional operators suppressed by the Planck mass M_P. These operators couple the gauginos and scalars of the visible sector to the hidden sector F-terms. It is when the F-fields acquire a vev that the soft terms are generated.

Scalar masses may arise from the dimension-6 operators

$$-\mathcal{L}_{dim-6} = \frac{\kappa^i{}_j}{M_P^2}|F_X|^2\tilde{\phi}_i\tilde{\phi}^{*j}, \tag{3.54}$$

where F_X is an F-term of a hidden sector superfield $\hat{X}$, $\tilde{\phi}$ is the scalar component of a visible sector superfield $\hat{\Phi}$ with mass $m_{\tilde{\phi}}$, $\kappa^i{}_j$ a dimensionless coupling and M_P is the Planck mass. If the F-term F_X has a non-vanishing expectation value, the scalar masses take the form

$$\left(m^2_{\tilde{\phi}}\right)^i_{\ j} \equiv \frac{\kappa^i{}_j}{M_P^2}|\langle F_X\rangle|^2. \tag{3.55}$$

The quadratic term in the superpotential (3.29) has a corresponding SSB bilinear term of the form $-\frac{1}{2}b^{ij}\phi_i\phi_j$, which may arise from dimension-6 operators

$$-\mathcal{L}_{dim-6} = \frac{1}{2}\frac{\beta_{ij}}{M_P^2}|F_X|^2\tilde{\phi}_i\tilde{\phi}_j + h.c. \tag{3.56}$$

When the F-term develops an expectation value, the soft bilinear coupling is

$$b_{ij} \equiv \frac{\beta_{ij}}{M_P^2}|\langle F_X\rangle|^2, \tag{3.57}$$

3.3.2. Soft Trilinear Couplings

As for the bilinear terms b_{ij}, the cubic terms in the superpotential have their corresponding soft counterparts. Soft trilinear terms may arise from dimension five operators of the form

$$-\mathcal{L}_{dim-5} = \frac{1}{6}\frac{\eta^{ijk}}{M_P}F_X\tilde{\phi}_i\tilde{\phi}_j\tilde{\phi}_k + h.c. \tag{3.58}$$

When the F-terms of $\hat{X}$ develop an expectation value, such terms generate the scalar trilinear couplings

$$a^{ijk} \equiv \frac{\eta^{ijk}}{M_P}\langle F_X \rangle. \tag{3.59}$$

3.3.3. Gaugino Masses

For the discussion below, and since the main topic of this thesis is Grand Unification, it is instructive to assume that the SM symmetry is described by some unification gauge group G_U with gauge coupling unification (see chapter 5). Gaugino masses may arise from a gauge-kinetic term of the form [93–100]

$$\begin{aligned}\mathcal{L}_{g-k} &= \int d^2\theta f_{ab}\left(\hat{X}_i\right)\hat{W}^{\alpha a}\hat{W}^b_\alpha + h.c. \\ &= -\frac{1}{4}Re f_{ab}F^a_{\mu\nu}F^{b\mu\nu} + \frac{1}{4}e^{-G/2}\frac{\partial f^*_{ab}}{\partial\varphi^{j*}}\left(G^{-1}\right)^j_k G^k\tilde{\lambda}^a\cdot\tilde{\lambda}^b + \cdots\end{aligned} \tag{3.60}$$

$\hat{W}^{\alpha a}$ is the gauge field strength superfield, $F^a_{\mu\nu}$ is the field strength tensor and $\tilde{\lambda}^a$ is a gaugino fermion; a and b are gauge indices, α is a spinor index, and as usual μ and ν are Lorentz indices. $\hat{X}_i$ are again the hidden sector superfields but now we include an index i in order to recognize that there may be more than one. The gauge-kinetic function $f_{ab}\left(\hat{X}_i\right)$ is an analytic function of the $\hat{X}_i$ superfields transforming as a symmetric product of two adjoint representations of the G_U so that the the Lagrangian is gauge invariant. $G\left(\hat{X}_i, \hat{X}^*_i\right)$ is a real function $G = K + \log|W|^2$ where K is the Kähler potential, which is a general real valued function of the superfields X_i and $X^\dagger_i$. W is the superpotential defined earlier. $G^k \equiv \partial G/\partial\varphi_k$ and $G^j_k \equiv \partial^2 G/\partial\varphi_j\partial\varphi^{k*}$ with $\left(G^{-1}\right)^i_k G^k_j = \delta^i_j$, where φ_i is the scalar component of $\hat{X}_i$. When an F-term F_X develops an expectation value, it spontaneously breaks supersymmetry and enters Eq. (3.60) by identifying

$$F^j_X = \frac{1}{2}e^{-G/2}\left[\left(G^{-1}\right)^j_k G^k\right], \tag{3.61}$$

generating a gaugino mass term of the form

$$\frac{1}{2}\langle F^j_X\rangle\left\langle\frac{\partial f^*_{ab}}{\partial\varphi^{j*}}\right\rangle\tilde{\lambda}^a\cdot\tilde{\lambda}^b. \tag{3.62}$$

The representations of the $\hat{X}_i$ are unknown, but we may expand the gauge-kinetic function in terms of trivial $\hat{X}^S$ and non-trivial $\hat{X}^N$ superfield representations

$$f_{ab}\left(\hat{X}^i\right) = f_0\left(\hat{X}^S\right)\delta_{ab} + \sum_N f_N\left(\hat{X}^S\right)\frac{\hat{X}^N_{ab}}{M_P} + O\left(1/M_P^2\right), \tag{3.63}$$

where f_0 and f_N are functions of the trivial field representations only. When this is inserted into the first term in the right-hand-side of Eq. (3.60) we have additional five-dimensional operators which generate an extra contribution to the canonical gauge-kinetic terms $-\frac{1}{4}F^a_{\mu\nu}F^{a\mu\nu}$. It has been shown [97, 100–104] that such operators do not spoil the unification of the gauge couplings both at one-loop and two-loop level and we indeed return to the canonical form by a rescaling of the superfields.

After such rescaling, the gaugino mass terms take the form

$$\frac{1}{2}\frac{\langle F_X^j\rangle}{\langle Ref_{ab}\rangle}\left\langle\frac{\partial f^*_{ab}}{\partial\varphi^{j*}}\right\rangle\tilde{\lambda}^a\cdot\tilde{\lambda}^b, \tag{3.64}$$

where the coefficient is a group theoretic factor that depends on a representation (or combination of representations) belonging to the symmetric product of two adjoint representations of G_U. If it is a singlet only the first term of Eq. (3.63) is relevant and we have a universal gaugino mass for the SM gauge groups,

$$M_{1/2} = \frac{\langle F_X^j\rangle}{\langle Ref_0\rangle}\left\langle\frac{\partial f_0^*}{\partial\varphi^{j*}}\right\rangle. \tag{3.65}$$

However, if the group theoretical factor is derived from a non-trivial representation (or a combination of them), this results in $SU(3)$, $SU(2)$ and $U(1)$ gauginos that have non-universal masses at the high scale. The effective soft gaugino-mass terms are then

$$\frac{1}{2}\left[M_1\tilde{\lambda}_1\cdot\tilde{\lambda}_1 + M_2\tilde{\lambda}_2\cdot\tilde{\lambda}_2 + M_3\tilde{\lambda}_3\cdot\tilde{\lambda}_3 + h.c.\right]. \tag{3.66}$$

It is noteworthy that eq. (7.11) is diagonal. In fact, the twelve $SU(3)_C$, $SU(2)_L$ and $U(1)_Y$ generators are block diagonal elements when embedded in a larger simple gauge group.

The soft terms, which involve only the scalar and gaugino fields, are clearly responsible for the explicit breakdown of supersymmetry. Particularly, as required by a correct phenomenology, both scalars and gauginos acquire masses of the order of the SSB scale, while its fermionic and bosonic counterparts have masses proportional to the electroweak scale. Despite some pressure posed by the ATLAS and CMS SUSY searches [105, 106] on low scale supersymmetry, the current non-observation of any superpartner is accommodated by these new parameters. It is generally expected to observe supersymmetry at the LHC or future colliders if the hierarchy problem is in fact to be solved by SUSY. Otherwise, if the superpartner masses are much beyond the TeV scale, a little-hierarchy problem emerges and, as eq. (3.52) tells, it becomes increasingly severe for larger SSB scales.

4. The Minimal Supersymmetric Standard Model

4.1. Superfields in the MSSM

The Minimal Supersymmetric Standard Model (MSSM), is a supersymmetric framework with the minimal particle extension to the SM. In the MSSM, for each observed fermion there is a scalar counterpart, a sfermion, belonging to the same chiral supermultiplet, whereas for each observed gauge bosons there is a gaugino superpartner, placed into the same gauge supermultiplet. However, it is not sufficient to extend the Higgs sector with a single *Higgsino* fermion. One of the reasons for this is the analyticity of the superpotential W, that we will discuss in 4.2. An other reason is related with anomalies, which are quantum mechanical effects that break the classical theory at loop level. In quantum filed theories, anomalies that violate the gauge symmetry of the classical Lagrangian are called gauge anomalies, and can be generated from triangle diagrams of the form

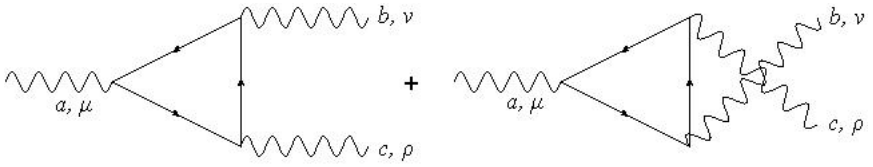

Figure 4.1. *Triangle diagrams that generate gauge anomalies*

where a, b and c are the adjoint representation indices of the A^a_μ, A^b_ν and A^c_ρ gauge bosons, and the result of the loop-integration yields

$$\mathcal{A}^{abc} \propto tr\Big(\Omega^a \left\{\Omega^b, \Omega^c\right\}\Big). \tag{4.1}$$

In the Standard Model, eq. (5.39) vanishes for all possible combinations of gauge currents, which is only possible with complete generations of chiral fermions. However, the introduction of one single chiral $SU(2)_L$ Higgsino doublet, provides extra non-zero contributions to (5.39) and the gauge theory becomes anomalous. Particularly relevant for this discussion is the *Witten anomaly* [107], which arises in gauge theories with an odd number of left-handed fermion doublets. To cancel such anomalies, an extra Higgs supermultiplet with opposite charges to the original one is introduced.

The gauge group of the MSSM is the same as in the SM, $G_{SM} = SU(3)_C \times SU(2)_L \times U(1)_Y$. The complete set of chiral and gauge supermultiplets with the respective G_{SM} charges is summarized in Tables 4.1 and 4.2.

Chiral Supermultiplet Fields in the MSSM				
Names		Spin 0	Spin 1/2	$SU(3)_c \times SU(2)_L \times U(1)_y$
Squarks, Quarks (× 3)	$\hat{Q}_L$	$(\tilde{u}_L, \tilde{d}_L)$	(u_L, d_L)	**3**, **2**, 1/3
	$\hat{\bar{u}}_R$	$\tilde{\bar{u}}_L = \tilde{u}_R^*$	$\bar{u}_L = (u_R)^c$	$\bar{\mathbf{3}}$, **1**, -4/3
	$\hat{\bar{d}}_R$	$\tilde{\bar{d}}_L = \tilde{d}_R^*$	$\bar{d}_L = (d_R)^c$	$\bar{\mathbf{3}}$, **1**, 2/3
Sleptons, Leptons (× 3)	$\hat{L}_L$	$(\tilde{\nu}_{eL}, \tilde{e}_L)$	(ν_{eL}, e_L)	**1**, **2**, -1
	$\hat{\bar{e}}_R$	$\tilde{\bar{e}}_L = \tilde{e}_R^*$	$\bar{e}_L = (e_R)^c$	**1**, **1**, 2
Higgs, Higgsinos	$\hat{H}_u$	(H_u^+, H_u^0)	$(\tilde{H}_u^+, \tilde{H}_u^0)$	**1**, **2**, 1
	$\hat{H}_d$	(H_d^0, H_d^-)	$(\tilde{H}_d^0, \tilde{H}_d^-)$	**1**, **2**, -1

Table 4.1. *Chiral supermultiplet fields in the MSSM. The leftmost column provides the usual designation for the fundamental particles, the two middle ones the spin and the rightmost the charges under the SM gauge group.*

Gauge Supermultiplet Fields in the MSSM				
Names		Spin 1/2	Spin 1	$SU(3)_c \times SU(2)_L \times U(1)_y$
Gluinos, Gluons	$\hat{G}^a$	$\tilde{g}$	g	**8**, **1**, 0
Winos, W bosons	$\hat{W}^a$	$\tilde{W}^{\pm}$, $\tilde{W}^0$	$W^{\pm}$, W^0	**1**, **3**, 0
Bino, B Boson	$\hat{B}$	$\tilde{B}$	B	**1**, **1**, 0

Table 4.2. *Gauge supermultiplet fields in the MSSM. The left column provides the usual designation for the gauge fields, the middle one the spin and the right one the SM charges.*

4.2. Superpotential and Soft Lagrangian

It is of common use to write superpotentials in terms of the superfields rather than the scalar fields as it was introduced in 3.2.1. In the MSSM, the superpotential is written as

$$W_{MSSM} = \varepsilon_{\alpha\beta}\left[(y_u)_{ij}\hat{\bar{u}}_{Rix}\hat{Q}_{Lj}^{\alpha x}\hat{H}_u^{\beta} - (y_d)_{ij}\hat{\bar{d}}_{Rix}\hat{Q}_{Lj}^{\alpha x}\hat{H}_d^{\beta} - (y_e)_{ij}\hat{\bar{e}}_{Ri}\hat{L}_{Lj}^{\alpha}\hat{H}_d^{\beta} + \mu\hat{H}_u^{\alpha}\hat{H}_d^{\beta}\right], \tag{4.2}$$

where i and j are generation indices, $\varepsilon_{\alpha\beta}$ is the usual $SU(2)_L$ metric defined here as

$$\varepsilon_{\alpha\beta} = \left(i\tau^2\right)_{\alpha\beta} = \begin{pmatrix} 0 & 1 \\ -1 & 0 \end{pmatrix} \tag{4.3}$$

and $x = 1,2,3$ is a colour index representing triplet **3** when raised and anti-triplet $\bar{\mathbf{3}}$ when lowered. $\hat{Q}_L$ and $\hat{L}_L$ are quark and lepton left-handed superfields containing spin-1/2 quarks and leptons and spin-0 squarks and sleptons respectively. The right-handed counterparts are

the $\hat{u}_R$, $\hat{d}_R$ and $\hat{e}_R$ superfields. $\hat{H}_{u(d)}$ are the up(down)-type Higgs superfields whose spin-0 components are Higgs bosons and spin-1/2 components up(down)-type Higgsino fermions. $\left(y_{u,d,e}\right)_{ij}$ are 3×3 matrices of the Yukawa couplings in the generation space and the bilinear term is the traditionally called the MSSM μ-*term*. The superpotential (4.2) describes a minimal phenomenologically viable model which is invariant under a new $\mathbb{Z}_2$ symmetry, commonly denoted as *R-parity* and defined as $P_R = (-1)^{3(B-L)+2s}$. Here B, L and s are the barion, lepton and spin quantum numbers. All observed SM particles have $P_R = +1$ while the superpartners $P_R = -1$. However, it is possible to write gauge-invariant and analytic terms in the chiral superfields that violate P_R. In addition to W, the most general superpotential would therefore include

$$W_{RPV} = \varepsilon_{\alpha\beta}\left[\lambda_{ijk}\hat{L}^{\alpha}_{Li}\hat{L}^{\beta}_{Lj}\hat{\bar{e}}_{Rk} + \lambda'_{ijk}\hat{L}^{\alpha}_{Li}\hat{Q}^{\beta x}_{Lj}\hat{\bar{d}}_{Rkx} + \mu'^{i}L^{\alpha}_{Li}H^{\beta}_{u}\right] + \frac{1}{2}\varepsilon^{xyz}\lambda''^{ijk}\hat{\bar{u}}_{Rix}\hat{\bar{d}}_{Rjy}\hat{\bar{d}}_{Rkz} \quad , \tag{4.4}$$

where the λ coefficients are Yukawa couplings, μ' a new bilinear coupling and x, y, z $SU(3)_C$ indices. The presence of B and L violating terms may disturb proton stability if λ' and λ'' are not small enough to suppress its decay rate (see discussion in [58]). Furthermore, decays of superpartners to an even number of daughter sparticles is permitted and the *lightest supersymmetric particle* (LSP) may become unstable, with allowed decay channels to SM particles. In the research presented in this thesis, we forbid terms as in eq. (4.4) by imposing R-parity. Therefore, the models that we will discuss provide a stable LSP which can match criteria for a dark matter candidate.

The introduction of two Higgs chiral superfields is necessary for anomaly cancellation. However, there is a purely mathematical argument to justify this requirement that becomes clear from (4.2). As it was pointed out in section 3.2.1, the superpotential is by construction an analytic function, therefore, if z is a complex variable, then W only depends on z, $W(z)$, and not on z^*, $W(z,z^*)$. In the latter case the Cauchy-Riemann conditions fail and $W(z,z^*)$ is not analytic. Therefore, the introduction of a term like $\hat{\bar{u}}_R\hat{Q}_L\hat{H}^{\dagger}_d$ as it is done in the SM for giving masses to the up type quarks, see eqs. (2.58 - 2.61), is not allowed and instead, an extra Higgs chiral superfield is required.

If we want to construct a realistic model, we need to break supersymmetry explicitly. The soft supersymmetry breaking terms in the MSSM are of the form of those already

discussed in section 3.3 and, in particular, take the form

$$\begin{aligned}
-\mathcal{L}_{soft} &= m_{H_d}^2 |H_d|^2 + m_{H_u}^2 |H_u|^2 + \tilde{Q}_{Li}^{\alpha x} \left(m_{\tilde{Q}_L}^2\right)^i{}_j \tilde{Q}_{L\alpha x}^{* j} + \tilde{L}_{Li}^{\alpha} \left(m_{\tilde{L}_L}^2\right)^i{}_j \tilde{L}_{L\alpha}^{* j} \\
&+ \tilde{u}_{Ri}^{* x} \left(m_{\tilde{u}_R}^2\right)^i{}_j \tilde{u}_{Rx}^{j} + \tilde{d}_{Ri}^{* x} \left(m_{\tilde{d}_R}^2\right)^i{}_j \tilde{d}_{Rx}^{j} + \tilde{e}_{Ri}^{*} \left(m_{\tilde{e}_R}^2\right)^i{}_j \tilde{e}_R^{j} \\
&+ \varepsilon_{\alpha\beta} \left[a_{uij} H_u^{\alpha} \tilde{u}_{Rix} \tilde{Q}_{Lj}^{\beta x} - a_{dij} H_d^{\alpha} \tilde{d}_{Rix} \tilde{Q}_{Lj}^{\beta x} - a_{eij} H_d^{\alpha} \tilde{e}_{Ri} \tilde{L}_{Lj}^{\beta} + b H_d^{\alpha} H_u^{\beta} + h.c.\right] \\
&+ \frac{1}{2}\left[M_1 \tilde{B} \cdot \tilde{B} + M_2 \tilde{W}^a \cdot \tilde{W}^a + M_3 \tilde{g}^a \cdot \tilde{g}^a + h.c.\right], \qquad (4.5)
\end{aligned}$$

where the adjoint index a runs from 1 to 3 in the wino term representing a weak isospin triplet and from 1 to 8 in the gluino term representing a colour octet. The trilinear couplings are often written in terms of the Yukawa couplings as $\left(a_{u,d,e}\right)_{ij} = \left(y_{u,d,e}\right)_{ij} \left(A_{u,d,e}\right)_{ij}$. Since the first and second generation Yukawa couplings are very small, we will only consider contributions from the third generation trilinears and Yukawa couplings throughout this thesis. The $\left(a_{u,d,e}\right)_{ij}$ are then effectively diagonal with only one non-zero entry each $(a_u)_{33} \equiv a_t$, $(a_d)_{33} \equiv a_b$ and $(a_e)_{33} \equiv a_\tau$.

4.3. Physical Masses in the MSSM

4.3.1. Electroweak Symmetry Breaking

As we discussed in section 3.2.2, the scalar potential of a supersymmetric theory is entirely derived from the F and D-term contributions. In particular, for the Higgs sector, the interactions in the MSSM determine that

$$\begin{aligned}
V_H &= \left(|\mu|^2 + m_{H_u}^2\right)\left(\left|H_u^0\right|^2 + \left|H_u^+\right|^2\right) + \left(|\mu|^2 + m_{H_d}^2\right)\left(\left|H_d^0\right|^2 + \left|H_d^-\right|^2\right) \\
&+ b\left[(H_u^+ H_d^- - H_u^0 H_d^0) + h.c.\right] + \frac{1}{2} g^2 \left|H_u^+ H_d^{0*} + H_u^0 H_d^{-*}\right|^2 \\
&+ \frac{1}{8}\left(g^2 + g'^2\right)\left(\left|H_u^0\right|^2 + \left|H_u^+\right|^2 - \left|H_d^0\right|^2 - \left|H_d^-\right|^2\right)^2, \qquad (4.6)
\end{aligned}$$

where the terms proportional to $|\mu|^2$ come from F-terms contributions in the MSSM as in eq. (3.45), the terms proportional to the gauge couplings g and g' are D-terms but also in (3.45) and finally, since the model contains softly broken supersymmetry, the terms in (4.6) proportional to the soft couplings $m_{H_u}^2$, $m_{H_d}^2$ and b, are introduced.

In a pure supersymmetric theory, the scalar potential is automatically bounded from below. However, since we have explicitly broken supersymmetry with the introduction of soft terms, we must be careful. The total scalar potential also includes squark and slepton fields carrying both colour and electric charges. This may not only generate charge and

colour breaking minima (CCB) deeper than the realistic minimum (the one provided by the Higgs potential), as well as directions in field space where the scalar potential becomes unbounded from below (UFB). When the neutral components of scalar doublets H_u and H_d develop expectation values

$$\langle H_u \rangle = \frac{1}{\sqrt{2}} \begin{pmatrix} 0 \\ v_u \end{pmatrix} \text{ and } \langle H_d \rangle = \frac{1}{\sqrt{2}} \begin{pmatrix} v_d \\ 0 \end{pmatrix} \tag{4.7}$$

we need to ensure that the origin is not a stable point, as well as certifying that the potential is not unbounded from below and that the Higgs minimum is indeed the deepest one. If so, we guarantee that the electroweak symmetry is spontaneously broken while QCD and QED are preserved. A broad analysis of the possible UFB and CCB directions in the MSSM was carried out in [108] and we will use their constraints in the numerical analysis presented throughout this thesis in order to ensure a stable vacuum.

It is possible to use the freedom of $SU(2)_L$ rotations to gauge away one of the charged components of the Higgs doublets, say $H_u^+ = 0$. After this operation, the condition of minimization $\partial V_H / \partial H_d^- = 0$ implies that $H_d^- = 0$. Therefore, the Higgs potential can be rewritten only in terms of the neutral components as

$$\begin{aligned} V_H &= \left(|\mu|^2 + m_{H_u}^2\right)|H_u^0|^2 + \left(|\mu|^2 + m_{H_d}^2\right)|H_d^0|^2 - b\left(H_u^0 H_d^0 + h.c.\right) \\ &+ \frac{1}{8}\left(g^2 + g'^2\right)\left(|H_u^0|^2 - |H_d^0|^2\right)^2 . \end{aligned} \tag{4.8}$$

The b term is the only one in the potential dependent on the phases of the neutral Higgs fields. However, it is possible to redefine the phases of H_u and H_d in order to absorb any possible complex phase in b. Furthermore, since at the minimum the product $H_u^0 H_d^0$ must be real, their phases have to be opposite. In this context b, $\left\langle H_u^0 \right\rangle$ and $\left\langle H_d^0 \right\rangle$ can be taken as real and positive modulus of complex numbers. It is instructive to write down the potential at the minimum as

$$V_0(x,y) = \alpha x^2 + \beta y^2 - 2bxy + \gamma\left(x^2 - y^2\right)^2 , \tag{4.9}$$

where the variables x, y and the coefficients α, β and γ can be read off from (4.8).

The quartic terms in V_0 guarantee that the potential is indeed bounded from below for almost all arbitrary large values of the fields. However, near D-flat directions, i.e. $x \approx y$, the D-terms vanish and V_0 is only bounded from below if $\alpha + \beta > 2b$. In order to allow EWSB,

the origin cannot be a minimum. We can then evaluate the Hessian matrix of V_0 at $x = y = 0$,

$$H(0,0) = \begin{pmatrix} \frac{\partial^2 V_0}{\partial x^2} & \frac{\partial^2 V_0}{\partial x \partial y} \\ \frac{\partial^2 V_0}{\partial y \partial x} & \frac{\partial^2 V_0}{\partial y^2} \end{pmatrix}_{x=y=0} = \begin{pmatrix} 2\alpha & -2b \\ -2b & 2\beta \end{pmatrix} \tag{4.10}$$

If the discriminant of $H(0,0)$ is positive, the origin is a minimum and EWSB does not occur, otherwise, if it is negative, i.e. $\alpha\beta - b^2 < 0$, the origin is a saddle point and EWSB is allowed for non-zero values of the the expectation values. To summarize, the necessary conditions for electroweak symmetry breaking are

$$\left(|\mu|^2 + m_{H_u}^2\right)\left(|\mu|^2 + m_{H_d}^2\right) < b^2 \tag{4.11}$$

$$2|\mu|^2 + m_{H_u}^2 + m_{H_d}^2 > 2b. \tag{4.12}$$

From (4.11), we see that if either $(|\mu|^2 + m_{H_u}^2)$ or $(|\mu|^2 + m_{H_d}^2)$ become negative, the condition for EWSB is automatically satisfied. Although it is also possible to satisfy (4.11) even if both terms on the LHS are positive, in particular if b is rather large, the renormalization group evolution of the $m_{H_u}^2$ (see Chapter 7) soft mass has a contribution proportional to the top-Yukawa coupling that naturally pushes $m_{H_u}^2$ to negative or small values at electroweak scale. In the MSSM, the breaking of the electroweak symmetry is therefore driven by quantum corrections and the mechanism is known as *radiative electroweak symmetry breaking* (REWSB).

When the two Higgs doublets develop expectation values as in (4.7), the minimization condition of the potential, $\partial V_0/\partial x = \partial V_0/\partial y = 0$, yields

$$\left(|\mu|^2 + m_{H_u}^2\right) v_u = b v_d + \frac{1}{4}\left(g^2 + g'^2\right)\left(v_d^2 - V_u^2\right) v_u \tag{4.13}$$

$$\left(|\mu|^2 + m_{H_d}^2\right) v_d = b v_u - \frac{1}{4}\left(g^2 + g'^2\right)\left(v_d^2 - V_u^2\right) v_d. \tag{4.14}$$

4.3.2. Higgs and Gauge Boson Masses

The steps to calculate the masses of the gauge bosons is equivalent to what is done in the SM. The difference here is that instead of a single scalar ϕ as in (2.33), we need the two Higgs doublets H_u and H_d. The result is that of section 2.3.1 but with the replacement

$$v^2 = v_u^2 + v_d^2. \tag{4.15}$$

The W and Z bosons masses take the form

$$M_Z = \sqrt{\frac{1}{2}\left(g^2+g'^2\right)\left(v_u^2+v_d^2\right)} \tag{4.16}$$

$$M_W = \sqrt{\frac{1}{2}g^2\left(v_u^2+v_d^2\right)}, \tag{4.17}$$

where a massless photon is also obtained when the Lagrangian is diagonalized. If we now introduce the traditional ratio of the expectation values

$$\tan\beta = \frac{v_u}{v_d}, \tag{4.18}$$

it is possible to rewrite the minimization conditions (4.19 - 4.20) of the Higgs potential as

$$\left(\left|\mu\right|^2+m_{H_u}^2\right) = b\cot\beta+\frac{M_Z^2}{4}\cos 2\beta \tag{4.19}$$

$$\left(\left|\mu\right|^2+m_{H_d}^2\right) = b\tan\beta-\frac{M_Z^2}{4}\cos 2\beta. \tag{4.20}$$

from where eliminating b and performing an expansion in powers of $1/(\tan\beta)$, M_Z^2 becomes

$$M_Z^2 = -2\left(m_{H_u}^2+\left|\mu\right|^2\right)+\frac{2}{\tan^2\beta}\left(m_{H_d}^2-m_{H_u}^2\right)+O\left(1/\tan^4\beta\right). \tag{4.21}$$

We see in (4.21) that if m_{H_u}, m_{H_d} and $\tan\beta$ are inputs, as for the research discussed in this thesis, the value of $|\mu|$ at the low scale will be fixed by the experimental value of $M_Z = 91.1876$ GeV [110].

In the SM, we found the Higgs mass considering radial oscillations about the minimum of the potential. However, for the present scenario, the determination of the Higgs spectrum involves some additional complications. We should note that, in the MSSM, there are *eight* real degrees of freedom coming from the four complex scalars, H_u^0, H_d^0,H_u^+ and $\mathrm{H_d^-}$, and the appropriate mass matrices have to be calculated. To illustrate how to obtain such matrices in a theory with n real scalars, consider the Lagrangian given by

$$\mathcal{L} = \frac{1}{2}\partial^\mu\Phi\partial_\mu\Phi - V(\Phi), \tag{4.22}$$

where the Higgs-type potential $V(\Phi)$ is the analog to (4.6). When Φ develops an expectation value $\langle\Phi\rangle = v$, where v should be regarded as a generic vector of vevs, $V(\Phi)$ is at its minimum, or mathematically

$$\left.\frac{\partial V}{\partial\Phi_i}\right|_{\Phi=v} = 0. \tag{4.23}$$

Since we want to find the quadratic deviations away from the symmetry breaking minimum, the potential is expanded about v up to second order yielding

$$V(v) = \frac{1}{2}\left.\frac{\partial^2 V}{\partial\Phi_i\partial\Phi_j}\right|_{\Phi=v}(\Phi-v)_i\,(\Phi-v)_j + O\left(\Phi^3\right). \tag{4.24}$$

We now redefine the fields as

$$\hat{\varphi}_i = \sqrt{2}(\Phi-v)_i, \tag{4.25}$$

and rewrite the Lagrangian as

$$\mathcal{L} = \frac{1}{2}\partial^\mu\hat{\varphi}^i\partial_\mu\hat{\varphi}_i - \frac{1}{2}\,\hat{\varphi}^i\mathbf{M}^2_{ij}\hat{\varphi}^j, \tag{4.26}$$

where the mass matrix $\mathbf{M}^2_{ij}$ is

$$\mathbf{M}^2_{ij} = \frac{1}{2}\left.\frac{\partial^2 V}{\partial\Phi_i\partial\Phi_j}\right|_{\Phi=v}. \tag{4.27}$$

We now apply this formalism to obtain the Higgs spectrum. Note however that since we can choose to have all the parameters in the potential (4.6) real, the respective imaginary and real parts do not mix. Furthermore, the mixing is only in pairs and we can consider separately the $\hat{\varphi}$ components

$$\begin{pmatrix} I_u \\ I_d \end{pmatrix},\ \begin{pmatrix} R_u - v_u \\ R_d - v_d \end{pmatrix},\ \begin{pmatrix} \phi_1^+ \\ \phi_1^- \end{pmatrix},\ \begin{pmatrix} \phi_2^+ \\ \phi_2^- \end{pmatrix}. \tag{4.28}$$

Here I_u, I_d, R_u, R_d are the imaginary and real parts of the neutral components H_u^0 and H_d^0 respectively, and the charged components are defined as $H_u^+ = \frac{1}{\sqrt{2}}(\phi_1^+ + i\phi_2^+)$ and $H_d^- = \frac{1}{\sqrt{2}}(\phi_1^- - i\phi_2^-)$.

For the imaginary neutral parts the potential takes the form

$$\begin{aligned} V_{I_u,I_d} &= \left(|\mu|^2 + m_{H_u}^2\right)I_u^2 + \left(|\mu|^2 + m_{H_d}^2\right)I_d^2 + 2bI_uI_d \\ &+ \frac{1}{2}g^2\left(I_u^2\left|H_u^+\right|^2 + \left|H_d^-\right|^2 I_d^2 + I_uI_dH_u^{+*}H_d^{-*} + H_d^-H_u^+I_uI_d\right) \\ &+ \frac{1}{8}\left(g^2+g'^2\right)\left(|R_u|^2 + |I_u|^2 - |R_d|^2 - |I_d|^2\right)^2. \end{aligned} \tag{4.29}$$

The next step is to calculate the second derivatives and evaluate them at the electroweak

minimum.

$$\frac{\partial^2 V}{\partial I_u \partial I_u} = (|\mu|^2 + m_{H_u}^2) + \frac{g^2+g'^2}{4}(v_u^2 - v_d^2) = b\cot\beta, \tag{4.30}$$

$$\frac{\partial^2 V}{\partial I_d \partial I_d} = (|\mu|^2 + m_{H_d}^2) - \frac{g^2+g'^2}{4}(v_u^2 - v_d^2) = b\tan\beta, \tag{4.31}$$

$$\frac{\partial^2 V}{\partial I_u \partial I_d} = \frac{\partial^2 V}{\partial I_d \partial I_u} = b. \tag{4.32}$$

The mass terms in (4.26) of the imaginary part of the neutral components take the form

$$\mathcal{L}_{I_u,I_d} = -\frac{1}{2}\begin{pmatrix} I_u & I_d \end{pmatrix}\begin{pmatrix} b\cot\beta & b \\ b & b\tan\beta \end{pmatrix}\begin{pmatrix} I_u \\ I_d \end{pmatrix}, \tag{4.33}$$

where upon diagonalization we obtain a massless neutral Goldstone boson G^0 which is absorbed into the longitudinal state of the Z boson, and a massive neutral pseudoscalar Higgs A^0 with mass

$$m_A^2 = \frac{2b}{\sin 2\beta}. \tag{4.34}$$

For the neutral real parts the relevant terms in the potential have the same form as (4.29) but with $I_{u,d}$ replaced by $R_{u,d}$. Evaluating the second derivatives at the minimum we get

$$\frac{\partial^2 V}{\partial R_u \partial R_u} = (|\mu|^2 + m_{H_u}^2) + \frac{g^2+g'^2}{4}(v_u^2 - v_d^2) + \frac{1}{4}(g^2+g'^2)v_u^2 = b\cot\beta + M_Z^2\sin^2\beta, \tag{4.35}$$

$$\frac{\partial^2 V}{\partial R_d \partial R_d} = (|\mu|^2 + m_{H_d}^2) - \frac{g^2+g'^2}{4}(v_u^2 - v_d^2) + \frac{1}{4}(g^2+g'^2)v_d^2 = b\tan\beta + M_Z^2\cos^2\beta, \tag{4.36}$$

$$\frac{\partial^2 V}{\partial R_u \partial R_d} = \frac{\partial^2 V}{\partial R_d \partial R_u} = -b - \frac{1}{2}(g^2+g'^2)v_u v_d = -b - \frac{1}{2}M_Z^2\sin 2\beta, \tag{4.37}$$

which results in the mass terms

$$\mathcal{L}_{R_u,R_d} = -\frac{1}{2}\begin{pmatrix} R_u - v_u & R_d - v_d \end{pmatrix}\begin{pmatrix} b\cot\beta + M_Z^2\sin^2\beta\cot\beta & -b - \frac{1}{2}M_Z^2\sin 2\beta \\ -b - \frac{1}{2}M_Z^2\sin 2\beta & b\tan\beta + M_Z^2\cos^2\beta \end{pmatrix}\begin{pmatrix} R_u - v_u \\ R_d - v_d \end{pmatrix}. \tag{4.38}$$

Diagonalizing (4.38), the physical masses of the neutral CP-even Higgs bosons h^0 and H^0 are obtained,

$$m_{h,\,H}^2 = \frac{1}{2}\left\{M_Z^2 + m_A^2 \mp \left[\left(M_Z^2 + m_A^2\right)^2 - 4m_A^2 M_Z^2\cos^2 2\beta\right]^{\frac{1}{2}}\right\}. \tag{4.39}$$

Finally, for the charged components, we consider once again the real and imaginary parts

separately. The potential has the same structure as (4.29) but with the replacements

$$I_u \rightarrow \phi_1^+, \phi_2^+ \tag{4.40}$$
$$I_d \rightarrow \phi_1^-, \phi_2^- \tag{4.41}$$

for the real and imaginary parts respectively, as well as

$$H_u^+ \rightarrow H_u^0 \tag{4.42}$$
$$H_d^- \rightarrow H_d^0 \tag{4.43}$$
$$R_u \rightarrow H_u^0 \tag{4.44}$$
$$R_d \rightarrow H_d^0. \tag{4.45}$$

Here, for the real components $\phi_1^\pm$, the derivatives take the form

$$\frac{\partial^2 V}{\partial\phi_1^+\partial\phi_1^+} = (|\mu|^2 + m_{H_u}^2) + \frac{g^2 v_d^2}{2} + \frac{g^2+g'^2}{4}(v_u^2 - v_d^2) = b\cot\beta + \frac{g^2 v_d^2}{2}, \tag{4.46}$$
$$\frac{\partial^2 V}{\partial\phi_1^-\partial\phi_1^-} = (|\mu|^2 + m_{H_d}^2) + \frac{g^2 v_u^2}{2} - \frac{g^2+g'^2}{4}(v_u^2 - v_d^2) = b\tan\beta + \frac{g^2 v_u^2}{2}, \tag{4.47}$$
$$\frac{\partial^2 V}{\partial\phi_1^+\partial\phi_1^-} = \frac{\partial^2 V}{\partial\phi_1^-\partial\phi_1^+} = b + \frac{1}{2}g^2 v_u v_d, \tag{4.48}$$

and the quadratic terms in the Lagrangian are

$$\mathcal{L}_1 = -\frac{1}{2}\begin{pmatrix}\phi_1^+ & \phi_1^-\end{pmatrix}\begin{pmatrix} b\cot\beta + \frac{g^2 v_d^2}{2} & b + \frac{1}{2}g^2 v_u v_d \\ b + \frac{1}{2}g^2 v_u v_d & b\tan\beta + \frac{g^2 v_u^2}{2}\end{pmatrix}\begin{pmatrix}\phi_1^+ \\ \phi_1^-\end{pmatrix}. \tag{4.49}$$

For the imaginary components $\phi_2^\pm$ the result is the same and once we diagonalize the Lagrangian, we obtain the physical massive charged complex fields $H^\pm$, as well as two massless charged Goldstone bosons $G^\pm$, which are absorbed into the longitudinal modes of the $W^\pm$ bosons. At last, the mass of the charged Higgs is

$$m_{H^\pm}^2 = M_W^2 + m_A^2. \tag{4.50}$$

It is important to note here that while H^0, $H^\pm$ and A^0 are nearly degenerate in the decoupling limit[1], the light Higgs h^0 mass is bounded from above having a maximum tree-level value of $m_h < M_Z|\cos 2\beta|$ which is far way from the experimental measured value of $125-126$ GeV. However, the Higgs mass relies quite significantly on radiative corrections where the largest contributions typically come from top and stop loops. It is therefore imperative to include such quantum corrections when calculating the Higgs mass and, at

[1]The decoupling limit is defined by $m_A \gg M_Z$.

one-loop level, the dominant contributions come from the diagrams 2.4, 3.1 and 3.2 together with the appropriate counterterms to cancel the divergent part. The dominant contribution to the one-loop corrections to the Higgs mass takes the form [111]

$$\Delta m_h^2 = \frac{3G_F\overline{m}_t^4}{\sqrt{2}\pi^2\sin^2\beta}\left[\log\frac{m_{\tilde{t}}^2}{m_t^2} + \frac{\tilde{A}_t^2}{m_{\tilde{t}}^2}\left(1 - \frac{\tilde{A}_t^2}{12m_{\tilde{t}}^2}\right)\right], \tag{4.51}$$

Where $G_F \approx 1.166\times10^5$ GeV^{-2} is the Fermi constant, $\overline{m}_t = 160$ GeV the top running mass, $m_{\tilde{t}} \equiv \sqrt{m_{\tilde{t}_L} m_{\tilde{t}_R}}$ the stop mass geometric average and $\tilde{A}_t = a_t/y_t - \mu\cot\beta$ a mixing term. It is clear from (4.51) that one-loop corrections push the maximum tree-level value of m_h upwards by several GeV. In particular, the coefficient of (4.51) is approximately 1600 GeV^2 and the second term inside the square brackets has a maximum value of 3. If we take $m_{\tilde{t}} \approx 1$ TeV, such contribution would rise the Higgs mass from M_Z to a maximum value of approximately $m_h \lesssim 135$ GeV.

4.3.3. Fermion and Sfermion Masses

In the MSSM, the masses of the observed quarks and charged leptons are determined from the superpotential after electroweak symmetry breaking, yielding mass terms of the form [2]

$$W_{FM} = \frac{1}{\sqrt{2}}\left[v_u\,(y_u)_{ij}\,\overline{u}_{Rix}u^x_{Lj} + v_d\,(y_d)_{ij}\,\overline{d}_{Rix}d^x_{Lj} + v_d\,(y_e)_{ij}\,\overline{e}_{Ri}e_{Lj}\right], \tag{4.52}$$

The fermion masses depend on the Yukawa couplings as well as on the $\tan\beta$ parameter. The expectations values of the up and down type Higgs can be written as $v_u = v\sin\beta$ and $v_d = v\cos\beta$ respectively, from where we take that

$$m_{u,c,t} = y_{u,c,t}\frac{v}{\sqrt{2}}\sin\beta\,, \quad m_{d,s,b} = y_{d,s,b}\frac{v}{\sqrt{2}}\cos\beta\,, \quad m_{e,\mu,\tau} = y_{e,\mu,\tau}\frac{v}{\sqrt{2}}\cos\beta. \tag{4.53}$$

Once again, the MSSM predicts massless neutrinos since it does not contain any extra fields or interactions capable of making them massive. The simplest way out is invoking the presence of a singlet right-handed neutrino superfield, where neutrino masses can be generated as we discussed in the first paragraph of sec. 2.5.

The physical masses of the sfermions are generated by SUSY-invariant F and D-terms after REWSB as well as from soft interacting terms. Since the Yukawa couplings of the first and second generation are rather small, the superpotential (4.2) can be written to a good

[2] Fermion masses in MSSM are entirely determined from the superpotential and no Lagrangian terms are allowed, otherwise, such terms would explicitly break $SU(2)_L$ invariance.

approximation as

$$\begin{aligned} W &\approx y_t \tilde{t}_R^* \left(\tilde{t}_L H_u^0 - \tilde{b}_L H_u^+\right) - y_b \tilde{b}_R^* \left(\tilde{t}_L H_d^- - \tilde{b}_L H_d^0\right) - y_\tau \tilde{\tau}_R^* \left(\tilde{\nu}_L H_d^- - \tilde{\tau}_L H_d^0\right) \\ &+ \mu \left(H_u^+ H_d^- - H_u^0 H_d^0\right). \end{aligned} \tag{4.54}$$

After symmetry breaking, the F-term contributions (see the Lagrangian (3.33)) to the stop quarks are

$$-\left|\frac{\partial W}{\partial \tilde{t}_R^\dagger}\right|^2 \rightarrow -y_t^2 \frac{v_u^2}{\sqrt{2}} \tilde{t}_L^* \tilde{t}_L = -m_t^2 \tilde{t}_L^* \tilde{t}_L \tag{4.55}$$

$$-\left|\frac{\partial W}{\partial \tilde{t}_L}\right|^2 \rightarrow -y_t^2 \frac{v_u^2}{\sqrt{2}} \tilde{t}_R^* \tilde{t}_R = -m_t^2 \tilde{t}_R^* \tilde{t}_R \tag{4.56}$$

$$-\left|\frac{\partial W}{\partial H_u^0}\right|^2 \rightarrow -\left|y_t \tilde{t}_R^* \tilde{t}_L - \mu \frac{v_d}{\sqrt{2}}\right|^2 = y_t \mu \frac{v}{\sqrt{2}} \cos\beta \left(\tilde{t}_R^* \tilde{t}_L + \tilde{t}_L^* \tilde{t}_R\right) + \cdots . \tag{4.57}$$

The D-terms in the scalar potential (3.45) are purely scalar quartic interactions if all the groups of G_{SM} are unbroken. However, when we break the electroweak symmetry some of the $SU(2)_L \times U(1)_Y$ representations, the Higgs, acquire expectation values and quadratic mass terms emerge:

$$\frac{1}{2} \sum_G \sum_a \sum_{i,j} g_G^2 \left(\phi_i^* \Omega^a \phi_i\right)\left(\phi_j^* \Omega^a \phi_j\right) \rightarrow \Delta_{\phi_{L,R}} \phi_{L,R}^* \phi_{L,R}. \tag{4.58}$$

Here $\Delta_{\phi_{L,R}}$ is generation independent and splits apart the components of the $SU(2)_L$ doublets sleptons and squarks.

$$\Delta_{\phi_{L,R}} = M_Z^2 (T_{3\phi_{L,R}} - Q_{\phi_{L,R}} \sin^2\theta_W) \cos 2\beta \,, \tag{4.59}$$

with $T_{3\phi_{L,R}}$ the third component of the weak isospin, $Q_{\phi_{L,R}}$ the electric charge and $\sin\theta_W$ the sine of the Weinberg angle. Therefore, the D-term contributions to the stop masses are

$$-\Delta_{\tilde{u}_L} \tilde{t}_L^* \tilde{t}_L \,, \tag{4.60}$$

$$-\Delta_{\tilde{u}_R} \tilde{t}_R^* \tilde{t}_R \,. \tag{4.61}$$

Finally, from the soft Lagrangian (4.5) we find both diagonal and off-diagonal terms. While the former come from quadratic terms, the later ones emerge from the trilinear terms. In particular we have

$$-\tilde{Q}_{L3} \left(m_{\tilde{Q}_L}^2\right)_3^3 \tilde{Q}_L^{*\,3} - \tilde{u}_{R3} \left(m_{\tilde{u}_R}^2\right)_3^3 \tilde{u}_R^3 = m_{\tilde{Q}_3}^2 \tilde{t}_L^* \tilde{t}_L - m_{\tilde{t}_R}^2 \tilde{t}_R^* \tilde{t}_R \tag{4.62}$$

and

$$-\varepsilon_{\alpha\beta}\left[a_t H_u^{\alpha}\tilde{t}_R\tilde{Q}_{L3}^{\beta}+h.c.\right] \;\rightarrow\; -\frac{v}{\sqrt{2}}\sin\beta\left(a_t\tilde{t}_R^{*}\tilde{t}_L+a_t\tilde{t}_L^{*}\tilde{t}_R\right). \tag{4.63}$$

Tidying up everything, the mass terms in the gauge eigenstates basis is

$$\mathcal{L}_{stop-mass}=-\begin{pmatrix}t_L^{*} & t_R^{*}\end{pmatrix}\begin{pmatrix} m_{\tilde{Q}_3}^2+m_t^2+\Delta_{\tilde{u}_L} & \frac{v}{\sqrt{2}}\sin\beta\,(a_t-y_t\mu\cot\beta)\\ \frac{v}{\sqrt{2}}\sin\beta\,(a_t-y_t\mu\cot\beta) & m_{\tilde{t}_R}^2+m_t^2+\Delta_{\tilde{u}_R}\end{pmatrix}\begin{pmatrix}t_L\\ t_R\end{pmatrix}. \tag{4.64}$$

Changing to a basis $\{\tilde{t}_1,\tilde{t}_2\}$ where the mass matrix is diagonal, we find the physical masses for the stops,

$$\begin{aligned} m_{\tilde{t}_1,\,\tilde{t}_2}^2 &= \frac{1}{2}\Bigg[\left(m_{\tilde{Q}_3}^2+m_{\tilde{t}_R}^2+2m_t^2+\Delta_{u_L}+\Delta_{u_R}\right)\\ &\mp \sqrt{\left(m_{\tilde{Q}_3}^2-m_{\tilde{t}_R}^2+\Delta_{u_L}-\Delta_{u_R}\right)^2+2v^2\sin^2\beta\,(a_t-y_t\mu\cot\beta)^2}\Bigg], \end{aligned} \tag{4.65}$$

where we denote $\tilde{t}_1$ as the light stop and $\tilde{t}_2$ as the heavy one. Following the same steps, once the electroweak symmetry is broken, the physical masses of the sbottoms and of the staus are

$$\begin{aligned} m_{\tilde{b}_1,\,\tilde{b}_2}^2 &= \frac{1}{2}\Bigg[\left(m_{\tilde{Q}_3}^2+m_{\tilde{b}_R}^2+2m_b^2+\Delta_{d_L}+\Delta_{d_R}\right)\\ &\mp \sqrt{\left(m_{\tilde{Q}_3}^2-m_{\tilde{b}_R}^2+\Delta_{d_L}-\Delta_{d_R}\right)^2+2v^2\cos^2\beta\,(a_b-y_b\mu\tan\beta)^2}\Bigg] \end{aligned} \tag{4.66}$$

and

$$\begin{aligned} m_{\tilde{\tau}_1,\,\tilde{\tau}_2}^2 &= \frac{1}{2}\Bigg[\left(m_{\tilde{L}_3}^2+m_{\tilde{\tau}_R}^2+2m_\tau^2+\Delta_{e_L}+\Delta_{e_R}\right)\\ &\mp \sqrt{\left(m_{\tilde{L}_3}^2-m_{\tilde{\tau}_R}^2+\Delta_{e_L}-\Delta_{e_R}\right)^2+2v^2\cos^2\beta\,(a_\tau-y_\tau\mu\tan\beta)^2}\Bigg]. \end{aligned} \tag{4.67}$$

In the minimal version of the MSSM where no right-handed neutrinos exist, the sneutrino mass of the third generation is simply given by its soft term and the electroweak D-term splitting

$$m_{\tilde{\nu}_3}^2=m_{\tilde{L}_3}^2+\Delta_{\nu_L}. \tag{4.68}$$

The smallness of the Yukawa and trilinear couplings dictates that for the first and second generation sfermions, which we take to be degenerate for the same flavour, we can neglect the off-diagonal terms in the mass Lagrangian. Therefore, the mass terms in the

gauge eigenstate space are given by

$$\mathcal{L}_{mass} = -\sum_{\varphi} \begin{pmatrix} \varphi_L^* & \varphi_R^* \end{pmatrix} \begin{pmatrix} m_{\varphi_L}^2 + \Delta_{\varphi_L} & 0 \\ 0 & m_{\varphi_R}^2 + \Delta_{\varphi_R} \end{pmatrix} \begin{pmatrix} \varphi_L \\ \varphi_R \end{pmatrix}, \tag{4.69}$$

where $\varphi_{L,R} \in \left\{\tilde{u}_L, \tilde{u}_R, \tilde{d}_L, \tilde{d}_R, \tilde{e}_L, \tilde{e}_R, \tilde{\nu}_L\right\}$, coincides to a good approximation with the mass eigenstates Lagrangian.

4.3.4. Gluino, Neutralino and Chargino Masses

In the gaugino sector, once the electroweak symmetry is broken, the gluinos are still protected by the $SU(3)_C$ symmetry and there is no mixing between gauge eigenstates. This is easily seen from the scalar-fermion-gaugino cubic terms in (3.42)

$$-\sqrt{2}g\left(\phi^*\Omega^a\psi\right)\lambda^a - \sqrt{2}g\lambda^{a\dagger}\left(\psi^\dagger\Omega^a\phi\right), \tag{4.70}$$

where ϕ, a color triplet **3**, does not develop expectation values and no quadratic terms mixing Higgsinos ψ and gluinos λ^3 are generated. Gluino masses are directly obtained from (4.5)

$$m_{\tilde{g}} = M_3. \tag{4.71}$$

This is not the case for the interactions involving binos, winos and higgsinos. Here, without the protection of the $SU(2)_L \times U(1)_Y$ symmetry, they are free to mix. The diagonal elements come from the last line of (4.5) where for the neutral and charged components we have respectively

$$-\frac{1}{2}\left[M_1\tilde{B}\cdot\tilde{B} + M_2\tilde{W}^0\cdot\tilde{W}^0 + h.c.\right], \tag{4.72}$$

and

$$-\frac{1}{2}\left[M_2\tilde{W}^1\cdot\tilde{W}^1 + M_2\tilde{W}^2\cdot\tilde{W}^2 + h.c.\right]. \tag{4.73}$$

The SUSY-invariant μ-term in the superpotential (4.2) also provides mixing between the neutral $\tilde{H}_u^0$ and $\tilde{H}_d^0$, and the charged $\tilde{H}_u^+$ and $\tilde{H}_d^-$ Higgsino components,

$$\begin{aligned} &-\mu\left(\tilde{H}_u^+\cdot\tilde{H}_d^- - \tilde{H}_u^0\cdot\tilde{H}_d^0 + h.c.\right) + \cdots = \\ &-\frac{1}{2}(-\mu)\left(\tilde{H}_u^0\cdot\tilde{H}_d^0 + \tilde{H}_d^0\cdot\tilde{H}_u^0\right) - \frac{1}{2}\mu\left(\tilde{H}_u^+\cdot\tilde{H}_d^- + \tilde{H}_d^-\cdot\tilde{H}_u^+\right) + h.c. \end{aligned} \tag{4.74}$$

Once the electroweak symmetry is broken and the Higgs doublets develop vevs as in (4.7), the cubic terms (4.70) generate quadratic terms that mix higgsinos, winos and binos. For the

neutral components we have

$$-\sqrt{2}g\begin{pmatrix}H_u^{+*} & H_u^{0*}\end{pmatrix}\frac{\tau^3}{2}\begin{pmatrix}\tilde{H}_u^+\\ \tilde{H}_u^0\end{pmatrix}\cdot\tilde{W}^3+h.c. \;\rightarrow\; -\frac{1}{2}\left(-\frac{gv_u}{2}\right)\left(\tilde{H}_u^0\cdot\tilde{W}^0+\tilde{W}^0\cdot\tilde{H}_u^0\right)+h.c. \tag{4.75}$$

$$-\sqrt{2}g'\begin{pmatrix}H_u^{+*} & H_u^{0*}\end{pmatrix}\frac{Y_{H_u}}{2}\begin{pmatrix}\tilde{H}_u^+\\ \tilde{H}_u^0\end{pmatrix}\cdot\tilde{B}+h.c. \;\rightarrow\; -\frac{1}{2}\left(\frac{g'v_u}{2}\right)\left(\tilde{H}_u^0\cdot\tilde{B}+\tilde{B}\cdot\tilde{H}_u^0\right)+h.c. \tag{4.76}$$

$$-\sqrt{2}g\begin{pmatrix}H_d^{0*} & H_d^{-*}\end{pmatrix}\frac{\tau^3}{2}\begin{pmatrix}\tilde{H}_d^0\\ \tilde{H}_d^-\end{pmatrix}\cdot\tilde{W}^3+h.c. \;\rightarrow\; -\frac{1}{2}\left(\frac{gv_d}{2}\right)\left(\tilde{H}_d^0\cdot\tilde{W}^0+\tilde{W}^0\cdot\tilde{H}_d^0\right)+h.c. \tag{4.77}$$

$$-\sqrt{2}g'\begin{pmatrix}H_d^{0*} & H_d^{-*}\end{pmatrix}\frac{Y_{H_d}}{2}\begin{pmatrix}\tilde{H}_d^0\\ \tilde{H}_d^-\end{pmatrix}\cdot\tilde{B}+h.c. \;\rightarrow\; -\frac{1}{2}\left(-\frac{g'v_d}{2}\right)\left(\tilde{H}_d^0\cdot\tilde{B}+\tilde{B}\cdot\tilde{H}_d^0\right)+h.c. \tag{4.78}$$

where $\tilde{W}^0\equiv\tilde{W}^3$, and for the charged components

$$\begin{aligned}&-\sqrt{2}g\begin{pmatrix}H_u^{+*} & H_u^{0*}\end{pmatrix}\left[\frac{\tau^1}{2}\begin{pmatrix}\tilde{H}_u^+\\ \tilde{H}_u^0\end{pmatrix}\cdot\tilde{W}^1+\frac{\tau^2}{2}\begin{pmatrix}\tilde{H}_u^+\\ \tilde{H}_u^0\end{pmatrix}\cdot\tilde{W}^2\right]+h.c.\\ \rightarrow\;& -\frac{1}{2}\left(\frac{gv_u}{2}\right)\left(\tilde{H}_u^+\cdot\tilde{W}^-+\tilde{W}^-\cdot\tilde{H}_u^+\right)+h.c.\end{aligned} \tag{4.79}$$

$$\begin{aligned}&-\sqrt{2}g\begin{pmatrix}H_d^{0*} & H_d^{-*}\end{pmatrix}\left[\frac{\tau^1}{2}\begin{pmatrix}\tilde{H}_d^0\\ \tilde{H}_d^-\end{pmatrix}\cdot\tilde{W}^1+\frac{\tau^2}{2}\begin{pmatrix}\tilde{H}_d^0\\ \tilde{H}_d^-\end{pmatrix}\cdot\tilde{W}^2\right]+h.c.\\ \rightarrow\;& -\frac{1}{2}\left(\frac{gv_d}{2}\right)\left(\tilde{H}_d^-\cdot\tilde{W}^++\tilde{W}^+\cdot\tilde{H}_d^-\right)+h.c.\end{aligned} \tag{4.80}$$

where $\tilde{W}^\pm\equiv(\tilde{W}^1\pm i\tilde{W}^2)$. The mass Lagrangian of the neutral components in the gauge eigenstate basis takes the form

$$\mathcal{L}_{neutral}=-\frac{1}{2}\begin{pmatrix}\tilde{B} & \tilde{W}^0 & \tilde{H}_d^0 & \tilde{H}_u^0\end{pmatrix}\begin{pmatrix}M_1 & 0 & -g'v_d/2 & g'v_u/2\\ 0 & M_2 & gv_d/2 & -gv_u/2\\ -g'v_d/2 & gv_d/2 & 0 & -\mu\\ g'v_u/2 & -gv_u/2 & -\mu & 0\end{pmatrix}\begin{pmatrix}\tilde{B}\\ \tilde{W}^0\\ \tilde{H}_d^0\\ \tilde{H}_u^0\end{pmatrix}+h.c.\,, \tag{4.81}$$

whereas for the charged ones we get

$$\mathcal{L}_{charged}=-\frac{1}{2}\left[\begin{pmatrix}\tilde{W}^+ & \tilde{H}_u^+\end{pmatrix}\mathbf{C}^{\mathbf{T}}\begin{pmatrix}\tilde{W}^-\\ \tilde{H}_d^-\end{pmatrix}+\begin{pmatrix}\tilde{W}^- & \tilde{H}_d^-\end{pmatrix}\mathbf{C}\begin{pmatrix}\tilde{W}^+\\ \tilde{H}_u^+\end{pmatrix}\right]+h.c. \tag{4.82}$$

with the mass matrix of the charged components given by

$$\mathbf{C}=\begin{pmatrix}M_2 & gv_u/2\\ gv_d/2 & \mu\end{pmatrix}. \tag{4.83}$$

The physical masses are obtained by diagonalizing the mass matrices in (4.81 and 4.82). Nonetheless, in most of the cases, the electroweak symmetry breaking effects can be regarded as small perturbations, $M_z \ll |\mu \pm M_{1,2}|$, and the off-(block)diagonal elements can be neglected to a good approximation. Therefore, the mass eigenstates of the neutral components, called *neutralinos*, only depend on the M_1, M_2 and μ parameters. For instance, if $M_1 < M_2 \ll \mu$, the lightest neutralino is dominantly *bino-like*, the next-to-lightest one is *wino-like* and the heavy ones are *higgsino-like* neutralinos. Accordingly, the mass eigenstates of the charged components, called *charginos*, are *wino-like* and *higgsino-like* respectively. However this needn't be the case and we can have symmetries at the high scale, yielding $M_2 < M_1$. Here, the lightest neutralino is wino-like and is approximately degenerate with the lightest wino-like chargino. An other possibility is to have $\mu \ll M_{1,2}$ and the two lightest neutralinos as well as the lightest chargino, are Higgsino-like. Recall that the gluinos are protected by the $SU(3)_C$ symmetry and do not mix with other gauginos or higgsinos. However, if $M_3 \ll M_{1,2}, \mu$, the gluino may become LSP, which is unacceptable since it would provide a colored Dark Matter candidate. In this thesis we will explore all these scenarios and will denote the charginos as $\tilde{\chi}_i^{\pm}$, the neutralinos as $\tilde{\chi}_i^0$, and label them according to the mass hierarchy

$$m_{\tilde{\chi}_1^{\pm}} < m_{\tilde{\chi}_2^{\pm}} \tag{4.84}$$

$$m_{\tilde{\chi}_1^0} < m_{\tilde{\chi}_2^0} < m_{\tilde{\chi}_3^0} < m_{\tilde{\chi}_4^0}. \tag{4.85}$$

When the lightest neutralino is also the lightest particle of the supersymmetric spectrum (LSP), it becomes an attractive candidate for Dark Matter (DM). Scenarios where the gaugino masses at the high scale are universal, typically predict bino dominated neutralinos as the LSP with a relic density a few orders of magnitude beyond the upper limit set by the Wilkinson Microwave Anisotropy Probe (WMAP) [120] and Planck [121] satellites. On the other hand, non-universal gauginos are compatible with higgsino and wino dominated DM, and for particular regions of the parameter space, the neutralino relic density can be within or below the WMAP and Planck bounds. The other weakly interacting massive particle (WIMP) in the MSSM that could become a DM candidate if the LSP, is the third generation sneutrino. However, such scenarios appears to be severely constrained by the latest XENON100 WIMP-nucleon cross section bounds [122], for direct Dark Matter detection.

4.4. Running of the Gauge Couplings in the MSSM

The new fields that are introduced in the MSSM, see tables 4.1 and 4.2, modify the slopes of the one-loop renormalization group equations for the gauge couplings (2.72). This is due to the additional terms in the Lagrangian, which provide extra contributions to the β-function once the appropriate loop-diagrams are calculated. In particular, for the example in figure

2.2, the additional one-loop contributions to the fermion-fermion-gauge vertex are

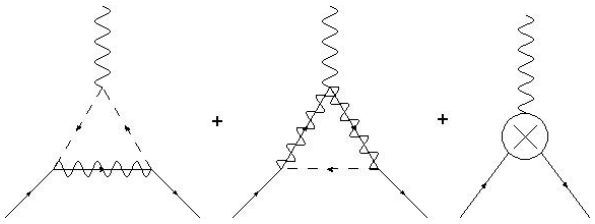

Figure 4.2. *One-loop SUSY corrections to the fermion-fermion-gauge vertex. The continuous and wavy lines represent fermions and gauge bosons respectively. The dashed lines represent scalars and a wavy line on top of a continuous one represents a gaugino.*

Once the counterterms of these diagrams (as well as all the other corrections not shown in the figure) are calculated, the β-function takes the form

$$\beta(g_i) = \frac{g_i^3}{16\pi^2}\left[-\frac{11}{3}C_2(V) + \frac{2}{3}C_2(G)\Theta_{gaugino} + \frac{4}{3}T_2\left(R_f\right) + \Theta_s\frac{1}{3}T_2(R_s)\right], \tag{4.86}$$

where $\Theta_{gaugino}$ and Θ_s are step-functions to switch superpartners on or off, depending on whether they are present or not at some energy scale. Using the formulas of section 2.4, the coefficients b_i become

$$b_1 = \frac{35}{3}\ ,\ b_2 = 1\ ,\ b_3 = -3, \tag{4.87}$$

which modifies the running of the gauge couplings, Fig (4.3), in comparison to the SM.

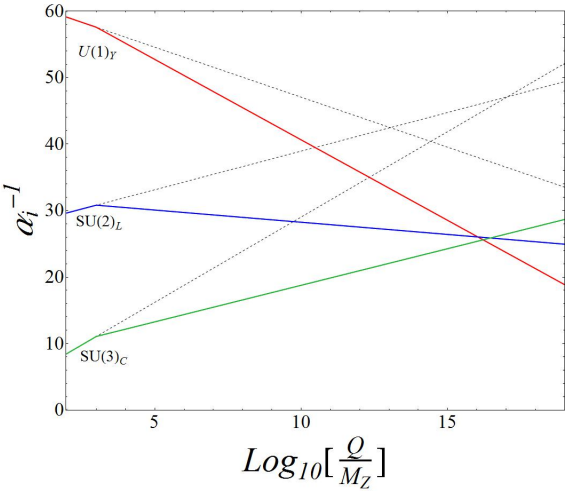

Figure 4.3. *Running of the Gauge Couplings in the MSSM. Dashed lines represent the running in the SM.*

Although not perfect, there is a tantalizing convergence of the gauge couplings to a common value at a scale of about $M_{GUT} \approx 2\times10^{16}$ GeV. While it can be simply regarded as a coincidence, it is on the other hand a strong motivation for a Grand Unified Theory. This

suggests, that beyond M_{GUT}, there is a larger symmetry described by some simple gauge group with one unified gauge coupling. The most popular candidates for a unified gauge symmetry are the $SU(5)$, $SO(10)$ and E_6 groups [123], and, as we will discuss, these gauge structures may constrain the soft supersymmetry breaking parameters at the high scale, with important consequences for the low scale physics.

5. Grand Unification

The unification of the gauge couplings in the MSSM, Fig. 4.3, suggests that the $SU(3)_C \times SU(2)_L \times U(1)_Y$ symmetry, which we abbreviate as G_{SM} throughout, is a remnant of some larger symmetry spontaneously broken at M_{GUT}. This idea is comparable to the electroweak theory, where $SU(2)_L \times U(1)_Y$ is partially broken at the scale M_{EW}, leaving behind a residual $U(1)_Q$. We should however be careful to bear in mind that the electroweak unification is a "*false*" unification framework. Indeed, it does not predict any unification between the g and g' gauge couplings, and we would like, instead, to embed G_{SM} in a structure capable of unifying the three gauge couplings into a single one. In such a model, not only a natural explanation for the values of the gauge couplings at the low scale is possible, but also, the charges of the SM particles are fixed by the larger symmetry. In particular, there is no *a-priori* reason for the assigned values of the hypercharges in the SM, besides needing to be compatible with experiment. However, when a generic $U(1)_x$ symmetry is a remnant of some spontaneously broken larger group, the x-hypercharges are, up to a normalization factor, fixed by the original larger symmetry.

To study Grand Unification it is instructive to get familiar with the tools and terminology. We provide a discussion in appendix A which aims to offer an overview of the basic elements of *representation theory*.

5.1. $SU(5)$ Grand Unification

The gauge group of the Standard Model, G_{SM}, is a semi-simple Lie algebra of rank *four*. Embedding G_{SM} in an $SU(5)$ gauge symmetry, which is also rank four, seems an appropriate choice for a starting point. The idea is to find a subalgebra of the larger symmetry that contains G_{SM} and it is indeed the case of $SU(5)$. If we pick up the highest weight of the adjoint representation (1 0 0 1), successive subtractions of simple roots, that can be read off from the Cartan matrix

$$A_{SU(5)} = \begin{pmatrix} 2 & -1 & 0 & 0 \\ -1 & 2 & -1 & 0 \\ 0 & -1 & 2 & -1 \\ 0 & 0 & -1 & 2 \end{pmatrix}, \tag{5.1}$$

produces 24 states which correspond to the gauge bosons of $SU(5)$. The generators associated with these gauge bosons are represented by 5×5 matrices. These contain the generators of G_{SM},

$$SU(3): \quad \Omega_{a_3} = \begin{pmatrix} \frac{1}{2}\lambda_{a_3} & 0 \\ 0 & 0 \end{pmatrix}, \; a_3 = 1,...,8 \tag{5.2}$$

$$SU(2): \quad \Omega_{a_2} = \begin{pmatrix} 0 & 0 \\ 0 & \frac{1}{2}\tau_{a_2-20} \end{pmatrix}, \; a_2 = 21,22,23 \tag{5.3}$$

$$U(1): \quad \Omega_{24} = \frac{1}{2}\sqrt{\frac{3}{5}} \begin{pmatrix} -\frac{2}{3} & 0 & 0 & 0 & 0 \\ 0 & -\frac{2}{3} & 0 & 0 & 0 \\ 0 & 0 & -\frac{2}{3} & 0 & 0 \\ 0 & 0 & 0 & 1 & 0 \\ 0 & 0 & 0 & 0 & 1 \end{pmatrix}, \tag{5.4}$$

as well as 12 off-diagonal generators Ω_{a_4} with $a_4 = 9,...,20$.

The next step is to find out which irreps of $SU(5)$ can embed the fields of the MSSM, summarized in tables 4.1 and 4.2. We detail here the simple example of the fundamental irrep, **5**, which highest weight is (1 0 0 0). Using the simple roots of $SU(5)$ extracted form (5.1), one can determine the weights of the five Hilbert state vectors as in the weight diagram of Fig. 5.1. We need now to project such states into G_{SM}, which is accomplished separately for

$$\begin{array}{c} (1\,0\,0\,0) \\ \downarrow \; \alpha_1 \\ (-1\,1\,0\,0) \\ \downarrow \; \alpha_2 \\ (0\,-1\,1\,0) \\ \downarrow \; \alpha_3 \\ (0\,0\,-1\,1) \\ \downarrow \; \alpha_4 \\ (0\,0\,0\,-1) \end{array}$$

Figure 5.1. *Weight diagram for the fundamental representation of $SU(5)$.*

$SU(3)\times SU(2)$ and for the $U(1)$ factor. In order to determine the projection matrix, a common convention is to demand that the state of highest weight of the **5**, which can accommodate a colour triplet weak singlet and a colour singlet weak doublet, branches to the state of highest weight of the first one, which weights are (1 0) and (0) respectively. Therefore

$$P(1\,0\,0\,0) = (1\,0\,0) \tag{5.5}$$

with the first two entries on the rhs of (5.5) the $SU(3)$ labels and the last entry the $SU(2)$ label.

It is then immediate that for the conjugate representation we have

$$P(0\ 0\ 0\ 1) = (0\ 1\ 0). \tag{5.6}$$

Hwever, We need further constraints in order to fully determine the projection. The second smallest representations of $SU(5)$ are the **10**, with highest weight (0 1 0 0), and its conjugate, $\overline{\mathbf{10}}$, with highest weight (0 0 1 0). They can both embed a colour triplet weak doublet, a colour triplet weak singlet and a singlet of $SU(3)\times SU(2)$. The choice here is to demand that the highest weights of the ten-dimensional representations branch to the highest weights of the colour triplet weak doublet fields. We then have

$$P(0\ 1\ 0\ 0) = (1\ 0\ 1) \tag{5.7}$$

$$P(0\ 0\ 1\ 0) = (0\ 1\ 1), \tag{5.8}$$

and from (5.5), (5.6), (5.7) and (5.8), the projection matrix takes the form

$$P\left(SU(5) \supset SU(3)\times SU(2)\right) = \begin{pmatrix} 1 & 1 & 0 & 0 \\ 0 & 0 & 1 & 1 \\ 0 & 1 & 1 & 0 \end{pmatrix}. \tag{5.9}$$

From (5.7), for example, we see that it clearly projects the highest weight of **10** into the state of highest weight of a $(\mathbf{3},\mathbf{2})$, which we identify with a left-handed quark field with hypercharge $Y^w = \frac{1}{3}$, which uniquely defines the hypercharge axes. The I_3^w, Y^w as well as the electric charge Q can be identified, and in the dual basis take the form

$$\overline{Y}^w = \frac{1}{3}[-2\ 1\ -1\ 2], \tag{5.10}$$

$$\overline{I}_3^w = \frac{1}{2}[0\ 1\ 1\ 0], \tag{5.11}$$

$$\overline{Q} = \frac{1}{3}[-1\ 2\ 1\ 1]. \tag{5.12}$$

Projecting out the **5** of $SU(5)$ we obtain the branching rule

$$\mathbf{5} \to (\mathbf{1},\mathbf{2})_1 \oplus (\mathbf{3},\mathbf{1})_{-\frac{2}{3}}, \tag{5.13}$$

which can be identified with either a $\hat{\bar{L}}\oplus\hat{d}$ or a $\hat{H}_u\oplus\hat{T}_u$, where $\hat{T}_u$ is a up-type Higgs colour triplet superfield. Following the same recipe for the anti-fundamental representation of $SU(5)$ as well as the **10** irrep, we find the branching rules

$$\overline{\mathbf{5}} \to (\mathbf{1},\mathbf{2})_{-1} \oplus \left(\overline{\mathbf{3}},\mathbf{1}\right)_{\frac{2}{3}}, \tag{5.14}$$

$$\mathbf{10} \to (\mathbf{1},\mathbf{1})_2 \oplus \left(\overline{\mathbf{3}},\mathbf{1}\right)_{-\frac{4}{3}} \oplus (\mathbf{3},\mathbf{2})_{\frac{1}{3}}, \tag{5.15}$$

from where we can identify either a $\hat{L}\oplus\hat{\bar{d}}$ or a $\hat{H}_d\oplus\hat{T}_d$ within the $\bar{\mathbf{5}}$ and a $\hat{\bar{e}}\oplus\hat{\bar{u}}\oplus\hat{Q}$ embedded in the **10**. We should further note that the tensor product of two fundamental irreps yields

$$\mathbf{5}^{\alpha}\otimes\mathbf{5}^{\beta}=\mathbf{15}_s^{\alpha\beta}\oplus\mathbf{10}_a^{\alpha\beta}, \tag{5.16}$$

where the labels s and a mean symmetric and anti-symmetric representation respectively, and the Greek letters are spinor indices. The matter and Higgs fields of the MSSM are therefore embedded as

$$\bar{\mathbf{5}}^{\alpha}=\begin{pmatrix}\bar{d}_R^1\\ \bar{d}_R^2\\ \bar{d}_R^3\\ e_L\\ -\nu_L\end{pmatrix};\quad \mathbf{5'}^{\alpha}=\begin{pmatrix}T_u^1\\ T_u^2\\ T_u^3\\ H_u^+\\ H_u^0\end{pmatrix};\quad \bar{\mathbf{5}}'^{\alpha}=\begin{pmatrix}\bar{T}_d^1\\ \bar{T}_d^2\\ \bar{T}_d^3\\ H_d^-\\ -H_d^0\end{pmatrix}; \tag{5.17}$$

$$\mathbf{10}^{\alpha\beta}=\begin{pmatrix}0 & \bar{u}_R^3 & -\bar{u}_R^2 & u_L^1 & d_L^1\\ -\bar{u}_R^3 & 0 & \bar{u}_R^1 & u_L^2 & d_L^2\\ \bar{u}_R^2 & -\bar{u}_R^1 & 0 & u_L^3 & d_L^3\\ -u_L^1 & -u_L^2 & -u_L^3 & 0 & \bar{e}_R\\ -d_L^1 & -d_L^2 & -d_L^3 & -\bar{e}_R & 0\end{pmatrix}, \tag{5.18}$$

where the primed and unprimed five-dimensional representations serve to distinguish between Higgs and matter fields respectively. We conclude from this minimal embedding that the standard matter of the MSSM belongs to a reducible $\bar{\mathbf{5}}\oplus\mathbf{10}$ complete representation, whereas the Higgs are in two distinct five-dimensional representations.

5.1.1. Proton Decay via Heavy Boson Exchange

The twelve off-diagonal gauge bosons of the adjoint representation of $SU(5)$ are not present in the MSSM. However, their appearance in GUT models have some important consequences. When the $SU(5)$ symmetry is broken to G_{SM} at, or at least close, to the GUT scale, in a minimal model, it may be accomplished by a Higgs in the adjoint **24** representation of $SU(5)$. Similarly to what we studied for the SM, this first breaking of the gauge structure will generate mass for the off-diagonal gauge bosons. The vector superfields can be represented by a 5×5 matrix, which in a compact form is given as

$$V_\mu=\frac{1}{\sqrt{2}}\begin{pmatrix}0 & \overline{X}_\mu\\ X_\mu & 0\end{pmatrix}. \tag{5.19}$$

The diagonal elements, which are set to zero in 5.19, are the SM gauge bosons. We know that they acquire their masses at the low scale being massless at the higher scales. For that reason, and for ease of notation, we remove them from this calculation. Note also that X_μ is a 3×2 matrix. The adjoint Higgs field, Σ^a, that gives masses to the x_μ bosons, develops an expectation value taking the form

$$\langle\Sigma\rangle = \frac{v_{24}}{\sqrt{30}}\begin{pmatrix}2 & 0\\ 0 & -3\end{pmatrix}, \tag{5.20}$$

where once again we used a compact block notation, where the first entry in the diagonal is actually a 3×3 block, and the second one is a 2×2 block. Recall now the Yang-Mills covariant derivative 2.20, which now is rewritten as

$$D_\mu = \partial_\mu + ig_5\Omega^a V^a_\mu, \tag{5.21}$$

where g_5 is the unified gauge coupling of $SU(5)$, and $V_\mu = V^a_\mu\Omega^a$. From the definition of the adjoint representation we have that $(\Omega^a)^{bc} = -if^{abc}$, (5.21) when acting on Σ^a takes the form

$$D_\mu\Sigma^c = \partial_\mu\Sigma^c + ig_5(-if^{abc})V^a_\mu\Sigma^b. \tag{5.22}$$

Defining $\Sigma = \Sigma^a\Omega^a$, (5.22) becomes

$$D_\mu\Sigma = \partial_\mu\Sigma + ig_5(-if^{abc})V^a_\mu\Sigma^b\Omega^c = \partial_\mu\Sigma - ig_5\Big[V_\mu,\Sigma\Big]. \tag{5.23}$$

We can now calculate the commutator in (5.23) and obtain

$$\Big[V_\mu,\Sigma\Big] = \frac{5v_{24}}{\sqrt{60}}\begin{pmatrix}0 & -\overline{X}_\mu\\ X_\mu & 0\end{pmatrix}. \tag{5.24}$$

The part of the high scale Lagrangian that will provide masses for the off-diagonal bosons is

$$\begin{aligned}\mathcal{L}_\Sigma &= \left(D_\mu\Sigma_a\right)^\dagger D^\mu\Sigma^a = Tr\Big[\left(D_\mu\Sigma\right)^\dagger D^\mu\Sigma\Big]\\ &= -\frac{5}{6}g_5^2v_{24}^2X_\mu X^\mu.\end{aligned} \tag{5.25}$$

This spontaneous GUT symmetry breaking takes place at the hight scale with $v_{24}\sim M_{GUT}$. The off diagonal bosons are indeed very heavy and all their interactions are highly suppressed. Their mass is then,

$$M_X = \sqrt{\frac{5}{6}}g_5M_{GUT}. \tag{5.26}$$

Although not directly observable, the X_μ fields allow baryon and lepton number violating interactions, which predicts proton decay, due to non diagonal terms in the full Lagrangian proportional to $\overline{L}X_\mu d$, $\bar{e}X_\mu Q$ and $\overline{Q}X_\mu u$. As an analogy, we can think of these interactions as for Feynman-Gell-Mann weak interactions [109], where the effective Lagrangian is given in terms of leptonic and hadronic currents J_μ as

$$\mathcal{L}_p = \frac{g_5^2}{M_X^2\sqrt{2}} J_\mu J^\mu. \tag{5.27}$$

In the theory of the weak interactions proposed by Feynman and Gell-Mann, it is possible to calculate the decay width of the muon as

$$\Gamma\left(\mu^- \to e^- \overline{\nu}_e \nu_\mu\right) = \frac{g_2^4}{192\pi^3}\frac{m_\mu^5}{M_W^4}, \tag{5.28}$$

which is suppressed by *four* powers of the electroweak scale. However, the calculation of the proton width is not so trivial as for weak interactions. At the proton mass scale, QCD is not perturbative, and calculations are done using *Lattice Gauge Theory*. However, and since a proton is made up by three quarks, *uud*, it is also rather challenging for a computer to perform the calculation. The proton width can be estimated using an analogy with the weak decay of the muon. We can then say that

$$\Gamma\left(p \to e^+\pi^0\right) \approx \frac{g_5^4}{192\pi^3}\frac{m_p^5}{M_X^4} = \frac{3}{400\pi^3}\frac{m_p^5}{M_{GUT}^4}. \tag{5.29}$$

The proton lifetime τ_p is then approximately predicted to be

$$\Gamma^{-1} \approx \frac{400\pi^3}{3}\frac{M_{GUT}^4}{m_p^5} \times 2.09 \times 10^{-32} \text{ yrs}. \tag{5.30}$$

The unification scale is defined to be the scale where the $SU(2)_L$ and $U(1)_Y$ gauge couplings meet $g_1 = g_2$. There are now two important distinct scenarios to consider: the first one is Grand Unification within the Standard Model, where from Fig. 2.3 we take that $M_{GUT} \approx 10^{13}$ GeV, and the second, is supersymmetric Grand Unification where, from Fig. 4.3 we take that $M_{GUT} \approx 2\times10^{16}$ GeV. Plugging these values in (5.30), and knowing that $m_p = 0.938$ GeV, we find

$$\Gamma^{-1}(SM) \approx 1.2\times10^{24}\text{yrs} \tag{5.31}$$

$$\Gamma^{-1}(SUSY) \approx 1.2\times10^{36}\text{yrs}. \tag{5.32}$$

Current limits constrain the proton lifetime to be above $\Gamma^{-1}_{p\to e^+\pi^0} > 8.2\times10^{33}$ yrs [125].

We see then that a Grand Unification scenario is, at least under an $SU(5)$ gauge symmetry with no further modification, ruled out for non-supersymmetric scenarios. The addition of extra fields pushes the GUT scale to higher values and a minimal supersymmetric $SU(5)$ GUT model ensures proton stability.

5.1.2. Doublet-Triplet Splitting Problem

As the reader might have noticed, there are extra fields that were not present in the MSSM before the $SU(5)$ embedding. We are obviously talking about the Higgs triplets T_u and T_d as well as their fermionic superpartners. Such fields are problematic since they not only spoil the unification of the gauge couplings, but also mediate fast proton decay through baryon number violating interactions [126–134]. The Yukawa interactions in the $SU(5)$ superpotential look like

$$W_y = \varepsilon_{\alpha\beta\gamma\rho\sigma}\,(y_{\mathbf{5}'})_{ij}\,\mathbf{10}_i^{\alpha\beta}\mathbf{10}_j^{\gamma\rho}\mathbf{5}'^{\sigma} + \left(y_{\overline{\mathbf{5}}'}\right)_{ij}\mathbf{10}_i^{\alpha\beta}\overline{\mathbf{5}}_{j\alpha}\overline{\mathbf{5}}'_{\beta}, \tag{5.33}$$

with i, j generation indices. Using (5.18) and (5.17) we may obtain cubic terms of the form $(y_{5'})_{ij}\,u_i^c e_j^c T_u$, $(y_{5'})_{ij}\,Q_i Q_j T_u$, $\left(y_{\overline{5}'}\right)_{ij} Q_i L_j \overline{T}_d$ and $\left(y_{\overline{5}'}\right)_{ij} u_i^c d_j^c \overline{T}_d$, which are allowed by the $SU(5)$ symmetry. Exchange of Higgs triplets leads once more to Fermi-like interactions of the type of the dimension-six operators

$$\frac{(y_{5'})_{ij}\left(y_{\overline{5}'}\right)_{kl}}{M_T^2}(Q_iQ_j)(Q_kL_l), \quad \frac{(y_{5'})_{ij}\left(y_{\overline{5}'}\right)_{kl}}{M_T^2}(u_i^c e_j^c)(u_k^c d_l^c), \tag{5.34}$$

where we can use (5.29) again to estimate the width of the triplet exchange interaction,

$$\Gamma\left(p \to e^+\pi^0\right) \approx \frac{(y_u y_d)^2}{192\pi^3}\frac{m_p^5}{M_T^4}. \tag{5.35}$$

Since nucleons are composed of first generation quarks, the Yukawa couplings are indeed those of the *up* and *down* quarks. In a supersymmetric model we see from (4.53) that

$$y_u y_d = 2\frac{m_u m_d}{v^2 \sin\beta\cos\beta} \approx 1.8\times10^{-8}. \tag{5.36}$$

for $\tan\beta = 30$ and with $v = 246$ GeV, $m_u = 3$ MeV and $m_d = 6$ MeV. Requiring the proton lifetime to be $\tau_p > 10^{31}$ yrs, we find a lower bound on the Higgs triplet mass of

$$M_T \gtrsim \left(\frac{\tau_p\, m_p^5\, (y_u y_d)^2}{192\pi^3\; 2.09\times10^{-32}}\right)^{\frac{1}{4}} = 6.6\times10^{10}\ \text{GeV}. \tag{5.37}$$

However, one should also consider the contribution from dimension-five operators of the form

$$O_5 = \frac{(y_{5'})_{ij}\left(y_{\bar{5}'}\right)_{kl}}{M_T}(Q_i\tilde{Q}_j)(Q_k\tilde{L}_l), \tag{5.38}$$

where the suppression factor is only proportional to one power of $1/M_T$. In order to estimate the constraint on the triplets mass arising from O_5, we need to further consider the exchange of gauge or Higgs fermions, transforming the scalars in its fermionic partners. Dressing loops convert dimension-five into effective dimension-six operators, which for the $p \to e^+\pi^0$ decay channel can be represented by

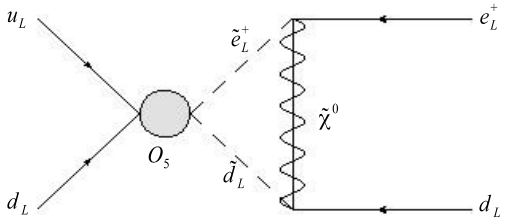

Figure 5.2. *Proton decay via dimension-five operators.*

The triangle diagram in figure 5.2 provides an extra contribution to the decay width of

$$\frac{2g'^2}{(4\pi)^2}f(m,M) \ , \tag{5.39}$$

with m the mass of the assumed degenerate superpartners and M the neutralino mass. Here we consider a Bino-dominated neutralino, and for the limit where $M \ll m$, eq. (5.39) takes the simple form

$$\frac{2g'^2}{(4\pi)^2}\frac{M}{m^2} = \frac{1}{256\pi}\frac{M}{m^2} \ , \tag{5.40}$$

see [135] for further details. With these ingredients we can estimate a lower bound for M_T of about

$$M_T \gtrsim \left(\frac{\tau_p\, m_p^5\, (y_u y_d)^2}{192\pi^3\; 2.09\times10^{-32}}\frac{M}{256\pi m^2}\right)^{\frac{1}{2}} = 4.3\times10^{17}\ \text{GeV}, \tag{5.41}$$

for $M = 200$ GeV and $m = 5000$ GeV. We therefore see that if we want to suppress dangerous nucleon decay, dimension-five operators allowed by supersymmetric interactions provide rather strong bounds on the triplets mass. Furthermore, if we relax the neutralino-scalar mass difference, this bound becomes even stronger. We know on the other hand that the $SU(2)_L$ Higgs doublets are significantly lighter with electroweak scale masses. It is then not understood why fields in the same $SU(5)$ multiplet, the up type doublets and triplets in the

$\mathbf{5}'$ irrep and the down type counterparts in the $\bar{\mathbf{5}}'$, have such a huge mass hierarchy. The difficulty in naturally keeping a heavy colour triplet and a light doublet in the same five-plet is the so called *doublet-triplet splitting problem*.

The extra triplets are excluded from the low scale theory. However, there is no obvious way of doing so in four dimensions. Some solutions have nonetheless been proposed, many of them involving model extension in higher dimensions [136–140]. As an example, if the model is embedded in a five dimensional orbifold [136], it is possible to assign odd parities to the Higgs triplets so that they become very heavy Kaluza-Klein excitations without zero modes. Therefore, they are removed from the *four* dimensional MSSM Lagrangian. The surviving fields are those of the MSSM and the doublet-triplet splitting problem is solved in a natural way.

5.1.3. Yukawa Coupling Unification

Besides matter unification, where quarks and leptons share common representations, and gauge coupling unification, the Yukawa interactions determined by W_y, eq. (5.33), provide another unified object in $SU(5)$ GUTs. Expanding (5.33) for the MSSM fields, we find

$$W_y = \varepsilon_{\alpha\beta}\left[(y_{5'})_{ij}\hat{\bar{u}}_{Rix}\hat{Q}^{\alpha x}_{Lj}\hat{H}^{\beta}_{u} - \left(y_{\bar{5}'}\right)_{ij}\hat{\bar{d}}_{Rix}\hat{Q}^{\alpha x}_{Lj}\hat{H}^{\beta}_{d} - \left(y_{\bar{5}'}\right)_{ij}\hat{\bar{e}}_{Ri}\hat{L}^{\alpha}_{Lj}\hat{H}^{\beta}_{d}\right]. \tag{5.42}$$

Consequently one obtains the unification condition $\mathbf{y}_e = \mathbf{y}_d^T$, which is basically telling us that the Yukawa couplings of the down type quarks and charged leptons are the same at the GUT scale. The renormalization group running of the Yukawa couplings yields different values at the low scale, but their ratio, and in particular the third generation one m_b/m_τ, can be predicted by this unification condition. However, this doesn't always happen and SUSY threshold corrections to the bottom mass may provide important contributions destroying the unification prediction [141]. The extension of this idea to lighter generations, foresees the unacceptable equality $m_s/m_d = m_\mu/m_e$. This unification picture usually refers only to the third generation and is called *bottom-tau Yukawa unification*. However, the condition $\mathbf{y}_e = \mathbf{y}_d^T$ is not necessarily unique. As it was discussed in [231, 250] (and references therein), group theoretical Clebsch-Gordan factors may arise from GUT symmetry breaking, altering the quark-lepton mass relations and providing plenty of new predictions for GUT scale Yukawa ratios. Particularly interesting is the prediction $y_\tau/y_b = 3/2$, which we may consider in chapters 8 and 9. Furthermore, these setups also fix Yukawa relations for lighter generations. An other possibility is embedding the model in $SO(10)$ GUTs.

5.2. $SO(10)$ Grand Unification

The rank *five* $SO(10)$ group, is the smallest gauge structure capable of accommodating all the SM fermions (and accompanying sfermions) of each generation in a single anomaly-free *sixteen* dimensional irrep **16**. Compared to $SU(5)$, this leaves room for an extra SM singlet which is identified with a right-handed neutrino (sneutrino) field. A $SO(10)$ GUT makes it possible to build the mass matrices of the Dirac and heavy Majorana neutrinos [142, 143], permits the determination of the charged fermion masses and mixing angles, and provides a seesaw mechanism [144–147], which remarkably predicts neutrino oscillations. In the minimal version, the two Higgs doublets of the MSSM are embedded in a single fundamental representation **10**.

5.2.1. Breaking Chains

The embedding of the $SO(10)$ representations in the SM gauge group is achieved by projecting the $SO(10)$ weights onto one of its maximal subgroups. The breaking chains to G_{SM} are either through $SU(5)\times U(1)$ (normal [148] or flipped [149–151] embedding), or through the Pati-Salam (PS) route $SU(4)\times SU(2)_L\times SU(2)_R$ [152]. Motivated by the running of the gauge couplings in the MSSM, Fig. 4.3, we consider here that this process is entirely carried out at the GUT scale or very close to it.

Let us start by considering the $SU(5)$ route,

$$SO(10) \xrightarrow{M_{GUT}} SU(5)\times U(1)_Z \xrightarrow{M_1\sim M_{GUT}} SU(3)\times SU(2)\times U(1)_X\times U(1)_Z \xrightarrow{M_2\sim M_1} G_{SM}, \quad (5.43)$$

where the branching rules at M_{GUT} for the **16** and **10** plets are

$$\mathbf{16} \rightarrow \mathbf{1}_{-5}\oplus\bar{\mathbf{5}}_{3}\oplus\mathbf{10}_{-1}, \quad (5.44)$$

$$\mathbf{10} \rightarrow \mathbf{5}_{2}\oplus\bar{\mathbf{5}}_{-2}, \quad (5.45)$$

with the subscript indices the $U(1)_Z$ hypercharge, and at M_1

$$\mathbf{1} \rightarrow (\mathbf{1},\mathbf{1})_0, \quad (5.46)$$

$$\mathbf{5} \rightarrow (\mathbf{1},\mathbf{2})_3\oplus(\mathbf{3},\mathbf{1})_{-2}, \quad (5.47)$$

$$\bar{\mathbf{5}} \rightarrow (\mathbf{1},\mathbf{2})_{-3}\oplus\left(\bar{\mathbf{3}},\mathbf{1}\right)_2, \quad (5.48)$$

$$\mathbf{10} \rightarrow (\mathbf{1},\mathbf{1})_6\oplus\left(\bar{\mathbf{3}},\mathbf{1}\right)_{-4}\oplus(\mathbf{3},\mathbf{2})_1. \quad (5.49)$$

where the subscript indicates the $U(1)_X$ Abelian charge. The field embeddings are identified in the same way as we did for $SU(5)$ with the addition of a right-handed neutrino field as a $(\mathbf{1},\mathbf{1})_0$ SM singlet. Both the $U(1)$ generators are in the Cartan subalgebra of $SO(10)$ and its axes

are orthogonal in a *five* dimensional Euclidean space. The weak hypercharge generator Y is then a linear combination of the $U(1)_X$ and $U(1)_Z$ generators, $U(1)_Y \subset U(1)_X \times U(1)_Z$, therefore, Y as well as $Y^\perp$, the $U(1)$ generator of $SO(10)$ that is orthogonal to the G_{SM} generators, are, for the Georgi-Glashow (GG) embedding [148], given by

$$Y = X \tag{5.50}$$
$$Y^\perp = -Z \tag{5.51}$$

Here, the X and Z charges as well as the decomposition rules were taken from Slansky [124].

For the flipped-$SU(5)$ route [149, 150], we can calculate the Y generator by demanding that it is a linear combination of the X and Z generators of the form

$$Y = aX + bZ. \tag{5.52}$$

Taking for example that for Q we have $Z = -1$, $X = 1$ and $Y = 1$, and that for $\bar{e}_R$ we have $Z = -5$, $X = 0$ and $Y = 6$, we can solve a linear system and deduce that

$$a = -\frac{1}{5} \tag{5.53}$$
$$b = -\frac{6}{5}. \tag{5.54}$$

The next step is to calculate the orthogonal generator $Y^\perp$. Here we use the same normalization as in [150], i.e.

$$Q_Z = \frac{1}{\sqrt{40}} Z\mathcal{N} \tag{5.55}$$
$$Q_X = \sqrt{\frac{3}{5}} X\mathcal{N}, \tag{5.56}$$

with $\mathcal{N}$ a normalization constant. Charge orthogonality requires that

$$\begin{pmatrix} Q_\theta \\ Q_\theta^\perp \end{pmatrix} = \begin{pmatrix} \cos\theta & \sin\theta \\ -\sin\theta & \cos\theta \end{pmatrix} \begin{pmatrix} Q_X \\ Q_Z \end{pmatrix}, \tag{5.57}$$

from where we find that $\theta = \arctan\sqrt{\frac{2}{3}}$ for a and b given as in (5.53) and (5.54). The $Y^\perp$ axes can now be obtained from (5.57), and the hypercharge generator as well as the $U(1)$ generator of $SO(10)$ orthogonal to G_{SM} takes the form

$$Y = -\frac{1}{5}(X + 6Z) \tag{5.58}$$
$$Y^\perp = -\frac{1}{5}(-Z + 4X). \tag{5.59}$$

In practice, if we explicitly write down the charges, the flipped (FL) embedding corresponds to swapping $\hat{u}_R^\dagger$ with $\hat{d}_R^\dagger$ and $\hat{e}_R^\dagger$ with $\hat{N}_R^\dagger$ in the GG identification.

For the Pati-Salam (PS) route [152],

$$\begin{aligned} &SO(10) \xrightarrow{M_{GUT}} SU(4)\times SU(2)_L \times SU(2)_R \xrightarrow{M_1 \sim M_{GUT}} \\ &SU(3)\times SU(2)_L \times SU(2)_R \times U(1)_W \xrightarrow{M_2 \sim M_1} G_{SM}, \end{aligned} \tag{5.60}$$

the decomposition of the **16** and **10** plets after the breaking of $SO(10)$ at M_{GUT} are

$$\mathbf{16} \rightarrow (\mathbf{4},\mathbf{2},\mathbf{1}) \oplus \left(\overline{\mathbf{4}},\mathbf{1},\mathbf{2}\right), \tag{5.61}$$

$$\mathbf{10} \rightarrow (\mathbf{1},\mathbf{2},\mathbf{2}) \oplus (\mathbf{6},\mathbf{1},\mathbf{1}), \tag{5.62}$$

where we can identify

$$(\mathbf{4},\mathbf{2},\mathbf{1}) = \begin{pmatrix} \hat{u}^x & \hat{\nu} \\ \hat{d}^x & \hat{e} \end{pmatrix}_L \tag{5.63}$$

$$\left(\overline{\mathbf{4}},\mathbf{1},\mathbf{2}\right) = \begin{pmatrix} \hat{d}_x^\dagger & \hat{e}^\dagger \\ \hat{u}_x^\dagger & \hat{N}^\dagger \end{pmatrix}_R \tag{5.64}$$

for matter fields, where $x = 1,2,3$ is a colour index, and

$$(\mathbf{1},\mathbf{2},\mathbf{2}) = \begin{pmatrix} \hat{h}_u^+ & \hat{h}_d^0 \\ \hat{h}_u^0 & \hat{h}_d^- \end{pmatrix}, \tag{5.65}$$

for the Higgs fields. We see from this prescription that we can interpret leptons as part of a four colour quark, unified in **4**-plets of $SU(4)$. The decomposition rules under the breaking at M_1 for the relevant fields are given as

$$(\mathbf{4},\mathbf{2},\mathbf{1}) \rightarrow (\mathbf{1},\mathbf{2},\mathbf{1})_3 \oplus (\mathbf{3},\mathbf{2},\mathbf{1})_{-1}, \tag{5.66}$$

$$\left(\overline{\mathbf{4}},\mathbf{1},\mathbf{2}\right) \rightarrow (\mathbf{1},\mathbf{1},\mathbf{2})_{-3} \oplus (\mathbf{3},\mathbf{1},\mathbf{2})_1, \tag{5.67}$$

$$(\mathbf{1},\mathbf{2},\mathbf{2}) \rightarrow (\mathbf{1},\mathbf{2},\mathbf{2})_0, \tag{5.68}$$

where the right-handed fields are grouped in $SU(2)_R$ doublets with right-isospin $\mathcal{I}_R = 1/2$ and eigenvalues $\mathcal{I}_{3R} = \pm 1/2$. Comparing the PS and the $SU(5)$ embeddings of the fields, we can express the Z and X generators in terms of $\mathcal{I}_{3R}$ and W:

$$Z = -4\mathcal{I}_{3R} + W, \tag{5.69}$$

$$X = -6\mathcal{I}_{3R} - W. \tag{5.70}$$

The hypercharge generator is distinct from the $U(1)_W$ generator and orthogonal to both the $SU(3)$ and $SU(2)_L$ generators. Therefore $U(1)_Y$ is not orthogonal to $SU(2)_R$ but instead, Y is a linear combination of the $U(1)_W$ and $SU(2)_R$ generators. At this stage, we have freedom for $SU(2)_R$ rotations in a plane perpendicular to the $U(1)_W$ axes. However, once fixing Y we will also fix the $SU(2)_R$ axes eliminating this freedom. The GG and FL hypercharge assignments in (5.50) and (5.58) respectively can be written as

$$Y_{GG} = -6\mathcal{I}_{3R} - W, \tag{5.71}$$

$$Y_{FL} = 6\mathcal{I}_{3R} - W, \tag{5.72}$$

where the flipped assignment is achieved after a π rotation in $SU(2)_R$. On the other hand, the orthogonal generators are expressed as

$$Y^{\perp}_{GG} = 4\mathcal{I}_{3R} - W, \tag{5.73}$$

$$Y^{\perp}_{FL} = 4\mathcal{I}_{3R} + W. \tag{5.74}$$

5.2.2. Yukawa Couplings and Higgs Representations

We have so far seen that in its minimal version, $SO(10)$ predicts full matter unification in a **16** irrep and full Higgs unification in a fundamental **10**. This prescription allows a single Yukawa term in the superpotential of the form

$$W_y = \mathbf{y}_{10}\mathbf{16}\cdot\mathbf{16}\cdot\mathbf{10}, \tag{5.75}$$

and if the third generation charged fermions obtain their masses entirely from Yukawa interactions involving exclusively the Higgs 10-plet, it is possible to achieve top-bottom-tau Yukawa unification (t-b-τ YU) [153–157]. However, this prescription fails to predict the correct fermion masses and mixings if we do not extend the Higgs sector.

One possible way of extending the Higgs sector can be understood by considering the tensor product of two **16**,

$$\mathbf{16}\times\mathbf{16} = \mathbf{10}_s \oplus \mathbf{120}_a + \mathbf{126}. \tag{5.76}$$

In order to find suitable Higgs representations **R**, the products $\mathbf{R}\times\mathbf{120}$ and $\mathbf{R}\times\mathbf{126}$ have to be singlets. The only possibilities here are $\overline{\mathbf{126}}$ and **120** Higgs. Although t-b-τ YU may be spoiled with the addition of extra fields, realistic charged fermions and neutrino masses can be obtained if we assume that the MSSM Higgs doublets $H_{u,d}$ are a superposition of the different components that reside in distinct $SO(10)$ representations [158]. If one wishes to preserve t-b-τ YU alongside with correct fermion masses, the contributions to $H_{u,d}$ from the

extra Higgs fields have to be sub-dominant, see [159] and references therein. On the other hand, if those contributions are sizable, we can still have top-bottom-tau quasi-Yukawa unification (QYU) as it was investigated in [160].

The presence of large representations in a $SO(10)$ GUT introduces extra colour triplet fields and thereby new higher dimensional operators contributing to proton decay. In [161], it is shown that such operators predict a proton lifetime evading the experimental bounds. For models compatible with a type-I seesaw mechanism, the heavy neutrino scale is kept rather large such that we do not need to worry about the running of the right-handed sneutrino soft mass. However, if we rely on a model where the MSSM is extended by three purely Dirac-type right-handed (s)neutrinos, the lightestst may become a cold dark matter (CDM) candidate [163–166]. In Chapter 7, we will assume a heavy Majorana mass term compatible with a type-I seesaw mechanism that protects the right-handed sneutrinos from acquiring large masses, allowing them to be viable CDM candidates.

5.3. E_6 Grand Unification

The unification under the exceptional E_6 gauge symmetry, which is well inspired by *String Theory*, is a natural extension of the $SO(10)$ ideas. The fundamental representation of this rank *six* group is a **27**-plet, where matter-Higgs unification is possible. In other words, we can embed the **16** and the **10** of $SO(10)$ in the **27**, still leaving space for an extra singlet. One of the most popular constructions inspired by an E_6 gauge symmetry is the so called *Exceptional Supersymmetric Standard Model* (E_6SSM) [167–174]. One of the maximal subalgebras of E_6 is $SO(10)\times U(1)$, and the braking chain down to the SM, is, like the previous examples, realized at the GUT scale by

$$E_6 \xrightarrow{M_{GUT}} SO(10)\otimes U(1)_\psi \xrightarrow{M1\sim M_{GUT}} SU(5)\otimes U(1)_\chi \xrightarrow{M2\sim M_1} G_{SM}\times U(1)_N, \tag{5.77}$$

where $U(1)_\psi$ and $U(1)_\chi$ are orthogonal and mix as in eq. (5.57) yielding the additional $U(1)_N$. The particular choice of $U(1)_N$ remaining at low energies is such that only the right-handed (s)neutrino is left neutral allowing it to naturally maintain a high mass, thereby facilitating the see-saw mechanism for neutrino masses. The branching rules at M_{GUT} are

$$\mathbf{27} \to \left(\mathbf{1}; \frac{4}{2\sqrt{6}}\right) \oplus \left(\mathbf{10}; \frac{-2}{2\sqrt{6}}\right) \oplus \left(\mathbf{16}; \frac{1}{2\sqrt{6}}\right), \tag{5.78}$$

and at M_1

$$\mathbf{1} \rightarrow \left(\mathbf{1}; \frac{1}{2\sqrt{10}}\right), \tag{5.79}$$

$$\mathbf{10} \rightarrow \left(\mathbf{5}; \frac{2}{2\sqrt{10}}\right) \oplus \left(\overline{\mathbf{5}}; \frac{-2}{2\sqrt{10}}\right), \tag{5.80}$$

$$\mathbf{16} \rightarrow \left(\mathbf{10}; \frac{-1}{2\sqrt{10}}\right) \oplus \left(\overline{\mathbf{5}}; \frac{3}{2\sqrt{10}}\right) \oplus \left(\mathbf{1}; \frac{-5}{2\sqrt{10}}\right). \tag{5.81}$$

With the Q_ψ and Q_χ charges above, the Q_N charge is calculated demanding that $Q_\theta\left(\overline{N}_e\right) = 0$, yielding

$$\theta = \arctan\sqrt{15} \Longrightarrow \mathbf{Q_N} = \frac{\mathbf{1}}{\mathbf{4}}\mathbf{Q}_\chi + \frac{\sqrt{15}}{\mathbf{4}}\mathbf{Q}_\psi. \tag{5.82}$$

With this new charge assignment, the branching of a **27** to $SU(5)\times U(1)_N$ takes the form

$$\mathbf{27} \rightarrow \mathbf{10}_1 \oplus \overline{\mathbf{5}}_2 \oplus \overline{\mathbf{5}}_{-3} \oplus \mathbf{5}_{-2} \oplus \mathbf{1}_5 \oplus \mathbf{1}_0, \tag{5.83}$$

where the $U(1)_N$ charge is normalized as $\sqrt{40}Q_N$. With the description of $SU(5)$ that we introduced earlier, we can identify here ordinary matter as well as new exotic matter, which is allowed at low energy due to the protection of $U(1)_N$. The charges of the quark and lepton superfields are

$$\mathbf{10}_1 \rightarrow (\mathbf{3},\mathbf{2})_{\frac{1}{3},1} \oplus \left(\overline{\mathbf{3}},\mathbf{1}\right)_{-\frac{4}{3},1} \oplus (\mathbf{1},\mathbf{1})_{2,1} = Q_L \oplus \overline{u}_R \oplus \overline{e}_R \tag{5.84}$$

$$\overline{\mathbf{5}}_2 \rightarrow (\mathbf{1},\mathbf{2})_{-1,2} \oplus \left(\overline{\mathbf{3}},\mathbf{1}\right)_{\frac{2}{3},2} = L_L \oplus \overline{d}_R \tag{5.85}$$

$$\mathbf{1}_0 \rightarrow (\mathbf{1},\mathbf{1})_{0,0} = \overline{N}_R, \tag{5.86}$$

whereas for the Higgs and exotics we have

$$\overline{\mathbf{5}}_{-3} \rightarrow (\mathbf{1},\mathbf{2})_{-1,-3} \oplus \left(\overline{\mathbf{3}},\mathbf{1}\right)_{\frac{2}{3},-3} = H_d \oplus \overline{T}_d \tag{5.87}$$

$$\mathbf{5}_{-2} \rightarrow (\mathbf{1},\mathbf{2})_{1,-2} \oplus (\mathbf{3},\mathbf{1})_{-\frac{2}{3},-2} = H_u \oplus T_u \tag{5.88}$$

$$\mathbf{1}_5 \rightarrow (\mathbf{1},\mathbf{1})_{0,5} = S. \tag{5.89}$$

The S field is a Higgs singlet that is responsible for the breaking of the $U(1)_N$ at the SUSY scale, generating an effective μ-term in the E_6SSM.

In order to preserve gauge coupling unification, two additional $SU(2)_L$ doublets, H' and $\overline{H}'$ are required. These are presumed to arise from incomplete **27′** and $\overline{\mathbf{27}}'$ irreps respectively and lead to a doublet-25plet splitting problem similar to the doublet-triplet splitting problem

that we can find both in $SU(5)$ and $SO(10)$ GUTs. The Higgs fields are now embedded in the **27**-plet, so three generations of Higgs are required (as well as an additional singlet Higgs for each generation), though only the third generation Higgs gain vevs. This latter requirement is arranged using an approximate Z_2^H symmetry, and additional Z_2^B or Z_2^L symmetries may be invoked to prevent Flavour Changing Neutral Currents. The theory gives rise to a distinctive low energy spectrum [169–174], which includes exotic fermions, extra gauginos, such as a Higgsino singlet $\tilde{S}$ and a $U(1)_N$ bino, and a new Z' boson which gets its mass when the $U(1)_N$ symmetry is broken by the $\langle S \rangle$ vev. Altogether, the E_6SSM may provide a vast and interesting phenomenology for the LHC.

6. Constraining Grand Unification using the First and Second Generation Sfermions

Most of the investigations of the MSSM have been in the context of the *constrained* Minimal Supersymmetric Standard Model (cMSSM, see [58] for a review), where the soft supersymmetry breaking parameters are universal at the scale where the gauge couplings unify. Besides $\tan\beta$ and $sign(\mu)$, which are fixed by the EWSB conditions, the boundary conditions of the cMSSM at the GUT scale are parametrized by a common soft scalar mass, m_0, a common gaugino mass, $M_{1/2}$, and a common trilinear coupling a_0. Yet, this choice of input parameters is not inspired by any Grand unification scenario and the cMSSM, by itself, does not provide any explanation for the G_{SM} gauge structure. It is however possible to impose some unified symmetry at the high scale, which may constrain the soft supersymmetry breaking parameters differently from the cMSSM.

Recent searches for squarks and gluinos at the Large Hadron Collider (LHC) [105, 106] have greatly constrained the parameter space of low energy supersymmetry. These searches have however been mostly inspired by the cMSSM. Within this framework, the experiments find that squarks must be heavier than about 1.5 TeV and gluinos above about 850 GeV to remain unobserved at the LHC.

While these results certainly put pressure on the cMSSM, there is still plenty of room for the discovery of supersymmetry at the LHC, particularly if one is willing to allow supersymmetry to have a relatively heavy spectrum. The desire to keep the supersymmetric spectrum light is driven by the desire for supersymmetry to be the solution of the hierarchy problem, using top squark loops to cancel the quadratic divergence of the Higgs mass arising from top quark loops. The remaining uncancelled logarithmic divergence will again require fine tuning if the stops become too heavy. Of course, this left over *little hierarchy problem* is still vastly less problematic than the required fine tuning of the Standard Model (SM) Higgs sector. Furthermore, searches for the third generation squarks remain relatively weak [175–177]. One could imagine a supersymmetric model where the first two generations are relatively heavy, avoiding the current LHC constraints, but the third generation is still rather light, diluting the required fine tuning. Indeed, such a scenario is perfectly reasonable even for GUT constrained supersymmetry, which has no *a priori* requirement for a common

supersymmetry breaking mass scale across the generations. While vastly differing scales would be difficult to generate using the same mechanism, hierarchies of a few orders of magnitude should not be surprising (and are present already in the SM masses).

Irrespective of the details of the mass spectrum, it is still not unreasonable to suppose that our first sight of supersymmetry will be the discovery of squarks and gluinos with masses of a few TeV. If a hierarchy between the generations does exist, the exclusion limits set by the LHC would be weakened [178] since only one generation of squarks could be available to produce instead of two. If this generation were the second generation (that is, an inverted hierarchy with the undetected third generation the lightest and the first generation the heaviest) the limits would be further reduced since one could not rely on the valence content of the proton to enhance squark production. After such a discovery, our task will be to examine the supersymmetric spectrum in detail, determine the underlying mechanism for supersymmetry breaking and hopefully build a new theory that explains some of the unanswered questions of the SM.

It is expected that the underlying gauge structure should leave an imprint on the low scale mass spectrum. In this chapter, we will examine how we may determine, or constrain, this choice of the underlying group using only the first or second generation of squarks and sleptons, and the accompanying gauge sector. To do this, we will use the RGEs for the first and second generations, which allows us to neglect Yukawa couplings and analytically integrate the one-loop RGEs. When we have a unification group of rank higher than four (the rank of the SM gauge group), the breaking mechanism generates extra D-term contributions to the soft SUSY breaking scalar masses [179]. This is the case of $SO(10)$ and E_6 and these D-terms will be included in our analysis.

6.1. Integration of the Renormalization Group Equations

The RGEs for the sfermion masses in the MSSM [180–187], to one-loop accuracy, are

$$16\pi^2 \frac{dm^2_{\tilde{Q}_L}}{dt} = (X_t + X_b) - \frac{32}{3} g_3^2 M_3^2 - 6 g_2^2 M_2^2 - \frac{2}{15} g_1^2 M_1^2 + \frac{1}{5} g_1^2 S, \tag{6.1}$$

$$16\pi^2 \frac{dm^2_{\tilde{u}_R}}{dt} = (2X_t) - \frac{32}{3} g_3^2 M_3^2 - \frac{32}{15} g_1^2 M_1^2 - \frac{4}{5} g_1^2 S, \tag{6.2}$$

$$16\pi^2 \frac{dm^2_{\tilde{d}_R}}{dt} = (2X_b) - \frac{32}{3} g_3^2 M_3^2 - \frac{8}{15} g_1^2 M_1^2 + \frac{2}{5} g_1^2 S, \tag{6.3}$$

$$16\pi^2 \frac{dm^2_{\tilde{L}_L}}{dt} = (X_\tau) - 6 g_2^2 M_2^2 - \frac{6}{5} g_1^2 M_1^2 - \frac{3}{5} g_1^2 S, \tag{6.4}$$

$$16\pi^2 \frac{dm^2_{\tilde{\tau}_R}}{dt} = (2X_\tau) - \frac{24}{5} g_1^2 M_1^2 + \frac{6}{5} g_1^2 S, \tag{6.5}$$

and for the Higgs masses,

$$16\pi^2 \frac{dm^2_{H_d}}{dt} = 3X_b + X_\tau - 6 g_2^2 M_2^2 - \frac{6}{5} g_1^2 M_1^2 - \frac{3}{5} g_1^2 S, \tag{6.6}$$

$$16\pi^2 \frac{dm^2_{H_u}}{dt} = 3X_t + X_\tau - 6 g_2^2 M_2^2 - \frac{6}{5} g_1^2 M_1^2 + \frac{3}{5} g_1^2 S, \tag{6.7}$$

where the terms in brakets in eq. (6.1) to (6.5) are proportional to the Yukawa couplings and given as

$$X_t = 2y_t^2 \left(m^2_{H_u} + m^2_{\tilde{Q}_3} + m^2_{\tilde{t}_R} \right) + 2a_t^2 \tag{6.8}$$

$$X_b = 2y_b^2 \left(m^2_{H_d} + m^2_{\tilde{Q}_3} + m^2_{\tilde{b}_R} \right) + 2a_b^2 \tag{6.9}$$

$$X_\tau = 2y_\tau^2 \left(m^2_{H_d} + m^2_{\tilde{L}_3} + m^2_{\tilde{\tau}_R} \right) + 2a_\tau^2. \tag{6.10}$$

Due to the smallness of the Yukawa couplings for the first two generations, we neglect the (6.8), (6.9) and (6.10) terms in the RGEs for the sfermion masses of the first and second families. Here $t \equiv \log(Q/Q_0)$, with Q the energy scale of interest and Q_0 the unification scale, for which we will use $Q_0 = 1.9 \times 10^{16}\,\text{GeV}$ throughout. $M_{1,2,3}$ are the gaugino masses corresponding to the usual $g_{1,2,3}$ gauge couplings, with RGEs

$$8\pi^2 \frac{dM_i}{dt} = b_i g_i^2 M_i, \tag{6.11}$$

and b_i given as in (4.87). S is only non-zero if the sfermion masses are not universal at the GUT scale; it is given by [188–193]

$$S \equiv Tr(Ym^2) = m_{H_u}^2 - m_{H_d}^2 + \sum_{\text{generations}} \left(m_{\tilde{Q}_L}^2 - 2m_{\tilde{u}_R}^2 + m_{\tilde{d}_R}^2 - m_{\tilde{L}_L}^2 + m_{\tilde{e}_R}^2 \right). \tag{6.12}$$

Notice that the sum over generations results in S also depending on the third generation soft scalar masses, and therefore implicitly on the third generation Yukawa couplings, which cannot be neglected. However, when constructing the evolution equation for S from the above definition, one finds that these Yukawa couplings cancel (for the same reason that the gravitational anomaly cancels), so an analytic solution is still possible. Indeed, only terms proportional to S itself survive and one finds

$$\frac{dS}{dt} = \frac{66}{5}\frac{\alpha_1}{4\pi}S \quad \Rightarrow \quad S(t) = S_0 \frac{\alpha_1(t)}{\alpha_1(0)}. \tag{6.13}$$

Here $S_0 \equiv S(0)$ is the value of S at the GUT scale and $\alpha_1 = g_1^2/4\pi$ as usual.

The absence of Yukawa and trilinear couplings allows equations (6.1) to (6.5) to be solved analytically. Furthermore, since only gauge interactions contribute to the running, if the sfermion squared mass-matrices are flavour-blind at the input scale, the squared masses of the gauge-eigenstates for the first two generations will remain diagonal at the supersymmetry breaking scale, with nearly degenerate left/right masses given by eq. (4.69). The solution of equations (6.1) to (6.5) is given by [188]

$$\begin{aligned}
m_{\tilde{u}_L}^2(t) &= m_{\tilde{Q}_L}^2(0) + C_3 + C_2 + \frac{1}{36}C_1 + \Delta_{u_L} - \frac{1}{5}K, && (6.14)\\
m_{\tilde{d}_L}^2(t) &= m_{\tilde{Q}_L}^2(0) + C_3 + C_2 + \frac{1}{36}C_1 + \Delta_{d_L} - \frac{1}{5}K, && (6.15)\\
m_{\tilde{u}_R}^2(t) &= m_{\tilde{u}_R}^2(0) + C_3 + \frac{4}{9}C_1 + \Delta_{u_R} + \frac{4}{5}K, && (6.16)\\
m_{\tilde{d}_R}^2(t) &= m_{\tilde{d}_R}^2(0) + C_3 + \frac{1}{9}C_1 + \Delta_{d_R} - \frac{2}{5}K, && (6.17)\\
m_{\tilde{e}_L}^2(t) &= m_{\tilde{L}_L}^2(0) + C_2 + \frac{1}{4}C_1 + \Delta_{e_L} + \frac{3}{5}K, && (6.18)\\
m_{\tilde{\nu}_L}^2(t) &= m_{\tilde{L}_L}^2(0) + C_2 + \frac{1}{4}C_1 + \Delta_{\nu_L} + \frac{3}{5}K, && (6.19)\\
m_{\tilde{e}_R}^2(t) &= m_{\tilde{e}_R}^2(0) + C_1 + \Delta_{e_R} - \frac{6}{5}K, && (6.20)
\end{aligned}$$

where we have

$$C_i(t) = M_i^2(0)\left[A_i \frac{\alpha_i^2(0) - \alpha_i^2(t)}{\alpha_i^2(0)}\right] \equiv M_i^2(0)\bar{c}_i(t), \quad i = \{1,2,3\}, \tag{6.21}$$

with

$$A_i = \left\{\frac{2}{11}, \frac{3}{2}, -\frac{8}{9}\right\}, \tag{6.22}$$

and

$$K(t) = \frac{1}{2b_1} S_0 \left(1 - \frac{\alpha_1(t)}{\alpha_1(0)}\right), \tag{6.23}$$

where $b_1 = 33/5$. The equivalence in equation (6.21) defines $\bar{c}_i(t)$. Since the squared mass-matrices of the squarks and sleptons in the gauge-eigenstate basis is diagonal for the first two generations, equations (6.14) to (6.20) represent the approximate physical masses.

The form of equations (6.14) to (6.20) immediately allows one to write down some simple sum rules relating the running sfermion masses that are independent of the specific GUT boundary conditions. For example,

$$m^2_{\tilde{u}_L} - m^2_{\tilde{d}_L} = m^2_{\tilde{e}_L} - m^2_{\tilde{\nu}_L} = M_Z^2(1 - \sin^2\theta_W)\cos 2\beta. \tag{6.24}$$

Since the right hand side of this equation is rather small, this also tells us that the left handed squarks and left handed sleptons will, separately, be approximately degenerate. Two other useful sum rules are

$$m^2_{\tilde{u}_L} + m^2_{\tilde{d}_L} - m^2_{\tilde{u}_R} - m^2_{\tilde{e}_R} = C_3 + 2C_2 - \frac{25}{18}C_1 \approx 4.8 M^2_{1/2}, \tag{6.25}$$

and

$$\frac{1}{2}\left(m^2_{\tilde{u}_L} + m^2_{\tilde{d}_L} - m^2_{\tilde{e}_L} - m^2_{\tilde{\nu}_L}\right) + m^2_{\tilde{d}_R} - m^2_{\tilde{e}_R} = 2C_3 - \frac{10}{9}C_1 \approx 8.1 M^2_{1/2}. \tag{6.26}$$

The left equality in equations (6.25) and (6.26) are independent of the GUT scale boundary conditions and true for all values of t. However, the right equality is assuming the boundary condition $M_1(0) = M_2(0) = M_3(0) = M_{1/2}$ and the values for C_i were obtained at a scale $Q = 1\,\text{TeV}$.

6.2. Boundary Conditions

We will now consider the effect of fixing boundary conditions at the GUT scale according to the GUT groups $SU(5)$, $SO(10)$ and E_6.

6.2.1. SU(5)

We first consider an $SU(5)$ supersymmetric GUT, breaking directly to $SU(3)\times SU(2)_L \times U(1)$ at the GUT scale, Q_0. Under this gauge group, all the SM fermions as well as their scalar partners are embedded in a $\mathbf{10}\oplus\bar{\mathbf{5}}$ dimensional representation, where $\tilde{L}_L$ and $\tilde{d}_R$ are in the $\bar{\mathbf{5}}$, and $\tilde{Q}_L$, $\tilde{u}_R$ and $\tilde{e}_R$ are in the $\mathbf{10}$. With this construction we do not have a universal scalar mass

m_0 at the GUT scale, as in the cMSSM, but instead have a common $m_{\mathbf{10}}$ for the matter in the 10-plet and a common $m_{\bar{\mathbf{5}}}$ for the matter in the 5-plet. For the minimal $SU(5)$ supersymmetric GUT, the Higgs fields H_u and H_d belong to two distinct five-dimensional representations, $\mathbf{5}'$ and $\bar{\mathbf{5}}'$ respectively, so their masses at the GUT scale are unrelated. For the gaugino mass, we consider the simplest scenario, where the chiral superfields in the gauge-kinetic function (3.60) are in a singlet representation of $SU(5)$ [194–196]. We then have a common gaugino mass, $M_{1/2}$, at the GUT scale. Leaving the doublet-triplet splitting problem aside, as we discussed in section 5.1.2, our boundary conditions are:

$$m^2_{\tilde{Q}_L}(0) = m^2_{\tilde{u}_R}(0) = m^2_{\tilde{e}_R}(0) = m^2_{\mathbf{10}}, \tag{6.27}$$

$$m^2_{\tilde{d}_R}(0) = m^2_{\tilde{L}_L}(0) = m^2_{\bar{\mathbf{5}}}, \tag{6.28}$$

$$m^2_{H_u}(0) = m^2_{\mathbf{5}'}, \tag{6.29}$$

$$m^2_{H_d}(0) = m^2_{\bar{\mathbf{5}}'}, \tag{6.30}$$

$$M_1^2(0) = M_2^2(0) = M_3^2(0) = M^2_{1/2}\ , \tag{6.31}$$

where the superpartner masses are running $\overline{\text{DR}}$ masses. Note that inserting equations (6.27) to (6.30) into equation (6.12), we find $S_0 = m^2_{\bar{\mathbf{5}}'} - m^2_{\bar{\mathbf{5}}} \neq 0$, so K, as defined by equation (6.23) does not vanish at the EW scale. Considering only the sfermion sector, we have five unknowns, $m_{\bar{\mathbf{5}}}$, $m_{\mathbf{10}}$, $M_{1/2}$, $\cos 2\beta$ and K, and seven equations, (6.14) to (6.20), that relate these unknowns to (in principle) measurable scalar masses. If we know the EW scale mass of five sfermions, say $\tilde{u}_L$, $\tilde{d}_L$, $\tilde{e}_R$, $\tilde{u}_R$ and $\tilde{d}_R$, we have an invertible system of equations and can fully determine our five parameters.

$$\begin{pmatrix} M^2_{\tilde{u}_L} \\ M^2_{\tilde{d}_L} \\ M^2_{\tilde{e}_R} \\ M^2_{\tilde{u}_R} \\ M^2_{\tilde{d}_R} \end{pmatrix} = \begin{pmatrix} 0 & 1 & c_{\tilde{u}_L} & \delta_{\tilde{u}_L} & -\frac{1}{5} \\ 0 & 1 & c_{\tilde{d}_L} & \delta_{\tilde{d}_L} & -\frac{1}{5} \\ 0 & 1 & c_{\tilde{e}_R} & \delta_{\tilde{e}_R} & -\frac{6}{5} \\ 0 & 1 & c_{\tilde{u}_R} & \delta_{\tilde{u}_R} & \frac{4}{5} \\ 1 & 0 & c_{\tilde{d}_R} & \delta_{\tilde{d}_R} & -\frac{2}{5} \end{pmatrix} \begin{pmatrix} m^2_{\bar{\mathbf{5}}} \\ m^2_{\mathbf{10}} \\ M^2_{1/2} \\ \cos 2\beta \\ K \end{pmatrix}. \tag{6.32}$$

In this equation, and throughout the rest of the chapter, we have used a capital M to denote the measured low energy masses, e.g. $M_{\tilde{u}_L} = m_{\tilde{u}_L}(M_{\tilde{u}_L})$. Also, we have defined

$$\Delta_\varphi \equiv \delta_\varphi \cos 2\beta, \qquad (\varphi = \tilde{u}_L, \tilde{d}_L, \tilde{e}_R, \tilde{u}_R, \tilde{d}_R) \tag{6.33}$$

$$c_{\tilde{u}_L} \equiv \bar{c}_3(M_{\tilde{u}_L}) + \bar{c}_2(M_{\tilde{u}_L}) + \frac{1}{36}\bar{c}_1(M_{\tilde{u}_L}), \tag{6.34}$$

$$c_{\tilde{d}_L} \equiv \bar{c}_3(M_{\tilde{d}_L}) + \bar{c}_2(M_{\tilde{d}_L}) + \frac{1}{36}\bar{c}_1(M_{\tilde{d}_L}), \tag{6.35}$$

$$c_{\tilde{e}_R} \equiv \bar{c}_1(M_{\tilde{e}_R}), \tag{6.36}$$

$$c_{\tilde{u}_R} \equiv \bar{c}_3(M_{\tilde{u}_R}) + \frac{4}{9}\bar{c}_1(M_{\tilde{u}_R}), \tag{6.37}$$

$$c_{\tilde{d}_R} \equiv \bar{c}_3(M_{\tilde{d}_R}) + \frac{1}{9}\bar{c}_1(M_{\tilde{d}_R}). \tag{6.38}$$

The explicit solutions determining $m_{\bar{\mathbf{5}}}$, $m_{\mathbf{10}}$, $M_{1/2}$, $\cos 2\beta$ and K as function of the low energy masses are then

$$\begin{aligned} m_{\bar{5}}^2 &= \frac{1}{5X_5}\Big[(c_{\tilde{u}_L}+c_{\tilde{d}_L})(M_{\tilde{u}_R}^2+5M_{\tilde{d}_R}^2-M_{\tilde{e}_R}^2)-c_{\tilde{u}_R}(M_{\tilde{u}_L}^2+M_{\tilde{d}_L}^2+5M_{\tilde{d}_R}^2-2M_{\tilde{e}_R}^2) \\ &\quad -5c_{\tilde{d}_R}(M_{\tilde{u}_L}^2+M_{\tilde{d}_L}^2-M_{\tilde{u}_R}^2-M_{\tilde{e}_R}^2)+c_{\tilde{e}_R}(M_{\tilde{u}_L}^2+M_{\tilde{d}_L}^2-2M_{\tilde{u}_R}^2-5M_{\tilde{d}_R}^2)\Big], \end{aligned} \tag{6.39}$$

$$\begin{aligned} m_{10}^2 &= \frac{1}{5X_5}\Big[(c_{\tilde{u}_L}+c_{\tilde{d}_L})(3M_{\tilde{u}_R}^2+2M_{\tilde{e}_R}^2)-c_{\tilde{u}_R}(3M_{\tilde{u}_L}^2+3M_{\tilde{d}_L}^2-M_{\tilde{e}_R}^2) \\ &\quad -c_{\tilde{e}_R}(2M_{\tilde{u}_L}^2+2M_{\tilde{d}_L}^2+M_{\tilde{u}_R}^2)\Big], \end{aligned} \tag{6.40}$$

$$M_{1/2}^2 = \frac{1}{X_5}\left(M_{\tilde{u}_L}^2+M_{\tilde{d}_L}^2-M_{\tilde{u}_R}^2-M_{\tilde{e}_R}^2\right), \tag{6.41}$$

$$\begin{aligned} \cos 2\beta &= \frac{1}{X_5 M_Z^2(\sin^2\theta_W-1)}\Big[c_{\tilde{u}_L}(2M_{\tilde{d}_L}^2-M_{\tilde{u}_R}^2-M_{\tilde{e}_R}^2)-c_{\tilde{d}_L}(2M_{\tilde{u}_L}^2-M_{\tilde{u}_R}^2-M_{\tilde{e}_R}^2) \\ &\quad +(c_{\tilde{u}_R}+c_{\tilde{e}_R})(M_{\tilde{u}_L}^2-M_{\tilde{d}_L}^2)\Big], \end{aligned} \tag{6.42}$$

$$\begin{aligned} K &= \frac{1}{6X_5(\sin^2\theta_W-1)}\Big[-3(c_{\tilde{u}_L}+c_{\tilde{d}_L})(M_{\tilde{u}_R}^2-M_{\tilde{e}_R}^2)+3c_{\tilde{u}_R}(M_{\tilde{u}_L}^2+M_{\tilde{d}_L}^2-2M_{\tilde{e}_R}^2) \\ &\quad -3c_{\tilde{e}_R}(M_{\tilde{u}_L}^2+M_{\tilde{d}_L}^2-2M_{\tilde{u}_R}^2) \\ &\quad +2\sin^2\theta_W\Big(c_{\tilde{u}_L}(4M_{\tilde{u}_R}^2-5M_{\tilde{d}_L}^2+M_{\tilde{e}_R}^2)+c_{\tilde{d}_L}(5M_{\tilde{u}_L}^2-M_{\tilde{u}_R}^2-4M_{\tilde{e}_R}^2) \\ &\quad -c_{\tilde{u}_R}(4M_{\tilde{u}_L}^2-M_{\tilde{d}_L}^2-3M_{\tilde{e}_R}^2)-c_{\tilde{e}_R}(M_{\tilde{u}_L}^2-4M_{\tilde{d}_L}^2+3M_{\tilde{u}_R}^2)\Big)\Big], \end{aligned} \tag{6.43}$$

where X_5 is given by:

$$X_5 = c_{\tilde{u}_L}+c_{\tilde{d}_L}-c_{\tilde{u}_R}-c_{\tilde{e}_R} \tag{6.44}$$

It is important to mention here that the work presented in this section follows the approach of [188]. We find inconsistencies in the results presented by the authors of [188] such as, in the expression for $\cos 2\beta$, the first term is absent. Furthermore, the plots in figures 1, 2 and 3 of the same reference are not correct. Therefore, after discussing this issue with the authors, it was agreed to redo the calculations as well as extending it with an E_6 analysis and compare the results with numerical calculations. We have also added extra observations in our discussion.

We had seven equations, (6.14) to (6.20), but only five unknowns, so we should have two constraints left over. These are provided by the sum rules. The unused equations are (6.18) and (6.19); their difference provides the second equality of equation (6.24) while their sum is part of equation (6.26), where it has been combined with other masses to remove

the non-C_i terms. The other sum rule, equation (6.25), is just a re-expression of equation (6.41).

Some simplification of equations (6.14) to (6.20) is possible by allowing more approximations. For example, since the running of the gauge couplings is logarithmic, $\bar{c}_i$ only have a rather small dependence on the scale where they are evaluated, and so $c_{\tilde{u}_L} \approx c_{\tilde{d}_L}$. Also $\bar{c}_1$ is numerically rather small and its contribution is diminished by its small coefficients in equations (6.37 - 6.38), so $c_{\tilde{u}_R} \approx c_{\tilde{d}_R}$ and $c_{\tilde{e}_R}$ can be neglected. Furthermore, for TeV scale sfermions, the contribution from the electroweak D-term is small, since it is added in quadrature, allowing one to neglect δ_φ. Finally, evaluating the masses at a common scale one finds

$$m_{\bar{5}}^2 \approx \frac{1}{5X_5}\Big[2c_L(m_{\tilde{u}_R}^2 + 5m_{\tilde{d}_R}^2 - m_{\tilde{e}_R}^2) - c_R(12m_{\tilde{u}_L}^2 + 5m_{\tilde{d}_R}^2 - 5m_{\tilde{u}_R}^2 - 7M_{\tilde{e}_R}^2)\Big], \tag{6.45}$$

$$m_{10}^2 \approx \frac{1}{5X_5}\Big[2c_L(3m_{\tilde{u}_R}^2 + 2m_{\tilde{e}_R}^2) - c_R(6m_{\tilde{u}_L}^2 - m_{\tilde{e}_R}^2)\Big], \tag{6.46}$$

$$M_{1/2}^2 \approx \frac{1}{X_5}\Big(2m_{\tilde{u}_L}^2 - m_{\tilde{u}_R}^2 - m_{\tilde{e}_R}^2\Big), \tag{6.47}$$

$$K \approx \frac{1}{X_5}\Big[c_L\Big(m_{\tilde{u}_R}^2 - m_{\tilde{e}_R}^2\Big) - c_R\Big(m_{\tilde{u}_L}^2 - m_{\tilde{e}_R}^2\Big)\Big], \tag{6.48}$$

and X_5 takes the simplified form

$$X_5 = 2c_L - c_R. \tag{6.49}$$

In an obvious notation, $c_L \equiv c_{\tilde{u}_L} \approx c_{\tilde{d}_L}$ and $c_R \equiv c_{\tilde{u}_R} \approx c_{\tilde{d}_R}$. The equation for $\cos 2\beta$ has dropped out of these approximate equations since the electroweak D-term has been neglected.

6.2.2. SO(10)

We now consider grand unification with boundary conditions of $SO(10)$. Now all the squarks and sleptons are embedded in the fundamental 16-dimensional irrep of $SO(10)$, including the right-handed sneutrino. We shall consider here the breaking scenario in (5.43), were, as discussed in section 5.2.1, we assume that the intermediate breakings all occur around the GUT scale. It is important to note that $SO(10)$ is a gauge group of rank-5, which means that the breaking chain (5.43) involves the reduction of rank from 5 to 4. In general, if one considers a supersymmetric model with n extra $U(1)$s and assume a Higgs type mechanism, the extra $U(1)$s may be spontaneously broken by the vevs of the scalar components of the Higgs superfields Φ and $\overline{\Phi}$, with charges $Q_{k\Phi}$ and $-Q_{k\Phi}$ respectively. The scalar supersymmetric potential with D-terms included is

$$V_{SUSY} = \frac{1}{M^{4n-6}}\left(|\Phi|^2 + |\overline{\Phi}|^2\right)|\Phi\overline{\Phi}|^{2n-2} + \sum_k \frac{g_k^2}{2}\left(Q_{k\Phi}\left(|\Phi|^2 - |\overline{\Phi}|^2\right) + \sum_a Q_{ka}|\varphi_a|^2\right)^2 \tag{6.50}$$

and the additional soft SUSY breaking terms have the form [179]

$$V_{\text{soft}} = m_{\Phi}^2|\Phi|^2 + m_{\overline{\Phi}}^2|\overline{\Phi}|^2, \tag{6.51}$$

where φ_a plays the role of the usual MSSM scalar fields, g_k are the diverse $U(1)_k$ gauge couplings, m_{Φ}^2 and $m_{\overline{\Phi}}^2$ are soft scalar masses and M is a mass of order the Planck scale. The scalar potential is assumed to receive a non-trivial vev in a nearly D-flat direction of the form

$$\langle\Phi\rangle^2 \approx \langle\overline{\Phi}\rangle^2 \approx \left[\frac{-\left(m_{\overline{\Phi}}^2 + m_{\Phi}^2\right)M^{4n-6}}{4n-2}\right]^{1/(2n-2)}, \tag{6.52}$$

where $m_{\overline{\Phi}}^2 + m_{\Phi}^2$ must be negative at the scale of $\langle\Phi\rangle$. After integrating out the superfields Φ and $\overline{\Phi}$, the corrections to the soft scalar masses for the surviving fields φ_a are proportional to their charges under the broken $U(1)_k$, having the form

$$\Delta m_a^2 = \sum_k Q_{ka} g_k^2 D_k, \tag{6.53}$$

where the D-term is given by[1]

$$D_k = \frac{\frac{1}{2}\left(m_{\overline{\Phi}}^2 - m_{\Phi}^2\right)Q_{k\Phi}}{\sum_l g_l^2 Q_{l\Phi}^2}. \tag{6.54}$$

One can see that the D-terms depend only on the soft masses m_{Φ}, $m_{\overline{\Phi}}$ and on the $U(1)_k$ charges, and not on the form of the scalar potential (6.50) itself. Even if the scale of spontaneous symmetry breaking governed by equation (6.52) is well above m_{soft}^2, the D-term contributions will remain of order the square of the soft scalar masses.

With this in mind, the breaking of the additional $U(1)_Z$ in the chain of equation (5.43) at the high scale will involve a D-term contribution of order m_{soft}^2. For the Higgs sector, we will consider a simple scenario where both the up-type and down-type Higgs fields are embedded in a 10-dimensional irrep of $SO(10)$. Then we have a common scalar mass $m_{\mathbf{16}}$ for the sfermions at the GUT scale, and a common mass $m_{\mathbf{10}}$ for the Higgs fields. Additionally, due to rank reduction after the breaking of $SO(10)$, one has D-term contributions of the form

[1] In principle, the form of the D-terms can be rather more complicated, reflecting non-trivial features of the breaking mechanism. Usually, one considers D_k to be a parameter of our ignorance of these details. We also add here that for both $SU(5)$ and $SO(10)$, there are no contributions for the $S = Tr(Ym^2)$ term arising from high scale heavy Higgs-triplets. As we discussed in subsec. 5.1.2, the doublet-triplet splitting problem may be solved by embedding the theory in higher dimensional models. Both the doublets and the triplets become Kaluza-Klein (KK) modes, forming complete representations of the GUT symmetry, which cancel out in the S-term. As such, the only contributions for S arise from the Higgs doublets zero modes, which are present in the model after the breaking of the GUT symmetry.

of equation (6.53). For the gaugino masses, the argument that justifies the common GUT scale mass $M_{1/2}$ for $SU(5)$ remains valid. We have then the following boundary conditions:

$$\begin{aligned} m^2_{\tilde{Q}_L}(0) &= m^2_{\tilde{u}_R}(0) = m^2_{\tilde{e}_R}(0) = m^2_{\mathbf{16}} + g^2_{10}D, && (6.55)\\ m^2_{\tilde{d}_R}(0) &= m^2_{\tilde{L}_L}(0) = m^2_{\mathbf{16}} - 3g^2_{10}D, && (6.56)\\ m^2_{H_u}(0) &= m_{\mathbf{10}^2} - 2g^2_{10}D, && (6.57)\\ m^2_{H_d}(0) &= m_{\mathbf{10}^2} + 2g^2_{10}D, && (6.58)\\ M_1(0) &= M_2(0) = M_3(0) = M_{1/2}, && (6.59) \end{aligned}$$

where g_{10} is the common value of the gauge couplings at the GUT scale.

One interesting difference between this scenario and $SU(5)$ unification is the extra relation between Higgs masses at the GUT scale, which, when inserted into equation (6.12), results in

$$S_0 = -4g^2_{10}D. \tag{6.60}$$

As before, considering only the sfermion sector we have five unknowns, $m_{\mathbf{16}}$, $g^2_{10}D$, $M_{1/2}$, $\cos 2\beta$ and K, with seven equations. The measurement of $M_{\tilde{u}_L}$, $M_{\tilde{d}_L}$, $M_{\tilde{e}_R}$, $M_{\tilde{u}_R}$ and $M_{\tilde{d}_R}$ is sufficient to determine these five parameters using the invertible system

$$\begin{pmatrix} M^2_{\tilde{u}_L} \\ M^2_{\tilde{d}_L} \\ M^2_{\tilde{e}_R} \\ M^2_{\tilde{u}_R} \\ M^2_{\tilde{d}_R} \end{pmatrix} = \begin{pmatrix} 1 & 1 & c_{\tilde{u}_L} & \delta_{\tilde{u}_L} & -\frac{1}{5} \\ 1 & 1 & c_{\tilde{d}_L} & \delta_{\tilde{d}_L} & -\frac{1}{5} \\ 1 & 1 & c_{\tilde{e}_R} & \delta_{\tilde{e}_R} & -\frac{6}{5} \\ 1 & 1 & c_{\tilde{u}_R} & \delta_{\tilde{u}_R} & \frac{4}{5} \\ 1 & -3 & c_{\tilde{d}_R} & \delta_{\tilde{d}_R} & -\frac{2}{5} \end{pmatrix} \begin{pmatrix} m^2_{\mathbf{16}} \\ g^2_{10}D \\ M^2_{1/2} \\ \cos 2\beta \\ K \end{pmatrix}. \tag{6.61}$$

Here, $M_{1/2}$ and $\cos 2\beta$ and K are given by the same expressions as for $SU(5)$, equations (6.41 - 6.43), whereas $m_{\mathbf{16}}$ and $g^2_{10}D$ are given by

$$\begin{aligned} m^2_{16} &= \frac{1}{4X_5}\Big[-c_{\tilde{u}_R}(2M^2_{\tilde{d}_L} + M^2_{\tilde{d}_R} - M^2_{\tilde{e}_R} + 2M^2_{\tilde{u}_L}) - c_{\tilde{e}_R}(M^2_{\tilde{d}_L} + M^2_{\tilde{d}_R} + M^2_{\tilde{u}_L} + M^2_{\tilde{u}_R}) \\ &\quad + (c_{\tilde{d}_L} + c_{\tilde{u}_L})(M^2_{\tilde{d}_R} + M^2_{\tilde{e}_R} + 2M^2_{\tilde{u}_R}) + c_{\tilde{d}_R}(-M^2_{\tilde{d}_L} + M^2_{\tilde{e}_R} - M^2_{\tilde{u}_L} + M^2_{\tilde{u}_R})\Big], && (6.62)\\ g^2_{10}D &= \frac{1}{20X_5}\Big[-c_{\tilde{u}_R}(2M^2_{\tilde{d}_L} - 5M^2_{\tilde{d}_R} + M^2_{\tilde{e}_R} + 2M^2_{\tilde{u}_L}) + c_{\tilde{e}_R}(-3M^2_{\tilde{d}_L} + 5M^2_{\tilde{d}_R} - 3M^2_{\tilde{u}_L} + M^2_{\tilde{u}_R}) \\ &\quad - (c_{\tilde{d}_L} + c_{\tilde{u}_L})(5M^2_{\tilde{d}_R} - 3M^2_{\tilde{e}_R} - 2M^2_{\tilde{u}_R}) + 5c_{\tilde{d}_R}(M^2_{\tilde{d}_L} - M^2_{\tilde{e}_R} + M^2_{\tilde{u}_L} - M^2_{\tilde{u}_R})\Big]. && (6.63) \end{aligned}$$

Once again, the $SO(10)$ results in [188] have some inconsistencies. In particular, we find that the term proportional to $c_{\tilde{d}_R}$ in the expression for $m_{\mathbf{16}}$ is not correct.

The choice of the Higgs fields in a 10-plet enables us to relate their GUT scale masses through the relation (6.60). If we plug this expression into equation (6.23), we obtain

$$K(t) = \frac{-4g_{10}^2 D}{2b_1}\left(1 - \frac{\alpha_1(t)}{\alpha_1(0)}\right). \tag{6.64}$$

Using the expressions for K, equation (6.43), and for $g_{10}^2 D$, equation (6.63), which are explicitly dependent on the low energy squark and slepton masses, we have a further constraint upon the sfermion masses. This constraint has not, to our knowledge, been previously reported in the literature.

This new relation is useful in distinguishing between GUT groups since it provides a direct constraint involving only the sfermion masses. If we do indeed find a first (and/or second) generation of sfermions at the LHC, measuring four of these masses will provide an $SO(10)$ prediction of the fifth. To see the significance of this, suppose that we find a first or second generation of sfermions, and measure the five masses $M_{\tilde{u}_L}$, $M_{\tilde{d}_L}$, $M_{\tilde{e}_R}$, $M_{\tilde{u}_R}$ and $M_{\tilde{d}_R}$. We cannot yet use equations (6.39 - 6.43) or (6.62 - 6.63) to determine the model parameters since we do not yet know which boundary conditions to apply. However, after inserting the expressions for K and $g_{10}^2 D$ found in equations (6.43) and (6.63) respectively, equation (6.64) provides an $SO(10)$ prediction of the $M_{\tilde{d}_R}$ which we can compare to the measured value. One can see an example of this in Table 6.1 (lower section), where we have presented three scenarios, whose details we will use for a numerical comparison with SOFTSUSY in Section 6.4.

In this table, values of the masses $M_{\tilde{u}_L}$, $M_{\tilde{d}_L}$, $M_{\tilde{e}_R}$ and $M_{\tilde{u}_R}$ have been chosen, consistent with unification and $-1 < \cos 2\beta < 0$. For $SU(5)$ we have no constraint on the value of $M_{\tilde{d}_R}$ so must also treat this as an input, but for $SO(10)$, expression (6.64) fixes the value of $M_{\tilde{d}_R}$ as shown. Also note that some choices for the masses $M_{\tilde{u}_L}$, $M_{\tilde{d}_L}$, $M_{\tilde{e}_R}$ and $M_{\tilde{u}_R}$, that are acceptable for $SU(5)$ and for which equation (6.64) provides a seemingly reasonable solution for $M_{\tilde{d}_R}$ in $SO(10)$, may actually be forbidden for $SO(10)$ since $m_{\mathbf{16}}^2 < 3g_{10}^2 D$ and thus $m_{\tilde{d}_R}^2(0) < 0$ (though this is not the case for any of the scenarios shown).

As mentioned earlier, some caution is required, since this additional sum rule is characteristic of choosing the Higgs fields to be in the **10** of $SO(10)$. It would be interesting to perform further studies to investigate which constraints on the masses would arise with Higgs embedded in a **120**, or a $\overline{\mathbf{126}}$, or even combinations of them.

6.2.3. E_6

For unification under the group E_6, the fundamental sfermions and Higgs are embedded in a **27** irrep together with additional exotic matter. For now, let us consider a simple scenario

		Scenario 1	Scenario 2	Scenario 3
$SU(5)$	$m_{\bar{\mathbf{5}}}$	781.7	893.7	2856.6
	$m_{\mathbf{10}}$	654.8	1385.0	2690.5
	$m_{\bar{\mathbf{5}}'}$	800	1800	2700
$SO(10)$	$m_{\mathbf{16}}$	669.9	1268.9	2811.6
	$m_{\mathbf{10}}$	800	1800	2700
	$g_{10}^2 D$	-19.971 $\times 10^3$	308.263 $\times 10^3$	-666.100 $\times 10^3$
$SU(5)$ & $SO(10)$	S_0	79.886 $\times 10^3$	-1233.05 $\times 10^3$	2664.40 $\times 10^3$
	$\tan\beta$	6.1	8.0	4.6
$SU(5)$ & $SO(10)$	$M_{\tilde{u}_L}$	1550	1951	3550
	$M_{\tilde{d}_L}$	1552	1953	3551
	$M_{\tilde{e}_R}$	700	1430	2700
	$M_{\tilde{u}_R}$	1500	1898	3500
$SU(5)$	$M_{\tilde{d}_R}$	1550	1600	3600
$SO(10)$	$M_{\tilde{d}_R}$	1518	1566	3830

Table 6.1. *Example scenarios to demonstrate the use of the additional $SO(10)$ sum rule and test the sum rules with SOFTSUSY. All masses are GeV (though S_0 and $g_{10}^2 D$ have dimension mass^2). For $SU(5)$, the $M_{\tilde{d}_R}$ mass is a free input parameter as the remaining superpartner masses, whereas for $SO(10)$ it is fixed by eq. (6.64) and is determined by $M_{\tilde{u}_L}$, $M_{\tilde{d}_L}$, $M_{\tilde{e}_R}$ and $M_{\tilde{u}_R}$.*

where all the extra fields (i.e. those that don't appear in the MSSM) are integrated out at the high scale and where the intermediate breaking of E_6 subgroups all occur around the GUT scale. Our motivation is to explore further constraints on the squark and slepton masses due to placing all our matter in a **27**-plet with a common scalar mass $m_{\mathbf{27}}$ at the GUT scale with GUT scale masses separated only by D-terms.

We consider the breaking

$$E_6 \to SO(10)\otimes U(1)_S \to SU(5)\otimes U(1)_S \otimes U(1)_X \to SU(3)\otimes SU(2)_L \otimes U(1). \tag{6.65}$$

E_6 is a rank-6 group, so the breaking to the SM group involves a rank reduction of two units and we have two D-term contributions from the breaking of $U(1)_S$ and $U(1)_X$ at the high scale, where the common gauge coupling has the value g_6^2. As for $SU(5)$ and $SO(10)$, we assume a common value $M_{1/2}$ for the gaugino masses at the high scale. The boundary

conditions are then:

$$\begin{aligned} m^2_{\tilde{Q}_L}(0) &= m^2_{\tilde{u}_R}(0) = m^2_{\tilde{e}_R}(0) = m^2_{\mathbf{27}} - g_6^2 D_S + g_6^2 D_X, && (6.66)\\ m^2_{\tilde{d}_R}(0) &= m^2_{\tilde{L}_L}(0) = m^2_{\mathbf{27}} - g_6^2 D_S - 3g_6^2 D_X, && (6.67)\\ m^2_{H_u}(0) &= m^2_{\mathbf{27}} + 2g_6^2 D_S - 2g_6^2 D_X, && (6.68)\\ m^2_{H_d}(0) &= m^2_{\mathbf{27}} + 2g_6^2 D_S + 2g_6^2 D_X, && (6.69)\\ M_1(0) = M_2(0) &= M_3(0) = M_{1/2}, && (6.70) \end{aligned}$$

where at the GUT scale we have

$$S_0 = -4g_6^2 D_X\,. \tag{6.71}$$

We have six unknowns, $m_{\mathbf{27}}$, $g_6^2 D_S$, $g_6^2 D_X$, $M_{1/2}$, $\cos 2\beta$ and K, with seven equations. However, all the sfermions have the same $U(1)_S$ charge[2], so $m^2_{\mathbf{27}}$ and $g_6^2 D_S$ always appears in the combination $m^2_{\mathbf{27}} - g_6^2 D_S$ in the sfermion boundary conditions, and cannot be disentangled without extra input from the Higgs sector. Given that we assume E_6 breaks to $SO(10)\otimes U(1)_S$ we may identify $m^2_{\mathbf{16}}$ with $m^2_{\mathbf{27}} - g_6^2 D_S$ and $m^2_{\mathbf{10}}$ with $m^2_{\mathbf{27}} + 2g_6^2 D_S$. Then the previous equations for $SO(10)$, equations (6.41 - 6.43) and (6.62 - 6.63), apply with $m^2_{\mathbf{16}}$ replaced by $m^2_{\mathbf{27}} - g_6^2 D_S$. The analysis is then reduced to that of $SO(10)$.

6.3. Including Additional Matter: The E_6SSM

In Section 6.2 we demonstrated that one may determine some of the free parameters of a grand unified model just by the measurement of the sfermion masses. For $SU(5)$ and $SO(10)$ we found analytic solutions for those parameters and additional constraints on the squark and slepton masses of the first two generations. In Subsection 6.2.3 we considered the GUT group E_6 and found that it is not possible to determine all the boundary condition parameters of the sfermion sector from the sfermion masses alone, since one could not disentangle the **27**-plet mass from the $U(1)_S$ D-term. The analysis of the mass spectrum reduced to that of $SO(10)$ with an effective $m_{\mathbf{16}}$.

However, this E_6 analysis was done with the assumption that the extra matter that fills up the **27**-plet remains at the high scale, so that the RGEs remain as they were for $SU(5)$ and $SO(10)$. In principle, there is no reason why this additional matter should not be present at low energy scales, as described by the Exceptional Supersymmetric Standard Model (E_6SSM).

To perform an analysis of the first and/or second generation sfermion sector, along the lines of our analysis of $SU(5)$ and $SO(10)$, we must take into account the contribution of the extra fields, and the extra $U(1)_N$ symmetry, to the RGEs. In particular we will have an extra S' contribution from the extra $U(1)_N$, a D-term from the breaking of $U(1)_N$ at the TeV

[2]The $U(1)_S$ charge is proportional to the normalized $U(1)_\psi$ charge in (5.78)

scale, $g_1'^2 D'$, analogous to the electroweak Δ_ϕ and a high scale D-term $g_6^2 D$ arising from the breaking of the additional $U(1)$ combination orthogonal to $U(1)_N$, which we shall refer to as $U(1)_M$. The charges of the fields in the **27** with respect to $U(1)_N$ and $U(1)_M$ are given in Table (6.2), where we used the techniques introduced in section A.1.1 to calculate Q_M. In particular,

	Q_L	u_R	d_R	L_L	e_R	N_R	S	H_2	H_1	T	$\overline{T}$
$\sqrt{40}Q_N$	1	1	2	2	1	0	5	-2	-3	-2	-3
$\sqrt{\frac{200}{3}}Q_M$	1	1	-2	-2	1	4	1	-2	1	-2	1

Table 6.2. *$U(1)_N$ and $U(1)_M$ normalized charges of the fields in the* **27** *of E_6*

the unnormalized charges Q_S and Q_X as in the breaking chain (6.65),were calculated using the dual basis vectors $\overline{Q}_S = [-1\ 1\ 4\ 3\ 1\ 0]$ and $\overline{Q}_X = [1\ -1\ 0\ 1\ -1\ 0]$, and the weights of the **27** irrep, given in table 21 of [124]. Upon normalization, the results in table 6.2 were obtained.

One finds that the RGEs for S and S' are coupled,

$$\frac{dS}{dt} = \frac{96}{5}\frac{\alpha_1}{4\pi}S - \frac{1}{5}\frac{\alpha_1'}{4\pi}S', \tag{6.72}$$

$$\frac{dS'}{dt} = -\frac{24}{5}\frac{\alpha_1}{4\pi}S + \frac{94}{5}\frac{\alpha_1'}{4\pi}S', \tag{6.73}$$

so a simple analytical expression of the form of equation (6.13), as one had for $SU(5)$ and $SO(10)$, is not available. Since most of the E_6 matter is now in a single multiplet, their contributions to S cancel, leaving only the contributions from H' and $\overline{H}'$, giving

$$S_0 \equiv S(0) = -m^2_{27'} + m^2_{\overline{27}'}, \tag{6.74}$$

$$S_0' \equiv S'(0) = 4m^2_{27'} - 4m^2_{\overline{27}'}. \tag{6.75}$$

Therefore in scenarios with unified H' and $\overline{H}'$ masses, the $S(t)$ and $S'(t)$ terms will be identically zero for all scales. Integrating (6.72) and (6.73) we get the coupled equations,

$$S(t) = S_0 + \frac{1}{5}K'(t) - \frac{96}{5}K(t), \tag{6.76}$$

$$S'(t) = -\frac{1}{4}S_0 - \frac{94}{5}K'(t) + \frac{24}{5}K(t), \tag{6.77}$$

where we have used $S_0' = -4S_0$. Here K' is the $U(1)_N$ equivalent of K with a definition analogous to equation (6.23).

The integrated RGEs are now,

$$m^2_{\tilde{u}_L}(t) = m^2_{\tilde{Q}_L}(0) + C_3^{E_6} + C_2^{E_6} + \frac{1}{36}C_1^{E_6} + \frac{1}{4}C_1' + \Delta_{u_L} + \Delta'_{u_L} - \frac{1}{5}K - \frac{1}{20}K' - g_6^2 D, \tag{6.78}$$

$$m^2_{\tilde{d}_L}(t) = m^2_{\tilde{Q}_L}(0) + C_3^{E_6} + C_2^{E_6} + \frac{1}{36}C_1^{E_6} + \frac{1}{4}C_1' + \Delta_{d_L} + \Delta'_{d_L} - \frac{1}{5}K - \frac{1}{20}K' - g_6^2 D, \tag{6.79}$$

$$m^2_{\tilde{u}_R}(t) = m^2_{\tilde{u}_R}(0) + C_3^{E_6} + \frac{4}{9}C_1^{E_6} + \frac{1}{4}C_1' + \Delta_{u_R} + \Delta'_{u_R} + \frac{4}{5}K - \frac{1}{20}K' - g_6^2 D, \tag{6.80}$$

$$m^2_{\tilde{d}_R}(t) = m^2_{\tilde{d}_R}(0) + C_3^{E_6} + \frac{1}{9}C_1^{E_6} + C_1' + \Delta_{d_R} + \Delta'_{d_R} - \frac{2}{5}K - \frac{1}{10}K' + 2g_6^2 D, \tag{6.81}$$

$$m^2_{\tilde{e}_L}(t) = m^2_{\tilde{L}_L}(0) + C_2^{E_6} + \frac{1}{4}C_1^{E_6} + C_1' + \Delta_{e_L} + \Delta'_{e_L} + \frac{3}{5}K - \frac{1}{10}K' + 2g_6^2 D, \tag{6.82}$$

$$m^2_{\tilde{\nu}_L}(t) = m^2_{\tilde{L}_L}(0) + C_2^{E_6} + \frac{1}{4}C_1^{E_6} + C_1' + \Delta_{\nu_L} + \Delta'_{\nu_L} + \frac{3}{5}K - \frac{1}{10}K' + 2g_6^2 D, \tag{6.83}$$

$$m^2_{\tilde{e}_R}(t) = m^2_{\tilde{e}_R}(0) + C_1^{E_6} + C_1' + \Delta_{e_R} + \Delta'_{e_R} - \frac{6}{5}K - \frac{1}{20}K' - g_6^2 D, \tag{6.84}$$

where

$$C_i^{E_6}(t) = M_i^2(0)\left[A_i^{E_6}\frac{\alpha_i^2(0) - \alpha_i^2(t)}{\alpha_i^2(0)}\right] = M_i^2(0)\bar{c}_i^{E_6}(t)\ , i = \{1,2,3,4\}\ , \tag{6.85}$$

with

$$A_i^{E_6} = \left\{\frac{1}{8}, \frac{3}{8}, \frac{20}{3}, \frac{1}{47}\right\}\ . \tag{6.86}$$

Note that here we have identified $C_4^{E_6} \equiv C_1'$, and M_4 as the mass of the $U(1)_N$ gaugino. Also, the $U(1)_N$ D-term is

$$\Delta'_\varphi = \frac{g_1'^2}{2\sqrt{40}}Q_\varphi^N D', \tag{6.87}$$

where we define

$$D' \equiv \sqrt{40}\left(Q_{H_1}^N v_d^2 + Q_{H_2}^N v_u^2 + Q_S^N v_s^2\right), \tag{6.88}$$

with Q_φ^N the $U(1)_N$ charges of the field φ and $v_{d,u,s}$ the down-type, up-type and singlet Higgs vevs respectively. In principle this D' is entirely measurable at low energies from the Higgs properties and Z' mass, but this will be very challenging and we will here assume that D' is an unknown.

Inserting the $U(1)_N$ charges into Δ'_φ in equations (6.78) to (6.84), we notice that the K' and the $g_1'^2 D'$ always appear in the combination

$$20\,D_N \equiv \frac{1}{4}g_1'^2 D' - K', \tag{6.89}$$

so cannot be disentangled without extra information (the factor 20 is for later notational convenience).

We have six unknowns and seven equations so this time we must make use of either $m^2_{\tilde{e}_L}(t)$ or $m^2_{\tilde{\nu}_L}(t)$. Unfortunately, neither is a good choice since they fail to provide orthogonal information on the system, preventing us from determining all six parameters. To overcome this, it may be possible to also consider the first and second generation exotic colored triplet fields, $T_{1,2}$ or $\overline{T}_{1,2}$, or more precisely their scalar partners. In order to provide analytic solutions, as our previous treatment, we require small Yukawa couplings, $\kappa_{1,2}$. Further discussion of these fields can be found in Ref. [169]. If $\kappa_{1,2}$ are small we have an extra equation for the $\tilde{T}_{1,2}$ mass,

$$m^2_{\tilde{T}_{1,2}}(t) = m^2_{\tilde{T}_{1,2}}(0) + C_3^{E_6} + \frac{1}{9}C_1^{E_6} + C_1' + \Delta_{T_{1,2}} + \Delta'_{T_{1,2}} + \frac{2}{5}K + \frac{1}{10}K' + 2g_6^2 D. \tag{6.90}$$

We now have sufficient equations to solve for the six unknowns $m_{\mathbf{27}}$, D_N, $M_{1/2}$, $\cos 2\beta$, K and $g_6^2 D$, which, as in the previous cases, are now fully determined by the low energy sfermion masses.

$$\begin{pmatrix} M^2_{\tilde{u}_L} \\ M^2_{\tilde{d}_L} \\ M^2_{\tilde{e}_R} \\ M^2_{\tilde{u}_R} \\ M^2_{\tilde{d}_R} \\ M^2_{\tilde{T}_{1,2}} \end{pmatrix} = \begin{pmatrix} 1 & c_{\tilde{u}_L} & \delta_{\tilde{u}_L} & -\frac{1}{5} & -1 & -1 \\ 1 & c_{\tilde{d}_L} & \delta_{\tilde{d}_L} & -\frac{1}{5} & -1 & -1 \\ 1 & c_{\tilde{e}_R} & \delta_{\tilde{e}_R} & -\frac{6}{5} & -1 & -1 \\ 1 & c_{\tilde{u}_R} & \delta_{\tilde{u}_R} & \frac{4}{5} & -1 & -1 \\ 1 & c_{\tilde{d}_R} & \delta_{\tilde{d}_R} & -\frac{2}{5} & -2 & 2 \\ 1 & c_{\tilde{T}_{1,2}} & \delta_{\tilde{T}_{1,2}} & \frac{2}{5} & 2 & 2 \end{pmatrix} \begin{pmatrix} m^2_{\mathbf{27}} \\ M^2_{1/2} \\ \cos 2\beta \\ K \\ D_N \\ g_6^2 D \end{pmatrix}. \tag{6.91}$$

This provides us with the same results as before for $M_{1/2}$, $\cos 2\beta$ and K, and the additional expressions

$$\begin{aligned} m^2_{27} &= \frac{1}{3X_5}\Big[-c_{\tilde{u}_R}(M^2_{\tilde{d}_L} + M^2_{\tilde{T}_{1,2}} + M^2_{\tilde{u}_L}) - c_{\tilde{e}_R}(M^2_{\tilde{d}_L} + M^2_{\tilde{T}_{1,2}} + M^2_{\tilde{u}_L}) \\ &\quad + (c_{\tilde{d}_L} + c_{\tilde{u}_L})(M^2_{\tilde{T}_{1,2}} + M^2_{\tilde{e}_R} + M^2_{\tilde{u}_R}) + c_{\tilde{T}_{1,2}}(-M^2_{\tilde{d}_L} + M^2_{\tilde{e}_R} - M^2_{\tilde{u}_L} + M^2_{\tilde{u}_R})\Big], \end{aligned} \tag{6.92}$$

$$\begin{aligned} D_N &= \frac{1}{20X_5}\Big[c_{\tilde{e}_R}(-2M^2_{\tilde{d}_L} + 5M^2_{\tilde{d}_R} - 5M^2_{\tilde{T}_{1,2}} - 2M^2_{\tilde{u}_L} + 4M^2_{\tilde{u}_R}) \\ &\quad + c_{\tilde{u}_R}(2M^2_{\tilde{d}_L} + 5M^2_{\tilde{d}_R} - 5M^2_{\tilde{T}_{1,2}} - 4M^2_{\tilde{e}_R} + 2M^2_{\tilde{u}_L}) \\ &\quad + (c_{\tilde{d}_L} + c_{\tilde{u}_L})(-5M^2_{\tilde{d}_R} + 5M^2_{\tilde{T}_{1,2}} + 2M^2_{\tilde{e}_R} - 2M^2_{\tilde{u}_R}) \\ &\quad + (c_{\tilde{d}_R} - c_{\tilde{T}_{1,2}})(M^2_{\tilde{d}_L} - M^2_{\tilde{e}_R} + M^2_{\tilde{u}_L} - M^2_{\tilde{u}_R})\Big]. \end{aligned} \tag{6.93}$$

$$\begin{aligned} g_6^2 D &= \frac{1}{12X_5}\Big[c_{\tilde{e}_R}(2M^2_{\tilde{d}_L} - 3M^2_{\tilde{d}_R} - M^2_{\tilde{T}_{1,2}} + 2M^2_{\tilde{u}_L}) + c_{\tilde{u}_R}(2M^2_{\tilde{d}_L} - 3M^2_{\tilde{d}_R} - M^2_{\tilde{T}_{1,2}} + 2M^2_{\tilde{u}_L}) \\ &\quad + (c_{\tilde{d}_L} + c_{\tilde{u}_L})(3M^2_{\tilde{d}_R} + M^2_{\tilde{T}_{1,2}} - 2M^2_{\tilde{e}_R} - 2M^2_{\tilde{u}_R}) \\ &\quad + (3c_{\tilde{d}_R} + c_{\tilde{T}_{1,2}})(-M^2_{\tilde{d}_L} + M^2_{\tilde{e}_R} - M^2_{\tilde{u}_L} + M^2_{\tilde{u}_R})\Big]. \end{aligned} \tag{6.94}$$

The sum rule of equation (6.24) remains unchanged since the extra E_6 contributions cancel (in particular $\tilde{u}_L$ and $\tilde{e}_L$ have the same $U(1)_N$ charges as $\tilde{d}_L$ and $\tilde{\nu}_L$ respectively).

However, equations (6.25-6.26) are changed by the presence of extra matter. Eliminating $m_\varphi^2(0)$, Δ_φ, K and D_N from equations (6.78-6.84), we find

$$m^2_{\tilde{u}_L} + m^2_{\tilde{d}_L} - m^2_{\tilde{u}_R} - m^2_{\tilde{e}_R} = C_3^{E_6} + 2C_2^{E_6} - \frac{25}{18}C_1^{E_6} - \frac{3}{4}C_1' \approx 2.8M^2_{1/2}, \tag{6.95}$$

and

$$\frac{1}{2}\left(m^2_{\tilde{u}_L} + m^2_{\tilde{d}_L} - m^2_{\tilde{e}_L} - m^2_{\tilde{\nu}_L}\right) + m^2_{\tilde{d}_R} - m^2_{\tilde{e}_R} = 2C_3^{E_6} - \frac{10}{9}C_1^{E_6} - \frac{3}{4}C_1' \approx 4.4M^2_{1/2}. \tag{6.96}$$

these are considerably different from the sum rules for $SU(5)$, $SO(10)$ and E_6 (with no extra matter) so should allow us to distinguish the E_6SSM even without seeing the additional exotic $T_{1,2}$, $\bar{T}_{1,2}$ or their scalar partners.

6.4. A Comparison with SOFTSUSY

In this Section, we will check that the $SU(5)$ and $SO(10)$ sum rules obtained from the one-loop RGEs for the first and second generations, are consistent with the results arising from SOFTSUSY 3.3.0 [197], when $SU(5)$ and $SO(10)$ boundary conditions are imposed. This will then assess the impact of including the full Yukawa couplings as well as the two-loop corrections. We will not compare the E_6SSM sum rule results, since this requires the implementation of new RGEs into SOFTSUSY. While this is in principle available (see Ref. [169]) we leave this for a future study.

6.4.1. $SU(5)$ Boundary Conditions

To test the sum rules of Eqs. (6.25) and (6.26), one would like to fix all but one of the sparticle masses on the left-hand-side of the equations. One could then vary $M_{1/2}$ and compare the remaining mass prediction from the sum rule with the equivalent prediction from SOFTSUSY including two loop running and a full dependence on the Yukawa couplings. This would tell us how robust these sum rules are under removal of the assumptions used to provide an analytic solution. However, since all of the masses on the left-hand-sides are outputs of SOFTSUSY, this is rather tricky to do. Instead, we define,

$$\Sigma_1 \equiv M^2_{\tilde{u}_L} + M^2_{\tilde{d}_L} - M^2_{\tilde{u}_R} - M^2_{\tilde{e}_R}, \tag{6.97}$$

$$\Sigma_2 \equiv \frac{1}{2}\left(M^2_{\tilde{u}_L} + M^2_{\tilde{d}_L} - M^2_{\tilde{e}_L} - M^2_{\tilde{\nu}_L}\right) + M^2_{\tilde{d}_R} - M^2_{\tilde{e}_R}, \tag{6.98}$$

so that the sum rules become,

$$\Sigma_1 = 4.8M^2_{1/2}, \tag{6.99}$$

$$\Sigma_2 = 8.1M^2_{1/2}. \tag{6.100}$$

Now we fix all the input parameters except for $M_{1/2}$ and compare the predictions for Σ_1 and Σ_2 both from these simple sum rules and from SOFTSUSY as $M_{1/2}$ is varied.

The required inputs are $\tan\beta$ and the boundary conditions at the unification scale. For $SU(5)$, these are the common scalar masses $m_{\bar{\mathbf{5}}}$, $m_{\mathbf{10}}$, $m_{\bar{\mathbf{5}}'}$ and $m_{\mathbf{5}'}$, the common universal gaugino mass $M_{1/2}$, and a common universal trilinear coupling a_0. Note that the choice of a_0 is unimportant, since the contributions from trilinear terms are negligible for the first and second generations. However, one should ensure that the choice of a_0 does not generate an unstable vacuum; a safe choice is to set $a_0 = 0$. For $m_{\bar{\mathbf{5}}}$ and $m_{\mathbf{10}}$ and $\tan\beta$, we choose $SU(5)$ inputs that generate the masses of scenarios 1, 2 and 3 we already examined in Section 6.2. These $SU(5)$ inputs are shown in Table 6.1. The Higgs masses $m_{\bar{\mathbf{5}}'}$ and $m_{\mathbf{5}'}$ are related through the parameter S_0, and we choose to fix S_0 to reproduce the three scenarios. Then, the only additional input required is $m_{\bar{\mathbf{5}}'}$, which wasn't needed in the earlier analysis. The chosen values for $m_{\bar{\mathbf{5}}'}$ are given in Table 6.1 and then $m_{\mathbf{5}'}$ is fixed by,

$$m_{\mathbf{5}'} = \sqrt{S_0 + m^2_{\bar{\mathbf{5}}'}}. \tag{6.101}$$

The results are shown in Figure 6.1, where the solid lines are the sum rules of equations (6.99 - 6.100) and the corresponding dashed lines are the results obtained from SOFTSUSY. We observe good agreement between the analytic sum rules and the masses obtained from SOFTSUSY at two-loops, indicating that these sum rules are robust.

6.4.2. $SO(10)$ Boundary Conditions

We also test the sum rules for $SO(10)$ boundary conditions. Now, in addition to $\tan\beta$, we have a common mass for the sfermions, $m_{\mathbf{16}}$, a common mass for the Higgs, $m_{\mathbf{10}}$, and D-term arising from the breaking of $SO(10)$, $g^2_{10}D$. As before, we chose our inputs, $m_{\mathbf{16}}$, $\tan\beta$ and $g^2_{10}D$ such that they reproduce our example scenarios. Again, the common Higgs mass wasn't needed for the earlier examples, but now we must fix it within SOFTSUSY and use the values given in Table (6.1). The results of this analysis are the two upper sets of curves in Figure (6.2). Once again, the analytic sum rules are in good agreement with SOFTSUSY.

We saw earlier that $SO(10)$ also implied an extra constraint, equation (6.64), which relates K (and therefore S_0) to the D-term. Since K and $g^2_{10}D$ are both functions of the low energy masses, equations (6.43) and (6.63), this provides us with an additional sum rule. As for the previous sum rules, this form is a little hard to check in SOFTSUSY since both sides of the equation are outputs of SOFTSUSY. We therefore first make a few manipulations to bring an input on to one side of the equation, allowing us to vary the input and check the

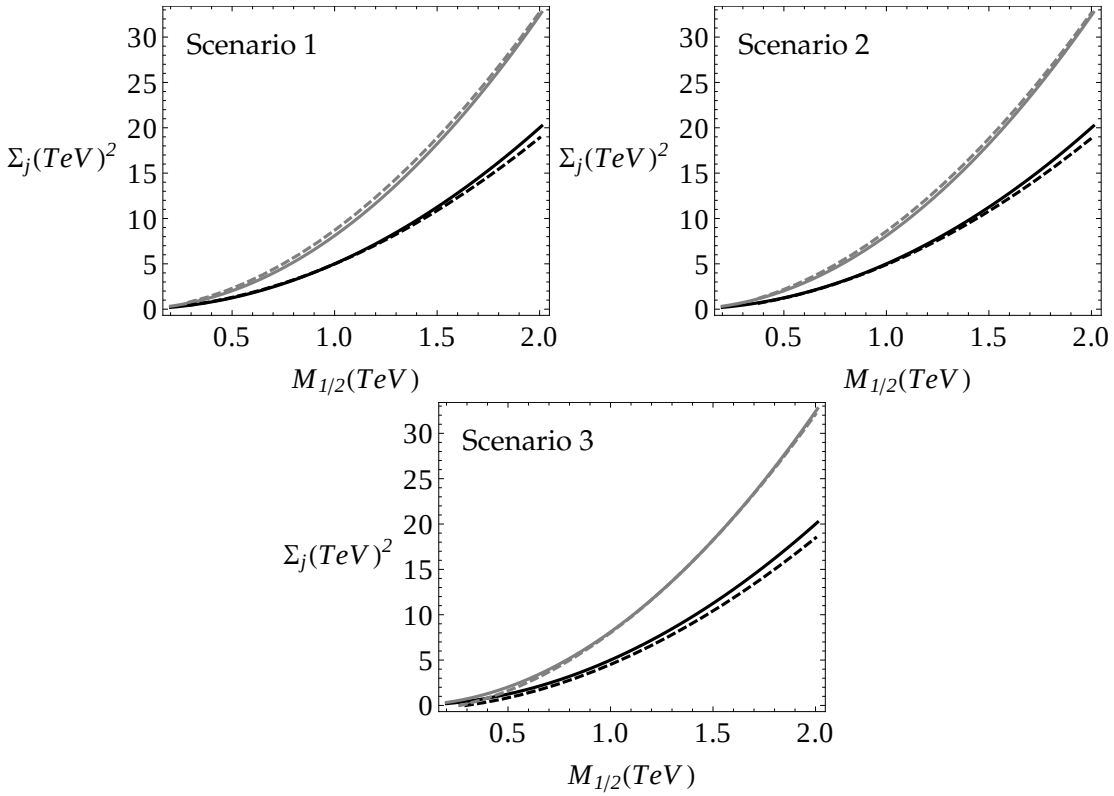

Figure 6.1. *A comparison of the SU(5) analytic sum rules with SOFTSUSY for example scenarios 1, 2 and 3. The lower solid line is the sum rule of equation (6.99) while the upper solid line is that for equation (6.100). The corresponding dashed lines are the results obtained from SOFTSUSY.*

robustness of the sum rule. Substituting equation (6.41) into (6.63) one can write,

$$g_{10}^2 D = \mathfrak{D} + 5c_{\tilde{d}_R}\frac{M_{1/2}^2}{20}, \tag{6.102}$$

where,

$$\begin{aligned}\mathfrak{D} \equiv \frac{1}{20X_5}\Big[&-c_{\tilde{u}_R}(2M_{\tilde{d}_L}^2 - 5M_{\tilde{d}_R}^2 + M_{\tilde{e}_R}^2 + 2M_{\tilde{u}_L}^2) - c_{\tilde{e}_R}(-3M_{\tilde{d}_L}^2 + 5M_{\tilde{d}_R}^2 - 3M_{\tilde{u}_L}^2 + M_{\tilde{u}_R}^2)\\ &+(c_{\tilde{d}_L} + c_{\tilde{u}_L})(5M_{\tilde{d}_R}^2 - 3M_{\tilde{e}_R}^2 - 2M_{\tilde{u}_R}^2)\Big].\end{aligned} \tag{6.103}$$

Substituting this back into the constraint, equation (6.64), and rearranging to place $M_{1/2}$ on the right-hand side, we find,

$$\Sigma_3 = \frac{1}{4}M_{1/2}^2, \tag{6.104}$$

where,

$$\Sigma_3 \equiv \frac{1}{c_{\tilde{d}_R}}\left(-\frac{1}{2}b_1 K\left[1 - \frac{\alpha_1(t)}{\alpha_1(0)}\right]^{-1} - \mathfrak{D}\right). \tag{6.105}$$

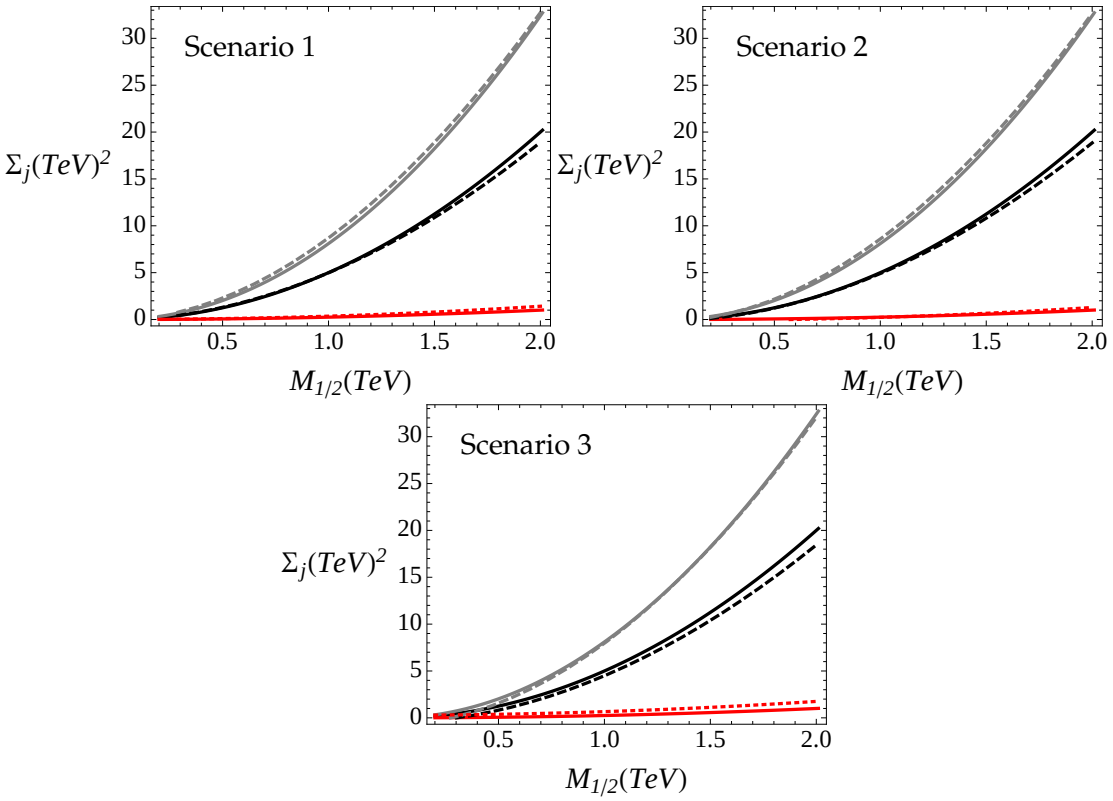

Figure 6.2. *A comparison of the SO(10) analytic sum rules with SOFTSUSY for example scenarios 1, 2 and 3. The lower solid line is now the sum rule of equation (6.104), while the middle solid line and the upper solid line are the sum rules given by equations (6.99) and (6.100) respectively. The corresponding dashed lines are the results obtained from SOFTSUSY.*

All the masses in K and $\mathfrak{D}$, and hence Σ_3, are outputs, so the sum rule may be compared with SOFTSUSY as the input $M_{1/2}$ is varied. These comparisons are shown as the lower set of curves in Figure 6.2, where the solid curve is the simple analytic expression and the dashed curve is the SOFTSUSY result. Once again we have good agreement indicating that these rules are robust.

6.5. Extension for Non-Universal Gaugino Masses

If the chiral superfields in the gauge-kinetic function (3.60) are no longer trivial representations of the GUT gauge group, we can have non-universal gaugino masses. Instead of a single unified $M_{1/2}$, we would have *three* distinct values for the gaugino masses for $SU(5)$ and $SO(10)$, and *four* high scale gaugino masses in E_6. We can however quantify this non-universality by defining *three* new parameters, ρ_1, ρ_2 and, for the E$_6$SSM, ρ_1' as

$$\rho_1 = \frac{M_1}{M_3}, \quad \rho_2 = \frac{M_2}{M_3}, \quad \rho_1' = \frac{M_1'}{M_3}. \tag{6.106}$$

The simplest way to probe these parameters is using the sum rules in (6.25), (6.26) and, for the case of the E$_6$SSM, (6.95) and (6.96).

For the first pair, the introduction of the ratios (6.106), and using eq. (6.21), yields

$$\Sigma_1 = C_3 + 2\rho_2^2 C_2 - \frac{25}{18}\rho_1^2 C_1 \approx \left(4.1 - 0.20\rho_1^2 + 0.89\rho_2^2\right) M_{1/2}^2, \tag{6.107}$$

$$\Sigma_2 = 2C_3 - \frac{10}{9}\,\rho_1^2 C_1 \approx \left(8.3 - 0.16\rho_1^2\right) M_{1/2}^2. \tag{6.108}$$

where $M_{1/2} \equiv M_3$ at the GUT scale. For the E$_6$SSM, we have

$$\begin{aligned}\Sigma_1^{E_6} &= C_3^{E_6} + 2\rho_2^2 C_2^{E_6} - \frac{25}{18}\rho_1^2 C_1^{E_6} - \frac{3}{4}\rho_1' C_1' \\ &\approx \left(2.29 - 0.17\rho_1^2 + 0.68\rho_2^2 - 0.02\rho_1'^2\right) M_{1/2}^2, \end{aligned}\tag{6.109}$$

$$\Sigma_2^{E_6} = 2C_3^{E_6} - \frac{10}{9}\rho_1^2 C_1^{E_6} - \frac{3}{4}\rho_1'^2 C_1' \approx \left(4.6 - 0.14\rho_1^2 - 0.02\rho_1'^2\right) M_{1/2}^2. \tag{6.110}$$

If the masses of first and second generation superpartners are determined experimentally, it becomes possible to probe models with fixed gaugino mass ratios using the sum rules above. In the following chapters we will discuss some of those models and their implications for the LHC and future colliders.

7. SU(5) Grand Unification Phenomenology

We will study in this chapter models of supersymmetric Grand Unification based on the gauge group $SU(5)$. Unlike the previous chapter, we use the high scale parameters as inputs to derive the low energy spectrum by means of the Renormalization Group Equations. Both the universality and non-universality of gaugino masses in a $SU(5)$ GUT are explored and the regions of the parameter space that favour a DM candidate with acceptable relic density are discussed. Our analysis is not only restricted to the gaugino sector; we also explore possible non-universalities arising from the $SU(5)$ boundary conditions, assuming that the GUT embedding should leave its signature in the sfermion masses, as well as in the soft trilinear couplings.

7.1. The $SU(5)$ GUT Model

We consider a $SU(5)$ GUT model with the superpotential given by

$$W_{SU(5)} = \varepsilon_{\alpha\beta\gamma\rho\sigma}\left(y_{\mathbf{5'}}\right)_{ij}\mathbf{10}_i^{\alpha\beta}\mathbf{10}_j^{\gamma\rho}\mathbf{5'}^{\sigma} + \left(y_{\overline{\mathbf{5}}'}\right)_{ij}\mathbf{10}_i^{\alpha\beta}\overline{\mathbf{5}}_{j\alpha}\overline{\mathbf{5}}'_{\ \beta} + \mu\overline{\mathbf{5}}'_{\ \alpha}\mathbf{5'}^{\alpha} + W_{\mathbf{X_R}}. \tag{7.1}$$

Here, $W_{\mathbf{X_R}}$ is the part of the superpotential that involves the chiral superfields $X_{\mathbf{R}}$, belonging to a $SU(5)$ symmetric representation $\mathbf{R}$, contained in the product of two adjoint representations, $\mathbf{24}\times\mathbf{24}$, and whose scalar components are responsible for the breaking of the GUT symmetry at the high scale. Greek letters are $SU(5)$ indices, Roman letters are generation indices and $\varepsilon_{\alpha\beta\gamma\rho\sigma}$ is the five dimensional generalization of the Levi-Civita symbol. We recall here that the left-handed quark doublet $\hat{Q}_L$, right-handed up-quark $\hat{u}_R^\dagger$ and right-handed charged lepton $\hat{e}_R^\dagger$ superfields are embedded in the $\mathbf{10}$ representation, while the left-handed lepton doublet $\hat{L}_L$ and right-handed down-quark $\hat{d}_R^\dagger$ superfields are in the $\overline{\mathbf{5}}$ representation. The Higgs superfields $\hat{H}_u$ and $\hat{H}_d$ are in the $\mathbf{5'}$ and $\overline{\mathbf{5}}'$ representations respectively. These are indeed the surviving fields after the breaking of the GUT symmetry to the SM gauge group G_{SM}, where we have assumed that the doublet-triplet splitting problem is solved by some unknown mechanism at the high scale, as discussed in 5.1.2.

7.1.1. Soft Scalar Masses

In the MSSM, the part of the Lagrangian (4.5) that includes the Higgs and sfermion soft masses is given by

$$\begin{aligned} -\mathcal{L}_{mass} &= m_{H_d}^2 |H_d|^2 + m_{H_u}^2 |H_u|^2 + \tilde{Q}_{Li}^{\alpha x} \left(m_{\tilde{Q}_L}^2\right)^i{}_j \tilde{Q}_{L\alpha x}^{* j} + \tilde{L}_{Li}^{\alpha} \left(m_{\tilde{L}_L}^2\right)^i{}_j \tilde{L}_{L\alpha}^{* j} \\ &+ \tilde{u}_{Ri}^{* x} \left(m_{\tilde{u}_R}^2\right)^i{}_j \tilde{u}_{Rx}^{j} + \tilde{d}_{Ri}^{* x} \left(m_{\tilde{d}_R}^2\right)^i{}_j \tilde{d}_{Rx}^{j} + \tilde{e}_{Ri}^{*} \left(m_{\tilde{e}_R}^2\right)^i{}_j \tilde{e}_{R}^{j}, \end{aligned} \tag{7.2}$$

with the indices having the same meaning as in (4.5). For a standard $SU(5)$ GUT, when the unified symmetry is broken to G_{SM}, the sfermions, which are embedded in **10** and $\bar{\mathbf{5}}$ dimensional representations, take soft masses $m_{\mathbf{10}}$ or $m_{\bar{\mathbf{5}}}$. Furthermore, we allow an hierarchy between the third generation and the first two generations, but keep the first two generations degenerate in order to avoid dangerous Flavour-Changing Neutral-Currents (FCNC) [198]. Therefore, this model has two extra parameters, $K_{\bar{\mathbf{5}}} > 0$ and $K_{\mathbf{10}} > 0$, which account for the third generation's non-universality at the GUT scale. For the Higgs sector, the masses of the doublets that couple to the up-type quarks and down type quarks take the high scale values $m_{\mathbf{5}'}$ and $m_{\bar{\mathbf{5}}'}$ respectively. Our boundary conditions for the scalar soft masses at the GUT scale are then given by:

$$m_{Q_{ij}}^2(0) = m_{u_{ij}}^2(0) = m_{e_{ij}}^2(0) = \begin{pmatrix} K_{\mathbf{10}} & 0 & 0 \\ 0 & K_{\mathbf{10}} & 0 \\ 0 & 0 & 1 \end{pmatrix} m_{\mathbf{10}}^2 \ , \tag{7.3}$$

$$m_{L_{ij}}^2(0) = m_{d_{ij}}^2(0) = \begin{pmatrix} K_{\bar{\mathbf{5}}} & 0 & 0 \\ 0 & K_{\bar{\mathbf{5}}} & 0 \\ 0 & 0 & 1 \end{pmatrix} m_{\bar{\mathbf{5}}}^2 \ , \tag{7.4}$$

$$m_{H_u}^2(0) = m_{\mathbf{5}'}^2 \ , \tag{7.5}$$

$$m_{H_d}^2(0) = m_{\bar{\mathbf{5}}'}^2 \ . \tag{7.6}$$

In the above, the RGEs are parameterized by $t \equiv \log(Q/Q_0)$, where Q the energy scale of interest and Q_0 is the unification scale.

To accompany the μ-term in Eq.(7.1) we also have the bilinear soft term in (4.5), $\varepsilon_{\alpha\beta}\left[bH_d^{\alpha}H_u^{\beta} + h.c.\right]$. However, b is determined from the electroweak symmetry breaking (EWSB) condition[1]

$$b = \frac{\sin 2\beta}{2}\left(m_{H_u}^2 + m_{H_d}^2 + 2\mu^2\right), \tag{7.7}$$

[1] In our analysis we use the two-loop generalisation of Eq. (7.7).

which is obtained from (4.19) and (4.20), so, unlike the other soft supersymmetry breaking parameters, it is not a high scale input for our analysis.

7.1.2. Soft Trilinear Couplings

The explicit soft susy-breaking terms that contain scalar trilinear couplings are given by

$$-\mathcal{L}_{trilinear} = \varepsilon_{\alpha\beta}\Big[a_{uij}H_u^\alpha \tilde{u}_{Rix}\tilde{Q}_{Lj}^{\beta x} - a_{dij}H_d^\alpha \tilde{d}_{Rix}\tilde{Q}_{Lj}^{\beta x} - a_{eij}H_d^\alpha \tilde{e}_{Ri}\tilde{L}_{Lj}^{\beta} + h.c.\Big], \tag{7.8}$$

where the indices have the same meaning as in Eq. (4.5). We impose the boundary conditions

$$a_t(0) = a_{\mathbf{5}'}, \tag{7.9}$$

$$a_b(0) = a_\tau(0) = a_{\bar{\mathbf{5}}'}. \tag{7.10}$$

Since the $\hat{t}_R^\dagger \hat{t}_L$ pair couples to a different $SU(5)$ Higgs multiplet from the $\hat{b}_R^\dagger \hat{b}_L$ and $\hat{\tau}_R^\dagger \hat{\tau}_L$ pairings, we make no attempt to unify the top Yukawa coupling with those of the bottom or τ at the high scale.

7.1.3. Gaugino Masses

The soft gaugino-mass terms in the Lagrangian (4.5) have the form

$$\frac{1}{2}\Big[M_1\tilde{\lambda}_1\tilde{\lambda}_1 + M_2\tilde{\lambda}_2\tilde{\lambda}_2 + M_3\tilde{\lambda}_3\tilde{\lambda}_3\Big]. \tag{7.11}$$

We will therefore examine two distinct sets of boundary conditions at the GUT scale:

I. universal gaugino masses: $M_1 = M_2 = M_3 \equiv M_{1/2}$,

II. non-universal gaugino masses: $M_1/\rho_1 = M_2/\rho_2 = M_3 \equiv M_{1/2}$,

where ρ_1 and ρ_2 are introduced to quantify the non-universality.

7.1.4. Summary of the Parameter Space

In addition to the usual SM parameters, our $SU(5)$ model is described by eleven high scale parameters, $m_{\bar{5}}$, $K_{\bar{5}}$, m_{10}, K_{10}, $M_{1/2}$, ρ_1, ρ_2, $m_{\bar{5}'}$, $m_{5'}$, $a_{\bar{5}'}$, $a_{5'}$, as well as $\tan\beta$ and the sign of μ. The value of μ^2 is fixed by the Z boson mass as usual.

7.2. Constraints on the Particle Spectrum

The next step is to use the RGEs to evolve the soft masses and couplings down to the electroweak scale, where the particle spectrum may be confronted with the various experimental constraints and possible fine-tunings examined. We perform this running

using SOFTSUSY 3.3.0 [197], starting from the boundary conditions described in section 7.1.

We allow the third generation GUT scale scalar masses, $m_{\bar{5}}^{(3)}$ and $m_{10}^{(3)}$ to lie between zero and 3.5 TeV and then choose K_{10}, $K_{\bar{5}}$ between zero and 10 to give the first and second generation scalar masses. The high scale masses of the Higgs multiplets, $m_{\bar{5}'}$ and $m_{5'}$ are constrained to be less then 4 TeV. We require M_3 to be less than 2 TeV; if examining scenarios with universal gaugino masses, this also sets M_1 and M_2, but if examining non-universal gauginos, we also vary $\rho_{1,2}$ between ±15. Finally the trilinear couplings, $a_{\bar{5}'}$ and $a_{5'}$, are allowed to vary between ±10 TeV, and our only (non-SM) low energy input $\tan\beta$ is constrained to lie in the range $1-60$.

We generate scenario points randomly within these ranges, separately for universal and non-universal gaugino masses. Although the input parameters for the generated scenarios are evenly distributed within their allowed ranges, we make no attempt to ascribe a significance to this distribution. Since the dynamics of the hidden sector are unknown to us, we assign no prior probability for the distribution of input parameters in theory space, and do not perform a Bayesian analysis of the low energy scenarios. The random inputs are then only an attempt to fill parameter space with possible scenarios and their density holds no significance. This is a rather different approach from some analyses in the literature [199–207] where theoretical priors are assigned.

7.2.1. Experimental Constraints

Each scenario must be confronted by experiment. Our first such constraints are the LHC direct searches for supersymmetry from ATLAS [105] and CMS [106]. These limits are rather non-trivial surfaces in parameter space (for example, the limit on the gluino mass is dependent on the squark masses) but here, in the interest of simplicity, we make simple, though more conservative cuts on individual masses. In particular, we require the first and second generation squarks to have masses greater than 1.4 TeV, the gluino to be heavier than 800 GeV and the lightest chargino heavier than 103.5 GeV. We do not explicitly constrain the third generation squarks since we find scenarios that violate the appropriate searches [175–177] are already ruled out by other experimental constraints. The only other direct cut we make is for the direct detection of Dark Matter; we use micrOMEGAS 2.4.5 [208] to calculate the spin independent cross section for the scattering of Weakly Interacting Massive Particles (WIMPs) and nucleons, σ_{SI}^{NW}, and compare with the 2σ bounds set by XENON100 [122].

We also confront our model with the newly measured Higgs boson mass as well as the Dark Matter relic density, and bounds on new physics from $b \to s\gamma$, $B_s \to \mu^+\mu^-$,

$B \to \tau\nu_\tau$ and the muon anomalous magnetic moment a_μ. For all of these, except for the Higgs boson mass, we again use micrOMEGAS to calculate their values for our scenarios and assume a 10% theoretical error. For each of these measurements we compare our prediction with experiment and determine the probability of the given deviation assuming Gaussian errors. We then combine the individual probabilities into a total probability $P_{\rm tot} = P_{m_h} \cdot P_{\Omega_c h} \cdot P_{b\to s\gamma} \cdot P_{\mathcal{R}_{\tau\nu_\tau}} \cdot P_{B_s\to\mu\mu} \cdot P_{a_\mu}$ and require that this is never smaller than 10^{-3}. This excludes scenarios with multiple predictions close to their $\pm 2\sigma$ bound, that would otherwise be accepted by imposing the contraints on a one-by-one basis.

For the Higgs boson mass, we use the ATLAS [1] and CMS [2] values $126 \pm 0.8\,\text{GeV}$ and $125.3 \pm 0.9\,\text{GeV}$ respectively. We combine these together and add a $\pm 2\,\text{GeV}$ theoretical uncertainty in quadrature. This theoretical uncertainty was estimated by the mass difference for the light CP-even Higgs obtained with SOFTSUSY and SUSPECT [209], as reported in [210]. This gives (1σ) uncertainty on our output Higgs boson mass of $125.7 \pm 2.1\,\text{GeV}$.

Constraints on $b \to s\gamma$ were taken from the Heavy Flavour Averaging Group [211], who report a measured value for the branching ratio $\text{Br}(b \to s\gamma) = (355 \pm 24 \pm 9) \times 10^{-6}$. Combining this with the theoretical error provides bounds of $\text{Br}(b \to s\gamma) = (355 \pm 43.8) \times 10^{-6}$.

First evidence of the decay $B_S \to \mu^+\mu^-$ was recently observed by LHCb [212]. A fit to data leads to the decay branching ratio $\text{Br}(B_S \to \mu^+\mu^-) = \left(3.2^{+1.5}_{-1.2} \times 10^{-9}\right)$. These errors are still sufficiently large that the theoretical uncertainty leaves them unchanged.

The latest Belle and BaBar results for the purely leptonic $B \to \tau\nu_\tau$ decay [213, 214], measured the branching ratio $\text{Br}(B \to \tau\nu_\tau) = (1.12 \pm 0.22) \times 10^{-4}$, which can be compared with the SM prediction of $(0.79 \pm 0.23) \times 10^{-4}$ [215]. MicrOMEGAS outputs the ratio of the predicted branching ratio with that of the SM, $\mathcal{R}_{\tau\nu_\tau}$. Again combining with a 10% theoretical uncertainty we find that this output should be constrained by $\mathcal{R}_{\tau\nu_\tau} = 1.42 \pm 0.70$.

The anomalous magnetic moment $a_\mu = (g-2)_\mu/2$ has been determined at BNL [52] to be $a_\mu(exp) = (11\ 659\ 208.9 \pm 6.3) \times 10^{-10}$, which may be compared to the SM prediction [53] $a_\mu(SM) = (11\ 659\ 183.4 \pm 4.9) \times 10^{-10}$. This 3-4$\sigma$ tension of (SM) theory and experiment could be a hint for physics beyond the SM, and may be attributed to supersymmetric contributions [216–219], but it is also possible that some other additional cause is responsible for some or all of the deviation. In this study, we only require that the supersymmetric contribution is not too large. We calculate the extra contribution arising from our model and compare it with $\Delta a_\mu(exp - SM) = (25.5 \pm 8.0) \times 10^{-10}$: if the additional contribution is less than this we set $P_{a_\mu} = 1$ for this scenario; but if it is more we use the uncertainty to quantify P_{a_μ} as described above.

Finally we turn to the relic abundance of Dark Matter. The cosmological parameters of the nine year WMAP observations were recently published in [120], where the fit to the cold Dark Matter relic density, $\Omega_c h^2$, provides a value of 0.1157 ± 0.0023. We estimate a 10% theoretical uncertainty arising from the LSP mass difference calculated with SOFTSUSY and micrOMEGAS and add this in quadrature with the experimental fit standard deviation. The resulting bounds for our micrOMEGAS relic density output are $\Omega_c h^2 = 0.1157 \pm 0.0118$. However, for the purposes of exclusion we only include the probability $P_{\Omega_c h}$ if the relic density is too high. Scenarios with values below $\Omega_c h^2 = 0.1157$ are accepted, but we then use $P_{\Omega_c h}$ in the usual way to determine if this mechanism provides the "preferred" relic density or too little. Scenarios with too little are kept because there may be some other contribution to Dark Matter such as an axion from a broken global $U(1)$ symmetry [220–224].

7.2.2. Fine-tuning

One of the original motivations for low energy supersymmetry was a solution to the fine-tuning (hierarchy) problem of the Higgs bosons mass, so it is sensible to also examine the fine-tuning of our scenarios. Of particular interest here is the fine-tuning of the Z-boson mass with respect to the input parameters. We use the measure of fine tuning introduced by Barbieri and Giudice [225], for which the *partial* fine-tuning is

$$\Delta_{\mathcal{P}_i} = \left| \frac{\mathcal{P}_i}{M_Z^2} \frac{\partial M_Z^2}{\partial \mathcal{P}_i} \right|, \tag{7.12}$$

where $\{\mathcal{P}_i\}$ is the set of input parameters. The fine-tuning of a specific scenario is the maximum of the partial fine tunings,

$$\Delta = \max\left\{\Delta_{\mathcal{P}_i}\right\}. \tag{7.13}$$

For an alternative measure of fine-tuning see [226].

The tree-level[2] the Z-boson mass is given by eq. (4.21), where we have expanded in $1/\tan\beta$, so in the MSSM, fine-tuning of the Z-boson mass arises principally from the parameters μ and m_{H_u}. Indeed, applying Eq. (4.21) to Eq. (7.12), the fine-tuning from μ alone is

$$\Delta_\mu \approx \frac{4|\mu|^2}{M_Z^2}, \tag{7.14}$$

which indicates that we need $\mu \lesssim \sqrt{5/2} M_Z \approx 150\,\text{GeV}$ if we want to keep $\Delta_\mu \lesssim 10$. Obviously

[2] This tree-level expression is appropriate at the scale $M_S = \sqrt{m_{\tilde{t}_1} m_{\tilde{t}_2}}$ where radiative corrections are minimal [227–230].

$\sqrt{-m_{H_u}^2}$ must then also be small to give the correct Z-boson mass ($m_{H_u}^2$ is typically negative). However, in our $SU(5)$ GUT model, $m_{H_u}^2$ is not a free parameter, but is a polynomial function of the input parameters,

$$m_{H_u}^2 = f\left(m_{\overline{5}}^{(3)}, m_{10}^{(3)}, K_{\overline{5}}, K_{10}, m_{\overline{5}'}, m_{5'}, M_3, \rho_1, \rho_2, a_{\overline{5}'}, a_{5'}\right), \tag{7.15}$$

with the largest contributions arising from $m_{10}^{(3)}$, $m_{5'}$, M_3 and $a_{5'}$ [231,238]. If the dimensionful input parameters are $O(\text{TeV})$ or higher, motivated by the desire to avoid the LHC direct searches described in Sec. 7.2.1, then small fluctuations in them will generally cause large fluctuations in our small $m_{H_u}^2$, which in turn spoils the Z-boson mass prediction and generates fine-tuning.

There are two potential ways out of this dilemma while still maintaining small μ. Firstly one might imagine a scenario with $O(\text{TeV})$ dimensionful input parameters such that the contributions to the derivative in Eq. (7.12) just happen to cancel. The smallness of the Z-boson mass would be a coincidence, but one that was stable to local fluctuations. Unfortunately, as we shall see in Sec. 7.3, a scan over parameter space looking for such scenarios with universal gaugino masses found no examples with fine tuning less than 1000. In Sec. 8.4 we will see that we can do significantly better if we allow the gaugino masses to deviate from universality at the GUT scale, but fine-tuning is still sizable.

A second possibility would be if the dimensionful input masses were not $O(\text{TeV})$ at all, but actually rather small. Then their natural fluctuations would be small and the fluctuations of $m_{H_u}^2$ and thus fine-tuning would be reduced. In order to avoid the direct LHC searches one would have to generate sizable electroweak scale soft masses via the RGE evolution. Although this turns out to be rather easy to do for the scalar masses, it is unfortunately not possible for the gaugino masses. The leading order contribution to the gaugino RGE is proportional to the gaugino mass itself, so if the gaugino mass is small at high scales, it is always small. In contrast, the leading order sfermion RGEs contain the gaugino masses, which, if sufficiently large, can push the sfermion masses to TeV scales at low energies. So while one may reduce (or remove entirely) the fine-tuning arising from the scalars, one will still have fine-tuning from the gauginos.

To move forward, we will here take a constructive approach and regard fine-tuning as an indicator of new physical mechanisms. Since the fine-tuning in μ seems to be unavoidable, as discussed above, we will regard this as evidence that μ should not be regarded on the same footing as the soft supersymmetry breaking parameters in the theory. Indeed, the origin of μ is still one of the unsolved problems in supersymmetry; it is present in the superpotential before supersymmetry breaking, so *a priori* should know nothing about the electroweak

scale. This is the well known μ-problem, and suggests an effective μ parameter generated (possibly at high scales) by some unknown mechanism. The most famous example of such a mechanism is the Next-to-Minimal Supersymmetric Standard Model (NMSSM) (for a review, see [233, 234]) which introduces a new Higgs scalar field, S, that couples to the two MSSM Higgs doublets. This generates an effective μ-term when S gains a vacuum expectation value, $\mu = \lambda\langle S\rangle$, where λ is the coupling of the new scalar to the doublets. Alternatively μ may be generated by the F-term vacuum expectation value of a hidden sector field [235–237], $\mu = \langle F_X\rangle/M_P$, in a similar way to the soft supersymmetry breaking masses. However, neither of these suggestions would solve this fine-tuning problem: in the NMSSM, μ is proportional to λ so one still has fine-tuning when varying λ; if μ is derived from an F-term one still has to fine-tune $\langle F_X\rangle$.

Nevertheless, we will assume here that some mechanism exists for generating an effective μ at the high scale that is insensitive to fluctuations in the true fundamental parameters and therefore does not provide a source of fine-tuning. Note that such a mechanism would not itself entirely solve the fine-tuning problem, since one must still require that the $m^2_{H_u}$, which contributes to M^2_Z though Eq. (4.21), is also insensitive to variations in the fundamental GUT scale parameters.

We will similarly consider that the ratios of the gaugino masses ρ_1 and ρ_2 must also have their origin in some underlying mechanism, otherwise, as we shall see in Sec. 8.4, they will also generate a large fine-tuning. Several mechanisms have been proposed in order to fix these ratios, and we have already discussed how these can be generated by non-trivial representations of hidden sector fields in Sec. 3.3.3. Additionally, orbifolds [238, 239] could be responsible for the non-universality of gaugino masses. We will explore both these possibilities in Sec. 7.5. Our fine-tuning is then only measured in terms of the soft supersymmetry breaking parameters at the GUT scale.

7.3. Universal Gaugino Masses

We will first study scenarios with universal gaugino masses, $\rho_1 = \rho_2 = 1$. We randomly chose our input parameters within the ranges given in Sec. 7.2 and run them down to the electroweak scale using the full two-loop RGEs within SOFTSUSY. We set the electroweak scale to be $M_z = 91.1876\,\text{GeV}$ and the top quark pole mass to be $m_t = 173.4$ GeV. We do not force *exact* gauge couplings unification in order to allow possible percent level shifts due to threshold corrections at unification scale, as well as shifts arising from possible higher dimensional operators.

As a preliminary cut, to avoid unnecessary computation, we discard scenarios with

Higgs boson masses outside the range 122.6 – 127 GeV, and also any scenarios that do not respect the LHC direct and XENON100 (2σ) bounds as described in Sec. 7.2.1. We ensure that our scenarios have a stable vacuum using the conditions proposed by Casas, Lleyda and Muñoz in [108]. Specifically, we implement the unbounded from below (UFB) constraints UFB-1,2,3 and the charge and colour breaking (CCB) minima constraint CCB-1. In the interest of computational efficiency we take a simplified approach to the CCB-2,3 constraints and implement the simple cuts $\left|a_{\overline{5}'}/m_{\overline{5}}\right| \lesssim 3$, $|a_{5'}/m_{10}| \lesssim 3$ and $\left|a_{\overline{5}'}/m_{10}\right| \lesssim 3$ to ensure they are satisfied. At this stage we also discard scenarios with a charged LSP (the majority of these have a stau LSP, caused by a low value of m_{10}). Out of 2,000,000 initial attempts, this leaves approximately 57,000 scenarios in our scan.

We then use the electroweak scale outputs of SOFTSUSY as inputs for micrOMEGAS to generate predictions for the remaining experimental observables, such as the relic density, and derive a value of P_{tot} for each scenario. Requiring $P_{\text{tot}} > 10^{-3}$ reduces the number of viable scenarios to 306, the vast majority of which have a Dark Matter relic density below the constraint described in Sec. 7.2.1; only 30 scenarios have the preferred relic density.

Fig. 7.1 shows the distribution of these surviving points in μ and $\tan\beta$, where scenarios with a Dark Matter relic density below the 2σ relic density bounds are shown in blue, while those with the preferred value are shown in green. Most scenarios are in the region $150 \gtrsim \mu \gtrsim 600\,\text{GeV}$, where the dark matter candidate is mainly a neutralino dominated by its Higgsino component with mass $m_{\tilde{\chi}_1^0} \approx \mu$. These scenarios generally have large values of $m_{5'} \gtrsim 2\,\text{TeV}$, which force a low value of $m^2_{H_u}$ due to the RGE running, and in a turn a relatively low value of μ from the Z-boson mass constraint. 30 scenarios have the preferred relic density: 28 of these have bino dominated neutralinos as the LSP; only 2 have higgsino dominated neutralinos as the LSP (the two green points in the figure with smallest μ).

In Fig. 7.2 we also show the viable scenarios with respect to the physical stop masses, and the Higgs boson and its pseudo-scalar partner. The lightest stop $\tilde{t}_1$ we found was 461 GeV (this is the blue point furthest to the left) though this has a Dark Matter relic density below observations. The lightest stop with the preferred relic density has mass 534 GeV (the furthest left green point). The other characteristics of these two scenarios can be found in the benchmarks BP1SU(5)$_1$ and BP2SU(5)$_1$ described in Sec. 7.6. From Fig. 7.2 (right) we see that we can produce a sufficiently heavy Higgs boson, but we require a CP-odd Higgs mass, m_A in the approximate region of 1–4.5 TeV. In a recent work by Baer et al [240] acceptable solutions were found with m_A in the interval 150–1500 GeV, where we find very few viable solutions. However, Bear et al consider m_A as an input and restrict to this range to generate a scan over parameter space; by contrast our m_A is an output derived from the running of the GUT scale parameters. It is possible that with our much wider parameter scan we fail to find viable

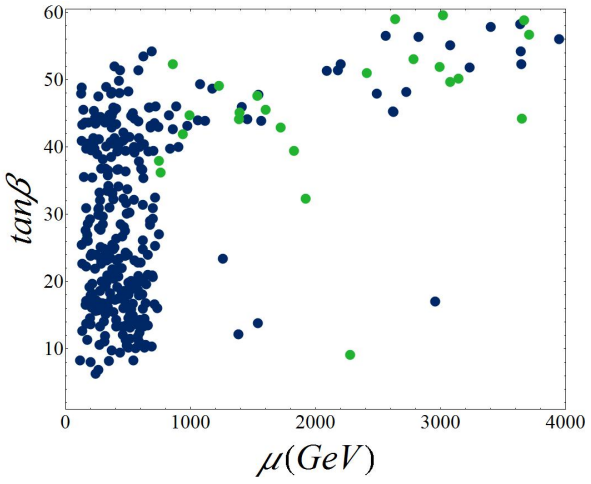

Figure 7.1. *Viable universal gaugino mass scenarios in the* μ - $\tan\beta$ *plane. Blue points represent scenarios with a Dark Matter relic density below* 2σ *bounds, while green points have the preferred relic density.*

solutions with $m_A < 1\,\text{TeV}$, but would find them if we greatly increased our initial number of scenarios tested. In Fig. 7.3 we show the viable scenarios regarding the sbottom and stau

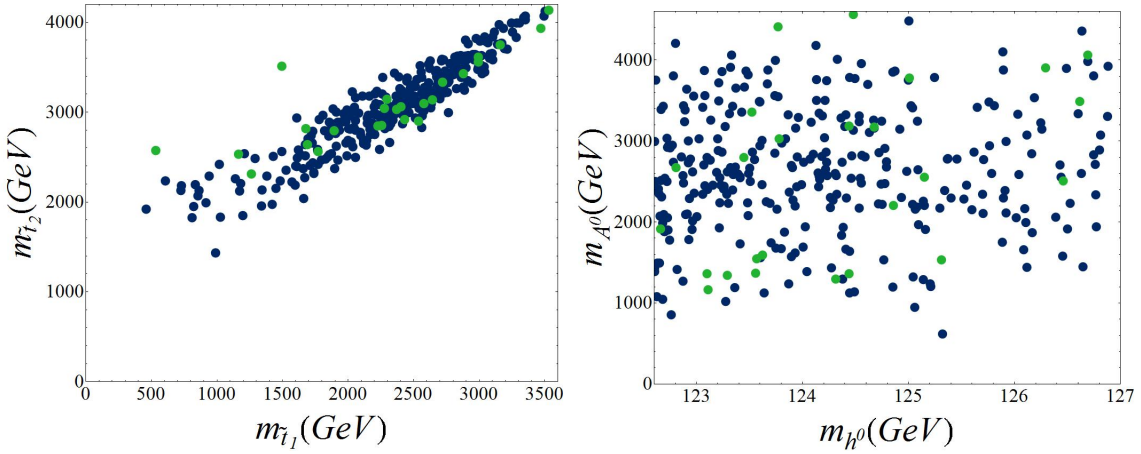

Figure 7.2. *Viable universal gaugino mass scenarios in the stop mass (left) and the lightest scalar - pseudoscalar mass (right) planes, with colours as in Fig. 7.1.*

masses. We find that the sbottoms are relatively heavy with the lightest one being precisely 1 TeV (the blue point furthest to the left). This is however a solution with little Dark Matter and the lightest one with the preferred relic density has a mass of 1285 GeV. On the other hand, the staus are significantly lighter with a lower band with plenty of solutions around 500 GeV. For instance, the lightest stau with the preferred relic density has mass 419 GeV and the lightest one with little Dark Matter has mass 416 GeV. Staus in this range of mass would be accessible to the next LHC runs and particularly interesting is that some heavy staus $\tilde{\tau}_2$ are also light enough to be probed. We find a solution where the pairing $(\tilde{\tau}_1, \tilde{\tau}_2)$ (bottom left end of the data distribution), has mass 519 GeV and 716 GeV respectively.

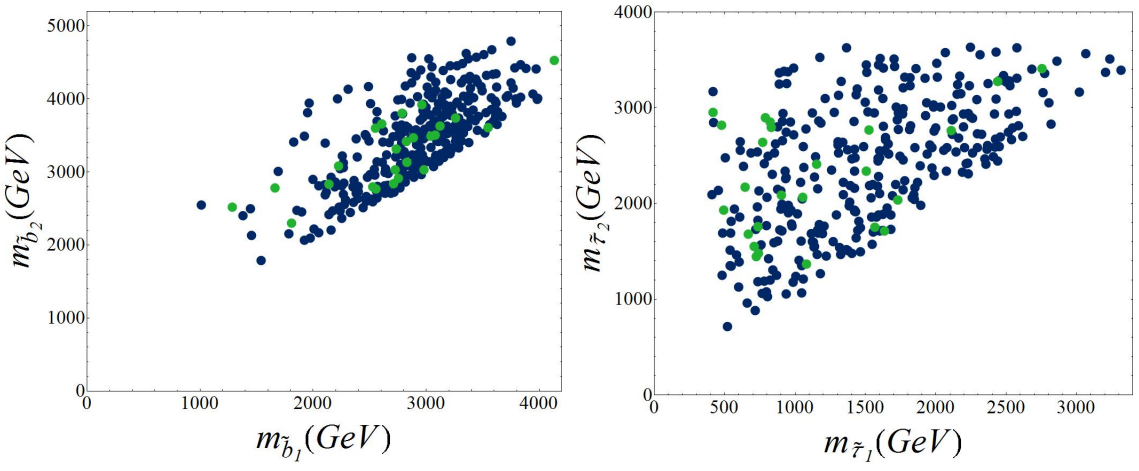

Figure 7.3. *Viable universal gaugino mass scenarios in the sbottom mass (left) and stau mass (right) planes, with colours as in Fig. 7.1.*

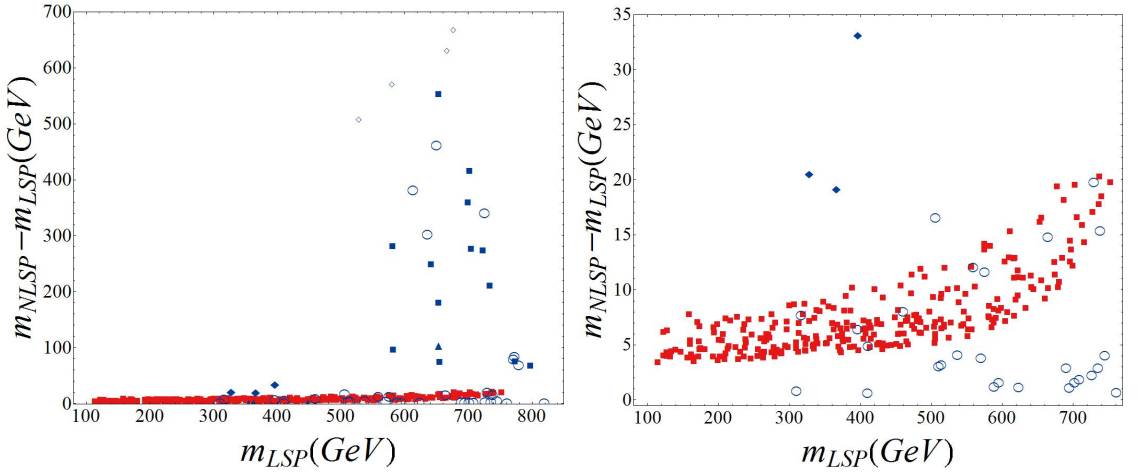

Figure 7.4. *Solutions in the plane of LSP mass vs. the NLSP-LSP mass splitting for universal gaugino mass scenarios. The colour indicates the flavour of LSP, with red and blue denoting higgsino and bino dominated Dark Matter respectively. The shape indicates the flavour of NLSP; squares, diamonds, triangles and circles denote chargino, stop, sneutrino and stau NLSP respectively. The right-hand plot is a zoomed in version of the left-hand plot.*

The LHC constraint on the gluino mass of $M_{\tilde{g}} \gtrsim 800\,\text{GeV}$ imposes a lower bound of about $M_{1/2} \gtrsim 300\,\text{GeV}$ on the common gaugino mass at the high scale. $M_{1/2} \approx 300\,\text{GeV}$ would result in a bino dominated neutralino with mass around 150 GeV. If the LSP, this would give too high a Dark Matter relic density unless one has an approximately degenerate Next-to-Lightest Supersymmetric Particle (NLSP) to facilitate coannihilation, or an appropriate particle at twice the LSP mass to provide resonant decay. Unfortunately we find no such scenarios that evade the experimental constraints and instead find that scenarios with a gluino near the LHC bound require a higgsino dominated neutralino as Dark Matter with a chargino as NLSP. These are the red squares shown in the low mass region of Fig. 7.4. When

$M_{1/2}$ is raised to 700 GeV or greater, the bino mass becomes greater than about 300 GeV and then we do indeed find viable scenarios with a bino dominated LSP and an acceptable Dark Matter relic density. All our viable scenarios are shown in Fig. 7.4.

We have so far seen that for $SU(5)$-inspired models with universal gaugino mass one has plenty of solutions that survive the experimental constraints and vacuum stability conditions, including an acceptable relic density of Dark Matter. Now we will examine these scenarios to see if they have significant fine-tuning from sources other than μ.

In particular we focus on fine-tuning of M_Z due to shifts in m_{10}, $m_{5'}$, $M_{1/2}$ and $a_{5'}$, which provide the dominant contribution to $m^2_{H_u}$. We use SOFTSUSY's implementation of fine-tuning throughout, which uses a discretised version of the definition in Eq. (7.12). The independent fine-tunings in these parameters are shown in Fig. 8.6. We see that the individual fine-tunings $\Delta_{m_{10}}$, $\Delta_{m_{5'}}$ and $\Delta_{a_{5'}}$ become small as their corresponding parameters are taken to zero, but we find no scenario with $\Delta_{M_{1/2}}$ less than about 330. This fine-tuning problem is exacerbated when these individual fine-tuning are combined into Δ, which is defined as the maximum value of the four tunings for each scenario (recall we are discounting the fine-tuning with respect to μ). In Fig. 7.6 we show this total fine-tuning in comparison to μ, and see that for the majority of scenarios we never have Δ less than about 1300. The minimum value of Δ found was 611 with a rather large value of μ (and thus Δ_μ). For viable scenarios in the region with Higgsino dominated dark matter, 100 GeV $\lesssim \mu \lesssim$ 800 GeV, Δ_μ may have been tolerable but unfortunately the fine-tuning in the other parameters make these unattractive.

The results obtained in this section show that it is possible to obtain physically viable solutions for GUT scale $SU(5)$-inspired scenarios with universal gaugino masses. However, all the scenarios found have a significant degree of fine tuning. We do however note that one may be able to find additional solutions with low fine tuning with a more intensive search [240], though such scenarios are undoubtedly rare.

7.4. Non-Universal Gaugino Masses

We expand our analysis by allowing the gaugino masses at the GUT scale to depend on the (SM) gauge group. This requires the introduction of two extra parameters, ρ_1 and ρ_2 which we vary in the interval $[-10, 10]$. We will continue to use the notation $M_{1/2}$ for the value of M_3 at the GUT scale in order to distinguish it from its value at other energies.

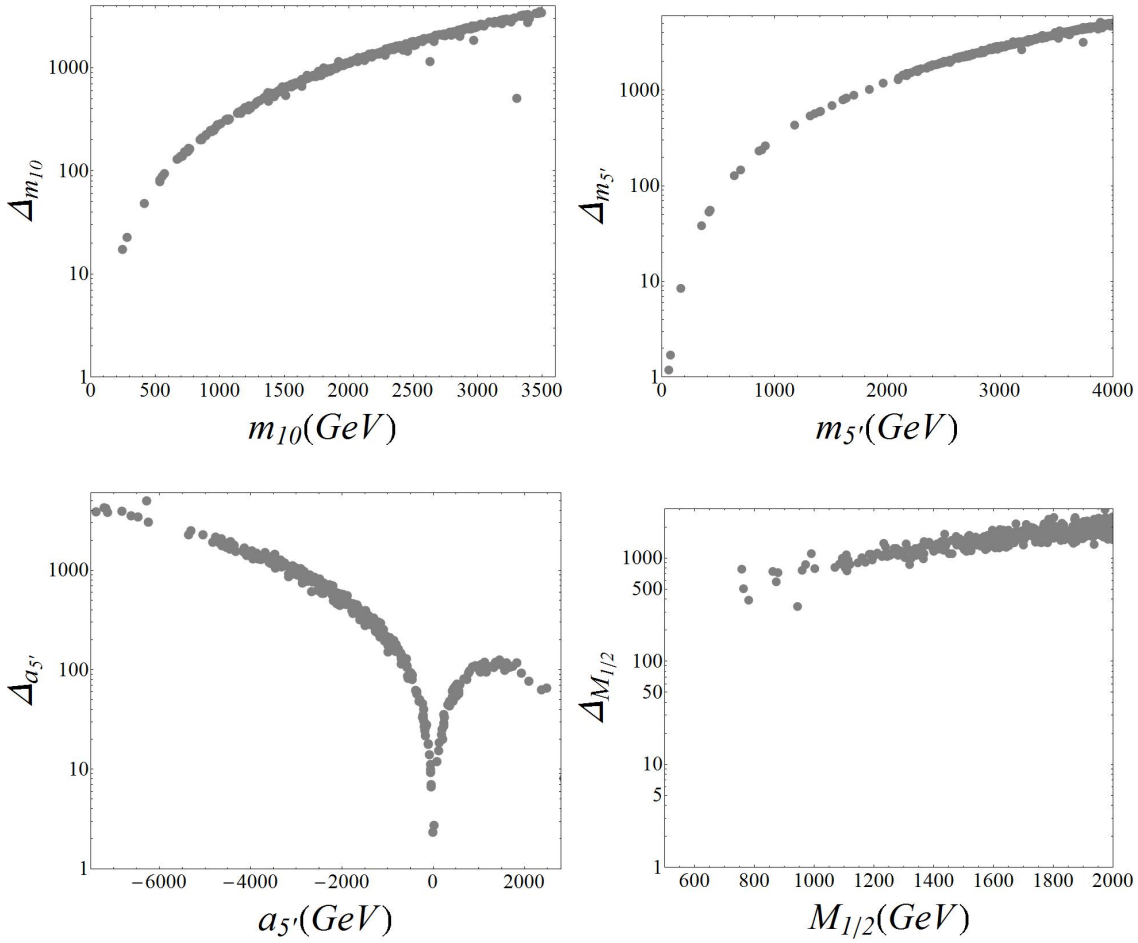

Figure 7.5. *Fine-tuning in M_Z with respect to the input parameters m_{10}, $m_{5'}$, $M_{1/2}$ and $a_{5'}$ for universal gaugino mass scenarios.*

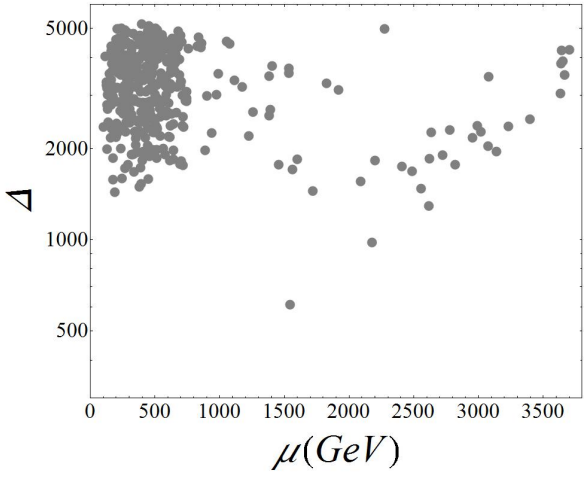

Figure 7.6. *The fine-tuning Δ compared to μ for universal gaugino mass scenarios.*

7.4.1. An Inclusive Scan

We begin our study of non-universal gaugino masses with an inclusive scan over parameter space to seek regions of interest, following a similar procedure to the universal gaugino mass scenarios described in Sec. 7.3. We increase the number of initial tries to 2,500,000 since we now have a larger parameter space to scan. After the preliminary Higgs mass cut, imposing the LHC and XENON100 direct search bounds, applying stability constraints and removing charged LSP scenarios we find only 22,418 scenarios (0.9%) survive, in comparison to approximately 57,000 (3%) for universal gaugino masses. This reduction in the number of accepted scenarios is due to the additional removal of scenarios with coloured dark matter in regions where $M_3 \ll M_{1,2}$. However, we find that the surviving scenarios are more accommodating to both the additional experimental constraints and the relic abundance of Dark Matter. After requiring $P_{\text{tot}} > 10^{-3}$ we find approximately 13,191 scenarios remain, 1581 of which have the preferred relic abundance of Dark Matter.

The gaugino masses feed into the RGEs of all superpartners playing an important role on their evolution, so it is not surprising that the range of physical masses is extended by relaxing the universality constraint. We show the viable scenarios projected onto the μ-$\tan\beta$ plane in Fig. 7.7. In contrast to the universal gaugino mass scenarios, we now have many examples of the preferred Dark Matter relic density, where the green band around 1 TeV predominantly represents scenarios with higgsino dominated Dark Matter. We find viable scenarios with stop and sbottom masses ranging from few hundred GeV up to 6 TeV, and a pseudoscalar Higgs mass extended to the interval $1.2 - 6$ TeV. We found however a wider range for the stau masses ranging between few hundred GeV up to 8 TeV. In non universal scenarios, it may happen that M_1 and/or M_2 provide stronger contributions than M_3 in the RG flow of the superpartners. While gaugino masses increase sfermions masses throughout the RG scale, the top Yukawa coupling, which contributes to decease the scalar masses as they are evolved, is not present in the RGE equations of the charged lepton superpartners, see eq. (6.1 -6.5) and (6.8-6.10). Therefore, scenarios with $M_{1,2} \gg M_3$ favour heavier staus which are not *"protected"* by the top Yukawa coupling.

The values of stop masses and the scalar/pseudoscalar Higgs masses are shown in Fig. 7.8 whereas the sbottom/stau masses are in Fig. 7.9. The scenarios with light sfermions (staus as well as stops) would be visible at the 14 TeV LHC. However, these solutions tend to have too little Dark Matter and we find very few scenarios with the preferred Dark Matter relic density while maintaining stops/staus below 1 TeV. The values of the non-universality parameters $\rho_{1,2}$ for viable scenarios are shown in Fig. 7.10. Notice that there are very few viable scenarios around $\rho_1 = \rho_2 = 1$ corresponding to universal gaugino masses.

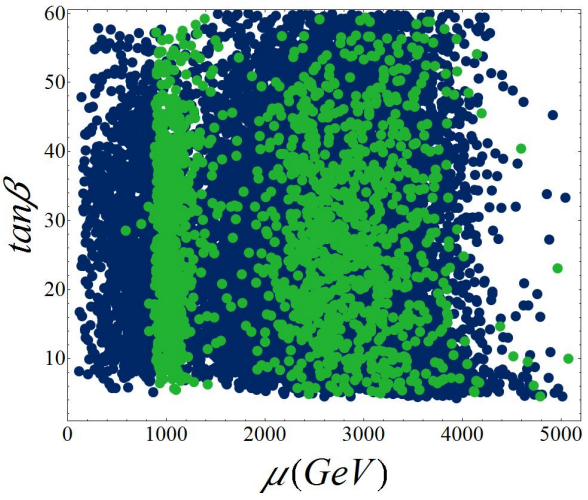

Figure 7.7. *Viable non-universal gaugino mass scenarios in the μ-tanβ plane, with colours as in Fig. 7.1.*

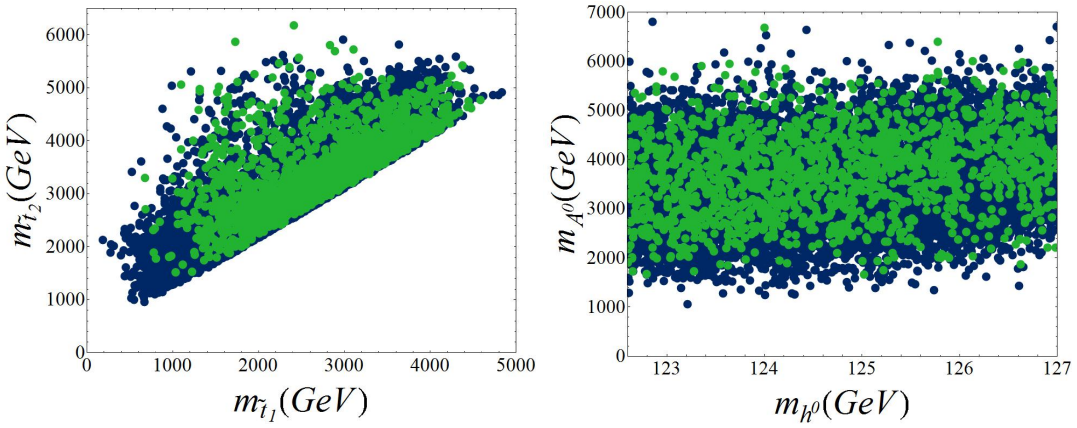

Figure 7.8. *Viable non-universal gaugino mass scenarios in the stop mass (left) and the lightest scalar – pseudoscalar mass (right) planes, with colours as in Fig. 7.1.*

In Fig. 7.11 we show the identity and masses of the LSP and NLSP for scenarios with the preferred relic density and now see many extra possibilities for LSP-NSLP pairings. Indeed the non-universality of gaugino masses now allows M_2 to be smaller than M_1, so we may also have wino dominated Dark Matter, and this can provide the correct relic density for higher LSP masses. As for the universal gaugino mass scenarios, the LSP and NLSP are typically close in mass in order to encourage co-annihilation but for bino dominated Dark Matter it is possible to have the NLSP as much as 300 GeV heavier than its LSP. (This particular scenario has a heavy Higgs boson twice the LSP mass allowing Dark Matter annihilation via a Higgs resonance.)

Although fine-tuning can be greatly reduced when the gaugino mass constraints are relaxed, there is still significant fine-tuning for much of the parameter space, and we find only

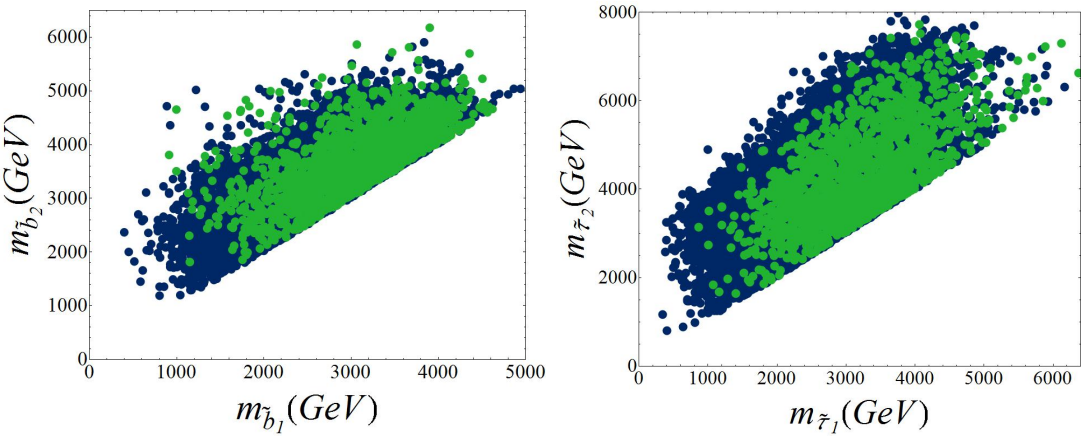

Figure 7.9. *Viable non-universal gaugino mass scenarios in the btottom mass (left) and stau mass (right) planes, with colours as in Fig. 7.1.*

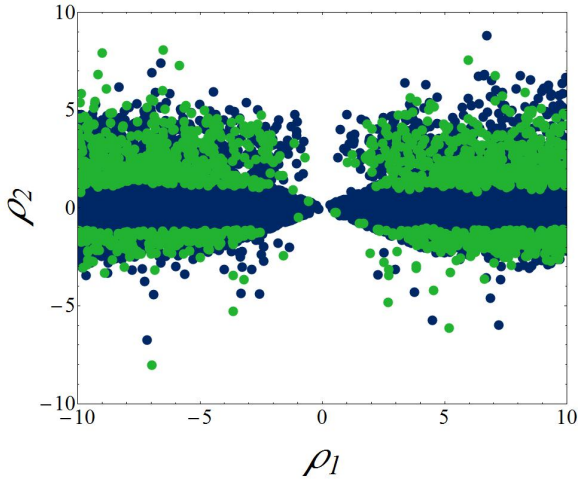

Figure 7.10. *Viable non-universal gaugino mass scenarios in the non-universality parameters $\rho_{1,2}$, with colours as in Fig. 7.1.*

one point with $\Delta < 100$. This has $\mu \approx 500\,\text{GeV}$ and a fine-tuning of approximately 60. Recall that the fine-tuning of μ is not included in Δ; the fine-tuning in μ as given by Eq. (7.14) is of order 120. In Fig. 7.12 we show the fine-tuning in the m_{10}-$M_{1/2}$ plane. The white area to the bottom-left of this plot is excluded by the experimental constraints. We see that increasing m_{10} very quickly gives unpalatable values for the fine-tuning, but increasing $M_{1/2}$ is not so problematic. This leads us to speculate that low values of the (GUT scale) soft scalar masses may provide attractive scenarios as long as a large $M_{1/2}$ feeds their evolution, making the scalars heavy enough to avoid the LHC constraints.

This conjecture is supported by the individual fine tunings of m_{10}, $m_{5'}$, $a_{5'}$ and $M_{1/2}$ in Fig. 7.13, where as before we see that in the limit of vanishing scalar masses the tuning tends to zero. This behaviour is in part due to the logarithmic form of the fine-tuning definition Eq. (7.12). The same behaviour is observed for the trilinear coupling but not for the gaugino

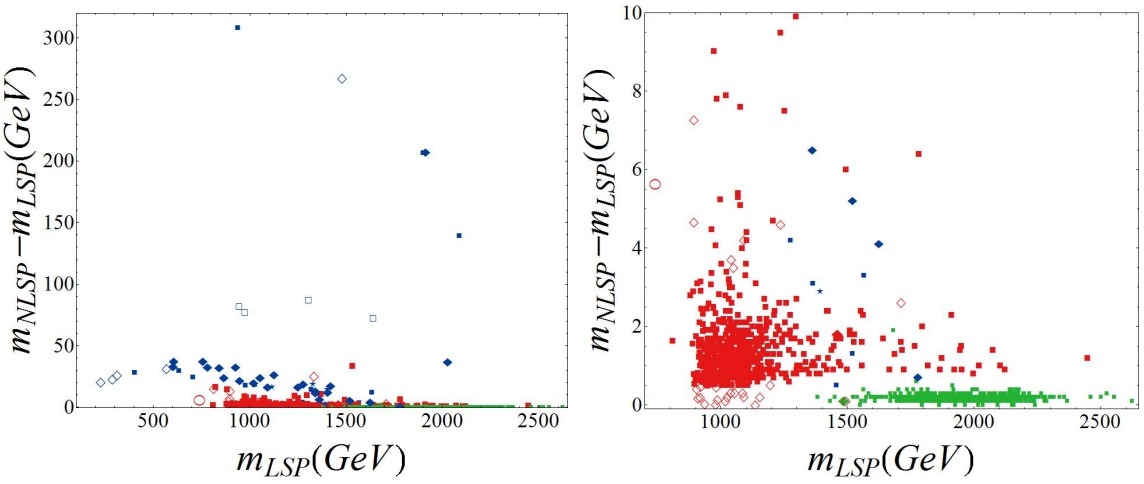

Figure 7.11. *Solutions in the plane of LSP mass vs. the NLSP-LSP mass splitting for non-universal gaugino mass scenarios. The colour indicates the flavour of LSP, with red, blue and green denoting higgsino, bino and wino dominated Dark Matter respectively. The shape indicates the flavour of NLSP; filled squares, empty squares, filled diamonds, empty diamonds, circles and stars denote chargino, gluino, stop, neutralino, stau and sbottom NLSP respectively. In contrast to Fig. 7.4, to keep the figure becoming too densely populated, we only show scenarios with the preferred Dark Matter relic density. The right-hand plot is a zoomed in version of the left-hand plot.*

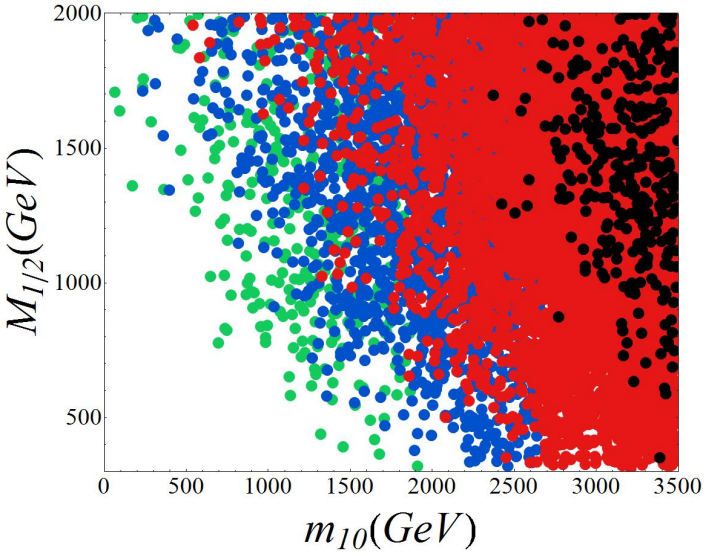

Figure 7.12. *Fine-tuning as a function of the input masses m_{10} and $M_{1/2}$ for non-universal gaugino mass scenarios. Green points represent scenarios with $\Delta \leq 1000$; blue points $1000 < \Delta \leq 2000$; red points $2000 < \Delta \leq 5000$; and black points $\Delta > 5000$.*

mass $M_{1/2}$. In contrast, for any value of the (GUT scale) gaugino mass, $M_{1/2}$, we find several points with no individual fine tuning of $M_{1/2}$, which suggests some other type of cancellation is taking place.

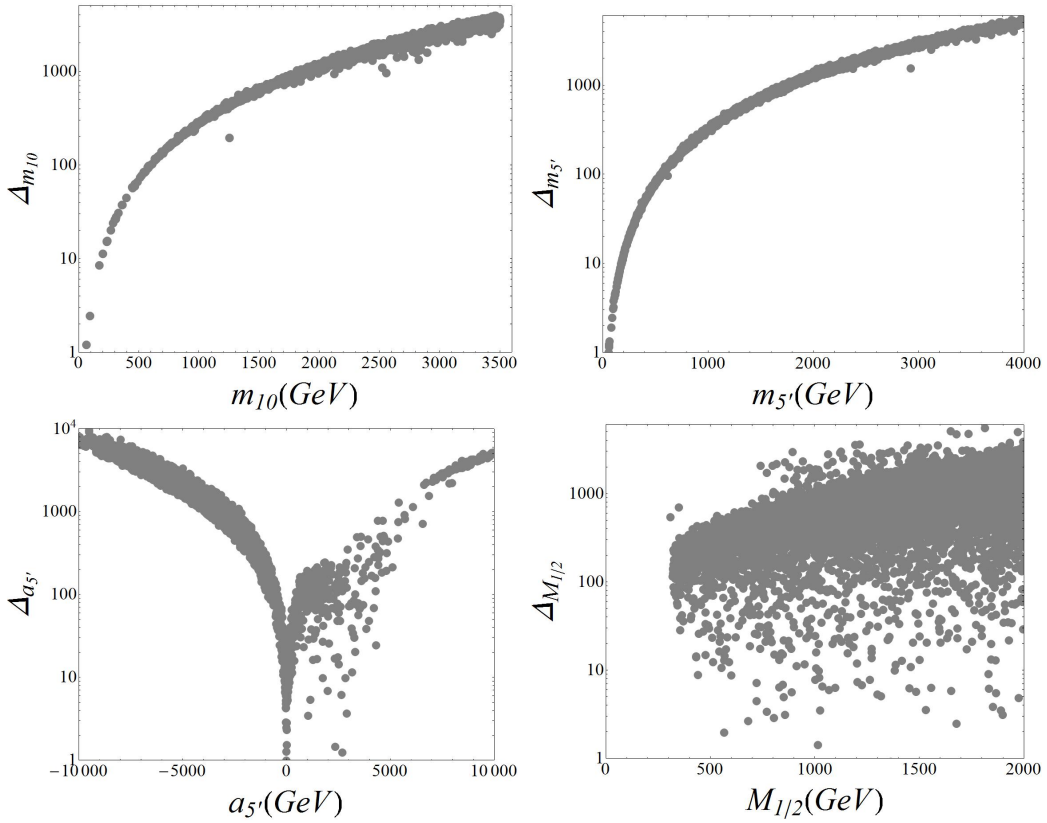

Figure 7.13. *Individual fine-tunings with respect to the input parameters m_{10}, $m_{5'}$, $M_{1/2}$ and $a_{5'}$ for non-universal gaugino mass scenarios.*

7.4.2. An Enhanced Scan Over $M_{1/2}$, ρ_1 and ρ_2

To search for regions where the fine tuning of the soft parameters is small, we set the scalar masses and trilinear couplings to zero at the GUT scale[3], but extend the range of the gaugino masses to $0 < M_{1/2} < 5000\,\text{GeV}$. We allow ρ_1 and ρ_2 to vary over the interval $[-15, 15]$, and only accept solutions where $\Delta < 100$ (again not including Δ_μ). Experimental and stability constraints are implemented as in the previous section. The surviving scenarios (3,832 out of approximately 130,000) are shown in the μ-$\tan\beta$, stop mass and Higgs mass planes in Fig. 7.14 and 7.15 and we now see not only points with fine-tuning less than 100 (lighter shades of green and blue) but also many with fine-tuning less than 10 (darker shades of green and blue). Furthermore, plenty points (1,028) provide a good description of the full Dark Matter relic density (green points) rather than describing only part of the relic density (blue points). We observe that insistence on the preferred dark matter abundance significantly restricts the allowed mass spectrum, and the preference for low fine-tuning narrows the allowed masses even further. In particular, for the optimal scenarios, we find μ restricted to be close to 1 TeV,

[3]Setting these to be *exactly* zero is for computational simplicity only; any small value at the GUT scale should be overwhelmed by the large contribution from the gluino. In Secs. 7.5.1 and 7.5.2 when we discuss explicity models we relax this and allow GUT scale scalar masses $< 100\,\text{GeV}$.

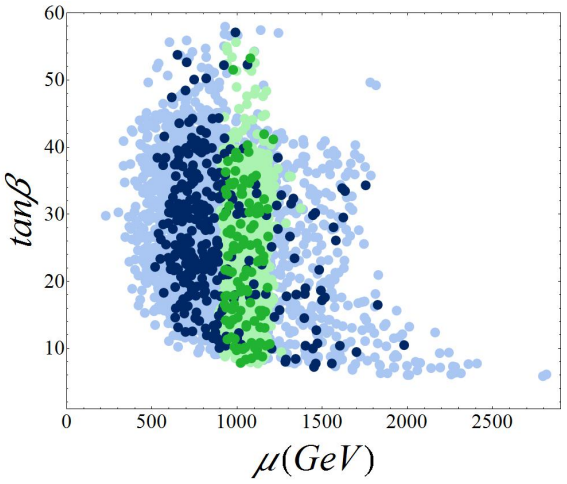

Figure 7.14. *Viable scenarios in the μ-tanβ plane for the enhanced scan with non-universal gaugino masses. Points with the preferred Dark Matter relic density are shown in green, while those with a relic density below the bounds are in blue. Darker and lighter shades denote the fine-tuning: darker shades have fine-tuning $\Delta < 10$ while lighter shades have $10 < \Delta < 100$.*

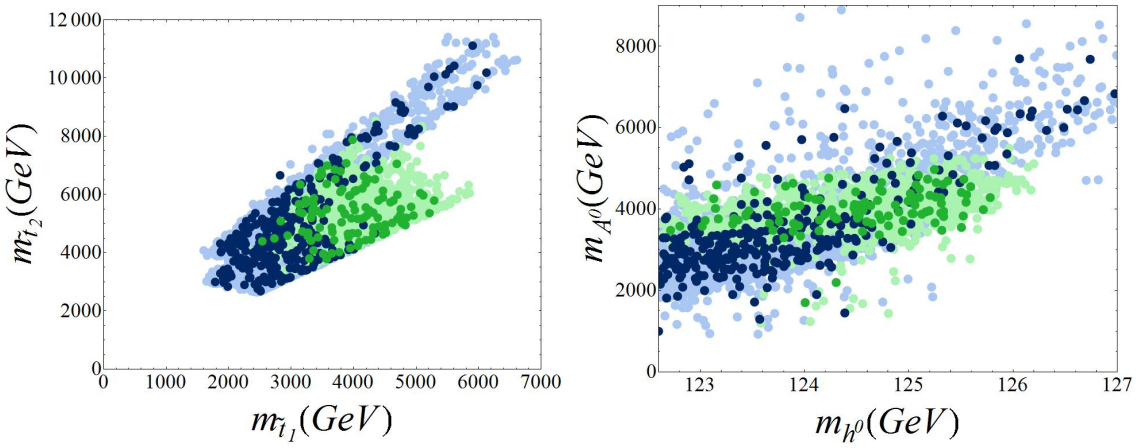

Figure 7.15. *Viable scenarios in the stop mass (left) and lightest scalar - pseudoscalar mass (right) planes for the enhanced scan with non-universal gaugino masses, with colours as in Fig. 7.14.*

lightest top and sbottom squarks confined to 2.5-6 TeV, lightest staus within 1-5.5 TeV and the pseudoscalar Higgs boson mass around 4 TeV. These ranges widen somewhat if we allow less dark matter or more fine-tuning.

It is instructive at this point to discuss why some scenarios can provide such a low fine-tuning. Since we are neglecting fine-tuning from μ, this is really a statement that m_{H_u} is insensitive to fluctuation in the fundamental (GUT scale) parameters. For the enhanced scan we have set the scalar masses and trilinears to zero, so the only dimensionful parameter that feeds the RGE's for m_{H_u} is $M_{1/2}$ and at leading order one expects $m^2_{H_u} = aM^2_{1/2}$ where a is a dimensionless coefficient that depends only on the dimensionless parameters (such as

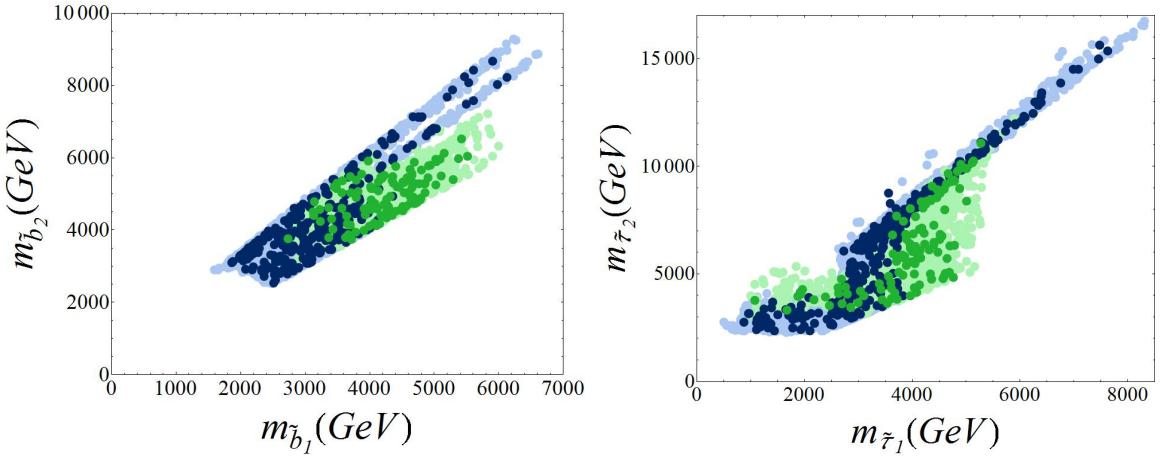

Figure 7.16. *Viable scenarios in the sbottom mass (left) and stau mass (right) planes for the enhanced scan with non-universal gaugino masses, with colours as in Fig. 7.14.*

the Yukawa couplings and $\rho_{1,2}$). Immediately this appears fine-tuned since a change in $M_{1/2}$ causes a proportionate change in m_{H_u} and therefore in M_Z, with fine-tuning

$$\Delta_{M_{1/2}} = 4|a|\frac{M_{1/2}^2}{M_Z^2}. \tag{7.16}$$

However, this expression is at leading order. One expects radiative corrections to electroweak symmetry breaking (such as tadpoles and self-energy) which are particularly important for the points on the ellipse, where a is rather small. Taking these into account makes a itself dependent on $M_{1/2}$ and a more complicated dependence results. This dependence on $M_{1/2}$ for typical parameters can be seen in Fig. 7.17. In this particular case a choice of $M_{1/2} \approx 3\,\text{TeV}$ sits close to a minimum, so $m_{H_u}^2$ (and all remaining low scale parameters including the stop mass) are insensitive to fluctuations in $M_{1/2}$ while still having large (absolute) values. However, we need to be careful in the interpretation of the low fine-tuning achieved, and remember that the behavior in Fig. 7.17 results from two-loop evolution of $m_{H_u}^2$ using the $\overline{\text{DR}}$ scheme implemented in SOFTSUSY 3.3.0. When we go from two to one-loop running of the RGE's, we observe a tiny shift in the value of the minimum, and it is expected that inclusion of further loops also affects this value, though not significantly. It is also important to check the effect of choosing different renormalization schemes, as well as verify whether the same behaviour is observed or not using distinct available software.

In Fig. 7.18, we show the LSP and NLSP masses and nature. We see that these scenarios are as usual dominated by neutralino LSPs with chargino NSLPs but the relaxation of the gaugino universality now allows the LSP to be wino dominated.

Fig. 7.19 is divided into two panes, showing the $\rho_{1,2}$ values for positive and negative μ

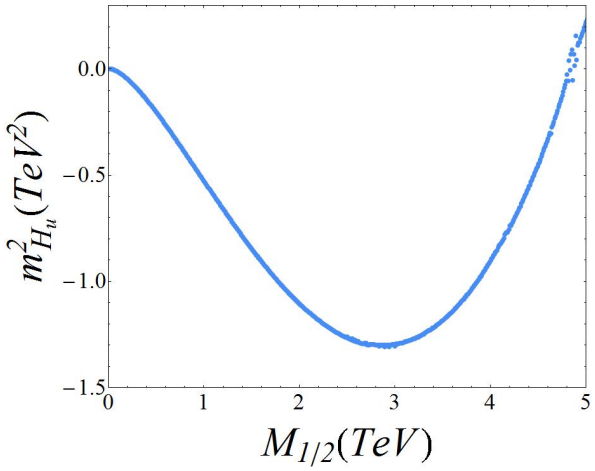

Figure 7.17. *The values of $m^2_{H_u}$ as $M_{1/2}$ is varied, for parameters as the BPO-I benchmark in Table 7.1 but with the scalar masses and trilinear couplings set to zero.*

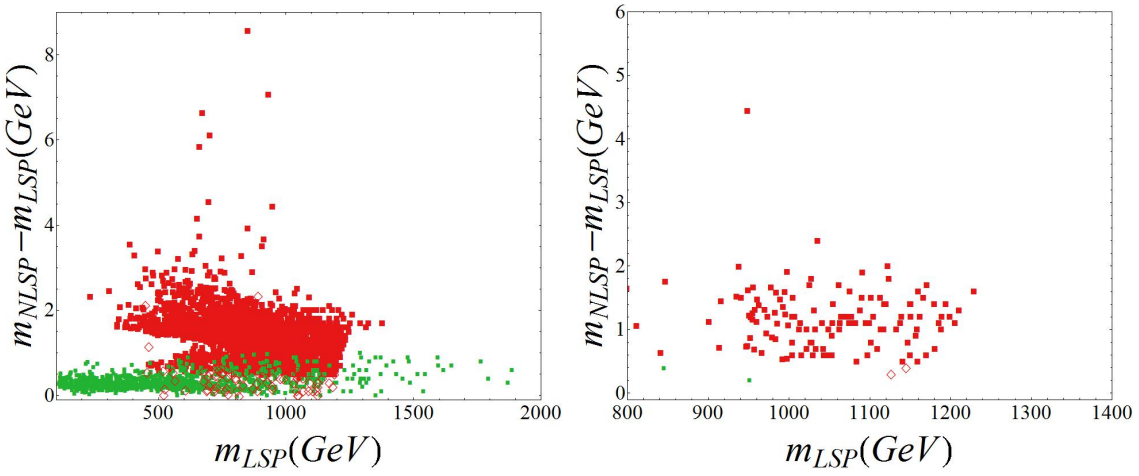

Figure 7.18. *Solutions in the plane of LSP mass vs. the NLSP-LSP mass splitting for the enhanced scan over non-universal gaugino mass scenarios. The colour indicates the flavour of LSP, with red, blue and green denoting higgsino, bino and wino dominated Dark Matter respectively. The shape indicates the flavour of NLSP; filled squares and empty diamonds denote chargino and neutralino NLSP respectively. The left-hand plot shows all scenarios with fine-tuning $\Delta < 100$ while the right-hand plot restricts to scenarios with $\Delta < 10$ and the preferred Dark Matter relic abundance.*

separately. We see that fine-tuning < 10 favours positive values of μ. It is interesting to note that all of these points fall on an ellipse. For $\mu > 0$ ($\mu < 0$) the points on the bottom (top) half of the ellipse are excluded by our experimental constraint $P_{\text{tot}} > 10^{-3}$. A similar analysis in Ref. [231] found a similar pattern.

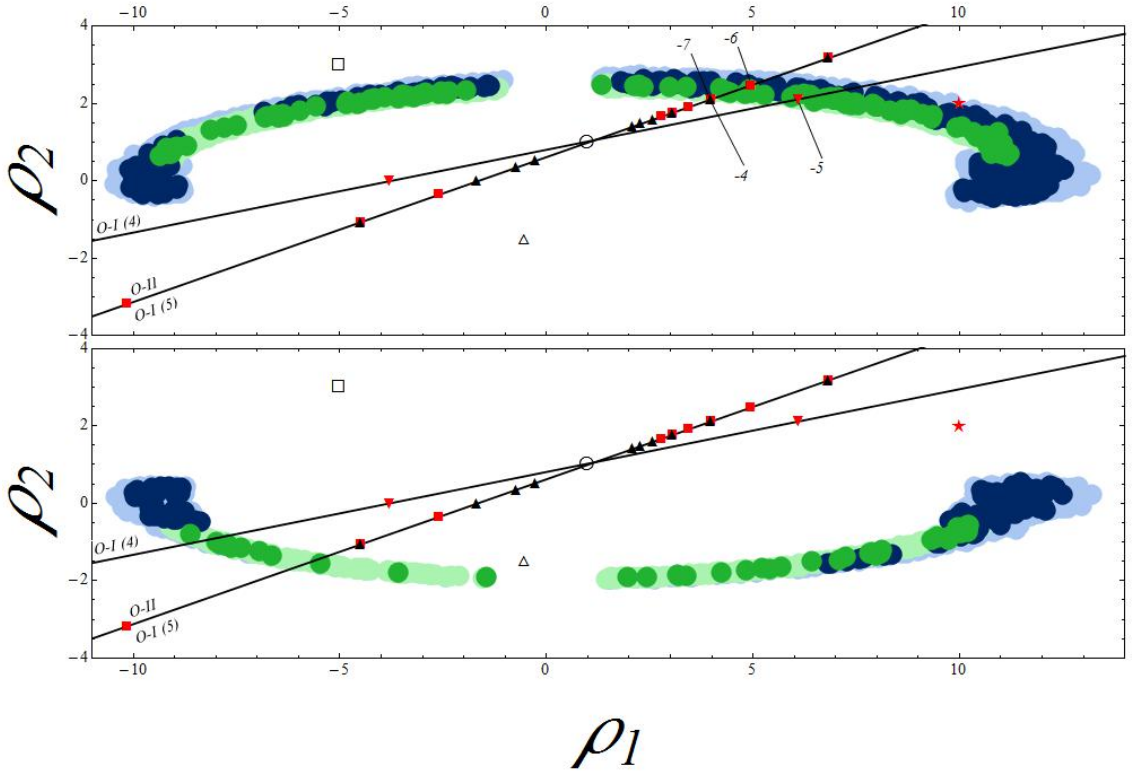

Figure 7.19. *Viable scenarios in ρ_1-ρ_2 plane for the enhanced scan with non-universal gaugino masses. Points with the preferred Dark Matter relic density are shown in green, while those with a relic density below the bounds are in blue. Darker and lighter shades denote the fine-tuning: darker shades have fine-tuning $\Delta < 10$ while lighter shades have $10 < \Delta < 100$. The upper pane is for scenarios with $\mu > 0$ while the lower pane is for $\mu < 0$. The additional symbols represent particular gaugino mass ratios as predicted by the mechanisms described in Sec. 3.3.3. Scenarios arising from embeddings in the* **1**, **24**, **75**, *and* **200** *representations of SU(5) are shown by an empty circle, an empty triangle, an empty square and a red star respectively. The orbifold inspired scenarios lie along the straight lines: the O-I model with $n_H + n_{\overline{H}} = -4$ lies on the shallower gradient line while those for the O-I model with $n_H + n_{\overline{H}} = -5$ share the steeper gradient line with the O-II orbifold. The numbers refer to δ_{GS} with those below the lines applicable to the O-I model and those above applicable to O-II.*

7.5. Scenarios with Fixed Gaugino Mass Ratios

In the above analysis we have implicitly assumed that the gaugino mass ratios are fixed by some GUT or string inspired mechanism. We here consider three classes of models as examples of how such mechanisms may be restricted by low energy constraints. For the reader not familiar with the notation below regarding the orbifold models, we encourage reading first the introductory sections of chapter 9.

1. The breaking of supersymmetry through a hidden sector field $\hat{X}$, with $f_{\alpha\beta}$ in a representation belonging to the product $(\mathbf{24}\times\mathbf{24})_{symm} = \mathbf{1}+\mathbf{24}+\mathbf{75}+\mathbf{200}$. The predicted gaugino mass ratios for embeddings in the **1**, **24**, **75**, and **200** representations are shown in Fig. 7.19 by an empty circle, an empty triangle, an empty square and a red star respectively.

2. The Brignole, Ibáñez and Muñoz (BIM) O-I orbifold [239] where the sum of the Higgs field modular weights[4] are $n_H + n_{\overline{H}} = -5$ or -4. For simplicity we will consider here only moduli dominated scenarios[5] with goldstino angles $\theta = 0$. Strictly speaking these models also restrict the scalar masses and force their mass-squared negative for $\sin^2\theta \leq 2/3$; here we disregard these scalar mass constraints and only use the orbifold to *inspire* values for the gaugino mass ratios. These ratios for the BIM O-I orbifold with $n_H + n_{\overline{H}} = -5$ are then given by[6]

$$\rho_1 = 1.18\,\frac{\delta_{GS}+54/5}{\delta_{GS}+6}, \qquad \rho_2 = 1.06\,\frac{\delta_{GS}+8}{\delta_{GS}+6}. \tag{7.17}$$

δ_{GS} is a negative integer arising from the Green-Schwarz counterterm and required for anomaly cancellation. For $n_H + n_{\overline{H}} = -4$ they are

$$\rho_1 = 1.18\,\frac{\delta_{GS}+51/5}{\delta_{GS}+6}, \qquad \rho_2 = 1.06\,\frac{\delta_{GS}+7}{\delta_{GS}+6}. \tag{7.18}$$

These scenarios are represented in Fig. 7.19 by filled black triangles triangles and inverted red triangles respectively. Note that each of these orbifold models provide scenarios that lie along a line in the ρ_1-ρ_2 plane (also drawn in Fig. 7.19).

3. The BIM O-II orbifold for which

$$\rho_1 = 1.18\,\frac{b_1-\delta_{GS}}{b_3-\delta_{GS}}, \qquad \rho_2 = 1.06\,\frac{b_2-\delta_{GS}}{b_3-\delta_{GS}}. \tag{7.19}$$

$b_{1,2,3} = (33/5, 1, -3)$ are the usual MSSM one-loop beta function coefficients. Again we are assuming moduli domination and neglecting the scalar mass predictions. These models share the line of the O-I models with $n_H + n_{\overline{H}} = -5$ in the ρ_1-ρ_2 plane and are identified in Fig. 7.19 by filled red squares. For completeness, we will explore in Chapter 8 the complete set of boundary conditions provided by the BIM O-I and BIM O-II orbifolds.

We observe that only five models provide mass ratios that lie close to our ellipse: hidden

[4] Here we use the notation adopted in [239].
[5] A dilaton dominated scenario would lie far from our ellipse.
[6] For the prefactors we use the values calculated in [239]. This is a different approach from Refs. [231] and [238] where these coefficients are set to 1.

sector breaking with a **200**; the BIM O-I orbifold with $n_H + n_{\overline{H}} = -4$ and $\delta_{GS} = -5$; the BIM O-I orbifold with $n_H + n_{\overline{H}} = -5$ and $\delta_{GS} = -4$ which coincides with the BIM O-II orbifold with $\delta_{GS} = -7$; and the BIM O-II orbifold with $\delta_{GS} = -6$. All of these models coincide with the upper half of the ellipse, so require sign(μ) = +. We will now study these cases individually.

7.5.1. $SU(5)_{200}$ Model

We first consider the model with a gauge-kinetic function embedded in a **200** of $SU(5)$, generating the GUT scale gaugino mass ratios $\rho_1 = 10$ and $\rho_2 = 2$. We note in advance that this model lies towards the edge of the ellipse in Fig. 7.19, in a light blue region, indicating that it may be difficult to generate points with small fine-tuning. When we perform a detailed scan we find that this is indeed the case; all viable scenarios have $\Delta \gtrsim 75$. However, despite its unattractive fine-tuning, this model also provides some predictions.

Firstly, the value of $\tan\beta$ is quite large, see Fig. 7.20, in the range $16-41$, and this becomes more resticted[7], $20-32$, if we insist that $\Delta < 80$. This favours $\mu \sim 500\,\text{GeV}$ with a corresponding higgsino-dominated neutralino as Dark Matter. Unfortunately, this contributes only $\sim 30\%$ of the preferred relic density, but unlike the sfermions, it should be within reach of the 14 TeV LHC.

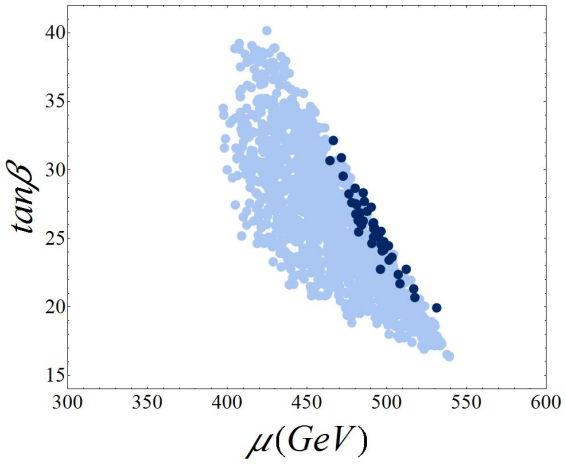

Figure 7.20. *Viable scenarios in the μ-$\tan\beta$ plane for the $SU(5)_{200}$ model. Darker and lighter shades denote the fine-tuning: darker shades have fine-tuning $\Delta < 80$ while lighter shades have $80 < \Delta < 100$. All these scenarios have a Dark Matter relic density below the preferred range.*

The allowed stop, sbottom and stau masses as well as the Higgs mass are also restricted to rather small regions of parameter space for viable scenarios. Scenarios in the stop and Higgs mass planes are shown in Fig. 7.21. The lightest stop has a mass of around 2.25 - 2.35 TeV for $\Delta < 80$. We see similar restrictions for the sbottom and stau masses, Fig. 7.22,

[7] Note that the definition of dark and light shades in Figs. 7.20 and 7.21 differ from those of Figs. 7.1, 7.2, 7.7 and 7.8 since we have no scenarios with $\Delta < 10$.

with the light sbottom within the same mass range and a stau around 2.65 - 2.75 TeV for $\Delta < 80$. The heavy stau $\tilde{\tau}_2$ has a mass which is almost twice the $\tilde{t}_2$ and $\tilde{b}_2$ masses due to the RG flow (see Tab. 7.3 for two typical scenarios). These are probably outside the reach of the 14 TeV LHC. It is also rather difficult to keep the Higgs mass heavy with $m_{h^0} \sim 122.6$ GeV for all solutions with $\Delta < 80$, though this is still compatible with the current combined experimental and theoretical uncertainties.

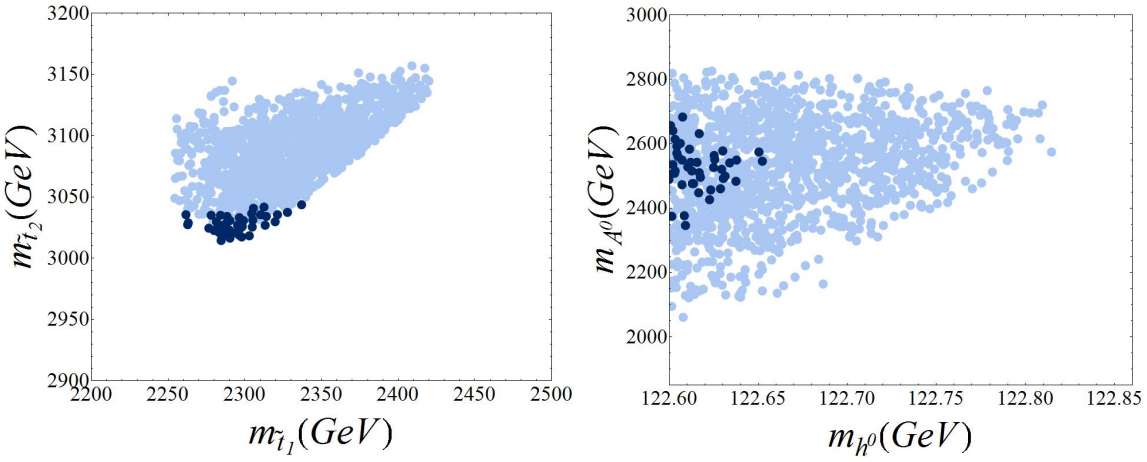

Figure 7.21. *Viable scenarios in the stop mass (left) and lightest scalar - pseudoscalar mass (right) planes for the SU(5)$_{\mathbf{200}}$ model, with colours as in Fig. 7.20.*

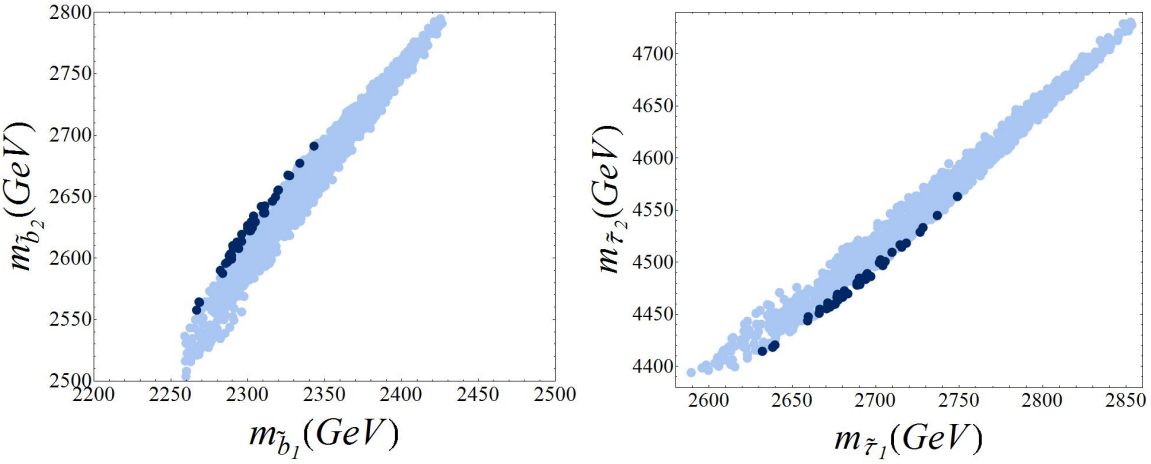

Figure 7.22. *Viable scenarios in the sbottom mass (left) and stau mass (right) planes for the SU(5)$_{\mathbf{200}}$ model, with colours as in Fig. 7.20.*

The LSP in this scenario is exclusively a higgsino dominated neutralino with mass that closely follows the value of μ. The NLSP is similarly a higgsino dominated chargino, always between 1 - 2 GeV heavier as shown in Fig. 7.23. Note that for these scenarios $\Delta_\mu \sim 120$ so comparable with the other fine-tunings.

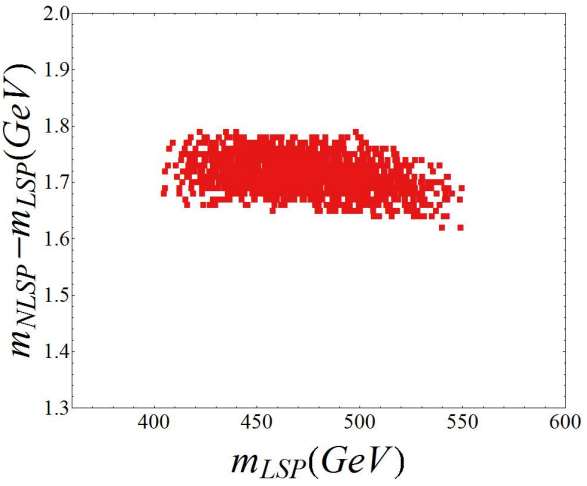

Figure 7.23. *Solutions in the plane of LSP mass vs. the NLSP-LSP mass splitting for the hidden sector chiral superfieds in a* **200** *of SU*(5). *The colours and shapes are as in Fig. 7.18. All scenarios have fine-tuning* $\Delta < 100$.

7.5.2. BIM Orbifold Models

The BIM O-I orbifold with $n_H + n_{\overline{H}} = -5$ and $\delta_{GS} = -7$ (and the coincident BIM O-II orbifold with $\delta_{GS} = -7$) also lies towards the edge of the ellipse with $\rho_1 = 4.01$ and $\rho_2 = 2.12$. However, in this case a dedicated scan finds no viable scenarios since the Dark Matter relic density is always too large (by about a factor of seven). Therefore we conclude that this model with $\Delta < 100$ is already ruled out.

The BIM O-I orbifold with $n_H + n_{\overline{H}} = -4$ and $\delta_{GS} = -5$ predicts $\rho_1 = 6.14$ and $\rho_2 = 2.12$. This lies very near the ellipse of Fig. 7.19 and when we perform a dedicated scan over its parameter space, we do indeed find plenty of solutions with low fine tuning. Rather intriguingly the majority of our points have a Dark Matter relic density in the preferred range. It is quite remarkable that this model agrees so well with all low energy data while still allowing (non-μ) fine-tuning to be very small.

In Fig. 7.24 we show the values of μ and $\tan\beta$ for the viable scenarios, indicating a preference for moderate to large values of $\tan\beta$, between 28 and 58 for fine-tuning $\Delta < 10$. μ is now necessarily quite large, around $0.9 - 1.2\,\text{TeV}$ for the least fine-tuned scenarios; lower values of μ produce an insufficient Dark Matter relic density. The distinct upper bound on $\tan\beta$ is due to our requirement for vacuum stability, while the distinct upper bound on μ is due to the upper bound on the Dark Matter relic density. The diagonal boundaries are caused by our fine-tuning constraint.

The stop masses and Higgs masses are shown in Fig. 7.25, and the sbottom and stau masses in Fig. 7.25. Now we have really very heavy stops, which in turn contribute to the Higgs mass radiative corrections, making it much easier to obtain the correct Higgs mass.

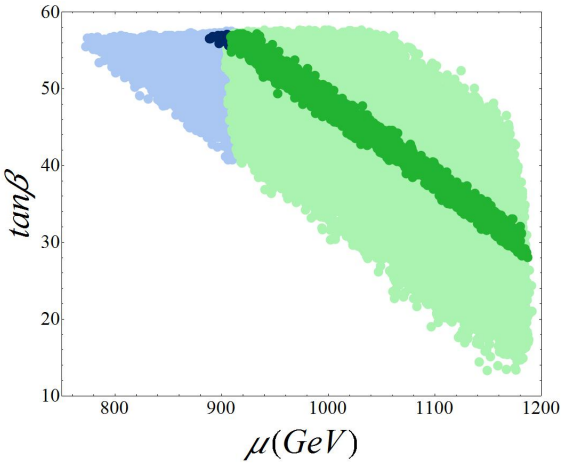

Figure 7.24. *Viable scenarios in the μ-tanβ plane for the O-I orbifold model with $\delta_{GS} = -5$. All points have the preferred Dark Matter relic density. Darker and lighter shades denote the fine-tuning: darker shades have fine-tuning $\Delta < 10$ while lighter shades have $10 < \Delta < 100$.*

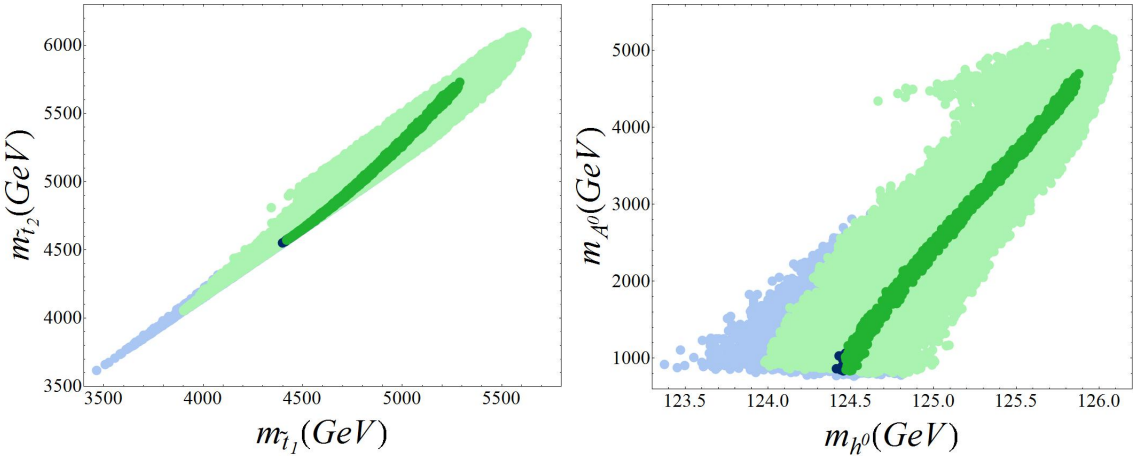

Figure 7.25. *Viable scenarios in the stop mass (left) and lightest scalar - pseudoscalar mass (right) planes for the O-I orbifold model with $\delta_{GS} = -5$, with colours as in Fig. 7.24.*

Indeed once the other constraints are applied these models seem to prefer a lightest scalar Higgs between 124.5 and 126 GeV. Since the pseudoscalar mass is now very heavy, this lightest scalar would look exactly like the SM Higgs boson, in accordance with the most recent findings. Stop, sbottom and stau masses are all approximately the same size. The LSP (neutralino) and NLSP (chargino) are both higgsino dominated and lie within roughly 1 GeV of each other as in Fig. 7.27.

The only other BIM orbifold that lies on the ellipse of Fig. 7.19 is the O-II orbifold with $\delta_{GS} = -6$. This predicts $\rho_1 = 4.96$ and $\rho_2 = 2.47$. The viable scenarios in the $\mu - \tan\beta$ plane are shown in Fig. 7.28. Now we see that most points have a Dark Matter relic density that lies below the preferred range, though we now have more moderate values of μ allowed, as

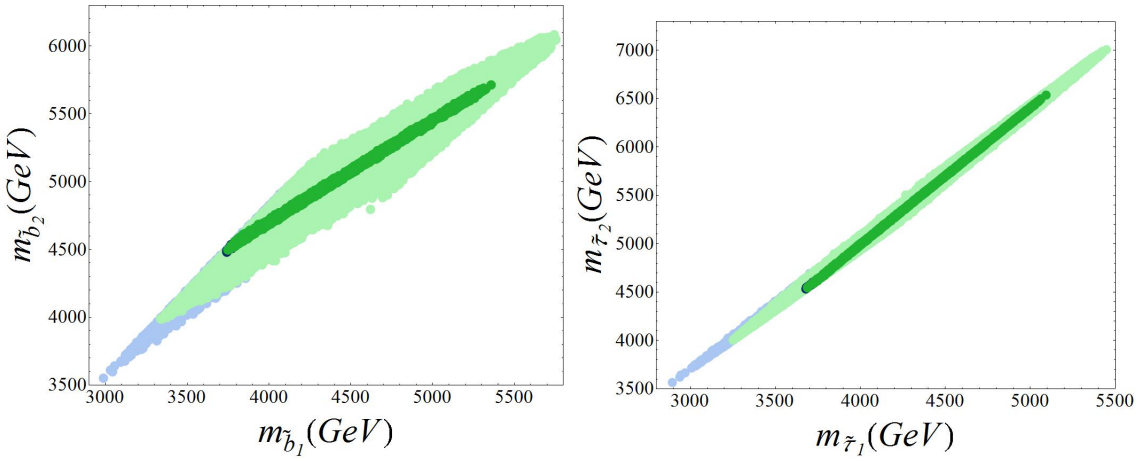

Figure 7.26. *Viable scenarios in the sbottom mass (left) and stau mass (right) planes for the O-I orbifold model with* $\delta_{GS} = -5$*, with colours as in Fig. 7.24.*

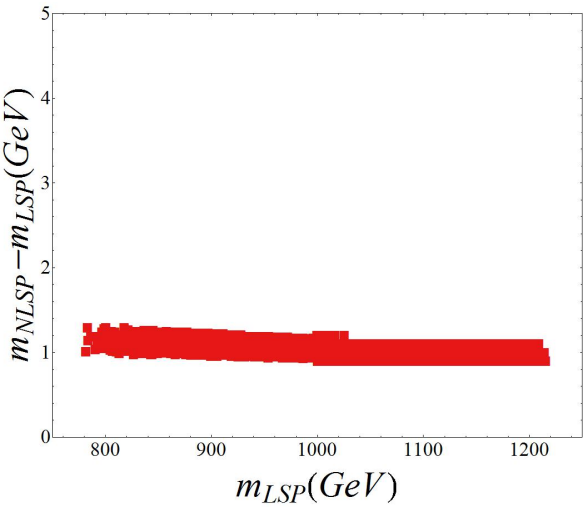

Figure 7.27. *Solutions in the plane of LSP mass vs. the NLSP-LSP mass splitting for the BIM O-I orbifold. The colours and shapes are as in Fig. 7.18. All scenarios have fine-tuning* $\Delta < 100$*.*

low as about 200 GeV. These low μ points still have fine-tuning of order $\Delta \sim 100$ from the other parameters, so having μ small gains us nothing in this regard. To keep $\Delta \leq 10$ requires μ larger than about 500 GeV. The scenarios with the preferred relic density all fall in the tail of the distribution, with quite low values of $\tan\beta$ and have fine-tuning $\Delta \sim 100$.

In Fig. 7.29 we show the results obtained in the stop mass and Higgs mass planes and in Fig. 7.30 the viable scenarios in the sbottom and stau mass planes. The third generation sfermions are considerably lighter than in the previous O-I example, even for scenarios with the preferred relic density, making them more attractive for LHC searches (though still very challenging). The corollary of lighter stops is that we also have a lighter Higgs boson, though as for the $SU(5)_{\mathbf{200}}$ this does not exclude the scenarios.

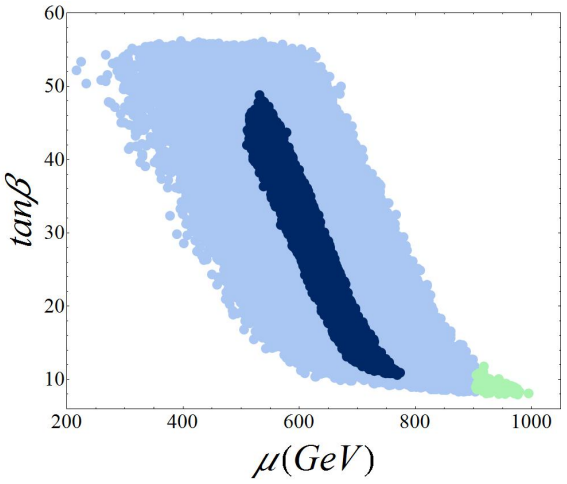

Figure 7.28. *Viable scenarios in the μ-tanβ plane for the O-II orbifold model with $\delta_{GS} = -6$. Points with the preferred Dark Matter relic density are shown in green, while those with a relic density below the bounds are in blue. Darker and lighter shades denote the fine-tuning: darker shades have fine-tuning $\Delta < 10$ while lighter shades have $10 < \Delta < 100$.*

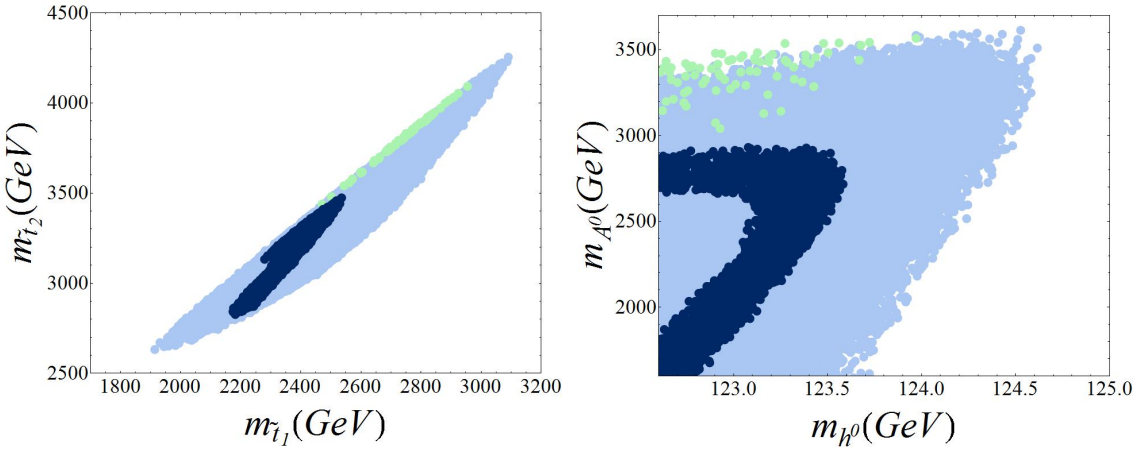

Figure 7.29. *Viable scenarios in the stop mass (left) and lightest scalar - pseudoscalar mass (right) planes for the O-II orbifold model with $\delta_{GS} = -6$, with colours as in Fig.(7.28).*

Once again, both the LSP and NLSP are higgsino dominated (neutralino and chargino respectively) and separated by about a GeV as can be seen on Fig. 7.31.

7.5.3. First and Second Generation Squarks and Gluinos

The masses of gluinos and first and second generation squarks are important for the potential discovery of supersymmetry [241, 242]. In Fig. 7.32, we show the gluino mass $m_{\tilde{g}}$ in comparison to the lightest squark mass for the three models with viable scenarios discussed

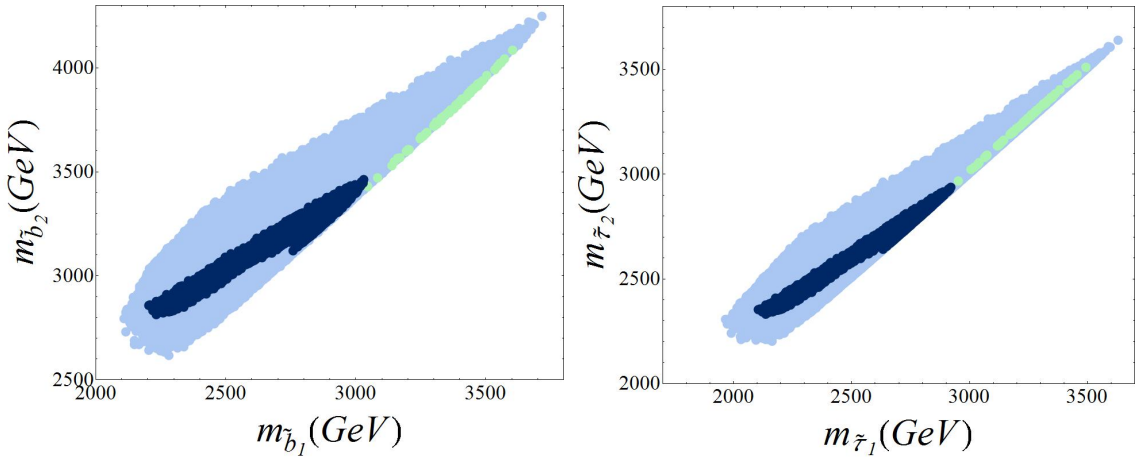

Figure 7.30. *Viable scenarios in the sbottom mass (left) and stau mass (right) planes for the O-II orbifold model with* $\delta_{GS} = -6$*, with colours as in Fig.(7.28).*

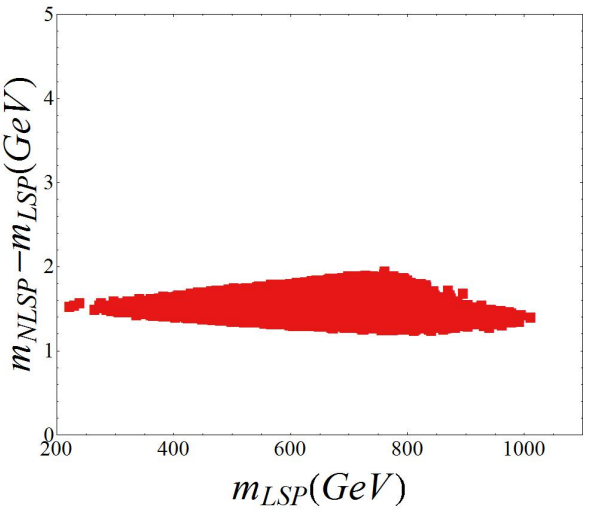

Figure 7.31. *Solutions in the plane of LSP mass vs. the NLSP-LSP mass splitting for the BIM O-II orbifold. The colours and shapes are as in Fig. 7.18. All scenarios have fine-tuning* $\Delta < 100$*.*

in Secs. 7.5.1 and 7.5.2. In all three cases we see a striking correlation between the gluino mass and the lighest squark mass. This can be easily understood analytically by making some simplifying approximations.

It is well known that the one-loop RGEs for the soft gaugino masses M_i, eq. (6.11), are analytically solvable, giving

$$M_i(t) = M_i(0)\frac{\alpha_i(t)}{\alpha_i(0)}. \tag{7.20}$$

Similarly, when one neglects the small Yukawa couplings, the one-loop RGEs for the first

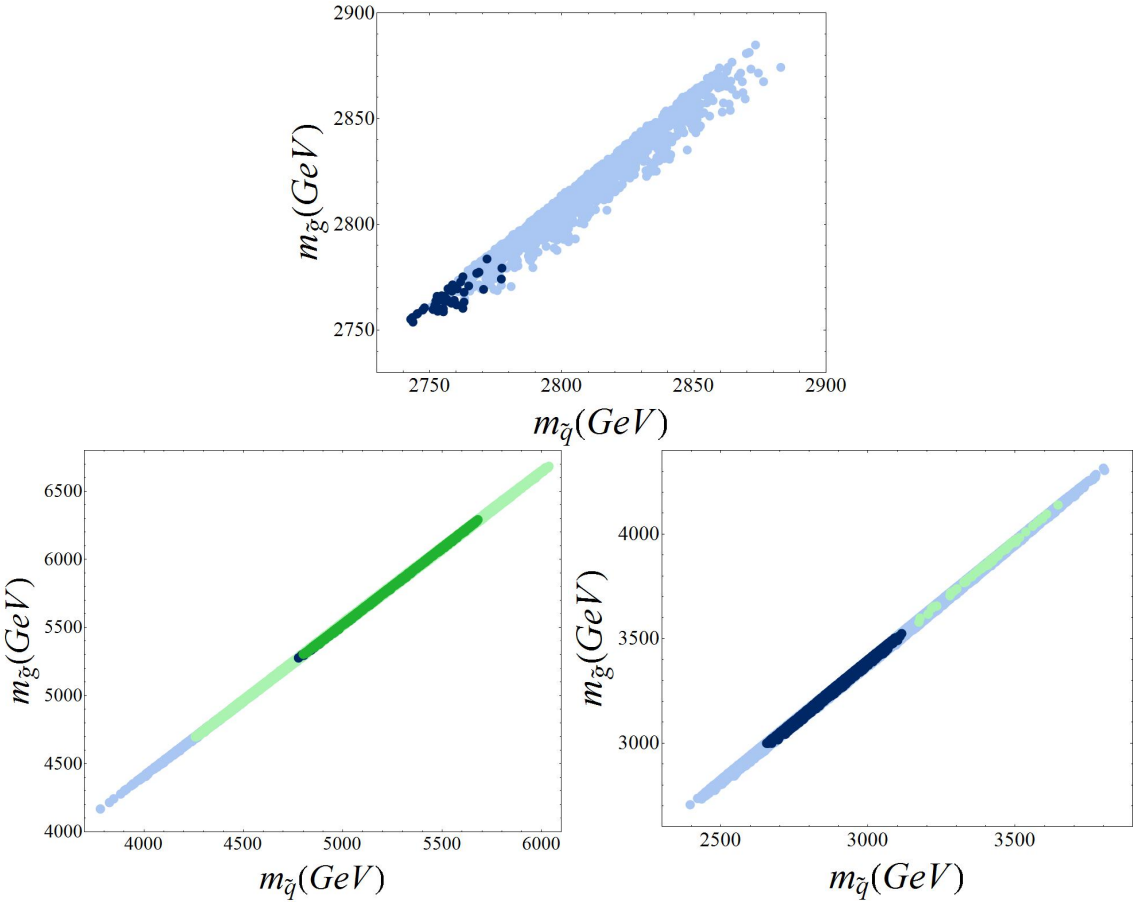

Figure 7.32. *The lightest squark mass and the gluino mass for the $SU(5)_{\mathbf{200}}$ model (top), the O-I orbifold model with $\delta_{GS} = -5$ (bottom-left) and O-II orbifold model with $\delta_{GS} = -6$ (bottom-right). Points with the preferred Dark Matter relic density are shown in green, while those with a relic density below the bounds are in blue. Darker and lighter shades denote the fine-tuning: in the upper plot ($SU(5)_{\mathbf{200}}$ scenarios), darker shades have fine-tuning $\Delta < 80$ while lighter shades have $80 < \Delta < 100$; in the two lower plots (orbifold scenarios) darker shades have fine-tuning $\Delta < 10$ while lighter shades have $10 < \Delta < 100$*

and second generation squarks are also analytically solvable, giving (6.14 - 6.22)

$$m^2_{\tilde{d}_R}(t) = m^2_{\tilde{d}_R}(0) - \frac{8}{9}M_3^2(0)\left[\frac{\alpha_3^2(0)-\alpha_3^2(t)}{\alpha_3^2(0)}\right] + \frac{2}{99}M_1^2(0)\left[\frac{\alpha_1^2(0)-\alpha_1^2(t)}{\alpha_1^2(0)}\right], \tag{7.21}$$

where we use the $\tilde{d}_R$ squark mass as an example, and ignore the contribution from the Higgs soft scalar masses which is always small for these scenarios. Using $M_1(0) = M_3(0)\rho_1$, applying Eq. (7.20), using the boundary condition $m^2_{\tilde{d}_R}(0) = K_{\bar{\mathbf{5}}} m^2_{\bar{\mathbf{5}}}$ and putting in numbers for the couplings, this gives approximately

$$m^2_{\tilde{d}_R}(t) = K_{\bar{\mathbf{5}}} m^2_{\bar{\mathbf{5}}} + M_3^2(t)\left[0.78 + 0.002\,\rho_1^2\right]. \tag{7.22}$$

When $m_{\tilde{d}_R}(0)$ is kept small, the dominant contribution arises from the gluino mass. For

the two orbifold models, ρ_1 is also rather small so one has $m_{\tilde{d}_R} \approx 0.9\, m_{\tilde{g}}$. For the $SU(5)_{\mathbf{200}}$ scenarios, the larger $U(1)$ gaugino mass ($\rho_1 = 10$) pushes this up a little to give $m_{\tilde{d}_R} \approx m_{\tilde{g}}$. The small spread in squark masses for a particular gluino mass is mainly caused by variations in $K_{\bar{\mathbf{5}}}$. Note that the apparent greater spread in masses for the $SU(5)_{\mathbf{200}}$ scenarios in Fig. 7.32 is only due to the different plot scales. Eq. (8.23) actually also works for the first two scenarios in Tab. 7.1 because coincidentally these scenarios have $m^2_{\mathbf{5}'} \approx m^2_{\bar{\mathbf{5}}}$, so that their contributions cancel, but does not work in general. Of course this argument is very approximate and ignores all the extra contributions that are included in the full two-loop SOFTSUSY analysis but nevertheless gives good qualitative agreement.

It is interesting that the $SU(5)_{\mathbf{200}}$ scenarios all require gluino and lightest squark masses in a rather restricted window, ranging from about 2740 GeV to about 2890 GeV, so well beyond current LHC limits. Requiring $\Delta < 80$ restricts them further to the very start of this already narrow mass window. If this model is a true reflection of reality, it is not surprising that the LHC has not yet seen supersymmetry. However, such gluino masses should be observable at the 14 TeV LHC.

The orbifold models also restrict the gluino and lightest squark masses but the window is much larger. For the O-I model we find viable scenarios only with the lightest squarks heavier than about 3.7 TeV and the gluinos about 10% heavier. Requiring $\Delta < 10$ results in the lightest squark being heavier than about 4.8 TeV. Unfortunately these scenarios are considerably beyond the expected reach of the 14 TeV LHC [243], which is unfortunate since this is our most attractive possibility, able to explain the entirety of Dark Matter while simultaneously keep the fine-tuning in the soft mass parameters small. Nevertheless, an energy-upgraded Super-LHC with $\sqrt{s} = 28$ TeV would enhance production rates of such squarks and gluinos by a factor of ten [244], allowing these scenarios to become accessible.

The O-II model is also restrictive, but like the $SU(5)_{\mathbf{200}}$ scenarios allows squarks and gluinos within reach of the 14 TeV LHC. If fine-tuning is our priority then we may achieve $\Delta < 10$ with lightest squark masses between about 2.6 TeV and 3.1 TeV, but if the preferred Dark Matter relic density is desired one requires a slightly heavier lightest squark between about 3.2 TeV and 3.7 TeV. Unfortunately this models does not allow low fine-tuning and the preferred relic density simultaneously.

7.6. Benchmark Points

In this section we present six benchmarks for viable $SU(5)$ GUT scenarios with non-universal masses that may be interesting to consider at either the 14 TeV LHC or the energy-upgraded Super-LHC with $\sqrt{s} = 28$ TeV. The GUT scale parameters for these scenarios can be found

in Tab. 7.1. In Tab. 7.2 we show the masses of the five Higgs bosons. The masses of the first and third generation sfermions are shown in Tab. 7.3. The second generation sfermions are assumed degenerate with the first. In Tab. 7.4 we show the gaugino masses. Finally in Tab. 7.5 we present μ, $\tan\beta$, the fine-tuning Δ, the fine-tuning from μ alone, the predicted relic density of Dark Matter, and the predominant component of the LSP.

	BP1SU(5)$_{\mathbf{1}}$	BP2SU(5)$_{\mathbf{1}}$	BP1SU(5)$_{\mathbf{200}}$	BP2SU(5)$_{\mathbf{200}}$	BPO-I	BPO-II
$m_{\mathbf{10}}$	3305	2632	78.86	70.97	9.33	24.75
$m_{\bar{\mathbf{5}}}$	2453	2442	47.83	75.03	17.71	60.12
$K_{\mathbf{10}}$	1.51	7.38	8.70	14.88	8.39	14.40
$K_{\bar{\mathbf{5}}}$	5.07	6.86	14.44	11.72	14.74	0.60
$m_{\mathbf{5}'}$	3735	3187	5.15	69.34	41.30	46.47
$m_{\bar{\mathbf{5}}'}$	3780	3179	64.78	14.29	88.26	17.43
$a_{\mathbf{5}'}$	-6283	-4436	-98.72	-97.67	8.94	-47.12
$a_{\bar{\mathbf{5}}'}$	4606	-1639	-88.26	-1.10	22.26	-10.12
$M_{1/2}$	944.8	781.2	1247	1249	2875	1611
ρ_1	1.00	1.00	10.00	10.00	6.14	4.96
ρ_2	1.00	1.00	2.00	2.00	2.12	2.47

Table 7.1. *GUT scale parameters for our six benchmark scenarios. Masses and trilinear couplings are in GeV. $M_{1/2}$ is the value of M_3 at the GUT scale.*

	BP1SU(5)$_{\mathbf{1}}$	BP2SU(5)$_{\mathbf{1}}$	BP1SU(5)$_{\mathbf{200}}$	BP2SU(5)$_{\mathbf{200}}$	BPO-I	BPO-II
m_{h^0}	123.8	124.9	122.6	122.6	125.5	123.6
m_{A^0}	4412	3144	2592	2375	3781	2635
m_{H^0}	4412	3144	2592	2375	3781	2635
$m_{H^\pm}$	4413	3145	2594	2377	3782	2636

Table 7.2. *Higgs masses in GeV for our six benchmark scenarios.*

The first two benchmarks BP1SU(5)$_{\mathbf{1}}$ and BP2SU(5)$_{\mathbf{1}}$ have universal gaugino masses consistent with breaking from a singlet of $SU(5)$ ($\rho_1 = \rho_2 = 1$) and only deviate from non-universality for the scalar masses. Although these scenarios have large fine-tuning (as did all the viable universal gaugino scenarios we found) and therefore are not aesthetically pleasing they are still consistent with experimental bounds so should not be dismissed out of hand.

The next two benchmarks, BP1SU(5)$_{\mathbf{200}}$ and BP2SU(5)$_{\mathbf{200}}$ are scenarios for which supersymmetry is broken by a gauge-kinetic function in a **200** dimensional representation of $SU(5)$. This allows non-universal gaugino masses, and in this case the $U(1)$ gaugino is a factor of 10 heavier than the $SU(3)$ gaugino at the GUT scale. Although the fine-tuning is still sizeable (~ 75 for both scenarios) it is considerably better than for the universal gaugino masses.

The final two benchmarks are for orbifold *inspired* values of gaugino mass ratios. The

	BP1SU(5)$_1$	BP2SU(5)$_1$	BP1SU(5)$_{200}$	BP2SU(5)$_{200}$	BPO-I	BPO-II
$m_{\tilde{t}_1}$	533.5	460.8	2303	2263	5039	2508
$m_{\tilde{t}_2}$	2572	1920	3018	3028	5354	3386
$m_{\tilde{b}_1}$	2557	1900	2309	2268	4848	2890
$m_{\tilde{b}_2}$	2764	2453	2642	2564	5332	3376
$m_{\tilde{\tau}_1}$	2437	2347	2704	2638	4681	2795
$m_{\tilde{\tau}_2}$	3277	2465	4497	4418	5960	2854
$m_{\tilde{\nu}^3}$	2436	2347	2703	2637	4680	2852
$m_{\tilde{u}_L}$	7609	7004	2877	2878	6315	3852
$m_{\tilde{u}_R}$	7596	6998	3797	3801	6551	3498
$m_{\tilde{d}_L}$	7610	7004	2878	2879	6316	3852
$m_{\tilde{d}_R}$	5702	6500	2751	2763	5416	3071
$m_{\tilde{e}_L}$	5534	6403	2790	2802	5012	2927
$m_{\tilde{e}_R}$	7449	6896	4605	4610	6478	2946
$m_{\tilde{\nu}^1}$	5534	6402	2789	2800	5011	2926

Table 7.3. *First and third generation sfermion masses (we assume the first and second generation sfermions are degenerate) for our six benchmark scenarios. All the masses are in GeV*

	BP1SU(5)$_1$	BP2SU(5)$_1$	BP1SU(5)$_{200}$	BP2SU(5)$_{200}$	BPO-I	BPO-II
$M_{\tilde{g}}$	2298	1934	2760	2763	5993	3476
$M_{\tilde{\chi}_1^0}$	414.9	342.0	534.9	495.6	1167	689.8
$M_{\tilde{\chi}_2^0}$	805.4	663.6	538.8	499.4	1169	692.6
$M_{\tilde{\chi}_3^0}$	2319	1288	2037	2041	5002	3242
$M_{\tilde{\chi}_4^0}$	2320	1292	5485	5496	7861	3490
$M_{\tilde{\chi}_1^\pm}$	805.5	663.6	536.6	497.3	1168	691.3
$M_{\tilde{\chi}_2^\pm}$	2321	1293	2037	2041	5002	3242

Table 7.4. *Gaugino masses in GeV for our six benchmark scenarios.*

	BP1SU(5)$_1$	BP2SU(5)$_1$	BP1SU(5)$_{200}$	BP2SU(5)$_{200}$	BPO-I	BPO-II
μ	2275	1256	512.2	471.6	1094	657.5
$\tan\beta$	9.14	23.43	22.75	30.90	38.40	26.65
Δ	4978	2638	75.55	78.83	2.94	9.59
Δ_μ	2433	750.1	141.7	119.0	646.3	232.7
$\Omega_c h^2$	1.01×10^{-1}	3.66×10^{-2}	3.02×10^{-2}	2.59×10^{-2}	1.30×10^{-1}	5.01×10^{-2}
LSP type	Bino	Bino	Higgsino	Higgsino	Higgsino	Higgsino

Table 7.5. *The Higgs parameters μ (in GeV) and $\tan\beta$ for our six benchmark scenarios. Also shown is the fine-tuning Δ (which does not include fine-tuning in μ as described in the text), the fine-tuning from μ alone, the predicted relic density of Dark Matter, and the predominant component of the LSP.*

benchmark BPO-I is inspired by the BIM O-I orbifold model with $n_H + n_{\bar{H}} = -4$ and $\delta_{GS} = -5$. The benchmark BPO-II is inspired by the BIM O-II orbifold with $\delta_{GS} = -6$. These both have very low (non-μ) fine-tuning. Remarkably BPO-I is also spot on for the relic density of Dark

Matter, but unfortunately its spectrum is very heavy and looks beyond the reach of the 14 TeV LHC.

8. $SO(10)$ Grand Unification Phenomenology

We turn now to the study of supersymmetric Grand Unified models based on the $SO(10)$ gauge symmetry. Our analysis is similar to the previous chapter. However we will develop our studies further for non-universal gauginos, by considering combinations of hidden sector fields in distinct $SO(10)$ representations. We examine the possible breaking chains following the $SU(5)$ and Pati-Salam routes and investigate which possible constraints are imposed on the parameter space.

8.1. The $SO(10)$ GUT Model

We consider the minimal realistic $SO(10)$ GUT model [245,246] with the superpotential given by

$$\begin{aligned} W_{SO(10)} &= (y_{\mathbf{10}})_{ij}\,\mathbf{16}_{ia}\,(\mathbf{C}\Gamma_\alpha)^{ab}\,\mathbf{16}_{jb}\mathbf{10}_\alpha + \frac{1}{5!}(y_{\mathbf{126}})_{ij}\,\mathbf{16}_{ia}\left(\mathbf{C}\Gamma_{[\alpha}\Gamma_\beta\Gamma_\rho\Gamma_\sigma\Gamma_{\lambda]}\right)^{ab}\mathbf{16}_{jb}\overline{\mathbf{126}}_{\alpha\beta\rho\sigma\lambda} \\ &+ \mu_1\mathbf{10}_\alpha\mathbf{10}_\alpha + \mu_2\mathbf{126}_{\alpha\beta\rho\sigma\lambda}\overline{\mathbf{126}}_{\alpha\beta\rho\sigma\lambda} + W_{\mathbf{X_R}}, \end{aligned} \tag{8.1}$$

where the Γ_μ matrices satisfy a rank 10 Clifford algebra, see eq. (2.9), and $\mathbf{C}$ is a $SO(10)$ charge conjugation matrix. Here, $W_{\mathbf{X_R}}$ is the part of the superpotential that involves the chiral superfields $X_{\mathbf{R}}$, belonging to a $SO(10)$ symmetric representation $\mathbf{R}$, contained in the product of two adjoint representations, $\mathbf{45}\times\mathbf{45}$, and whose scalar components are responsible for the breaking of the GUT symmetry at the high scale. $\{i,j\} = 1,2,3$ are generation indices and $\{a,b\} = 1,\ldots,16$ are spinor indices. All the MSSM quark and lepton superfields as well as the right-handed neutrino superfield, $\hat{Q}_L$, $\hat{u}^\dagger_R$, $\hat{e}^\dagger_R$, $\hat{L}_L$, $\hat{d}^\dagger_R$, and $\hat{\mathrm{N}}^\dagger_R$, are embedded in the $\mathbf{16}$ representation. The Higgs superfields $\hat{H}_u$ and $\hat{H}_d$ belong to a superposition of the $\mathbf{10}$ and of the $\overline{\mathbf{126}}$ representations in order to generate the correct fermion masses and mixings. In addition, we consider that terms involving a $\mathbf{126}$-plet, which do not couple to the ordinary matter in the $\mathbf{16}$-plet, are also present in $W_{\mathbf{X_R}}$. While such terms enhance proton decay lifetime by a factor of 10^3 over a minimal $SU(5)$ model, [162], D-terms arising from the expectation values of the $\overline{\mathbf{126}}$ will be canceled and the mass splittings at the GUT scale will be similar to a model with a single Higgs $\mathbf{10}$-plet. The doublet-triplet splitting problem is assumed to be solved by a mechanism similar to that discussed in [247–249]. We assume here that the MSSM μ-term is a combination of the bilinear terms μ_1 and μ_2. Finally $y_{\mathbf{10}}$ and $y_{\mathbf{126}}$ are Yukawa coupling matrices and typically $y_{\mathbf{126}}$ is much smaller than $y_{\mathbf{10}}$.

8.1.1. Soft Scalar Masses

The effective Lagrangian for the Higgs and sfermion masses is given as in eq. (7.2). For the $SO(10)$ GUT model described, when the unified symmetry is broken to G_{SM}, the sfermions, which are embedded in a single **16** dimensional representation, take a common soft mass $m_{\mathbf{16}}$, whereas the $\mathbf{10}\oplus\overline{\mathbf{126}}$ Higgs fields a common $m_{\mathbf{10+126}}$. The mass of the Higgs field arises from the individual masses of the **10** and of the $\overline{\mathbf{126}}$ (recall the field embeddings in Sec. 5.2). It is an effective mass parameter for the particular combination that acts as the Higgs. In a addition, D-term splittings in the scalar masses should be included due to the rank reduction after the breaking of the $U(1)$ orthogonal to G_{SM}. The boundary conditions for the Georgi-Glashow (GG) embedding follow from the charge assignments (5.50) and (5.51) yielding

$$m^2_{Q_{ij}}(0) = m^2_{u_{ij}}(0) = m^2_{e_{ij}}(0) = \begin{pmatrix} K_{\mathbf{16}} & 0 & 0 \\ 0 & K_{\mathbf{16}} & 0 \\ 0 & 0 & 1 \end{pmatrix}\left(m^2_{\mathbf{16}} + g^2_{10}D\right) \tag{8.2}$$

$$m^2_{L_{ij}}(0) = m^2_{d_{ij}}(0) = \begin{pmatrix} K_{\mathbf{16}} & 0 & 0 \\ 0 & K_{\mathbf{16}} & 0 \\ 0 & 0 & 1 \end{pmatrix}\left(m^2_{\mathbf{16}} - 3g^2_{10}D\right) \tag{8.3}$$

$$m^2_{N_{ij}}(0) = \begin{pmatrix} K_{\mathbf{16}} & 0 & 0 \\ 0 & K_{\mathbf{16}} & 0 \\ 0 & 0 & 1 \end{pmatrix}\left(m^2_{\mathbf{16}} + 5g^2_{10}D\right) \tag{8.4}$$

$$m^2_{H_u}(0) = m^2_{\mathbf{10+126}} - 2g^2_{10}D, \tag{8.5}$$

$$m^2_{H_d}(0) = m^2_{\mathbf{10+126}} + 2g^2_{10}D, \tag{8.6}$$

where $g^2_{10}D$ is the D-term contribution for the mass splittings and g_{10} is the unified gauge coupling of $SO(10)$. Here we also allow an hierarchy between the third generation and the first two generations, but keep the first two generations degenerate in order to avoid dangerous Flavour-Changing Neutral-Currents (FCNC) [198]. Therefore, this model has one extra parameter, $K_{\mathbf{16}} > 0$, which account for the third generation's non-universality at the GUT scale. In order to be consistent with a type-I seesaw mechanism, we add a large Majorana mass term $\mathcal{M}_{ij}$ to the right-handed sneutrino field boundary condition. This term may emerge when a neutral component of the $\overline{\mathbf{126}}$ Higgs acquires an expectation value at the high scale. Since N_R is a G_{SM} singlet, it does not run down to the low scale and its mass is dominated by the Majorana term. Therefore, the right-handed sneutrinos do not become Dark Matter candidates as they could if their masses were purely Dirac.

For the flipped embedding (FL), when we apply the charge assignments (5.58) and (5.59), the boundary conditions at the GUT scale have the same form as the GG ones, but

with opposite sign D-term splittings. If we consider both positive and negative D-term contributions, there is no difference between the GG and FL embeddings in the scalar sector, and the boundary conditions take the same form as in (8.2-8.6).

For the Pati-Salam (PS) route, the charge assignments in eqs. (5.73) and (5.74), yield the same D-term splittings as for the GG and FL embeddings respectively. Recall that we assume that the breaking to G_{SM} is accomplished at the GUT scale or very close to it. Once again we have boundary conditions as in (8.2-8.6).

8.1.2. Soft Trilinear Couplings

The explicit soft susy-breaking terms that contain scalar trilinear couplings are given as in (7.8). Since $y_{\mathbf{126}} \ll y_{\mathbf{10}}$, we consider contributions only from $y_{\mathbf{10}}$ and we impose the simplified boundary condition

$$a_t(0) = a_b(0) = a_\tau(0) = a_{\mathbf{10}}. \tag{8.7}$$

where $a_{\mathbf{10}}$ is a single unified trilinear coupling at the GUT scale.

8.1.3. Gaugino Masses

The hidden sector auxiliary fields $\hat{X}_i$ are now in a representation (or combination of representations) belonging to the symmetric product $(\mathbf{45}\times\mathbf{45})_{symm} = \mathbf{1}+\mathbf{54}+\mathbf{210}+\mathbf{770}$. As we discussed before, the coefficient in the gaugino mass term

$$\frac{1}{2}\frac{\langle F_X^j\rangle}{\langle Re f_{\alpha\beta}\rangle}\left\langle\frac{\partial f^*_{\alpha\beta}}{\partial\varphi^{j*}}\right\rangle\tilde{\lambda}^\alpha\tilde{\lambda}^\beta \tag{8.8}$$

will only generate universal masses when F_X is a trivial representation. It is in this sector where the GUT scale constraints arising from the GG, FL and PS embeddings will differ. In particular, the transformation properties of the F-terms under the full $SO(10)$ symmetry as well as under its maximal proper subgroups, fixes distinct coefficients in (8.8). A detailed description with all possible coefficients is provided in [104]. Once again, we will examine following sets of boundary conditions at the GUT scale:

I. universal gaugino masses: $M_1 = M_2 = M_3 \equiv M_{1/2}$,

II. non-universal gaugino masses: $M_1/\rho_1 = M_2/\rho_2 = M_3 \equiv M_{1/2}$.

8.1.4. Summary of the Parameter Space

In addition to the usual SM parameters, our $SO(10)$ model is described by eight high scale parameters, m_{16}, K_{16}, m_{10+126}, $g_{10}^2 D$, $M_{1/2}$, ρ_1, ρ_2, a_{10}, as well as $\tan\beta$ and the sign of μ (the

value of μ^2 is fixed by the Z boson mass as usual). Despite the common scalar masses, the $SO(10)$ model differs from the cMSSM or the *Non-Universal Higgs Mass* (NUHM) due to the D-term splittings.

8.2. Constraints on the Particle Spectrum

The common third generation GUT scale scalar mass as well as the high scale mass of the Higgs multiplets, $m_{16}^{(3)}$ and m_{10+126} respectively, are allowed to lie between zero and 4 TeV.The D-term splittings $g_{10}^2 D$, are allowed to vary in the range ±4 TeV. To ensure vacuum stability, we only accept points where the sum of the input scalar masses with the respective D-term splittings is positive. The first and second generation input scalar masses are obtained from multiplying m_{16} by K_{16} which we allow to be between zero and 15. We require M_3 to be less than 4 TeV; if examining scenarios with universal gaugino masses, this also sets M_1 and M_2, but if examining non-universal gauginos, we also vary $\rho_{1,2}$ between ±15. Finally the single trilinear coupling, a_{10} is allowed to vary between ±10 TeV, and our only (non-SM) low energy input $\tan\beta$ is constrained to lie in the range $1-60$.

We follow here the same approach for fine tuning studies and use the same experimental constraints as we did for $SU(5)$, see Sec. 7.2.1 and 7.2.2.

8.3. Universal Gaugino Masses

We start our analysis studying scenarios with universal gaugino masses, $\rho_1 = \rho_2 = 1$. We randomly generate points in the parameter space with inputs lying in the ranges given in Sec. 8.2, and using the full two-loop RGEs, run them down to the electroweak scale, $M_z = 91.1876\,\text{GeV}$. Once again we do not force *exact* gauge couplings unification.

We apply here the same LHC direct and XENON100 (2σ) bounds as described in the previous chapter, and discard scenarios with Higgs boson masses outside the range $122.6-127\,\text{GeV}$, avoiding unnecessary computation. We also follow the same approach for the vacuum stability conditions including the simplified approach to the CCB-2,3 constraints implementing the cuts

$$\left|\frac{a_{10}}{\sqrt{m_{16}^2 + g_{10}^2 D}}\right| \lesssim 3, \tag{8.9}$$

$$\left|\frac{a_{10}}{\sqrt{m_{16}^2 - 3g_{10}^2 D}}\right| \lesssim 3. \tag{8.10}$$

Note that eqs. (8.9 - 8.10) are equivalent to the $SU(5)$ ones identifying $m^2_{\mathbf{10}}$ with $m^2_{16} + g^2_{10}D$, and $m^2_{\bar{\mathbf{5}}}$ with $m^2_{16} - 3g^2_{10}D$. At this stage we also discard scenarios with a charged LSP. Out of 1,000,000 initial attempts, this leaves approximately 180,000 scenarios in our scan. We immediate notice that we have a lot more surviving points in comparison to $SU(5)$, 18% against 3% of the initial tries.

Using the electroweak scale outputs of SOFTSUSY as inputs for micrOMEGAS, we generate predictions for the remaining experimental observables, such as the relic density, and derive a value of P_{tot} for each scenario. We again require $P_{\text{tot}} > 10^{-3}$, reducing the number of viable scenarios to 2151, corresponding to 0.2% of the initial attempts, of which 458, (0.05%) of the initial attempts, have the preferred relic density. In comparison, we had approximately 0.02% of surviving scenarios for $SU(5)$ with just 0.002% of points with the preferred relic density.

Fig. 8.1 shows the distribution of the surviving points in μ and $\tan\beta$, where scenarios with a Dark Matter below the 2σ relic density bounds are shown in blue, while those with the preferred value are shown in green.

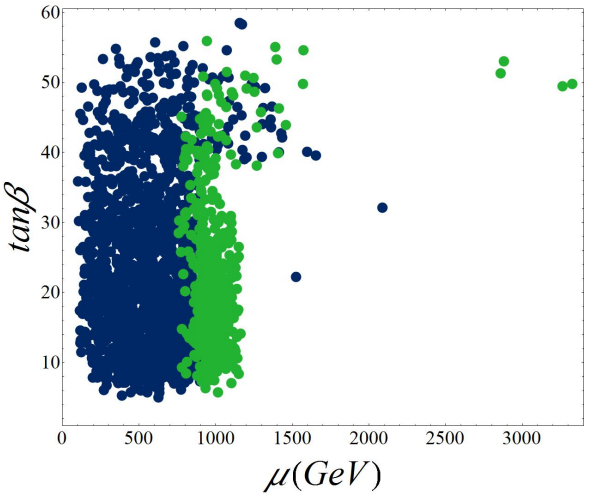

Figure 8.1. *Viable universal gaugino mass scenarios in the μ - $\tan\beta$ plane. Blue points represent scenarios with a Dark Matter relic density below 2σ bounds, while green points have the preferred relic density.*

For a sharper comparison with the $SU(5)$ results, we may consider only the points generated with $M_{1/2} \leq 2$ TeV. We have now approximately 500,000 attempts with 46,500 surviving points. Out of these solutions, 446, or 0.09% against 0.02% of $SU(5)$ survived the probability cut, of which 13, or 0.003% against 0.002% of the initial tries, have the preferred relic density. In figure 8.2 we show the distribution of the accepted solutions in the μ - $\tan\beta$ plane for this subset of the generated points. While the fraction of accepted solutions is more than four times larger in $SO(10)$, the number of points with the correct relic density is just a

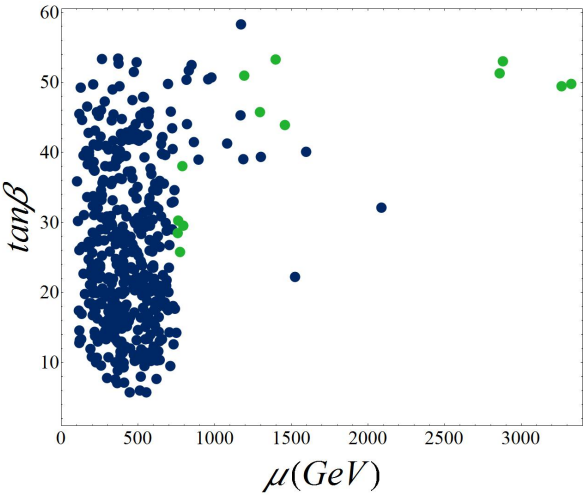

Figure 8.2. *Viable universal gaugino mass scenarios in the* μ - $\tan\beta$ *planefor the subset* $0 \leq M_{1/2} \leq 2$ TeV. *Blue points represent scenarios with a Dark Matter relic density below* 2σ *bounds, while green points have the preferred relic density.*

factor of 3/2 larger. One of the reasons for the higher fraction of good points in comparison to the $SU(5)$ results is the larger range of $M_{1/2}$ that we are implementing, 0 to 4 TeV against 0 to 2 TeV. The higher symmetry imposed by the $SO(10)$ group is responsible for the reduction of the number of input parameters, which is an other element contributing to a larger fraction of accepted solutions in comparison to $SU(5)$.

In Fig. 8.3 we show the viable scenarios with respect to the physical stop masses, and the Higgs boson and its pseudo-scalar partner. The furthest blue point to the left in the $m_{\tilde{t}_1} - m_{\tilde{t}_2}$ pane corresponds to the lightest stop found and has a mass of 432 GeV but too little Dark Matter. The lightest stop with the preferred relic density has mass 1785 GeV (the furthest left green point in the stops mass projection).

In Fig. 8.4 the viable scenarios with respect to the physical sbottom and stop masses are shown. The majority of the solutions with the preferred Dark Matter density have μ close to the 1 TeV band with neutralino-chargino co-annihilation, both dominated by its Higgsino component. However it is possible to have stops, staus or sneutrinos light enough to favour bino dominated neutralino-sfermion co-annihilation. In particular, one of such solutions provides the lightest stau $\tilde{\tau}_1$ we found with a mass of 502 GeV (the furthest left green point in the staus mass plane).

The higher symmetry provided by $SO(10)$ is equivalent to a parameter space with less dimensions and, instead of two distinct trilinear couplings, we have a single one. Despite similar results, the simplified CCB-2,3 conditions (8.9) and (8.10), are more restrictive

than those of $SU(5)$. As an example, there is a green point in Fig. 7.2 with coordinates $(m_{\tilde{t}_1}, m_{\tilde{t}_2}) = (1495, 3512)$ GeV, for which $m_{\bar{5}} = 960$ GeV and $a_{5'} = -9736$ GeV. While in $SU(5)$ this solution is accepted since there is no $\mathbf{5'}$ Higgs coupling to a $\bar{\mathbf{5}}$ sfermion, under $SO(10)$, if $\sqrt{m_{16}^2 - 3g_{10}^2 D} = 960$ GeV, then $|a_{10}|$ would have to be less than 2880 GeV. Therefore, such a point would not survive the $SO(10)$ vacuum stability conditions.

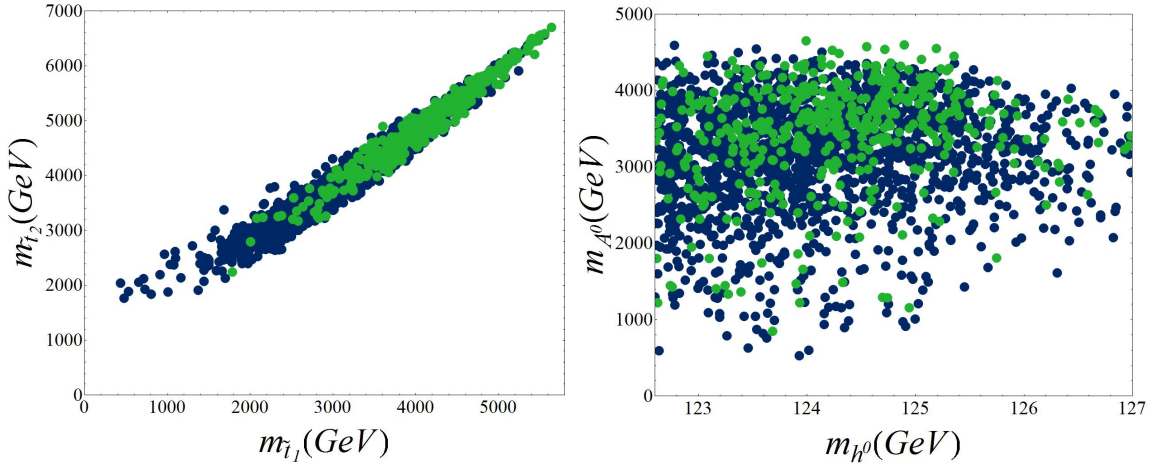

Figure 8.3. *Viable universal gaugino mass scenarios in the stop mass (left) and the lightest scalar - pseudoscalar mass (right) planes, with colours as in Fig. 8.1.*

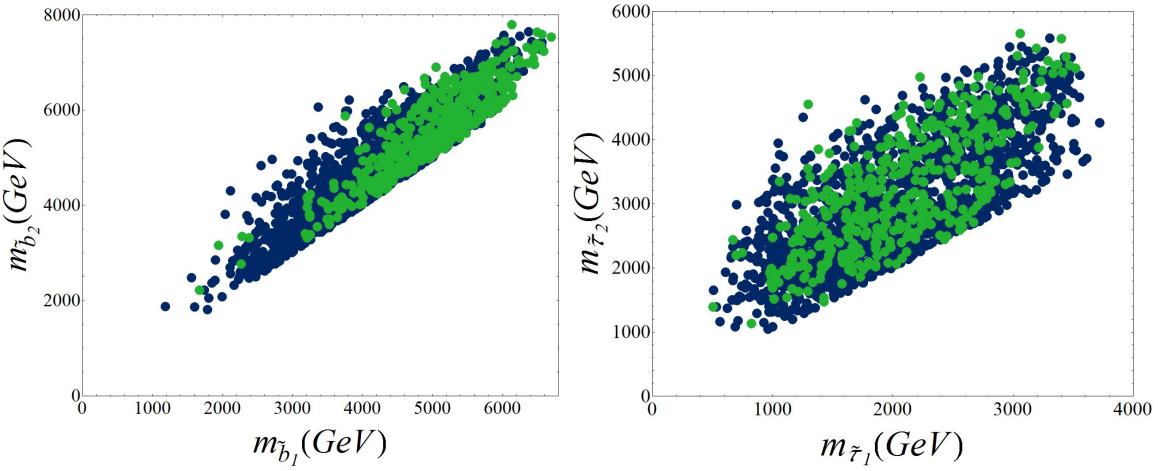

Figure 8.4. *Viable universal gaugino mass scenarios in the sbottom mass (left) and stau mass (right) planes, with colours as in Fig. 8.1.*

From Fig. 8.3 (right) we see that we can produce a sufficiently heavy Higgs boson, but we require a CP-odd Higgs mass, m_A in the approximate region of 0.6–6.6 TeV, reflecting once more the effect of the extended scan range.

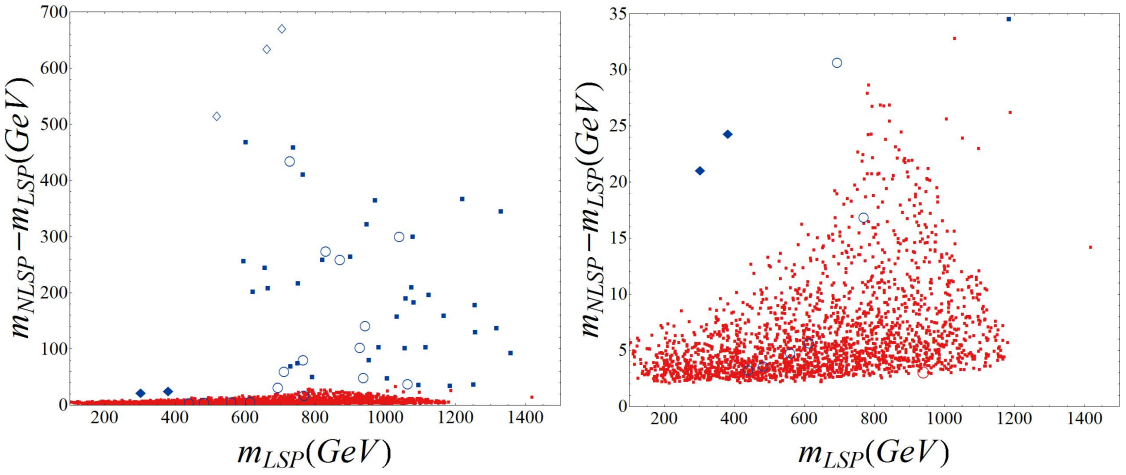

Figure 8.5. *Solutions in the plane of LSP mass vs. the NLSP-LSP mass splitting for universal gaugino mass scenarios. The colour indicates the flavour of LSP, with red and blue denoting higgsino and bino dominated Dark Matter respectively. The shape indicates the flavour of NLSP; squares, diamonds, triangles, circles and empty diamonds denote chargino, stop, sneutrino, stau and neutralino NLSP respectively. The right-hand plot is a zoomed in version of the left-hand plot.*

In Fig. 8.5, we found less points with stau-neutralino co-annihilation in comparison to $SU(5)$. Such solutions are represented by blue circles in regions where the LSP - NLSP mass splittings are small (see Fig. 7.4). Once again, it follows from the new stability conditions that further restrict the parameter space. This is actually the case of the $SU(5)$ point discussed above, where $m_{\bar{5}} = 960$ GeV yields a light stau (dominated by its left-handed component, see eq. (4.67)) with mass 824 GeV. In Fig. 8.5 (right) we also see a rare solution where the neutralino is dominated by its Higgsino component, but instead of a chargino, the NLSP is a stau. The mass of the third generation slepton for this point fell exactly in between the moderately degenerate neutralino-chargino pair, with the $M_{\tilde{\chi}_1^0}$, $m_{\tilde{\tau}_1}$ and $M_{\tilde{\chi}_1^\pm}$ masses being 940, 944 and 947 GeV respectively (red circle in the bottom of the data distribution). We also obtain plenty of viable scenarios where the NLSP can be as much as 700 GeV heavier. In particular, those solutions have a heavy Higgs boson mass approximately twice the mass of the neutralino, allowing Dark Matter annihilation via a Higgs resonance.

We have so far observed that like in $SU(5)$, $SO(10)$ GUT models with universal gaugino masses, provide plenty of solutions that survive the vacuum stability conditions and experimental constraints.We will now examine contributions to the fine-tuning of the Z boson mass M_Z that arise from parameters other than the μ-parameter.. We focus on the parameters that provide the dominant contribution to $m_{H_u}^2$, such as the scalar masses m_{16} and m_{10+126}, the D-term $g_{10}^2 D$, the gaugino mass $M_{1/2}$, and the trilinear coupling a_{10}. We use SOFTSUSY's implementation of fine-tuning throughout and the results for the independent fine-tunings in these parameters are shown in Fig. 8.6. We see that the individual fine-tunings

$\Delta_{m_{16}}$, $\Delta_{a_{10}}$ and $\Delta_{g_{10}^2 D}$ become smaller as their corresponding parameter goes to zero. On the other hand we find no such scenarios for $\Delta_{M_{1/2}}$ nor for $\Delta_{m_{10+126}}$. Both have fine-tuning above 1000 and only a single outlier at $\Delta_{M_{1/2}} \approx 100$ is found.

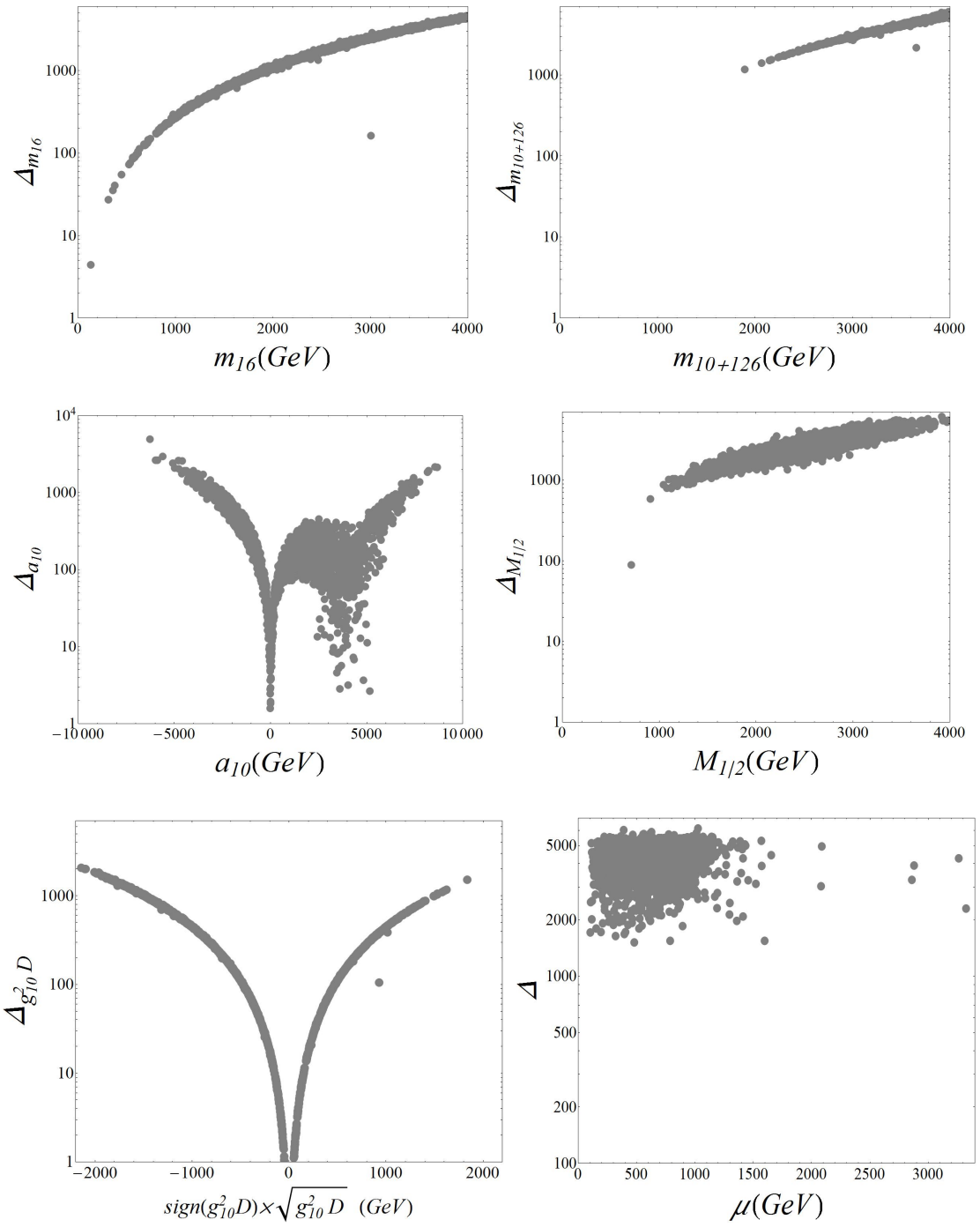

Figure 8.6. *Fine-tuning in M_Z with respect to the input parameters m_{16}, m_{10+126}, $M_{1/2}$, a_{10} and $g_{10}^2 D$ for universal gaugino mass scenarios. On the bottom-right corner the fine-tuning Δ compared to μ for universal gaugino mass scenarios.*

When the individual fine-tunings are combined into Δ, defined as the maximum of the individual ones, the problem is exacerbated (recall we are discounting the fine-tuning with respect to μ). We show in the bottom-right corner of Fig. 8.6 the total fine-tuning in comparison to μ, and see that the entire set of solutions has fine-tuning above 1500.

Once again we obtained plenty of physically viable solutions for GUT scale $SO(10)$-inspired scenarios with universal gaugino masses. Furthermore, the augmented range on the input masses together with the $SO(10)$ gauge symmetry, provided us remarkably more solutions with the preferred Dark Matter relic density. However, those scenarios are unattractive if we insist on low fine-tuning.

8.4. Non-Universal Gaugino Masses

In this section, we allow the gaugino masses at the GUT scale to depend on the (SM) gauge group, and extend our parameter space by introducing ρ_1 and ρ_2 and letting them vary in the interval $[-15, 15]$. We will preserve here the same notation, and identify $M_{1/2}$ with the value of M_3 at the GUT scale.

8.4.1. An Inclusive Scan

We follow here a similar procedure to the universal gaugino masses described in Sec. 8.3, performing an inclusive scan over the parameter space in order to identify regions of interest. The number of total initial tries is now 4,100,000 and when we remove the charged LSP scenarios, apply the stability constraints and impose the LHC and XENON100 direct search bounds, we find 97,457 (2.3%) of surviving scenarios, which is a sizable increase in the fraction of accepted points in comparison to $SU(5)$. The removal of solutions with coloured dark matter in regions where $M_3 \ll M_{1,2}$, is the reason for the typically lower fraction of accepted points when we have non-universal gaugino masses. Applying the probability cut by requiring $P_{\text{tot}} > 10^{-3}$, we are left with 59,833 scenarios, of which 9200 have the preferred Dark Matter relic density. We show in Fig. 8.7 the surviving scenarios projected onto the μ-$\tan\beta$ projection. In comparison to $SU(5)$, we find here a significant increase in the density of scenarios with the preferred Dark Matter relic density, essentially in the high μ region, where Dark Matter is either Bino or Wino. We also notice an increase in the range of possible values for μ of about a TeV, which follows from the increased range of $M_{1/2}$.

In Fig. 8.8 we show the results for the masses of the stops (left) as well as light CP-even Higgs and its pseudoscalar counterpart. Only 9 scenarios with stop masses below 1 TeV and the preferred relic abundance are encountered, with the lightest one having a mass of 576 GeV, the furthest left green point. In Fig. 8.9 we show the physical masses of the

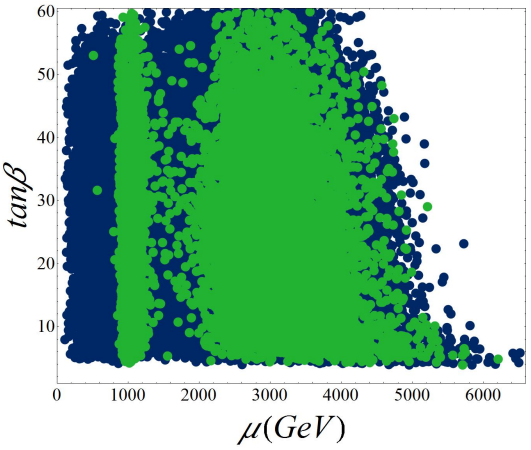

Figure 8.7. *Viable non-universal gaugino mass scenarios in the μ-tanβ plane, with colours as in Fig. 8.1.*

sbottoms (left) and staus (right). The extended range of $M_{1/2}$ is responsible for the larger intervals of masses, which is far most evident in the stop mass projection. The gaugino masses contributions compete with those of the Yukawa couplings due to an oposite sign in RGEs, and solutions with heavy staus are strongly favoured by large $M_{1,2} \gg M_3$.

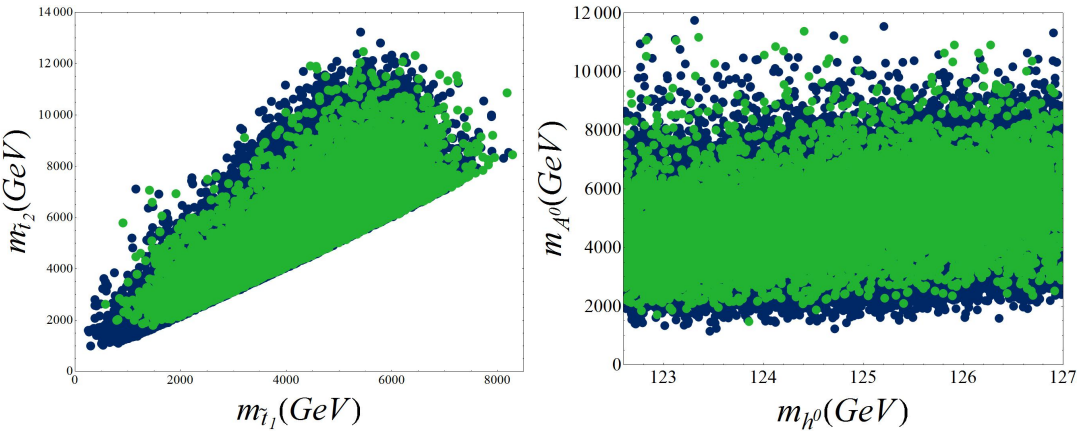

Figure 8.8. *Viable non-universal gaugino mass scenarios in the stop mass (left) and the lightest scalar – pseudoscalar mass (right) planes, with colours as in Fig. 8.1.*

The allowed scenarios projected onto the $\rho_{1,2}$ plane are shown in Fig. 7.10. Once again, we notice that in the region correspondent to universal gaugino masses, $\rho_1 = \rho_2 = 1$, there are very few viable scenarios. The asymmetry with respect to the ρ_1 axis is due to our choice of a positive μ parameter for this particular scan.

The identity and masses of the LSP and NLSP are shown in Fig. 7.11. Here we see many extra possibilities for LSP-NLSP pairings, including wino dominated Dark Matter that is achievable when $M_2 < 2M_1$. Such solutions can provide the correct relic density for higher

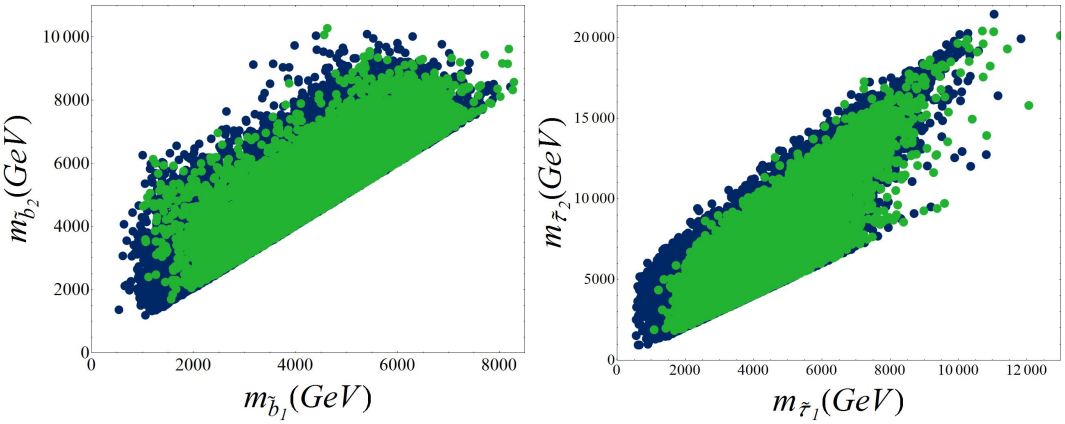

Figure 8.9. *Viable non-universal gaugino mass scenarios in the sbottom mass (left) and stau mass (right) planes, with colours as in Fig. 8.1.*

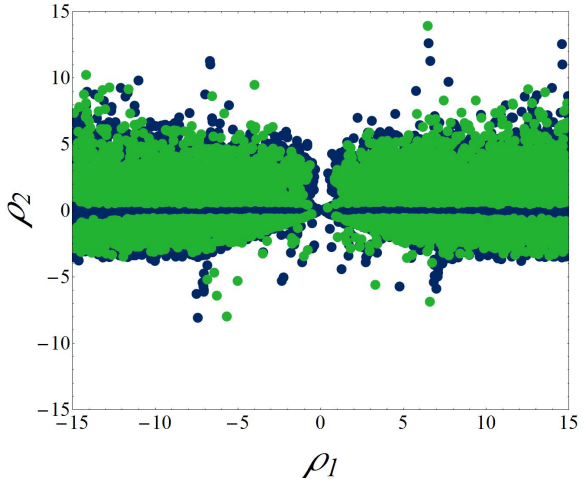

Figure 8.10. *Viable non-universal gaugino mass scenarios in the non-universality parameters $\rho_{1,2}$, with colours as in Fig. 8.1.*

LSP masses. Once again we find plenty of scenarios where the LSP and NLSP are close in mass permitting co-annihilation, as well as bino dominated Dark Matter, where the NLSP can be as much as 400 GeV heavier than its LSP, relying in Dark Matter annihilation via a heavy Higgs resonance. Recall that for $SU(5)$ we have just shown solutions with the correct relic density. Since the results are quite similar, and for complementarity, we show here all accepted solutions independent of the value of the relic density.

The individual fine-tunings for the $SO(10)$ parameters are shown in Fig. 8.12. We see that in comparison to the universal gaugino masses, we can now generate solutions where the Z boson mass is not fine-tuned with respect to $M_{1/2}$ and m_{10+126}. However, for the combined fine-tuning, bottom-right corner of Fig. 8.12, we find no points with $\Delta < 100$. Once again, and as we expected, we see that in the limit of vanishing scalar masses, trilinear couplings

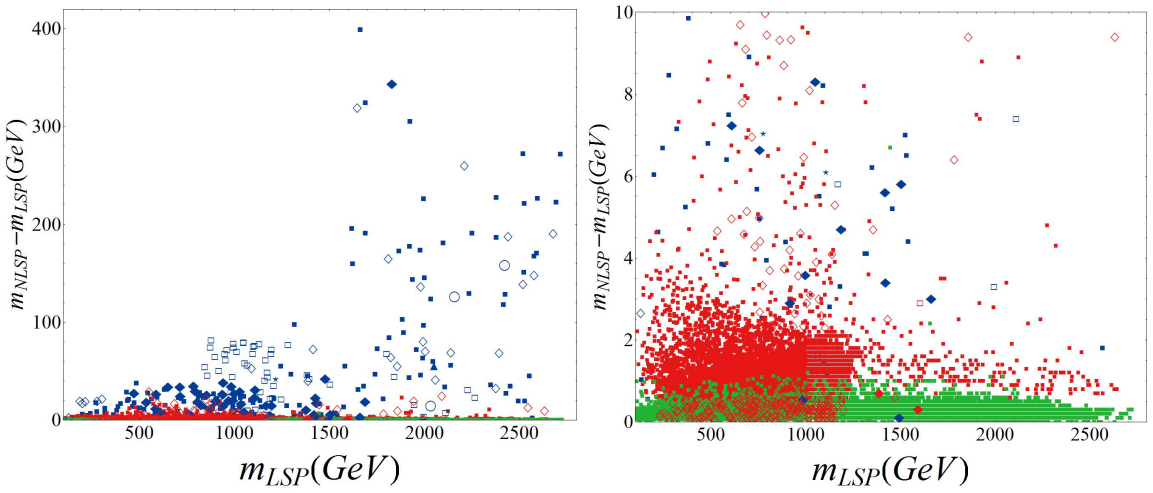

Figure 8.11. *Solutions in the plane of LSP mass vs. the NLSP-LSP mass splitting for non-universal gaugino mass scenarios. The colour indicates the flavour of LSP, with red, blue and green denoting higgsino, bino and wino dominated Dark Matter respectively. The shape indicates the flavour of NLSP; filled squares, empty squares, filled diamonds, empty diamonds, circles and stars denote chargino, gluino, stop, neutralino, stau and sbottom NLSP respectively. The right-hand plot is a zoomed in version of the left-hand plot.*

and D-terms, the tuning tends to zero. In contrast, we find several points with no individual fine tuning of $M_{1/2}$, for any value of the GUT scale gaugino mass.

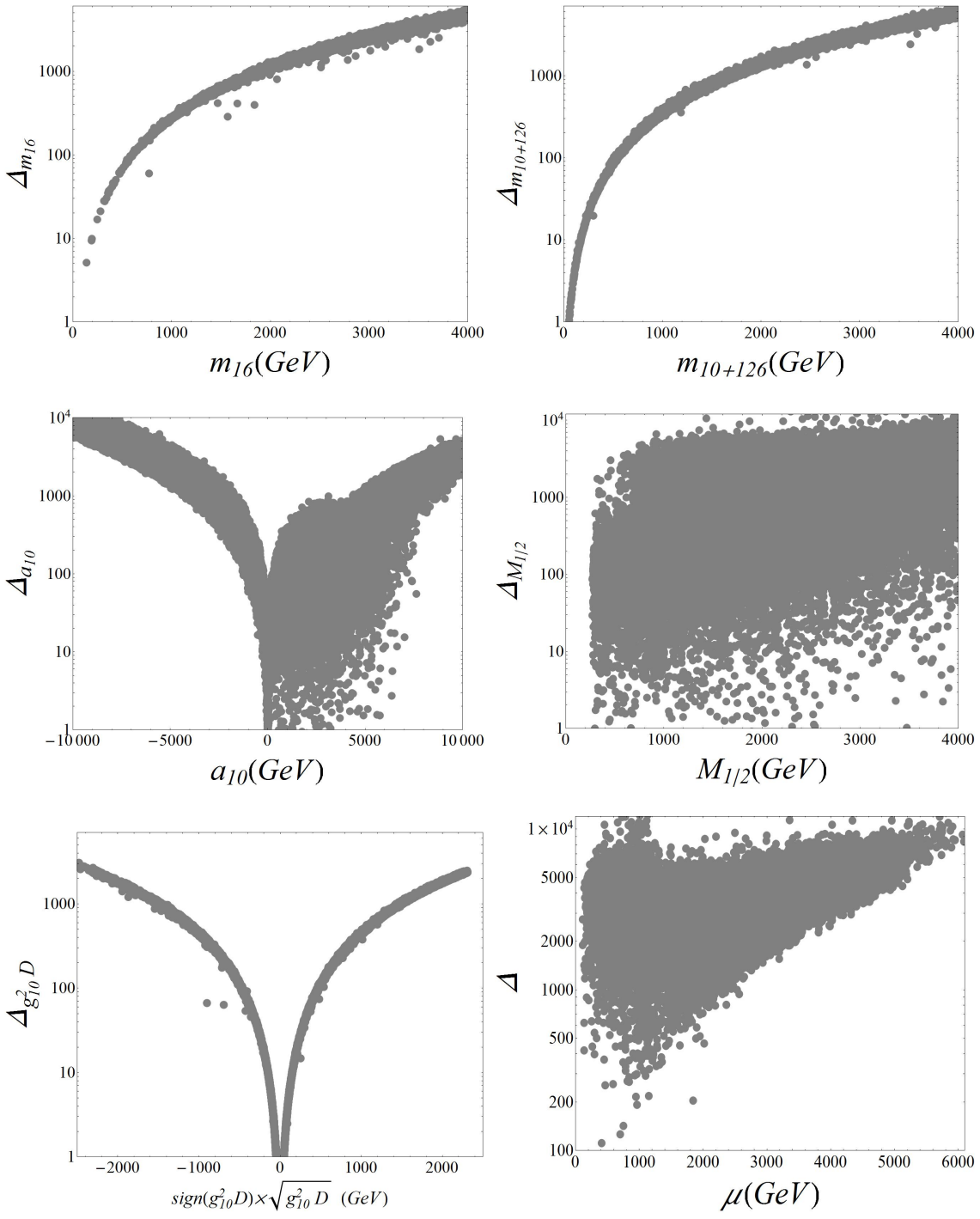

Figure 8.12. *Fine-tuning in M_Z with respect to the input parameters m_{16}, m_{10+126}, $M_{1/2}$, a_{10} and $g_{10}^2 D$ for non-universal gaugino mass scenarios. On the bottom-right corner the fine-tuning Δ compared to μ for non-universal gaugino mass scenarios.*

8.4.2. An Enhanced Scan Over $M_{1/2}$, ρ_1 and ρ_2

The search for regions with low fine tuning of the soft parameters requires an enhancement of the scanning region. In order guarantee that the natural fluctuations of the scalar masses and trilinear couplings are small, we set all these parameters to the ranges $0 < m_{scalar} < 150$ GeV, $0 < \left|g_{10}^2 D\right| < 150$ GeV and $0 < |a_{10}| < 150$ GeV. With the experience taken from $SU(5)$ studies, we allow ρ_1 and ρ_2 to vary over the intervals $[-13, 13]$ and $[-3.5, 3.5]$ respectively. We expect to increase the number of good solutions with $\Delta < 100$ (again not including Δ_μ). Experimental and stability constraints are implemented as usual. With approximately 2,000,000 initial attempts, 10,158 solutions survived the LHC and stability constraints, of which 5,760 were accepted by the probability and fine-tuning cuts. Such scenarios are shown in the μ-tanβ, stop and Higgs mass, and sbottom and stau mass planes in Fig. 8.13, 8.14 and 8.15 respectively. Once again we identify plenty of points with fine tuning less than 100 (lighter shades of green and blue) as well as several with fine-tuning less than 10 (darker shades of green and blue). The number of points that provide a good description of the full Dark Matter (green points) increased from 1,028 in $SU(5)$ to 1,478 in $SO(10)$, for reasons discussed in the previous sections.

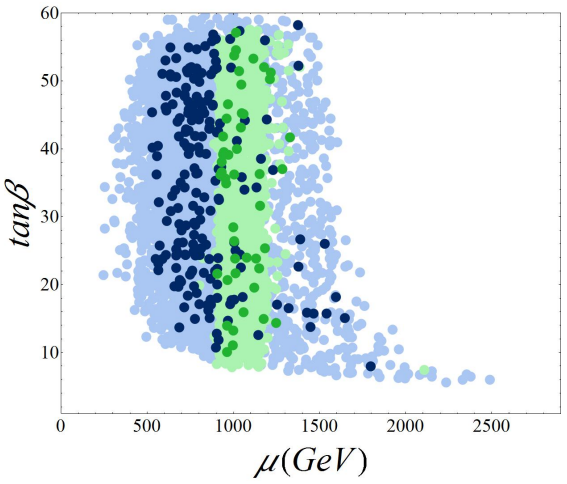

Figure 8.13. *Viable scenarios in the μ-tanβ plane for the enhanced scan with non-universal gaugino masses. Points with the preferred Dark Matter relic density are shown in green, while those with a relic density below the bounds are in blue. Darker and lighter shades denote the fine-tuning: darker shades have fine-tuning $\Delta < 10$ while lighter shades have $10 < \Delta < 100$.*

The allowed mass spectrum is restricted by the insistence on the preferred Dark Matter density and even further if we request a low fine-tuning. It is not surprising to find once more that the optimal scenarios have μ restricted to be close to 1 TeV. The lightest top and bottom squarks are confined to 2.5-6 TeV, lightest staus in the interval 1-6.0 TeV and the pseudoscalar Higgs boson mass is now allowed to vary in a wider region from 1-5 TeV.

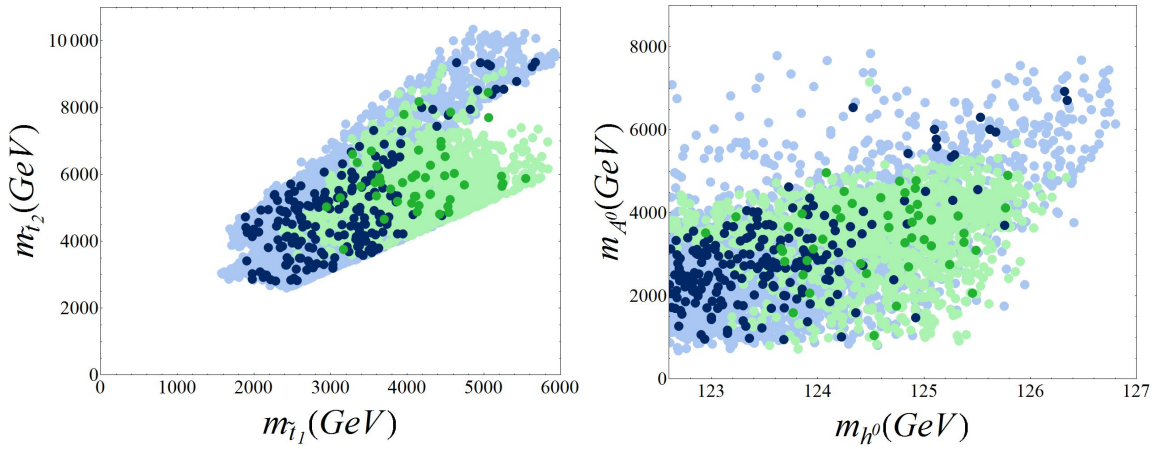

Figure 8.14. *Viable scenarios in the stop mass (left) and lightest scalar - pseudoscalar mass (right) planes for the enhanced scan with non-universal gaugino masses, with colours as in Fig. 8.13.*

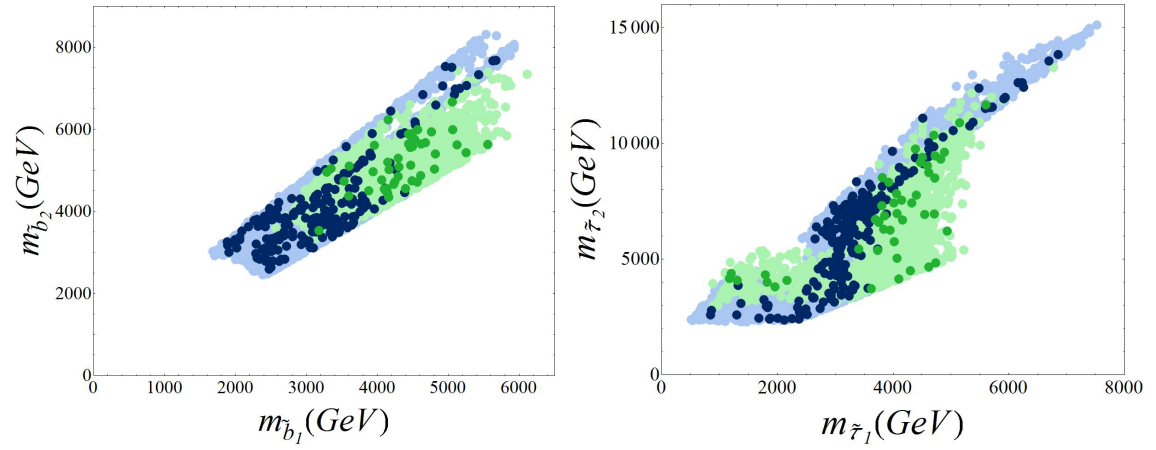

Figure 8.15. *Viable scenarios in the sbottom mass (left) and stau mass (right) planes for the enhanced scan with non-universal gaugino masses, with colours as in Fig. 8.13.*

The LSP and NLSP masses and nature is shown in Fig. 8.16. We observe that for scenarios with the preferred relic density (right panel), there are several points with neutralino NLSP (empty diamonds), though the majority of the solutions are still dominated by neutralino LSPs with chargino NSLPs. From eq. (4.81) and (4.82), we see that the leading contribution for the masses of Higgsino type neutralino and chargino is the μ-parameter, and their mass splitting is mostly due to M_1 and M_2. Since the $U(1)_Y$ gaugino mass term only contributes to the neutral components, the splitting $M_{\tilde{\chi}_1^0} - M_{\tilde{\chi}_2^0}$ is typically larger. However, in regions where $M_1 \ll M_2$, or equivalently small ρ_1, both light neutralinos become degenerate. This is indeed the case for those solutions represented by empty diamonds in Fig. 8.16, with ρ_1 constrained approximately to the interval $[-1.1, -2.3]$.

We use the definition of Yukawa coupling unification from [153] by, and quantify how

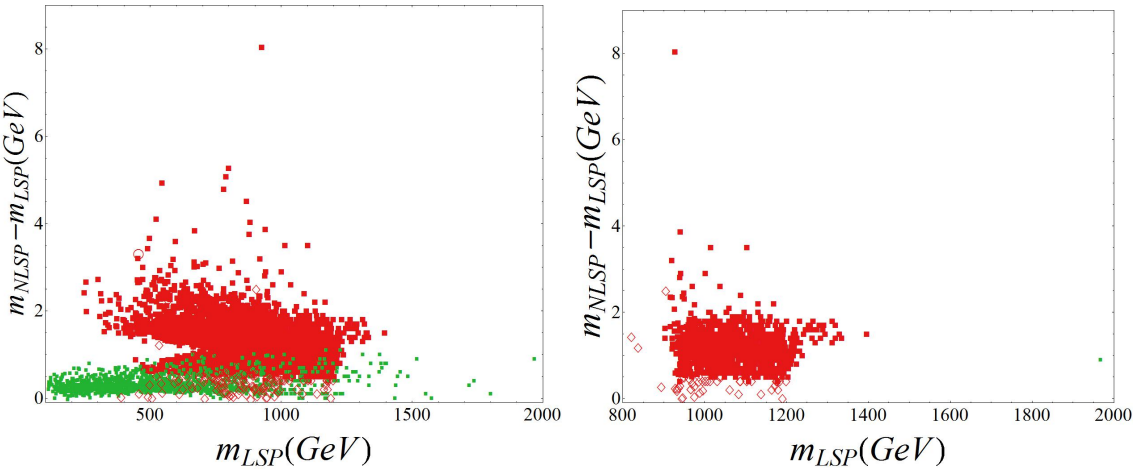

Figure 8.16. *Solutions in the plane of LSP mass vs. the NLSP-LSP mass splitting for the enhanced scan over non-universal gaugino mass scenarios. The colour indicates the flavour of LSP, with red, blue and green denoting higgsino, bino and wino dominated Dark Matter respectively. The shape indicates the flavour of NLSP; filled squares and empty diamonds denote chargino and neutralino NLSP respectively. The left-hand plot shows all scenarios with fine-tuning $\Delta < 100$ while the right-hand plot restricts to scenarios with $\Delta < 10$ and the preferred Dark Matter relic abundance.*

close to exact unification we are using this ratio

$$R_{tb\tau} = \frac{max(y_t, y_b, y_\tau)}{min(y_t, y_b, y_\tau)}. \tag{8.11}$$

Recalling the discussion carried out in secs. 5.1.3 and 5.2.2, we do not expect to have exact unification and therefore do not throw away the scenarios that don't have $R_{tb\tau} = 1$ or $R_{b\tau} = 1$. In Fig. 8.17 we show solutions with $\tan\beta$ between 40 and 60, where the left branch corresponds to points with $\mu < 0$ and the right branch to $\mu > 0$. We see that it is for negative values of μ that we get the best YU conditions with a point having $R_{tb\tau} = 1.07$ for $\tan\beta = 51.6$ (the dark blue point furthest to the left)[1]. For the μ positive branch we do not find exact YU, and the best we can have is a solution with the preferred relic density for which $R_{tb\tau} = 1.37$ and $\tan\beta = 51.6$, and a point with little dark matter for which $R_{tb\tau} = 1.37$ and $\tan\beta = 52.6$.

In Fig. 8.18 we show the $SO(10)$ version of the $\rho_{1,2}$ ellipse, where for $\mu > 0$ ($\mu < 0$) the points on the bottom (top) half of the ellipse are excluded due to predicting charged LSP.

8.5. Scenarios with Fixed Gaugino Mass Ratios

We have once again assumed that in the previous analysis, gaugino mass ratios are fixed by some GUT or string inspired mechanism. One of such possibilities is the breaking

[1] It is discussed in [154, 155] that threshold corrections to the Yukawa couplings at the GUT scale are dependent on the sign of μ as well as the sign of $M_{1,2,3}$. In particular, solutions with $\mu < 0$ may favour YU.

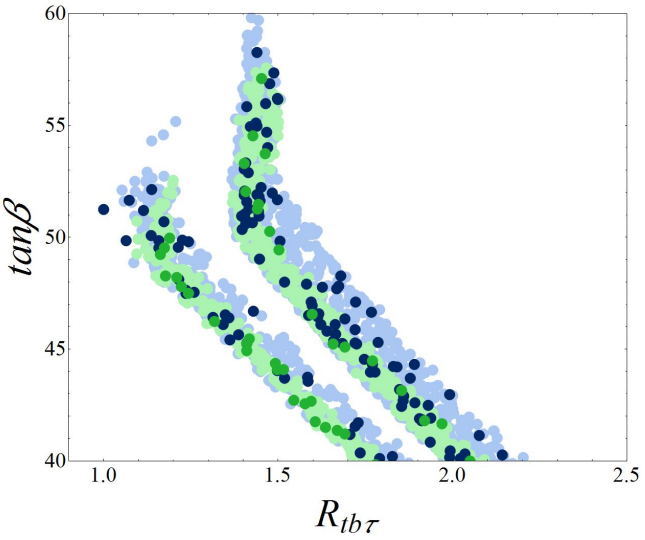

Figure 8.17. *Viable scenarios in the $R_{tb\tau}$-tanβ plane for the enhanced scan with non-universal gaugino masses, with colours as in Fig. 8.13. The left (right) branch is for solutions with $\mu < 0$ ($\mu > 0$).*

of supersymmetry through a hidden sector field $\hat{X}$ in a representation (or combination of representations) belonging to the product $(\mathbf{45}\times\mathbf{45})_{symm} = \mathbf{1}+\mathbf{54}+\mathbf{210}+\mathbf{770}$. In [104], the possible $M_1 : M_2 : M_3$ coefficients for the GG, FL and PS routes are introduced. In tables 8.1, 8.2 and 8.3 we show the fixed ratios that are closest to our ellipse. The $SU(5)$ route with GG embedding produces the same points that we have already studied in 7. In particular, the $SU(5)_{\mathbf{200}}$ model is equivalent to a $\mathbf{770}$-$\hat{X}$ that transforms as a $\mathbf{200}$ under its maximal proper subgroup. Out of the new $\rho_{1,2}$ ratios predicted by the FL and PS routes, there is only one that lies close to the ellipse, transforming as a singlet under $SU(4)\times SU(2)_R$. This model is represented by a yellow filled triangle in Fig. 8.18.

$SO(10) \to SU(5)$	ρ_1	ρ_2	Label in Fig. 8.18
$\mathbf{1} \to \mathbf{1}$ $\mathbf{210} \to \mathbf{1}$ $\mathbf{770} \to \mathbf{1}$	1	1	empty circle
$\mathbf{54} \to \mathbf{24}$ $\mathbf{210} \to \mathbf{24}$ $\mathbf{770} \to \mathbf{24}$	$-\frac{1}{2}$	$-\frac{3}{2}$	empty triangle
$\mathbf{210} \to \mathbf{75}$ $\mathbf{770} \to \mathbf{75}$	-5	3	empty square
$\mathbf{770} \to \mathbf{200}$	10	2	red star

Table 8.1. *Fixed gaugino mass ratios for hidden sector chiral superfield $\hat{X}$ in representations of $SU(5) \subset SO(10)$ with the Georgi-Glashow embedding.*

$SO(10) \to SU(5)'$	ρ_1	ρ_2
$\mathbf{210} \to \mathbf{1}$	$-\frac{19}{5}$	1
$\mathbf{210} \to \mathbf{24}$	$\frac{7}{10}$	$-\frac{3}{2}$
$\mathbf{210} \to \mathbf{75}$ $\mathbf{770} \to \mathbf{75}$	$-\frac{1}{5}$	3
$\mathbf{770} \to \mathbf{1}$	$\frac{77}{5}$	1
$\mathbf{770} \to \mathbf{24}$	$-\frac{101}{10}$	$-\frac{3}{2}$
$\mathbf{770} \to \mathbf{200}$	$\frac{2}{5}$	2

Table 8.2. *Fixed gaugino mass ratios for hidden sector chiral superfield $\hat{X}$ in representations of $SU(5) \subset SO(10)$ with the flipped embedding. All the ratios in this table are labeled by filled orange squares in Fig. 8.18.*

$SO(10) \to SU(4) \times SU(2)_R$	ρ_1	ρ_2	Label in Fig. 8.18
$\mathbf{210} \to (\mathbf{15},\mathbf{1})$	$-\frac{4}{5}$	0	red triangle
$\mathbf{770} \to (\mathbf{1},\mathbf{1})$	$\frac{19}{10}$	$\frac{5}{2}$	yellow triangle
$\mathbf{770} \to (\mathbf{84},\mathbf{1})$	$\frac{32}{5}$	0	red triangle

Table 8.3. *Fixed gaugino mass ratios for hidden sector chiral superfield $\hat{X}$ in representations of $SU(4) \times SU(2)_L \times SU(2)_R \subset SO(10)$. All the ratios in this table are labeled by filled triangles in Fig. 8.18.*

We may extend our analysis and assume possible mixings among the representations of $\hat{X}$. In $SU(5)$ we considered BIM inspired models which gave us plenty of scenarios to study initially. However, there is only one extra viable scenario in $SO(10)$ that is distinct from $SU(5)$, the yellow triangle on the ellipse. Therefore, we consider mixing between representations, and as consequence we find plenty of extra scenarios to study. Let $\mathbf{R}$ and $\mathbf{R'}$ be two of those irreps and $\theta_{RR'}$ the mixing angle. We define the gaugino masses at the input scale as

$$M_1 = M_{1/2}(\rho_1^R \cos\theta_{RR'} + \rho_1^{R'} \sin\theta_{RR'}), \tag{8.12}$$

$$M_2 = M_{1/2}(\rho_2^R \cos\theta_{RR'} + \rho_2^{R'} \sin\theta_{RR'}), \tag{8.13}$$

$$M_3 = M_{1/2}(\cos\theta_{RR'} + \sin\theta_{RR'}), \tag{8.14}$$

such that we recover the standard form when either $\theta_{RR'} = 0$ ($\hat{X} \in \mathbf{R}$), or $\theta_{RR'} = \pi/2$ ($\hat{X} \in \mathbf{R'}$). In eq. (8.12 - 8.13), $\rho_{1,2}^{R,R'}$ are the usual gaugino mass ratios fixed by the representation $\mathbf{R}, \mathbf{R'}$ and the transformation properties of the hidden sector fields under the maximal subgroups. Note that now M_3 is no longer $M_{1/2}$ at the GUT scale, unless the mixing angle is zero or $\pi/2$.

The gauino mass ratios are now slightly more complicated, and given as

$$\rho_1 = \frac{M_1}{M_3} = \frac{\rho_1^R \cos\theta_{RR'} + \rho_1^{R'} \sin\theta_{RR'}}{\cos\theta_{RR'} + \sin\theta_{RR'}}, \tag{8.15}$$

$$\rho_2 = \frac{M_2}{M_3} = \frac{\rho_2^R \cos\theta_{RR'} + \rho_2^{R'} \sin\theta_{RR'}}{\cos\theta_{RR'} + \sin\theta_{RR'}}. \tag{8.16}$$

From the equations above, we may obtain an expression for $\theta_{RR'}$ and eliminate it from (8.12 - 8.16) in order to get a general expression relating ρ_1 with ρ_2,

$$\theta_{RR'} = \arctan\left(\frac{\rho_1 - \rho_1^R}{\rho_1^{R'} - \rho_1}\right), \tag{8.17}$$

$$\rho_2 = \frac{\left(\rho_2^{R'} - \rho_2^R\right)\rho_1 + \rho_2^R\rho_1^{R'} - \rho_1^R\rho_2^{R'}}{\rho_1^{R'} - \rho_1^R}. \tag{8.18}$$

Note that ρ_2 is not divergent when $\rho_1^R = \rho_1^{R'}$ since the numerator of eq. (8.18) cancels. At this stage, the new ρ_1 and ρ_2 parameters are no longer a fixed value. They are allowed to vary with $\theta_{RR'}$ and are constrained to segments in the $\rho_1 - \rho_2$ plane. Eq. 8.18 gives a generic expression for such segments, where the end points correspond to the original fixed ratios $\rho_{1,2}^{R,R'}$, which characterize the representations that are mixing.

As we are seeking models with low fine tuning, we give preference to those scenarios that best overlap with the ellipse. We identify such models as:

1. The hidden sector fields $\hat{X}$ are embedded in the combinations $\mathbf{R} + \mathbf{R'} = \mathbf{210} + \mathbf{770}$ or $\mathbf{770} + \mathbf{770'}$ transforming as $\mathbf{75} + \mathbf{200}$ under standard $SU(5)$. The respective ρ_1^R, ρ_2^R, $\rho_1^{R'}$ and $\rho_2^{R'}$ fixed ratios are in table 8.1 and the mixed ρ_1 and ρ_2 are related by

$$\rho_2 = -\frac{1}{15}\rho_1 + \frac{8}{3}. \tag{8.19}$$

This model is identified by the red dashed line in 8.18 and we may call it $GG75 + 200$.

2. The second model relies again on the same combinations of $SO(10)$ irreps but transforms as $\mathbf{75} + \mathbf{1}$ of $SU(5)$ with flipped embedding. In table 8.2 we find the respective values for ρ_1^R, ρ_2^R, $\rho_1^{R'}$ and $\rho_2^{R'}$, and the new ρ_1 and ρ_2 are related by

$$\rho_2 = -\frac{5}{39}\rho_1 + \frac{116}{34}. \tag{8.20}$$

This model is identified by the upper orange line in the $\mu > 0$ half of Fig. 8.18 and we call it $FL75 + 1$.

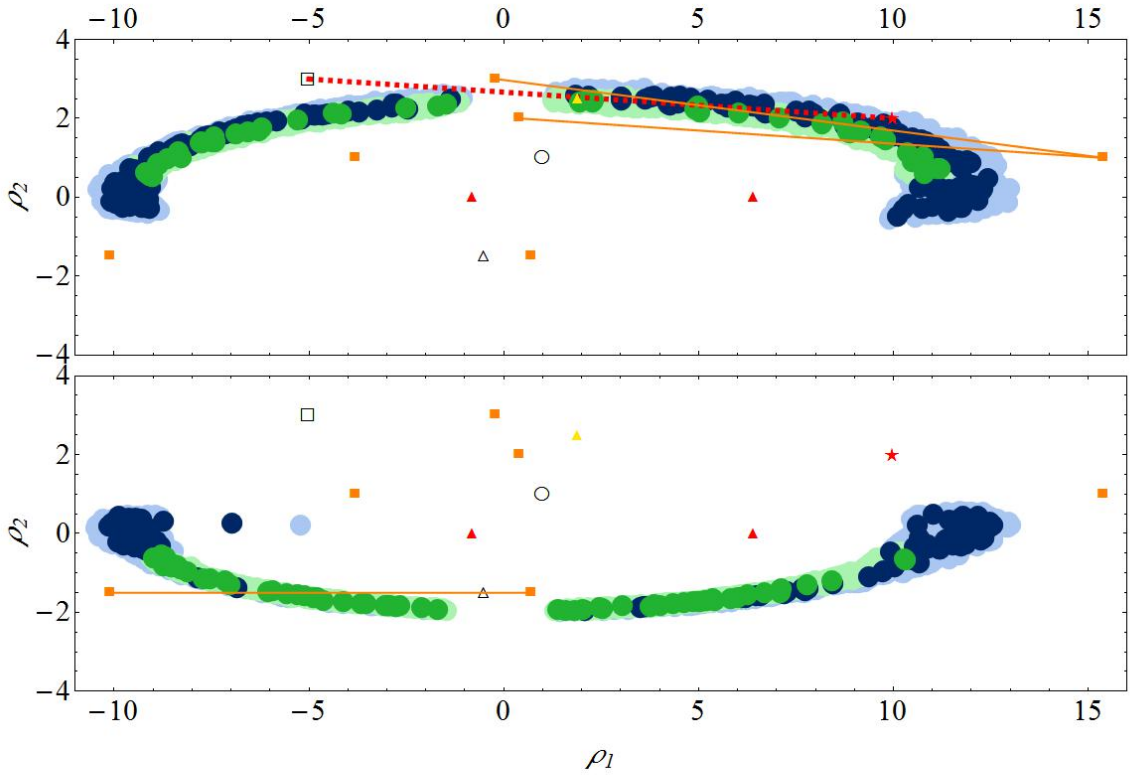

Figure 8.18. *Viable scenarios in ρ_1-ρ_2 plane for the enhanced scan with non-universal gaugino masses. Points with the preferred Dark Matter relic density are shown in green, while those with a relic density below the bounds are in blue. Darker and lighter shades denote the fine-tuning: darker shades have fine-tuning $\Delta < 10$ while lighter shades have $10 < \Delta < 100$. The upper pane is for scenarios with $\mu > 0$ while the lower pane is for $\mu < 0$. The additional symbols represent particular gaugino mass ratios as predicted by the mechanisms described in tables 8.1, 8.2 and 8.3. Scenarios arising from embeddings in the* **1**, **54**, **210**, *and* **770** *representations of SO(10) and transforming as a* **1**, **24**, **75**, *and* **200** *of $SU(5)$ with Georgi-Glashow embedding are shown by an empty circle, an empty triangle, an empty square and a red star respectively. Orange squares represent gaugino mass ratios when the proper maximal subgroup is $SU(5)$ with flipped embedding. Red and yellow triangles coincide with ratios as predicted by transformations under $SU(4) \times SU(2)_R$. Scenarios with combinations of two representations lie along the straight lines: the GG75 + 200 lies on the red dashed line, whereas the FL75 + 1, FL1 + 200 and FL24 + 24 lie on the uppermost, middle and lowermost orange lines respectively.*

3. The third model mixes two 770-dimensional irreps, $\mathbf{R} + \mathbf{R'} = \mathbf{770} + \mathbf{770'}$ which transform as $\mathbf{1} + \mathbf{200}$ under flipped $SU(5)$. The gaugino mass ratios are related through

$$\rho_2 = -\frac{1}{15}\rho_1 + \frac{152}{75}, \tag{8.21}$$

which corresponds to the lowermost orange segment in the $\mu > 0$ half of the $\rho_1 - \rho_2$ plane.

We name this model as $FL1+200$.

4. The fourth model considers that the hidden sector fields belong to the reducible $\mathbf{R}+\mathbf{R'}=\mathbf{210}+\mathbf{770}$ representation, which under its maximal $SU(5)$ subgroup transforms as $\mathbf{24}+\mathbf{24'}$ with flipped embedding. The gaugino mass ratios are related by the constant

$$\rho_2 = -\frac{3}{2}, \tag{8.22}$$

corresponding to the orange segment in the $\mu<0$ bottom half of the $\rho_1-\rho_2$ plane. This model is denoted as $FL24+24$.

5. Finally, we consider a model without mixing of representations, corresponding to a single **770** which transforms as a $(\mathbf{1},\mathbf{1})$ under the Pati-Salam maximal subgroup. This model is identified by the yellow triangle in the $\mu>0$ half of the ellipse, which corresponds to $\rho_1=10/19$ and $\rho_2=5/2$, and we call it $PS1$.

Before moving forward, we note that with mixed representations, we have extended the parameter space with $\theta_{RR'}$. We should therefore study the fine-tuning this new parameter contributes to points within the ellipse. Recall the discussion carried out in subsection 8.4.2 on the low fine-tuning of our solutions. We found that for particular choices of $M_{1/2}$, it may sit close to a minimum of $m^2_{H_u}$, rendering it insensitive to fluctuations of $M_{1/2}$. The solutions that we found in the $\rho_1-\rho_2$ ellipse manifest this type of stability upon fluctuations of the soft gaugino mass parameter. Unfortunately, fine-tuning in $\theta_{RR'}$ will destroy the vast majority of the solutions encountered, with Δ of several hundreds or even thousands. However, this is not the end of the game; $\theta_{RR'}$ is also dependent on the gaugino mass, see eq. (8.17), therefore $m^2_{H_u}$ must also be dependent on $\theta_{RR'}$. In Fig 8.19 we show the $m^2_{H_u}$ dependence as $\theta_{RR'}$ is varied, for a particular point of the $FL75+1$ model, where we also set $\tan\beta=31.9$, $M_{1/2}=2456.8$ GeV, $a_{10}=-2.3$ GeV, $m_{16}=49.3$ GeV, $m_{10}=75.9$ GeV, $\sqrt{g^2_{10}D}=75.9$ GeV and $K_{16}=12.2$. We see that the particular value $\theta_{RR'}\approx 0.65$ sits close to a minimum where $m^2_{H_u}$ is insensitive to fluctuations in $\theta_{RR'}$.

For most of the cases, the minimum of $m^2_{H_u}$ with respect to $\theta_{RR'}$ does not coincide with the minimum relative to variations in $M_{1/2}$. This is indeed the reason why most of the points in the ellipse of Fig. 8.18 become fine-tuned. However, it may happen that both $\theta_{RR'}$ and $M_{1/2}$ sit close to the same minimum of $m^2_{H_u}$. Those solutions are undoubtedly rare but do exist. In Fig. 8.20 we show the individual fine-tunings $\Delta_{M_{1/2}}$ and $\Delta_{\theta_{RR'}}$ as $\theta_{RR'}$ is varied for the same point described above. The green curve represents the fine tuning in $M_{1/2}$ whereas the red one correspond to $\Delta_{\theta_{RR'}}$. We see in the zoomed version (right panel) that the minimum of both curves are remarkably close when we vary $\theta_{RR'}$. Indeed, the point

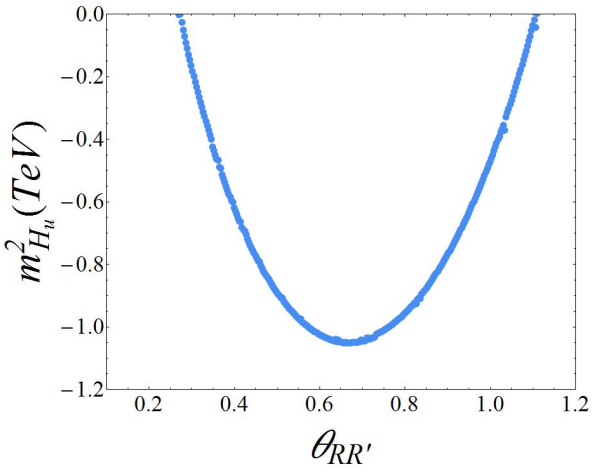

Figure 8.19. *The values of $m^2_{H_u}$ as $\theta_{RR'}$ is varied, for a particular point with gaugino mass ratios consistent with the FL75 + 1 model. The remaining parameters are defined in the main text.*

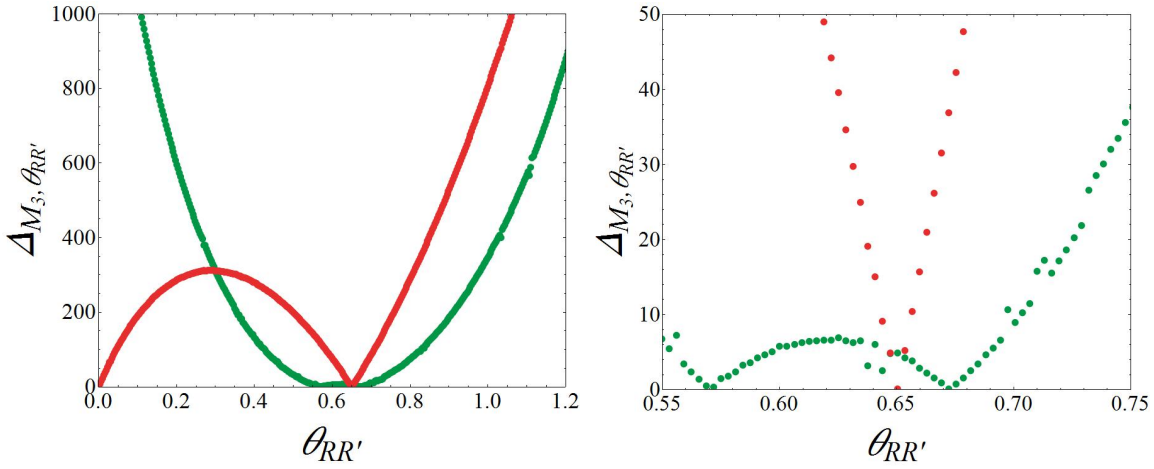

Figure 8.20. *Fine tuning in $M_{1/2}$ and $\theta_{RR'}$ as the mixing angle is varied, for a particular point with gaugino mass ratios consistent with the FL75 + 1 model. The remaining parameters are defined in the main text. The Red curve corresponds to $\Delta_{\theta_{RR'}}$ and the green curve to $\Delta_{M_{1/2}}$. The right pane is a zoomed in version of the left one.*

where $\Delta_{\theta_{RR'}} = 8.8 \times 10^{-2}$ corresponds to $\Delta_{M_{1/2}} = 4.9$ (the lowest red point and the green point straight above it in Fig. 8.20 right).

We will now study the $GG75 + 200$, $FL75 + 1$, $FL1 + 200$, $FL24 + 24$ and $PS1$ models individually, and investigate how such scenarios may be restricted by low energy constraints. We require here that non of the models exhibit fine tuning in $M_{1/2}$ and $\theta_{RR'}$ simultaneously. We then perform dedicated scans for each case searching for stable solutions along the segments in Fig. 8.18, but unfortunately, we did not find any of such solutions for the $FL1 + 200$ and $FL24 + 24$ models. However it does not mean that low fine tuned points do not exist for these models. They are instead very rare when compared to the $GG75 + 200$ and

$FL75+1$ cases, which are the ones the better overlap the ellipse. The $PS1$ model does not depend on $\theta_{RR'}$, therefore it is already free of fine tuning in the representation mixing angle. We will therefore consider only $GG75+200$, $FL75+1$ and $PS1$ as non-fine tuned models.

8.5.1. GG75 + 200 Model

We first consider the model with a gauge kinetic function transforming as a **75 + 200** of $SU(5)$ with conventional embedding, and gaugino mass ratios related through eq. (8.19). Use the same ranges for the soft parameters as described in the beginning of subsection 8.4.2 but now we restrict $M_{1/2}$ to vary in the interval $[1500, 3000]$ GeV. Note that $M_{1/2}$ no longer corresponds to the value of M_3 at the high scale. The three gaugino masses are now determined by $M_{1/2}$ and $\theta_{RR'}$ through eq. (8.12 - 8.14). Instead of defining a range for $\rho_{1,2}$, we implicitly determine it just by specifying a range for $\theta_{RR'}$. To avoid unnecessary computation we choose $\theta_{RR'}$ such that $\rho_{1,2}$ are within the ellipse. Using eq. (8.17), the values for $\rho_1^{R,R'}$ of the $GG75+200$ in table 8.1, and observing that the dashed red line overlaps the ellipse approximately from $\rho_1 = 1$ to $\rho_1 = 10$, we restrict $\theta_{RR'}$ to vary between $[0.58, \pi/2]$.

Firstly we show the $\mu - \tan\beta$ plane in Fig. 8.21 (left), which indicates preference for low to moderate $\tan\beta$, between 7 and 38, if we insist in solutions predicting the preferred relic density as well as fine-tuning $\Delta < 10$. It is also evident that such solutions are rare. In particular, we have generated approximately 1,165,000 initial scenarios of which 12,311 survived the experimental, stability and fine-tuning cuts ($\sim 1\%$), and 40 ($\sim 0.003\%$) have fine-tuning below 10.

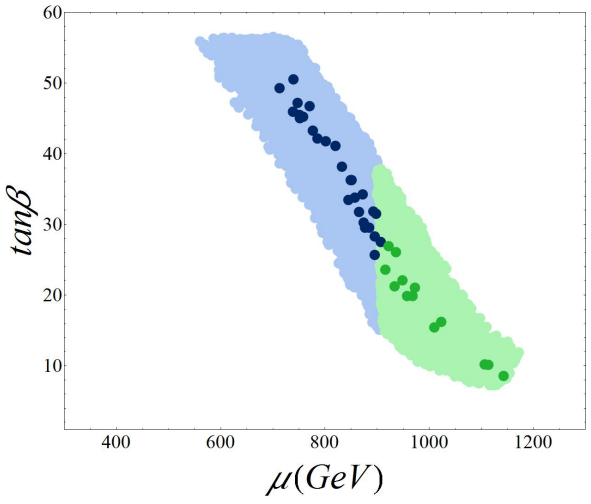

Figure 8.21. *Viable scenarios in the $\mu - \tan\beta$ plane for the $GG75+200$ model, with colours as in Fig. 8.13.*

The stop and Higgs masses are shown in Fig. 8.22 and the bottom and tau superpartner

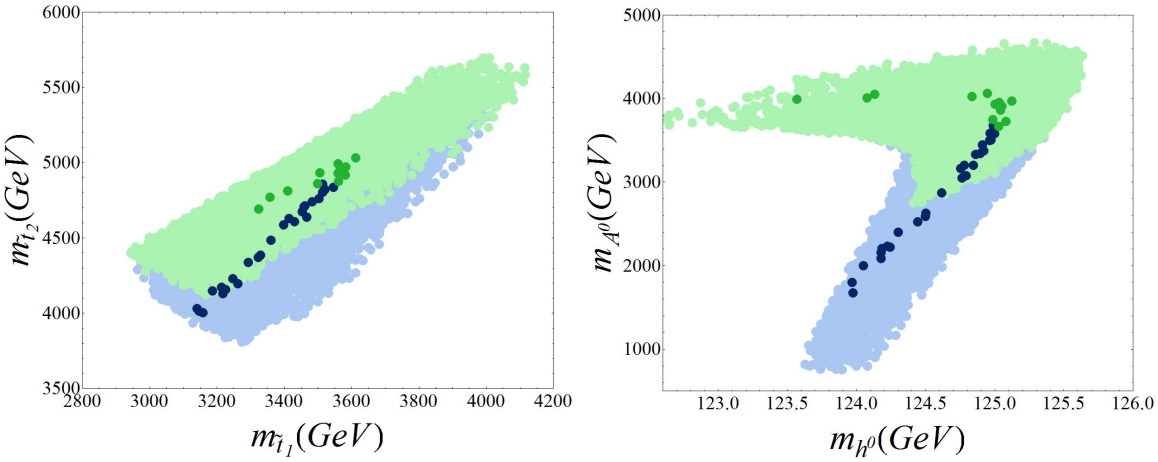

Figure 8.22. *Viable scenarios in the stop mass and lightest scalar - pseudoscalar mass planes for the GG75 + 200 model, with colours as in Fig. 8.13.*

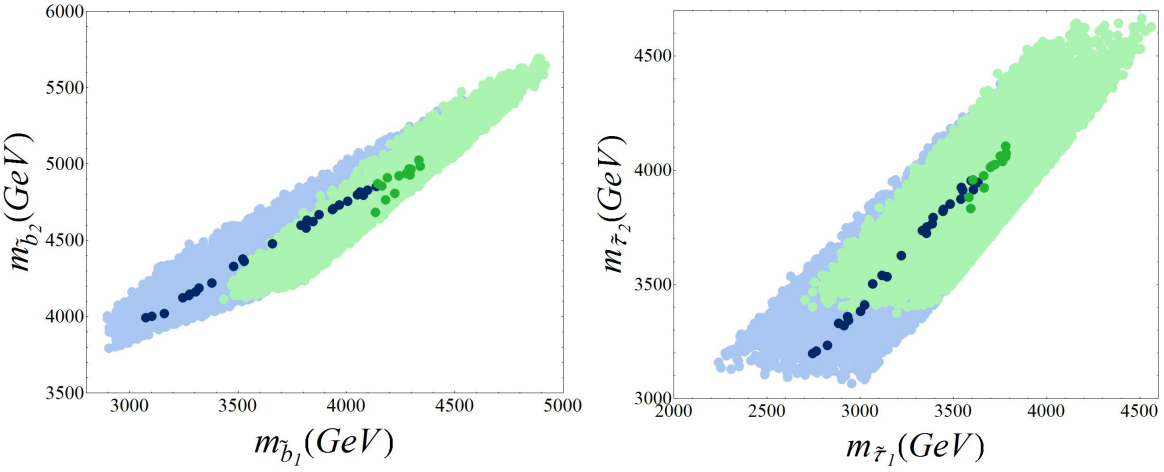

Figure 8.23. *Viable scenarios in the sbottom mass (left) and stau mass (right) planes for the GG75 + 200 model, with colours as in Fig. 8.13.*

masses in Fig. 8.23. Here we find solutions with 125.2 GeV Higgs together with low fine-tuning and the preferred relic density. Those solutions predict relatively heavy third generation sfermions, with 3.6 TeV stops, 3.8 TeV staus and 4.3 TeV sbottoms. Indeed, Higgs masses of 125.5 GeV are also possible requiring an increase in mass of about a half TeV for the supersymmetric spectrum. The pseudoscalar mass is also heavy enough such that the lightest scalar would look like the SM Higgs bosons, in accordance with the recent discovery.

The values of the allowed gaugino mass ratios for the *GG75 + 200* model are shown in Fig. 8.24, where the end points of the segment correspond approximately to $\theta_{RR'} \in [0.95, 1.14]$.

The $R_{tb\tau} - \tan\beta$ condition, Fig. 8.25 (top planes), shows that solutions with quasi-Yukawa

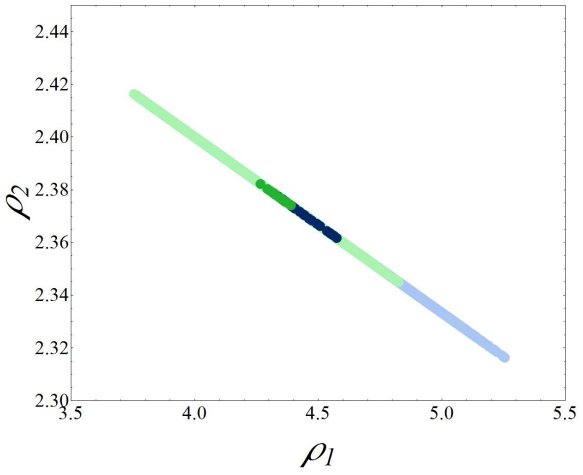

Figure 8.24. *Viable scenarios in the non-universal parameters $\rho_{1,2}$ for the GG75 + 200 model, with colours as in Fig. 8.13*

unification (QYU), with $R_{tb\tau}$ between 1.37 and 2.0, are unfortunately not reconcilable with the preferred Dark Matter abundance (top-right). However, bottom-tau unification, which is defined analogously to eq. (8.11) by removing the top-Yukawa contribution, is always between 1.30 and 1.44, which is not far off from the $y_\tau/y_b = 3/2$ GUT scale ratio prediction as discussed in [231, 250].

Both the LSP and the NLSP are nearly degenerated neutralino and chargino, dominated by their higgsino component, with masses separated roughly by $1-1.5$ GeV, as shown in Fig. 8.26. If we do not require Dark Matter relic density to be within the WMAP bounds, we can have neutralinos as light as 600 GeV, which may be accessible to the 14 TeV LHC.

8.5.2. FL75 + 1 Model

The second model that we study, assumes that the hidden sector fields transform as a **75 + 1** of $SU(5)$ with flipped embedding. The gaugino mass ratios are related through eq. (8.20) and the segment that represents the model in the $\rho_1 - \rho_2$ plane, intercepts the ellipse when ρ_1 is roughly between 2 and 12. These values corresponds to vary $\theta_{RR'}$ in the interval $0.16 - 1.30$. We also allow $M_{1/2}$ to be between $1.2 - 2$ TeV.

The viable scenarios in the $\mu - \tan\beta$ and $R_{tb\tau} - \tan\beta$ planes are shown in Fig. 8.27. This model produces similar results to those of the *GG*75 + 200, but now we have solutions with the preferred relic density up to $\tan\beta = 50$.

The *FL*75 + 1 model predicts slightly heavier mass spectra for the third generation superpartners, Figs. 8.28 and 8.29, which manifests as a marginal increase in the Higgs mass

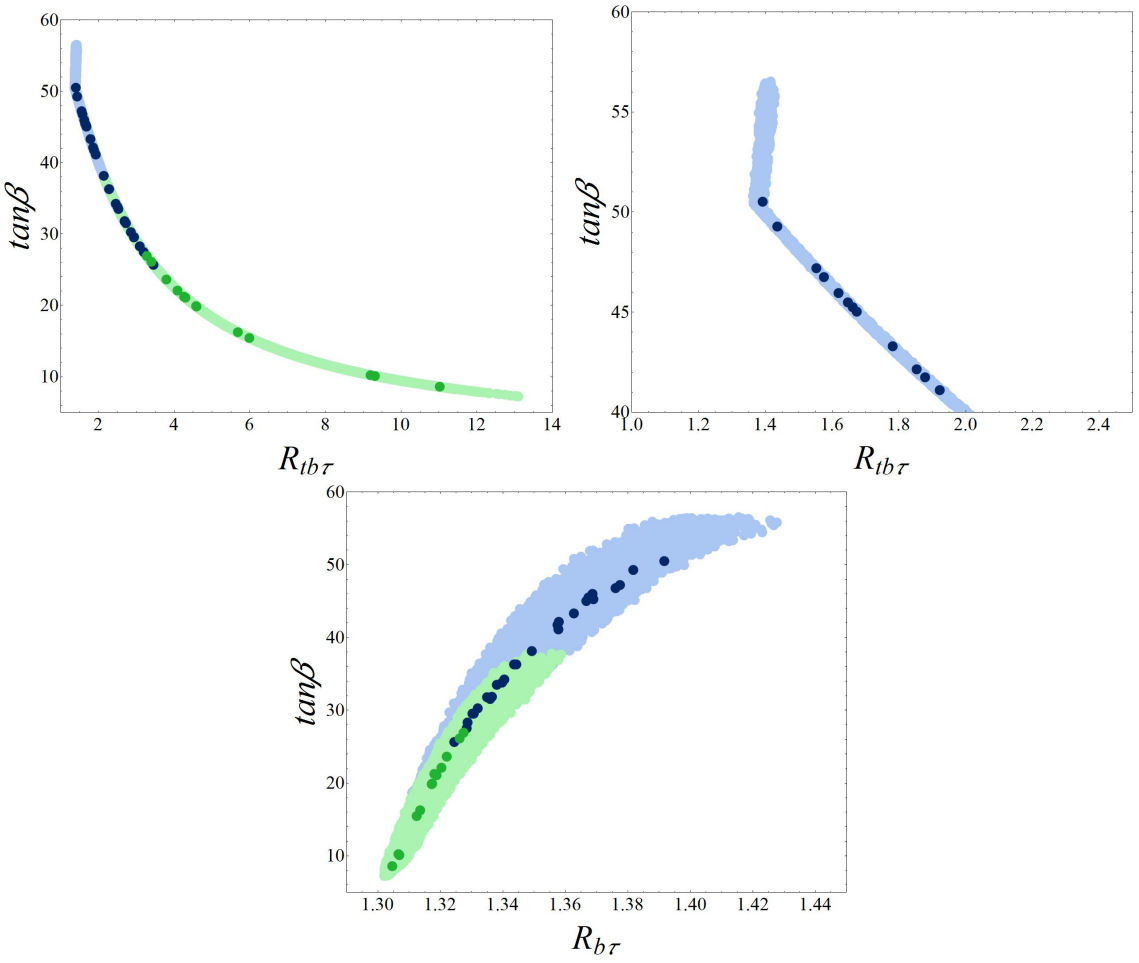

Figure 8.25. *Viable scenarios in the $R_{tb\tau} - \tan\beta$ (top) and $R_{b\tau} - \tan\beta$ (bottom) planes for the GG75 + 200 model, with colours as in Fig. 8.13. The top-right pane is a zoomed-in version of the top-left one.*

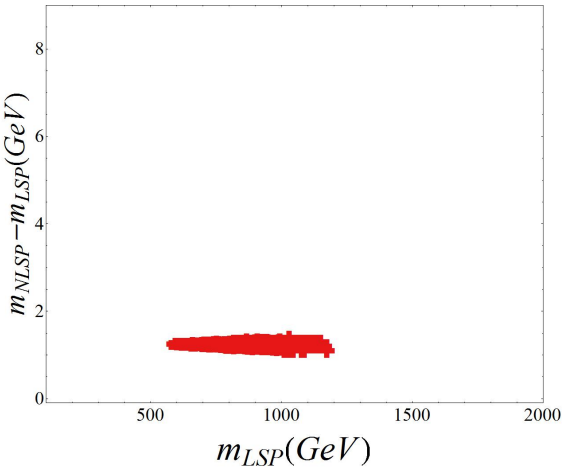

Figure 8.26. *Solutions in the plane of LSP mass vs. the NLSP-LSP mass splitting for the GG75 + 200 model. Red squares indicate higgsino LSP and filled squares chargino NLSP.*

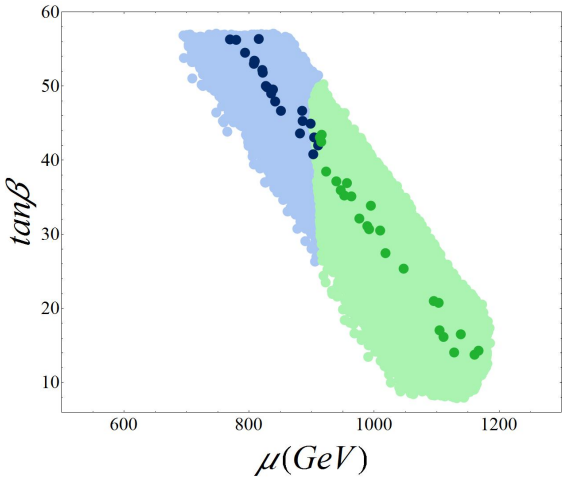

Figure 8.27. *Viable scenarios in the* $\mu - \tan\beta$ *plane for the FL*$75+1$ *model, with colours as in Fig. 8.13.*

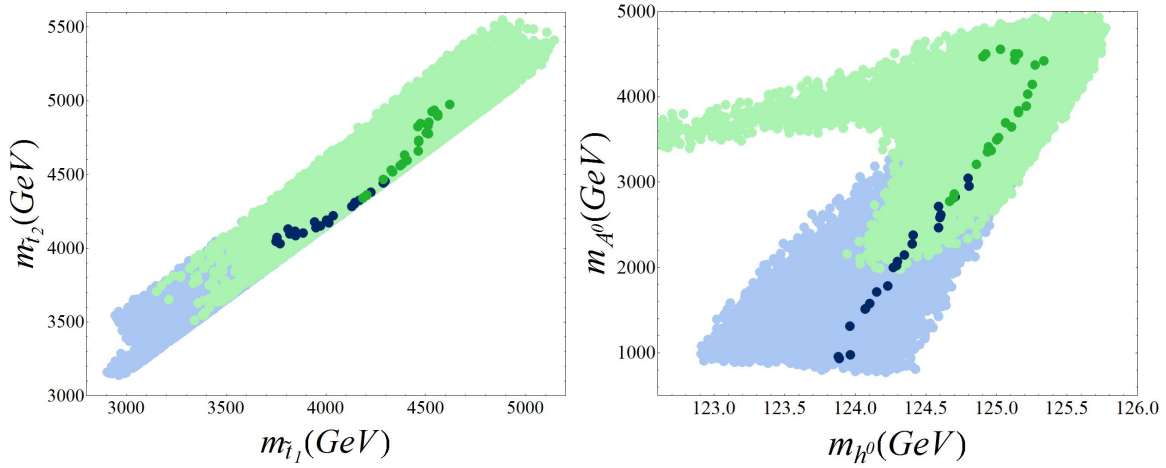

Figure 8.28. *Viable scenarios in the stop mass and lightest scalar - pseudoscalar mass planes for the FL*$75+1$ *model, with colours as in Fig. 8.13.*

upper bound. In particular, we can have Higgs as heavy as $125.5-125.8$ GeV with stops and staus of about 5 TeV and sbottoms with a mass close to 5.5 TeV. On the other hand, both the *GG*$75+200$ and *FL*$75+1$ models exhibit solutions with stops and sbottoms just below 3 TeV and staus as low as 2.5 TeV. Although not excessively heavy, these scenarios are still very challenging for the LHC.

We show the gaugino mass ratios for the *FL*$75+1$ model in Fig. 8.30. Once again we observe that the values of theta corresponding to the segment, form a quite narrow subset of the initial range of $\theta_{RR'}$, spreading over $0.56 < \theta_{RR'} < 0.82$.

The unification of Yukawa couplings predicts now that for solutions with the preferred relic density, we can have $R_{tb\tau}$ as good as 1.4. However, such solutions have fine-tunings in the

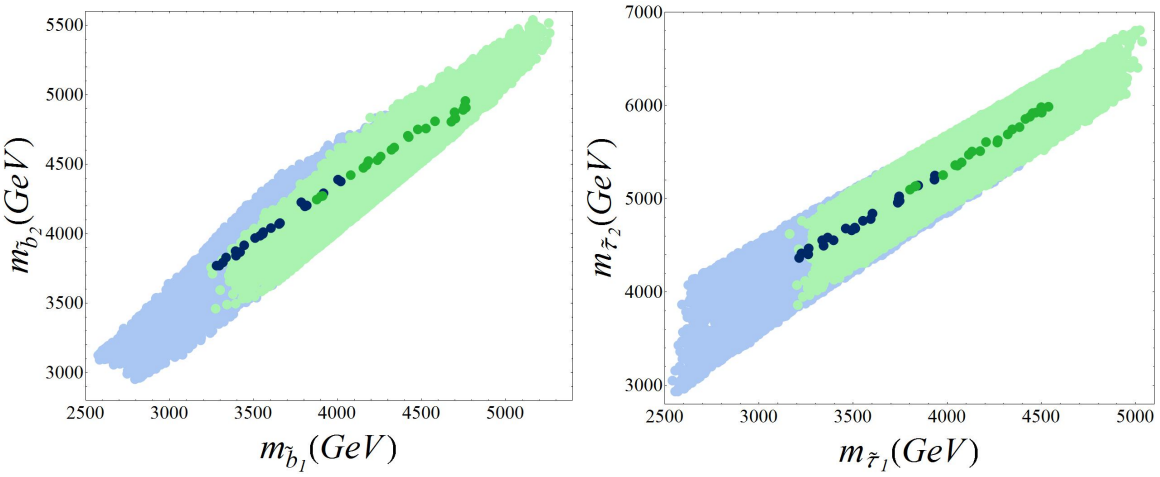

Figure 8.29. *Viable scenarios in the sbottom mass (left) and stau mass (right) planes for the FL75 + 1 model, with colours as in Fig. 8.13.*

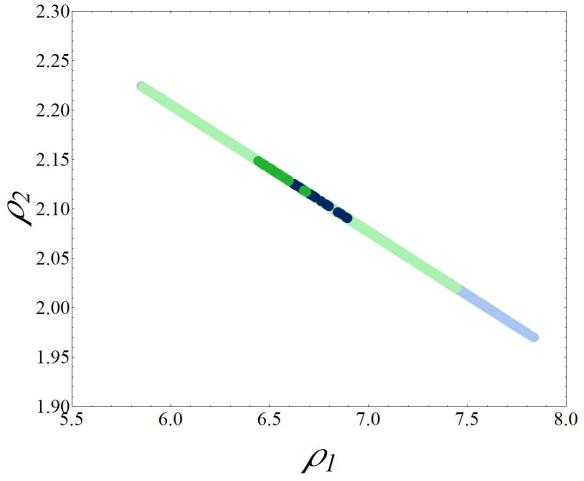

Figure 8.30. *Viable scenarios in the non-universal parameters $\rho_{1,2}$ for the FL75 + 1 model, with colours as in Fig. 8.13*

region $10 < \Delta < 100$. On the other hand, the bottom-tau unification condition yields $R_{b\tau} \approx 1.48$ in the high $\tan\beta$ regime, which further approaches to the $y_\tau/y_b = 3/2$ ratio, particularly if we do not insist in describing the full amount of Dark Matter density. If we require the preferred relic density as well as low fine-tuning (dark green points), we find $1.31 < R_{b\tau} < 1.37$.

The nature of the LSP and NLSP is equivalent to the *GG*75 + 200 model. The only difference resides in the mass range of both the (higgsino dominated) neutralino (LSP) and chargino (NLSP), which is now restricted to $0.7 - 1.2$ TeV. However, solutions with the preferred Dark Matter abundance require neutralinos heavier that 900 GeV.

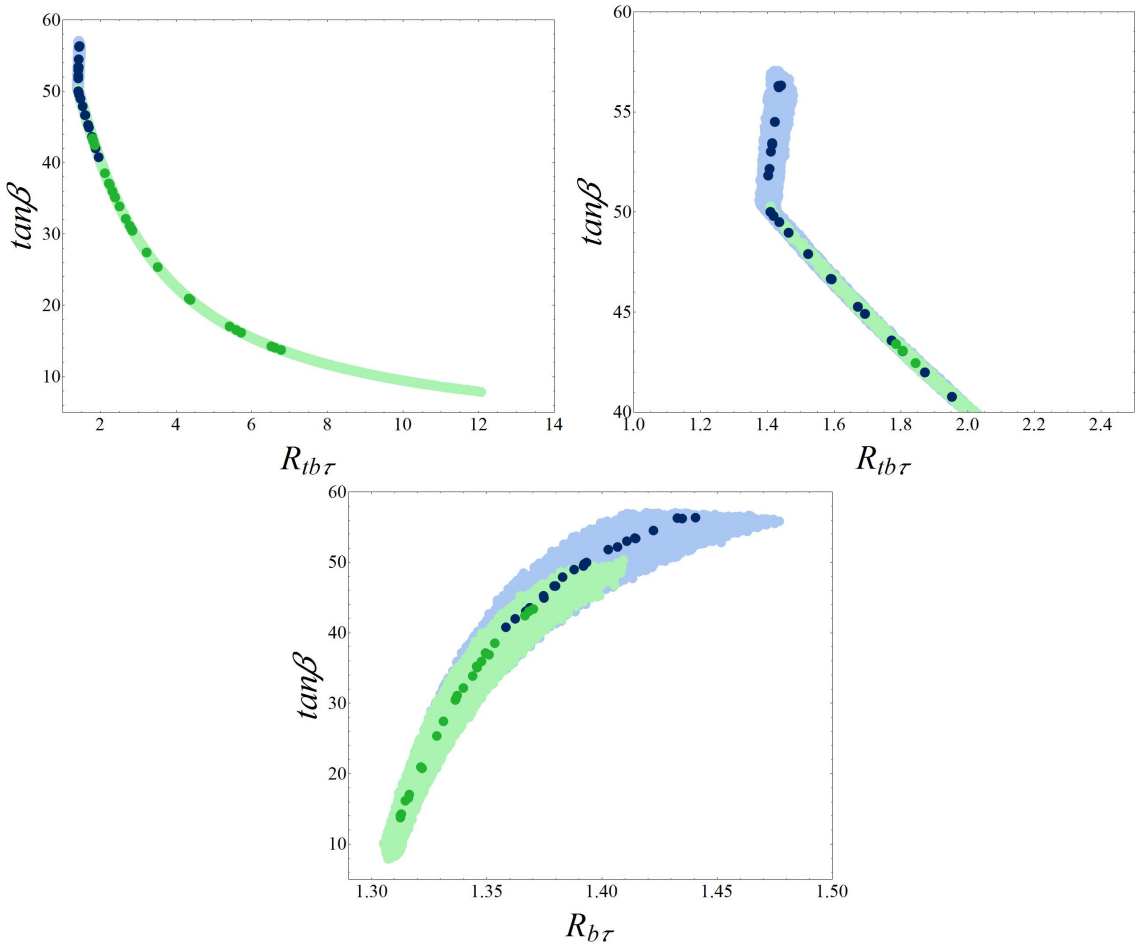

Figure 8.31. *Viable scenarios in the $R_{tb\tau} - \tan\beta$ (top) and $R_{b\tau} - \tan\beta$ (bottom) planes for the FL75 + 1 model, with colours as in Fig. 8.13. The top-right pane is a zoomed-in version of the top-left one.*

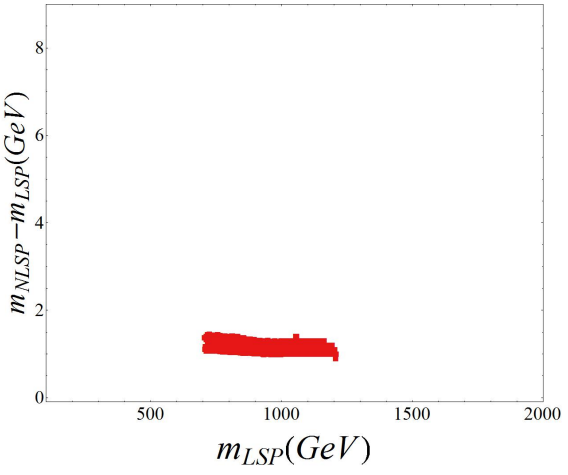

Figure 8.32. *Solutions in the plane of LSP mass vs. the NLSP-LSP mass splitting for the FL75 + 1 model. Red squares indicate higgsino LSP and filled squares chargino NLSP.*

8.5.3. PS1 Model

For the $PS1$ model, the gaugino mass ratios are entirely determined from the group theoretical coefficients predicted by a single representation of the $\hat{X}$ superfields. This scenario is analogous to the $SU(5)_{200}$ model that we studied in chapter 7, but now $\rho_1 = 19/10$ and $\rho_2 = 5/2$. The scan is performed using the same range for the input parameters as in Sec. 8.4.2.

We first note in Fig. 8.33 that $\tan\beta$ takes values from 7 up to 40, with some scattered solutions at 42. This range becomes slightly restricted, $8-38$, if we insist that $\Delta < 10$. The viable scenarios have moderate to large values of μ, $0.6-1.1$ TeV, with most of the points that agree with the preferred relic density being heavier than 900 GeV, as usual for higgsino DM. We see however a region for larger values of $\tan\beta$, where we find solutions that predict the preferred Dark Matter abundance, with μ between $750-850$ GeV. The reason for this, is that in this area, we can also have stau NLSPs, or very close to the chargino NLSP, which co-annihilate with the higgsino dominated neutralinos, yielding a Dark Matter density within or below the WMAP bounds. This is due to a relatively small value of ρ_1, which is equivalent to a small M_1, combined with a large $\tan\beta$. While gaugino mass terms contribute to increase the mass of the gauge eigenstates through the RG scale, the Yukawa coupling terms have the opposite sign. Therefore, for the $PS1$ model, the X_τ contribution (6.10) in the RGE equation of the right-handed stau, eq. (6.5), becomes dominant over M_1 for large $\tan\beta$. Light stau masses are therefore induced by the RG running with $\tilde{\tau}_1$ dominated by its right-handed component. On the other hand, the heavy stau, which is dominated by the $\tilde{\tau}_L$ component, may become heavy due to the M_2 contribution. Despite only one solution found with $\Delta < 10$ (the isolated dark green point), we observe several other light green points close enough to the dark blue bland, where the fine-tuning is still not large.

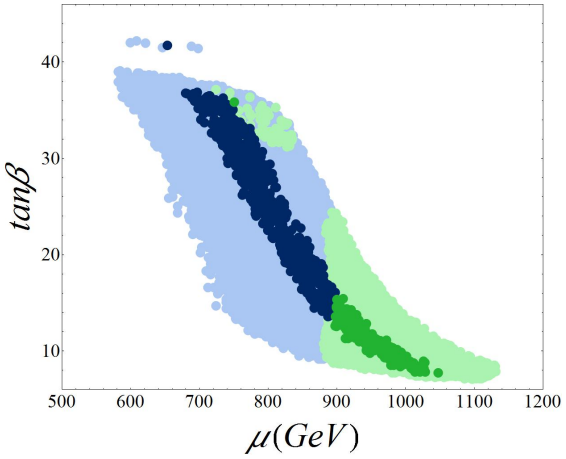

Figure 8.33. *Viable scenarios in the $\mu - \tan\beta$ (left) and $R_{tb\tau} - \tan\beta$ (right) planes for the $PS1$ model, with colours as in Fig. 8.13.*

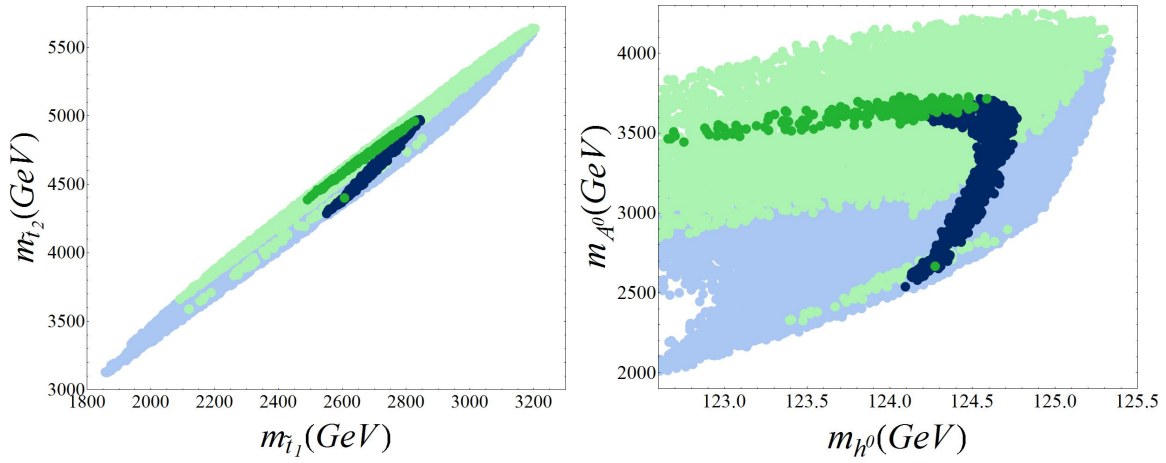

Figure 8.34. *Viable scenarios in the stop mass and lightest scalar - pseudoscalar mass planes for thePS*1 *model, with colours as in Fig. 8.13.*

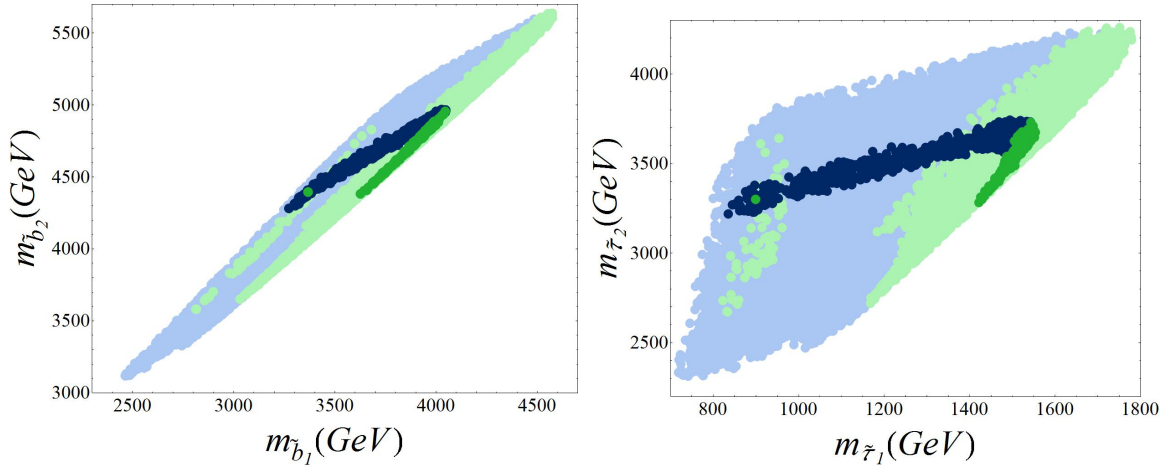

Figure 8.35. *Viable scenarios in the sbottom mass (left) and stau mass (right) planes for the PS*1 *model, with colours as in Fig. 8.13.*

The stop-Higgs and sbottom-stau masses are shown in Figs. 8.34 and 8.35. We see that the supersymmetric spectra is in general lighter than the previous *GG*75 + 200 and *FL*75 + 1 models, with stops as light as 1.8 TeV, sbottoms of 2.5 TeV and 750 GeV staus. However, these solutions have fine-tuning $10 < \Delta < 100$ and predict too little Dark Matter density. For the particular case of the stau-neutralino-chargino degenerate region, we find a solution with 900 GeV stops, which, even though challenging, may be accessible to the 14 TeV LHC, predicts the preferred Dark Matter relic density and is not fine-tuned $\Delta < 10$. However, the Higgs mass for this point is however below the average LHC value, having a mass of 124.3 GeV. If we insist in a 125 GeV Higgs (or heavier) together with the preferred relic density, we find plenty of such solutions but unfortunately with $10 < \Delta < 100$ and rather heavier sparticle spectra.

The values of $\tan\beta$ obtained here are not sufficiently large to reach the region preferred for Yukawa coupling unification, $R_{tb\tau} \to 1$. Therefore we consider that the $PS1$ model is not a good candidate for top-bottom-tau YU. However, the lowest value for $R_{tb\tau}$ we obtained here is 1.85, which may be close to a QYU condition. The bottom-tau unification is once again closer to the 3/2 ratio rather than an exact $y_b = y_\tau$ unification, with values between $1.30 - 1.41$.

In general, we have observed that for the three scenarios considered so far, solutions with the preferred relic density and fine-tuning $\Delta < 10$, are not reconcilable with top-bottom-tau YU and favour a $R_{b\tau}$ ratio approximately between 1.30 and 1.35.

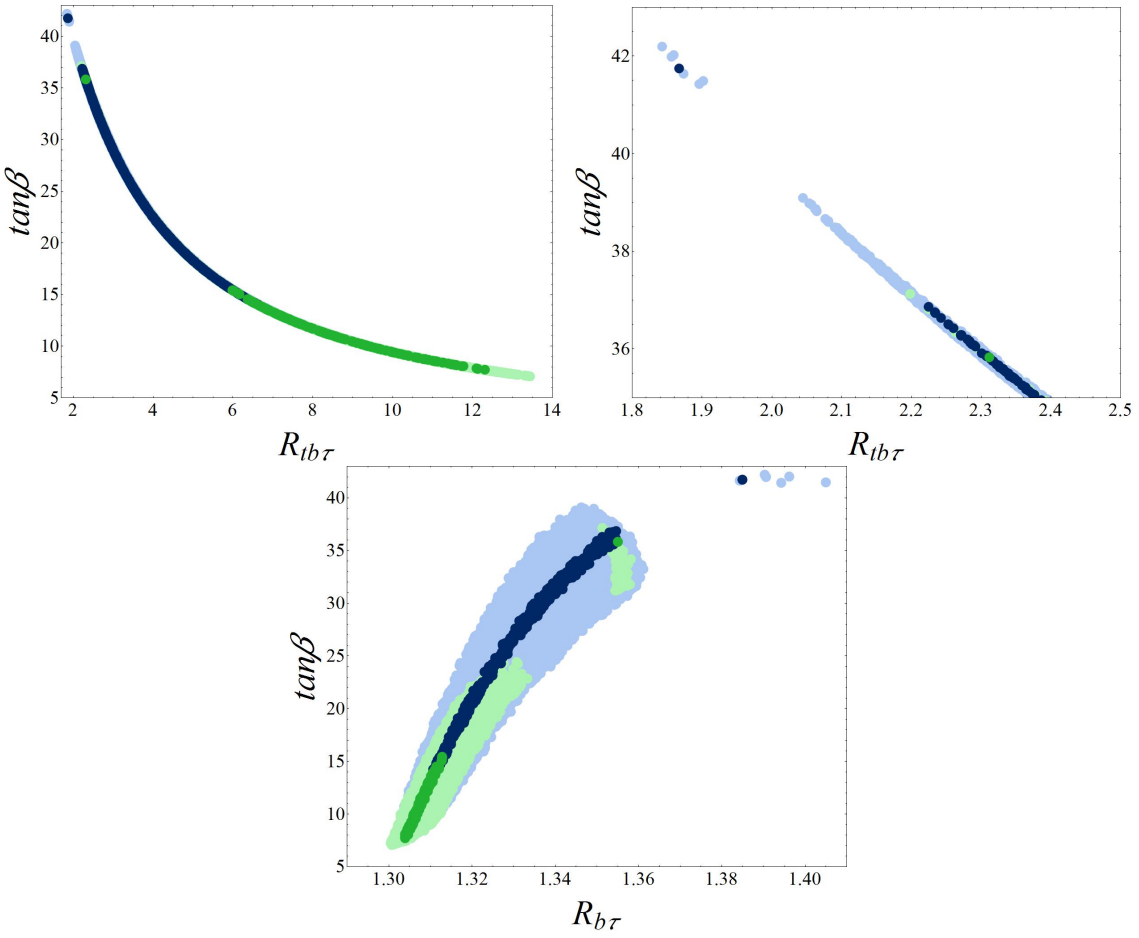

Figure 8.36. *Viable scenarios in the $R_{tb\tau} - \tan\beta$ (top) and $R_{b\tau} - \tan\beta$ (bottom) planes for the $PS1$ model, with colours as in Fig. 8.13. The top-right pane is a zoomed-in version of the top-left one.*

In Fig. 8.37 we see that for scenarios with stau NLSP (red circles), the mass separation to the LSP ranges from less than 0.5 GeV up to 3 GeV. For those points in the parameter space with chargino NLSP (red filled squares), the separation is roughly $2 - 4.5$ GeV. The solutions with the preferred relic density (right panel) reveal the two distinct areas that we

have been discussing. One has both higgsino dominated neutralino LSP and chargino NLSP, with masses in the range $0.9 < m_{LSP} < 1$ TeV; the other region predicts closely degenerate stau-neutralino-chargino masses in the interval $0.7 < m_{LSP} < 0.9$ TeV.

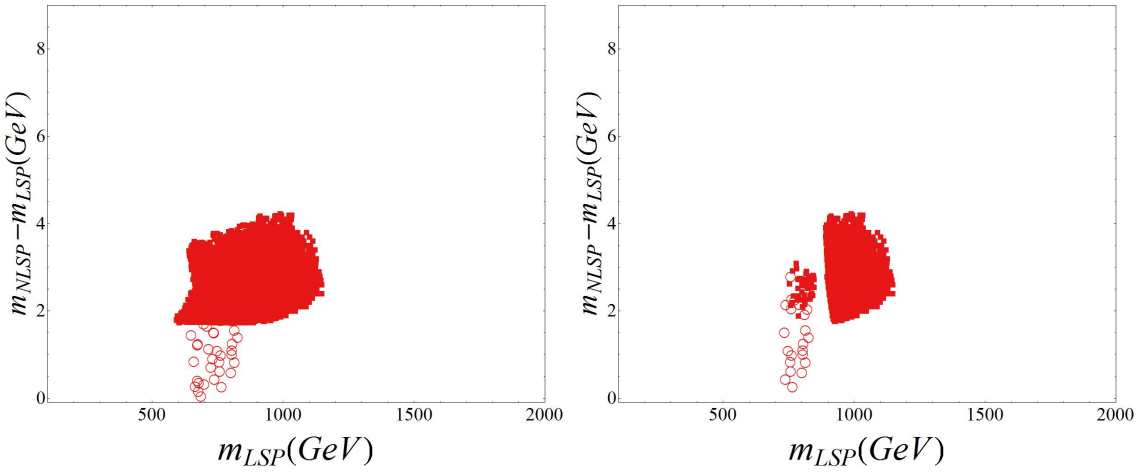

Figure 8.37. *Solutions in the plane of LSP mass vs. the NLSP-LSP mass splitting for the PS1 model. All the LSPs are higgsino. The shapes indicate the NLSP flavour where filled squares and circles indicate chargino and stau respectively. The right panel only shows solutions with the preferred relic density.*

8.5.4. First and Second Generation Squarks and Gluinos

The gluino and the lightest first and second generation squark masses are shown in Fig. 8.38 for the three models discussed in Secs. 8.5.1, 8.5.2 and 8.5.3. We see once again a correlation between the gluino mass and the lighest squark mass, which is due to the same reasons already discussed in Sec. 7.5.3.

Using the boundary condition (8.3), the $\tilde{d}_R$ squark mass, which is typically the lightest one, takes the approximate form

$$m^2_{\tilde{d}_R}(t) = K_{\mathbf{16}}\left(m^2_{\mathbf{16}} - 3g^2_{10}D\right) + M^2_3(t)\left[0.78 + 0.002\,\rho_1^2\right], \tag{8.23}$$

where, once again, we have ignored all two loop contributions that are implemented in SOFTSUSY. Since we keep $m_{\tilde{d}_R}(0)$ small, the dominant contribution arises from the gluino mass term. For the $GG75+200$ and the $PS1$ models, the gaugino mass ratios are $3.7 \lesssim \rho_1 \lesssim 5.3$ and $\rho_1 = 1.9$ respectively, so, to a good approximation, we have $m_{\tilde{d}_R} \approx 0.9 m_{\tilde{g}}$. For the $FL75+1$ model, since $5.8 \lesssim \rho_1 \lesssim 7.8$, this correlation may become $m_{\tilde{d}_R} \approx 0.95 m_{\tilde{g}}$ for larger values of ρ_1. If we require solutions with the preferred relic density and $\Delta < 10$, then the approximation $m_{\tilde{d}_R} \approx 0.9 m_{\tilde{g}}$ is valid for the three scenarios studied.

The $GG75+200$ allows solutions predicting the preferred Dark Matter abundance with

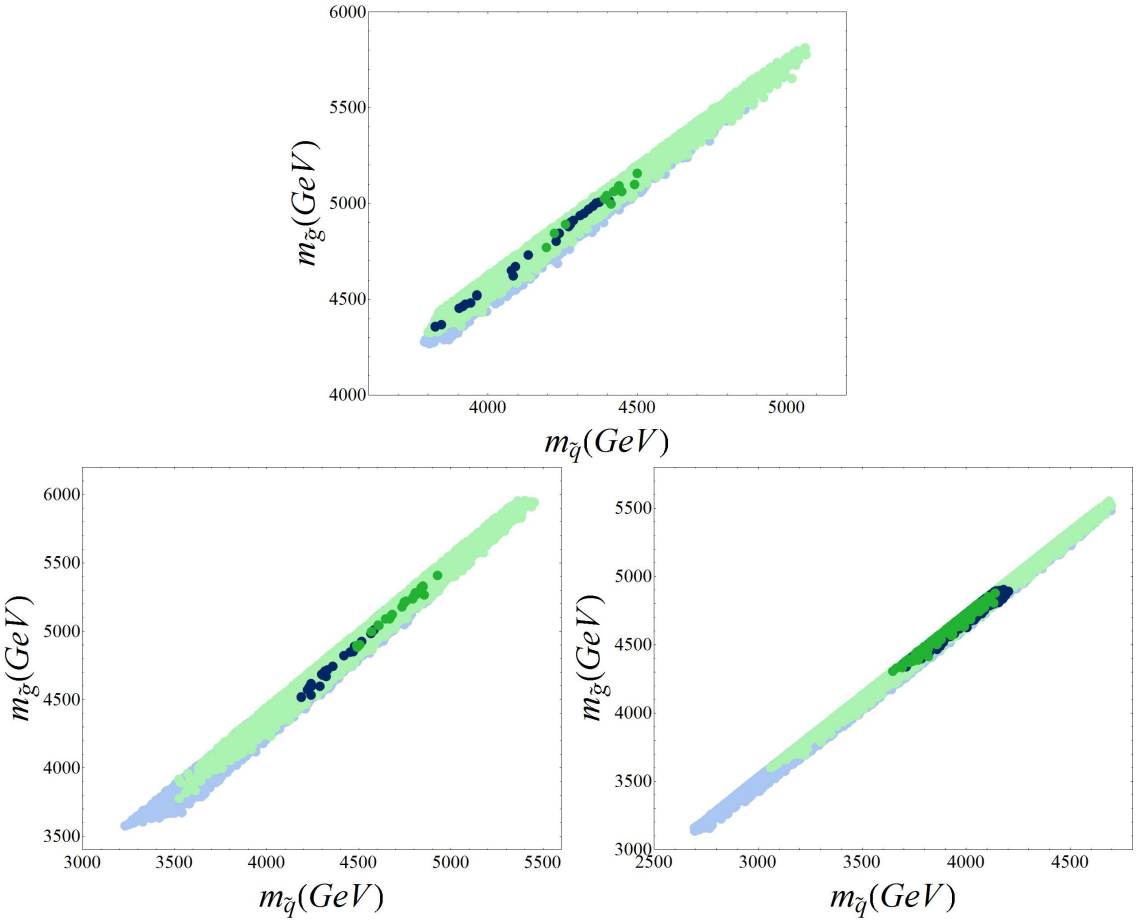

Figure 8.38. *The lightest squark mass and the gluino mass for the GG*$75+200$ *(top), FL*$75+1$ *(bottom-left) and PS*1 *(bottom-right) models. Points with the preferred Dark Matter relic density are shown in green, while those with a relic density below the bounds are in blue. Darker and lighter shades denote the fine-tuning, with darker shades have fine-tuning* $\Delta < 10$ *while lighter shades have* $10 < \Delta < 100$

squarks as light as 3.7 TeV and gluinos about 10% heavier. However, such scenarios are very challenging for the 14 TeV LHC, and, if we insist in low fine-tuning, the lightest squark becomes heavier than 4.2 TeV. We also found scenarios with $\Delta < 10$ for $m_{\tilde{q}} \approx 3.7$ TeV but too little Dark Matter density. Nevertheless, all these scenarios would become accessible to an energy-upgraded Super-LHC with $\sqrt{s} = 28$ TeV.

As discussed in the previous sections, the *FL*$75+1$ model is quite similar to the *GG*$75+200$. However, it predicts a slightly lighter mass spectrum, and $3.2-3.3$ TeV squarks are now allowed and maybe accessible to the 14 TeV LHC. Still, these low mass solutions have $10 < \Delta < 100$ and do not fulfill the total Dark Matter density of the Universe. However, this is possible to attain for squark masses between 3.5 and 5.5 TeV, or between 4.5 and 5.0 TeV if we require $\Delta < 10$. Unfortunately, these attractive scenarios are outside the expected reach of the 14 TeV LHC, and we do not expect to see them without an energy upgrade.

Like the $SU(5)_{200}$ and the $O-II$ models, we find squarks and gluinos which are accessible to the 14 TeV LHC in the $PS1$ model. Nevertheless, these solutions predict a relic density below the WMAP bounds and have $10 < \Delta < 100$. Although it is possible to satisfy both the low fine-tuning and preferred relic density requirements simultaneously, the lightest squarks would possible escape the region reachable by the LHC, with masses around $3.6 - 4.1$ TeV.

8.6. Benchmark Points

We present in this section seven benchmarks for viable $SO(10)$ GUT scenarios with non-universal masses that may be interesting to consider at either the 14 TeV LHC or the energy-upgraded Super-LHC with $\sqrt{s} = 28$ TeV. The GUT scale parameters for these scenarios can be found in Tab. 8.4. In Tab. 8.5 we show the masses of the five Higgs bosons. The masses of the first and third generation sfermions are shown in Tab. 8.6. The second generation sfermions are assumed degenerate with the first. In Tab. 8.7 we show the gaugino masses. Finally in Tab. 8.8 we present μ, $\tan\beta$, the Yukawa coupling ratios $R_{tb\tau}$ and $R_{b\tau}$, the fine-tuning Δ, the fine-tuning from μ alone and the predicted relic density of Dark Matter. In all seven scenarios, the LSP is predominantly dominated by the Higgsino component.

	GG_1	GG_2	GG_3	FL_1	FL_2	PS_1	PS_2
$m_{\mathbf{16}}$	138.2	106.0	28.92	104.0	138.4	147.5	113.8
$K_{\mathbf{16}}$	1.96	0.86	6.56	3.47	6.17	12.79	12.3
$m_{\mathbf{10+126}}$	110.0	127.8	78.47	132.7	107.4	130.6	132.5
$g_{10}^2 D$	5355	-21.86	0.12	-5025	5377	4065	-6674
$a_{\mathbf{10}}$	4.24	-149.6	5.10	-0.35	-4.41	-38.43	-116.7
$M_{1/2}$	1747	1924	1505	1781	1426	2105	2471
ρ_1	4.39	4.23	4.55	6.51	7.04	1.90	1.90
ρ_2	2.37	2.38	2.36	2.14	2.07	2.50	2.50
$\theta_{RR'}$	1.03	1.01	1.05	0.65	0.71	0	0

Table 8.4. *GUT scale parameters for our seven benchmark scenarios. Masses and trilinear couplings are in GeV.*

The first three benchmarks GG_1, GG_2 and GG_3 are scenarios for which supersymmetry is broken by the auxiliary components of chiral superfields belonging to a combination of a **210** and a **770** $SO(10)$, transforming respectively as a **75** and a **200** of $SU(5)$ with conventional embedding. The GG_1 benchmark has very low (non-μ) fine-tuning, predicts the preferred

	GG_1	GG_2	GG_3	FL_1	FL_2	PS_1	PS_2
m_{h^0}	125.0	125.5	124.1	125.2	123.7	124.3	125.0
m_{A^0}	3666	4139	1999	4030	891.1	2667	3842
m_{H^0}	3666	4139	1999	4030	891.1	2667	3842
$m_{H^\pm}$	3667	4140	2000	4031	895.5	2668	3843

Table 8.5. *Higgs masses in GeV for our seven benchmark scenarios.*

	GG_1	GG_2	GG_3	FL_1	FL_2	PS_1	PS_2
$m_{\tilde{t}_1}$	3561	3844	3141	4502	3534	2606	2987
$m_{\tilde{t}_2}$	4877	5396	4031	4783	3900	4401	5243
$m_{\tilde{b}_1}$	4144	4587	3159	4525	3132	3366	4240
$m_{\tilde{b}_2}$	4870	5390	4022	4757	3549	4396	5239
$m_{\tilde{\tau}_1}$	3663	3938	2823	4344	3026	900.0	1577
$m_{\tilde{\tau}_2}$	3976	4394	3234	5743	4247	3302	3955
$m_{\tilde{\nu}^3}$	3974	4393	3232	4343	3025	3300	3954
$m_{\tilde{u}_L}$	5519	6079	4761	5545	4508	4997	5785
$m_{\tilde{u}_R}$	4923	5359	4296	5867	4970	3898	4481
$m_{\tilde{d}_L}$	5519	6079	4761	5546	4508	4998	5786
$m_{\tilde{d}_R}$	4397	4816	3823	4794	3974	3786	4417
$m_{\tilde{e}_L}$	4075	4481	3520	4500	3708	3424	4036
$m_{\tilde{e}_R}$	3879	4132	3442	5972	5227	1594	1765
$m_{\tilde{\nu}^1}$	4074	4480	3518	4499	3707	3423	4035

Table 8.6. *First and third generation sfermion masses (we assume the first and second generation sfermions are degenerate) for our seven benchmark scenarios. All the masses are in GeV*

relic density but unfortunately is slightly heavier than the expected reach of the 14 TeV LHC. The GG_2 scenario is also spot on for the relic density of Dark Matter and has the correct Higgs mass. The fine-tuning is a bit larger (~ 47), but tolerable. The attractiveness of the GG_3 benchmark is that having ~ 3.8 TeV squarks and ~ 800 GeV neutralinos and charginos, it may be accessible to the 14 TeV LHC, thought undoubtedly very challenging.

	GG_1	GG_2	GG_3	FL_1	FL_2	PS_1	PS_2
$M_{\tilde{g}}$	5040	5542	4357	5252	4292	4450	5175
$M_{\tilde{\chi}_1^0}$	971.2	1069	801.9	1077	875.7	794.8	949.4
$M_{\tilde{\chi}_2^0}$	973.1	1070	804.1	1079	878.1	798.0	952.2
$M_{\tilde{\chi}_3^0}$	4642	4964	3960	4376	3414	1740	2050
$M_{\tilde{\chi}_4^0}$	4655	5170	4107	7217	6282	4288	5040
$M_{\tilde{\chi}_1^\pm}$	972.4	1070	803.1	1078	876.9	796.9	951.3
$M_{\tilde{\chi}_2^\pm}$	4648	5170	3960	4376	3414	4288	5040

Table 8.7. *Gaugino masses in GeV for our seven benchmark scenarios.*

	GG_1	GG_2	GG_3	FL_1	FL_2	PS_1	PS_2
μ	922.1	1016	746.9	1021.3	808.6	751.1	907.5
$\tan\beta$	26.94	24.32	47.19	27.44	56.56	35.83	19.13
$R_{tb\tau}$	3.27	3.67	1.55	3.21	1.46	2.31	4.76
$R_{b\tau}$	1.33	1.32	1.38	1.33	1.46	1.36	1.32
Δ	6.82	46.97	8.69	5.88	33.98	9.83	33.62
Δ_μ	459.6	560.1	302.5	561.9	358.4	302.3	453.5
$\Omega_c h^2$	0.0944	0.113	0.0647	0.112	0.0735	0.0944	0.0934

Table 8.8. *The Higgs parameters μ (in GeV) and $\tan\beta$ for our seven benchmark scenarios. Also shown is the fine-tuning Δ (which does not include fine-tuning in μ as described in the text), the fine-tuning from μ alone, and the predicted relic density of Dark Matter. The LSP is always predominantly Higgsino.*

The next two benchmarks, FL_1 and FL_2 are scenarios for which the auxiliary components of hidden sector chiral superfields belong to a combination of two distinct **770** $SO(10)$ irreps, transforming as a **75** and a **1** under $SU(5)$ with flipped embedding. While the first one allows for low fine-tuning together with the preferred Dark Matter abundance and a Higgs mass of 125.2 GeV, the second one predicts a bottom-tau Yukawa coupling ratio with just a 2.7% deviation from $y_\tau/y_b = 3/2$.

The final two benchmarks PS_1 and PS_2, are for scenarios with supersymmetry broken by a chiral superfield in a **770** of $SO(10)$ transforming as a singlet under $SU(4)\times SU(2)_R$. Both cases predict relatively light staus as a consequence of the smallness of ρ_1. In particular, PS_1 corresponds to the isolated dark green point in Figs. 8.33, 8.34 and 8.35.

9. BIM-OI and BIM-OII Orbifold Phenomenology

We have discussed in both Chapters 7 and 8 scenarios with non-universality among the gaugino masses at the high scale. In most of the cases we used fixed ratios set by hidden sector chiral superfields in distinct GUT representations, as the $SU(5)_{200}$ and the $PS1$ models, but we also considered possible combinations of such representations as in the $GG75+200$ and $FL75+1$ models. Besides these more conventional supersymmetry breaking frameworks, we have also studied possible non-universalities of gaugino masses inspired by the O-I and O-II orbifold models as discussed by Brignole, Ibáñez and Muñoz in [239]. However, we only considered moduli dominated scenarios and disregarded constraints from scalar masses in the models that we denoted as BIM O-I and BIM O-II. For completeness, we will revisit these scenarios and include the full trilinear couplings, gaugino and scalar masses boundary conditions, as derived in [239]. Furthermore, as we have a more definite theoretical motivation, we will allow for some relaxation of the fine-tuning constraints. However, as a point of interest, we also consider scenarios with low fine-tuning in the gravitino mass when possible.

9.1. Overview of the Parameter Space

In general *four*-dimensional string models, there are *three* types of of massless chiral fields, which include the complex Standard Model singlets *moduli* T and *dilaton* S fields, as well as charged fields that contain the quark, lepton and Higgs multiplets and its superpartners. In string theory, while moduli fields are associated with the size of the extra six dimensions, the dilaton provides a measure of the size of the eleventh dimension. To make a simple analogy, we can imagine the whole space represented by a cylinder where its height corresponds to a modulus field and the radius of the base, which represents the eleventh dimension, is the dilaton.

Although string inspired models allow for many extra chiral multiplets, in a minimal version, the breaking of supersymmetry may be accomplished only through non-vanishing expectation values of the auxiliary components, F^S and F^T, of the dilaton and modulus fields

respectively. For this class of theories, supersymmetry is realized locally, allowing for the presence of a fermion field, the gravitino, which acquires mass in the process of spontaneous SUSY-breaking. The gravitino is a spin-3/2 field with mass $m_{3/2}$, and is the superpartner of the spin-2 graviton, which, due to the apparent unlimited range of the gravitational interaction, is expected to be massless.

It is however important to know which of the fields, either S or T, provide the dominant contribution for SUSY-breaking. In this process, a massless goldstone fermion emerges, the goldstino ($\tilde{\eta}$), which is absorbed by the gravitino and can be expressed as

$$\tilde{\eta} = \tilde{S}\sin\theta + \tilde{T}\cos\theta, \tag{9.1}$$

where $\tilde{S}$ and $\tilde{T}$ are the fermionic partners of the S or T scalars, and θ is a mixing angle denoted as *goldstino angle*. This is the approach carried out in [239], where without specifying any particular mechanism for the breakdown of supersymmetry, the goldstino angle serves as an indicator on whether supersymmetry breaking is moduli or dilaton dominated. This mechanism produces a low energy effective theory containing global supersymmetry, explicitly broken by soft terms, that can be completely determined from the goldstino angle θ and the gravitino mass $m_{3/2}$.

For the orbifold models that we consider here, the Kähler potential is invariant under the modular group $SL(2,\mathbb{Z})$ where the moduli fields transform like

$$T \to \frac{aT - ib}{ict + d} \quad \text{with} \quad ad - bc = 1 \quad \text{and} \quad a,b,c,d \in \mathbb{Z}\,, \tag{9.2}$$

the dilaton is invariant at tree level, and the matter fields Ψ_i transform as

$$\Psi_i \to (icT + d)^{n_i}\,\Psi_i\,. \tag{9.3}$$

With the above transformation properties, the Kähler potential is *modular invariant*, and the integer coefficients n_i are the *modular weights*.

The computation of the soft terms is dependent on the string model considered, and one of the approaches taken by the authors of [239] relies on a class of four-dimensional strings based on orbifold compactifications. Phenomenological constraints can be imposed in order to further constrain the soft parameters, and within the framework of a Grand Unified Theory, it is adequate to invoke the matching of the gauge couplings at the GUT scale. However, it is not automatic in string models since there is a mismatch between M_{GUT} and the string scale given as $M_{string} \approx 5\times10^{17}$ GeV [251]. In order to explain this mismatch, the authors of [239] propose two distinct orbifold models called O-I and O-II.

For the first one, which we denoted as BIM O-I, the G_{SM} gauge couplings unify at the GUT scale and then diverge towards M_{string} due to large one-loop stringy threshold corrections. An appropriate choice for the modular weights[1] n_i, of the matter and Higgs fields contributes too the joining of the gauge couplings at M_{GUT}, in particular

$$\begin{aligned} n_{Q_L} = n_{d_R} &= -1, \\ n_{u_R} &= -2, \\ n_{L_L} = n_{e_R} &= -3, \\ n_H + n_{\overline{H}} &= -5, -4. \end{aligned} \tag{9.4}$$

For the second case, which we call BIM O-II, all the modular weights are set to $n_i = -1$, and the $M_{GUT} - M_{string}$ mismatch is explained assuming the presence of very massive fields close to the string scale.

9.1.1. Soft-SUSY Breaking Parameters in the BIM O-I Orbifold

With the formulae derived in [239], the scalar masses of the BIM O-I model are given as $m_i = m_{3/2}^2(1 - n_i \cos^2\theta)$, where using (9.4), we get

$$m_{\tilde{Q}_L}^2 = m_{\tilde{d}_R}^2 = m_{-1}^2 = m_{3/2}^2 \sin^2\theta, \tag{9.5}$$

$$m_{\tilde{u}_R}^2 = m_{-2}^2 = m_{3/2}^2\left(1 - 2\cos^2\theta\right), \tag{9.6}$$

$$m_{\tilde{L}_L}^2 = m_{\tilde{e}_R}^2 = m_{-3}^2 = m_{3/2}^2\left(1 - 3\cos^2\theta\right), \tag{9.7}$$

and for the Higgs fields, two possible choices are

$$m_{H_u}^2 = m_{H_d}^2 = m_{3/2}^2\left(1 - 2\cos^2\theta\right), \tag{9.8}$$

when $n_H + n_{\overline{H}} = -4$, and

$$m_{H_u}^2 = m_{3/2}^2\left(1 - 3\cos^2\theta\right), \tag{9.9}$$

$$m_{H_d}^2 = m_{3/2}^2\left(1 - 2\cos^2\theta\right), \tag{9.10}$$

when $n_H + n_{\overline{H}} = -5$. We see from eq. (9.7), that vacuum stability requires that $\cos^2\theta \leq 1/3$ or equivalently that $\sin^2\theta \geq 2/3$, which implies that the source of supersymmetry breaking is dilaton dominated.

[1] Negative integer coefficients arising from the transformation of matter fields in orbifold compactifications [253].

The trilinear couplings take the universal value

$$a_0 = -m_{3/2}\Big(\sqrt{3}\sin\theta + n_{H_d}\cos\theta\Big), \tag{9.11}$$

and the gugino masses acquire the form

$$\begin{aligned} M_1 &= 1.18\sqrt{3}m_{3/2}\Big[\sin\theta - \Big(\frac{51}{5}+\delta_{GS}\Big)2.9\times10^{-2}\cos\theta\Big], && (9.12)\\ M_2 &= 1.06\sqrt{3}m_{3/2}\Big[\sin\theta - (7+\delta_{GS})\,2.9\times10^{-2}\cos\theta\Big], && (9.13)\\ M_3 &= \sqrt{3}m_{3/2}\Big[\sin\theta - (6+\delta_{GS})\,2.9\times10^{-2}\cos\theta\Big], && (9.14) \end{aligned}$$

for $n_{H_u} + n_{H_d} = -4$, and

$$\begin{aligned} M_1 &= 1.18\sqrt{3}m_{3/2}\Big[\sin\theta - \Big(\frac{54}{5}+\delta_{GS}\Big)2.9\times10^{-2}\cos\theta\Big], && (9.15)\\ M_2 &= 1.06\sqrt{3}m_{3/2}\Big[\sin\theta - (8+\delta_{GS})\,2.9\times10^{-2}\cos\theta\Big], && (9.16)\\ M_3 &= \sqrt{3}m_{3/2}\Big[\sin\theta - (6+\delta_{GS})\,2.9\times10^{-2}\cos\theta\Big], && (9.17) \end{aligned}$$

for $n_{H_u} + n_{H_d} = -5$. In string theories, the emergence of extra chiral fermions may introduce anomalies. However, they can be canceled by the so called Green-Schwarz counterterm [252], form where the coefficient δ_{GS}, which is a negative integer, appears. In the limit $\sin\theta \to 0$, if we take the ratios ρ_1 and ρ_2, we recover the results for the BIM O-I model discussed in chapter 7. However, we see that such solutions generate unacceptable scalar masses which destabilize the vacuum.

9.1.2. Soft-SUSY Breaking Parameters in the BIM O-II Orbifold

The BIM O-II model aims to study a region where supersymmetry breaking is moduli dominated, which implies that $\sin\theta \to 0$. It is pointed out by the authors of [239] that, in this limit, one-loop corrections to the soft terms are much better known and easier to handle in the context of orbifolds rather than in other schemes such as Calabi-Yau-type compactifications. The scalar masses and trilinear couplings take universal values of the form

$$\begin{aligned} m_0 = m_i^2\,(\sin\theta \to 0) &\approx m_{3/2}^2\,(-\delta_{GS})\times10^{-3}, && (9.18)\\ a_0 &= -\sqrt{3}m_{3/2}\sin\theta, && (9.19) \end{aligned}$$

whereas the gaugino masses are given as

$$M_1 = 1.18\sqrt{3}m_{3/2}\left[\sin\theta - \left(\frac{-33}{5} + \delta_{GS}\right)4.6\times10^{-4}\cos\theta\right], \quad (9.20)$$

$$M_2 = 1.06\sqrt{3}m_{3/2}\left[\sin\theta - (-1+\delta_{GS})4.6\times10^{-4}\cos\theta\right], \quad (9.21)$$

$$M_3 = \sqrt{3}m_{3/2}\left[\sin\theta - (3+\delta_{GS})4.6\times10^{-4}\cos\theta\right]. \quad (9.22)$$

We see from the above equations, that in the limit $\sin\theta = 0$, from where we recover the results of chapter 7 with respect to the gaugino masses, the gravitino mass decouples from the scalar masses. We have in particular that $M_3 = -\sqrt{3}m_{3/2}(3+\delta_{GS})4.6\times10^{-4} = 0.0024m_{3/2}$ for $\delta_{GS} = -6$. The LHC limits on the gluino mass impose that $M_3 \gtrsim 300$ GeV which results in a gravitino mass $m_{3/2} \gtrsim 126$ TeV and a universal scalar mass $m_0 \gtrsim 10$ TeV.

For both models considered here, the effective low energy theory contain superpotential terms of the same form of the supergravity ones. The μ-term of the MSSM, which is generated by a rescaling of the high energy terms, is uncertain, but can either grow up to the order of $m_{3/2}$, or being generated at the scale of the soft parameters.

9.1.3. Summary of the Parameter Space

The parameter space of the BIM O-I and BIM O-II models is greatly reduced when compared to $SU(5)$ and $SO(10)$. In addition to the SM parameters, there are only three high scale parameters, $m_{3/2}$, θ and δ_{GS}, as well as $\tan\beta$ and the sign of μ.

9.2. BIM O-I Orbifold

The first scenario to study considers dilaton dominated supersymmetry breaking. As we have discussed, vacuum stability forces the goldstino angle to be larger than $\arcsin(\sqrt{2/3})$. We therefore consider the ranges $\arcsin(\sqrt{2/3}) < \theta < \pi/2 + \arcsin(\sqrt{2/3})$, as well as $\arcsin(\sqrt{2/3}) + \pi < \theta < 3\pi/2 + \arcsin(\sqrt{2/3})$, which correspond to the possible values of θ around $\pi/2$ and $3\pi/2$ where $\sin^2\theta > 2/3$. In this limit, it is possible to see from eqs. (9.5 - 9.17) that the soft parameters are of the same order of magnitude as $m_{3/2}$ and we allow the gravitino mass to vary between $0-5000$ GeV. We have now the ingredients needed to run the two-loop RGEs down to the electroweak scale and study the viability of this scenario when confronted with experimental constraints as described in chapters 7 and 8. The vacuum stability conditions are also implemented in the same way as described previously, and the simplified approach to the CCB2,3 conditions is now given as

$$\left|\frac{a_0}{m_i}\right| \lesssim 3. \quad (9.23)$$

However, if we look at eqs. (9.5, 9.6 and 9.11), we find that that

$$0.32 < \frac{a_0}{m_{-1}} < 1, \quad 0.45 < \frac{a_0}{m_{-2}} < \sqrt{3}, \tag{9.24}$$

which shows that in the range of the goldstino angle considered, the a_0/m_{-1} and a_0/m_{-2} constraints are always safe from dangerous charge and colour breaking minima. For the case of a_0/m_{-3} we should be careful since in the limit $\sin^2\theta \to 2/3$, we have $a_0/m_{-3} \to \infty$. Therefore, the stability cut to implement is

$$\left|\frac{a_0}{m_{-3}}\right| \lesssim 3. \tag{9.25}$$

With the input parameters considered, the mass of the up-type Higgs gauge eigenstate is given as $m^2_{H_u} = a_\theta m^2_{3/2}$, where we found that the coefficient a_θ, which depends on the goldstino angle, is always negative and of the order $O(1)$. Therefore any large fluctuation of $m_{3/2}$ will cause a proportionate change in $m^2_{H_u}$, which one may naively interpret as fine-tuning. However, in this case we expect a particular value of $m_{3/2}$ (and indeed θ) to be dictated by the String Theory; it is therefore not a parameter that should ever be tuned to provide an acceptable phenomenology. We will therefore relax our previous requirement for low fine-tuning in the scans over the parameter space.

We will consider two scenarios, one with $n_H + n_{\overline{H}} = -4$ and $\delta_{GS} = -5$, whose gaugino masses reduce to the BIM O-I scenario of chapter 7 when $\sin\theta = 0$, and another one with $\delta_{GS} = 0$ and $n_H + n_{\overline{H}} = -5$. We shall call these scenarios as OI4d5 and OI5d0 respectively. In the dilaton dominated region, the dependence of the soft parameters on θ, δ_{GS} as well as on the modular weights of the Higgs fields is not significant and this is the reason behind our choice of a non-smooth change in the input parameters.

9.2.1. OI4d5 Model

We first consider a model with $n_H + n_{\overline{H}} = -4$, which in terms of the MSSM Higgs doublets corresponds to $n_{H_u} = n_{H_d} = -2$ and with $\delta_{GS} = -5$. We have once again used SOFTSUSY to generate 435,458 initial scenarios, of which 89,915 survived the LHC bounds and stability constraints. We have then generated predictions for the remaining experimental constraints discussed in Sec. 7.2.1 using micrOMEGAS. Imposing the cut $P_{tot} > 10^{-3}$ in order to accept a solution, the number of viable scenarios is reduced to only 12 (0.003%), of which 5 have the preferred Dark Matter abundance. The vast majority of the solutions are rejected due to predicting a large relic density. However, we have observed that the few accepted solutions all lie very close to either $\theta = 4.95$ or $\theta = 4.25$. We have therefore preformed a new dedicated scan with the goldstino angle varying in the intervals $4.90 - 5.00$ and $4.20 - 4.30$, generating significantly more data.

We show in Fig. 9.1 (left) the $\mu - \tan\beta$ plane, from where we see a preference for large values of $\tan\beta$ in a relatively narrow band between 35 and 40. The values of μ are also larger than in previous cases, lying in the range $1700 - 3400$ GeV. The $m_{3/2} - \theta$ plane is shown on the right panel of the same figure, and we observe that all points accepted favour goldstino angles around $3\pi/2$, where $\sin\theta$, and therefore the gaugino masses, are negative. The OI4d5 model favours gaugino mass ratios approximately fixed to $\rho_1 \approx 1.18$ and $\rho_2 \approx 1.06$, which lies far from the ellipse of Figs. 8.18 and 7.19.

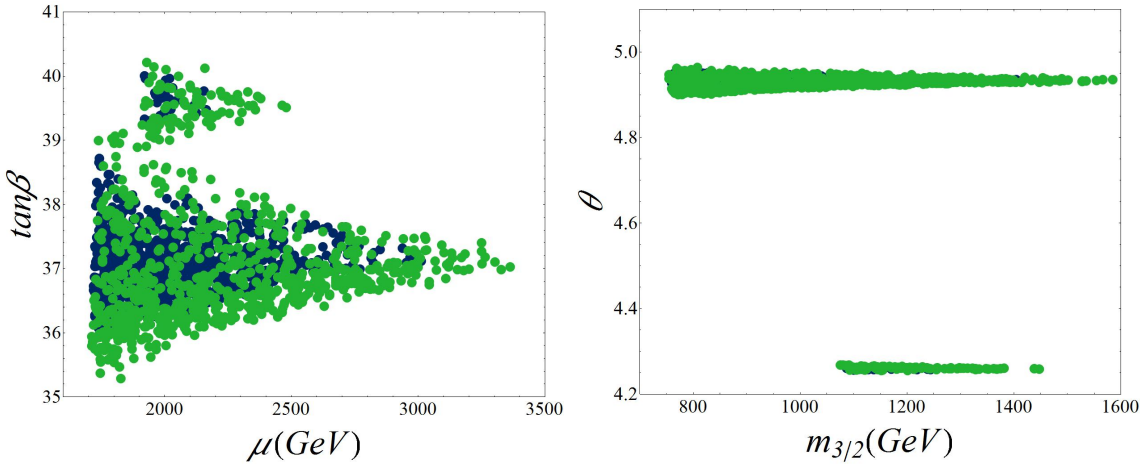

Figure 9.1. *Viable scenarios in the $\mu - \tan\beta$ (left) and $m_{3/2} - \theta$ (right) planes for the OI4d5 model. Blue points represent scenarios with a Dark Matter relic density below 2σ bounds, while green points have the preferred relic density.*

The stop-Higgs and sbottom-stau masses are shown in Figs. 9.2 and 9.3. Although the supersymmetric spectra is not too heavy, with stops having masses between 1.8 and 3.8 TeV and sbottoms in the range $2.1 - 4.4$ TeV, it is not expected to observe third generation squarks with the masses predicted by the OI4d5 model at the 14 TeV LHC. However, such solutions would be accessible to an energy upgraded super-LHC with $\sqrt{s} = 28$ TeV. On the other hand, the light stau can be as light as 650 GeV, which may be accessible to the 14 TeV LHC. It is also difficult to keep the Higgs mass heavy with the majority of solutions having mass bellow 125 GeV, and only a not densely populated tail with masses between 125 and 126 GeV. Though, all results are still compatible with the experimental bounds and theoretical uncertainties.

The masses of the gluinos and lightest first and second generation squarks for the OI4d5 model is shown in Fig. 9.4. Plenty of solutions accessible to the 14 TeV LHC and with the preferred relic density were encountered, with squarks below 3.5 TeV and gluinos roughly 10% heavier. Once again a striking correlation is observed but we no longer have small

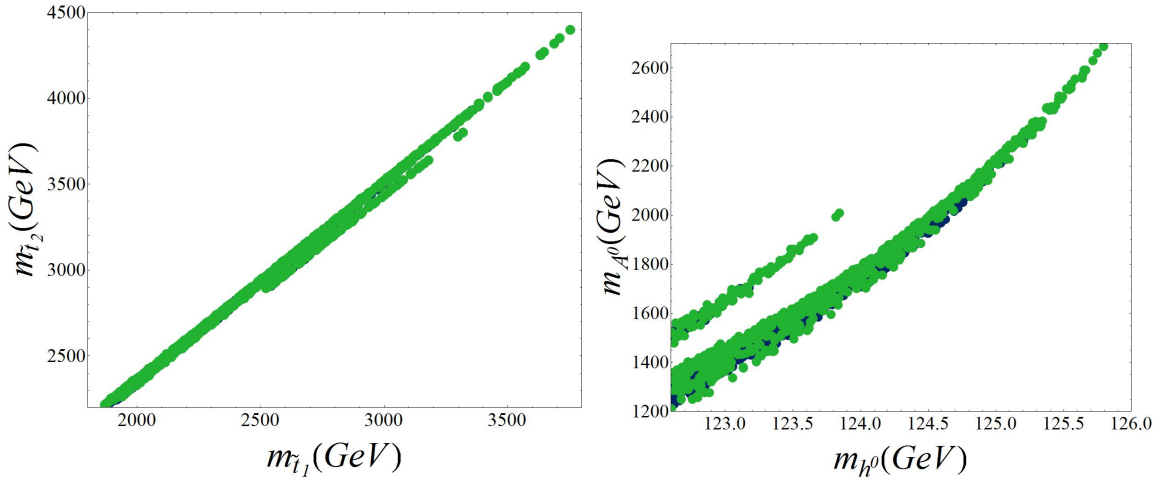

Figure 9.2. *Viable scenarios in the stop mass and lightest scalar - pseudoscalar mass planes for the OI4d5 model, with colours as in Fig. 9.1.*

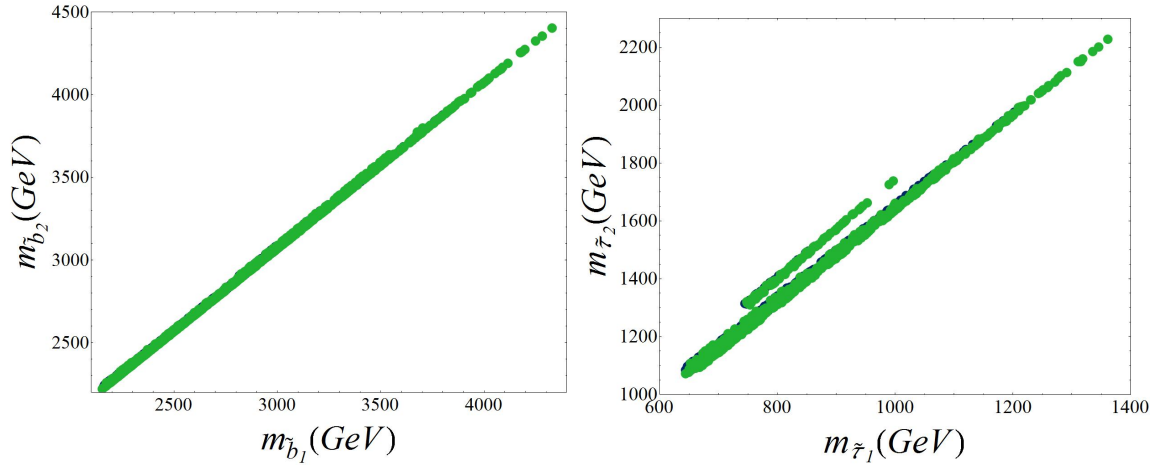

Figure 9.3. *Viable scenarios in the sbottom mass (left) and stau mass (right) planes for the OI4d5 model, with colours as in Fig. 9.1.*

scalar masses at the high scale and our boundary conditions are rather different than the cases studied previously. To understand the reason for this behavior, we consider once more the expression for $m^2_{\tilde{d}_R}(t)$ derived in Sec. 7.5.3. Here, it takes the form

$$m^2_{\tilde{d}_R}(t) = m^2_{3/2}\sin^2\theta + M^2_3(t)\left[0.78 + 0.002\,\rho_1^2\right], \tag{9.26}$$

where for the surviving points we have $\rho_1 \approx 1.18$ and $\sin^2\theta \approx 1$, yielding

$$m^2_{\tilde{d}_R}(t) \approx m^2_{3/2} + 0.78 M^2_3(t). \tag{9.27}$$

At the electroweak scale we have gluinos between 2.8 and 3.8 TeV whereas the gravitino

mass is smaller than 1.2 TeV (at the high scale), therefore $m_{3/2}^2/m_{\tilde{g}}^2 \lesssim 0.1$. If we rewrite eq. (9.28) as

$$m_{\tilde{d}_R}(t_{EW}) \approx \sqrt{0.78} m_{\tilde{g}} \sqrt{1 + 0.78 \frac{m_{3/2}^2}{m_{\tilde{g}}^2}}, \tag{9.28}$$

we can expand $m_{\tilde{d}_R}(t_{EW})$ in powers of $m_{3/2}^2/m_{\tilde{g}}^2$ obtaining

$$m_{\tilde{d}_R}(t_{EW}) \approx 0.9 m_{\tilde{g}} + O\left(m_{3/2}^2/m_{\tilde{g}}^2\right), \tag{9.29}$$

which is in good agreement with Fig. 9.4 and highlights the predictive power of the OI4d5 model.

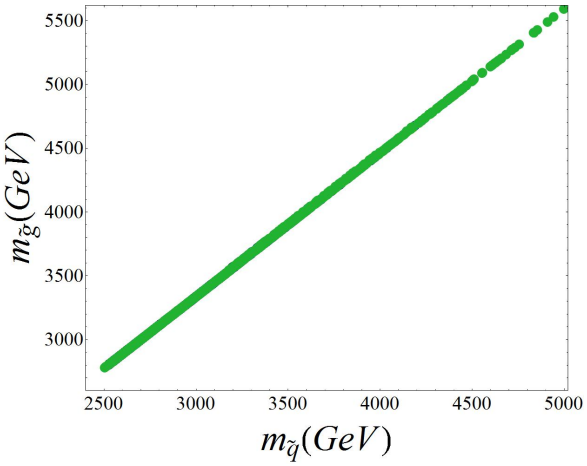

Figure 9.4. *The lightest squark mass and the gluino mass for the OI4d5 model with colours as in Fig. 9.1.*

The Yukawa unification conditions $R_{tb\tau}$ and $R_{b\tau}$ are shown in Fig. 9.5. We see that for the surviving solutions, it is difficult to achieve exact top-bottom-tau unification, with $R_{tb\tau}$ between 1.65 and 2, as expected for the $\tan\beta$ values encountered. However, bottom-tau unification deviates just 1% to 6% from the ratio $y_\tau/y_b = 1$, which differs from the results in chapter 8, where we were closer to the ratio $y_\tau/y_b = 3/2$ with an average deviation of about 10%.

The identity and masses of the LSP and NLSP are shown in Fig. 9.6, where we see that all our scenarios predict neutralino Dark Matter dominated by its $U(1)_Y$ component. The NLSP is always stau and its mass can be up to 30 GeV heavier than the LSP, favouring co-annihilation and reducing the relic density. Such small values for the stau mass, which is the lightest sfermion for the surviving points, are a direct consequence of the boundary conditions, where we always have $m_{-3} < m_{-2} < m_{-1}$ and not to heavy gravitinos. On the right panel we show the five surviving scenarios with the preferred relic density. It is

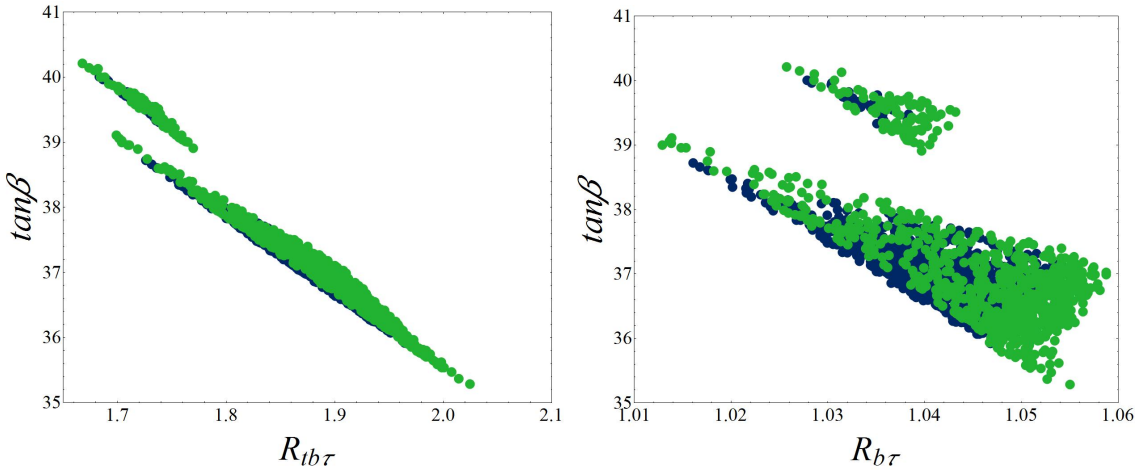

Figure 9.5. *Viable scenarios in the $R_{tb\tau} - \tan\beta$ (left) and $R_{b\tau} - \tan\beta$ (right) planes for the OI4d5 model, with colours as in Fig. 9.1.*

tantalizing to note that the OI4d5 model predicts solutions with neutralinos in the preferred relic abundance as light as 650 GeV, and staus equally light, which may be accessible to the 14 TeV LHC.

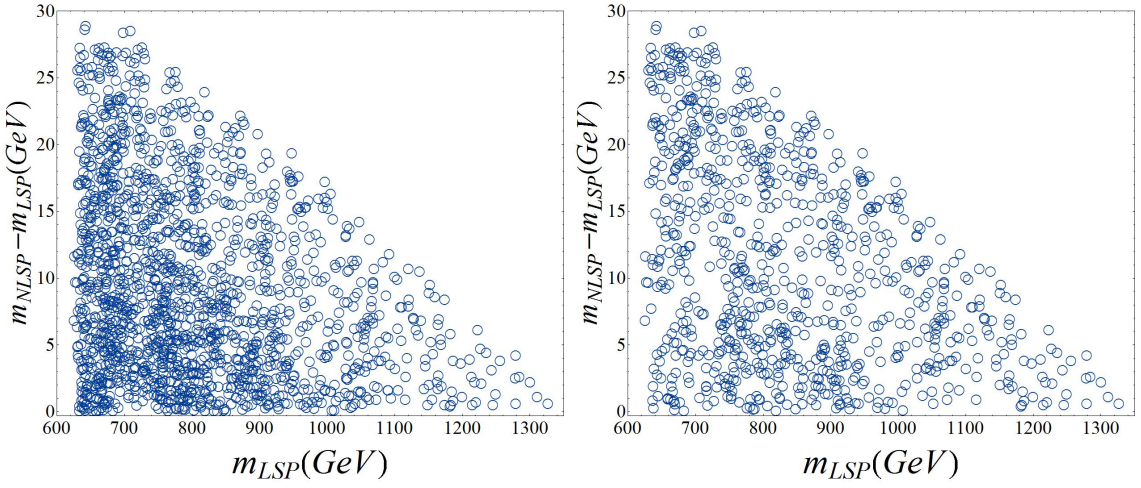

Figure 9.6. *Solutions in the plane of LSP mass vs. the NLSP-LSP mass splitting for the OI4d5 model. All the LSPs are bino dominated neutralinos with stau NLSP. The right panel only shows solutions with the preferred relic density.*

9.2.2. OI5d0 Model

We study now a scenario where the sum of the Higgs modular weights is $n_H + n_{\overline{H}} = -5$, which in terms of the MSSM Higgs doublets corresponds to $n_{H_u} = -2$ and $n_{H_d} = -3$, and where $\delta_{GS} = 0$.

The results obtained with respect to μ and $\tan\beta$, Fig. 9.7 (left), were quite similar to those obtained for the OI4d5 model. We also see that the preferred values of the goldstino angle lie within the bands $4.90 < \theta < 4.95$ and $4.20 < \theta < 4.25$, which indicates that the gaugino mass ratios are the same as for the OI4d5 model.

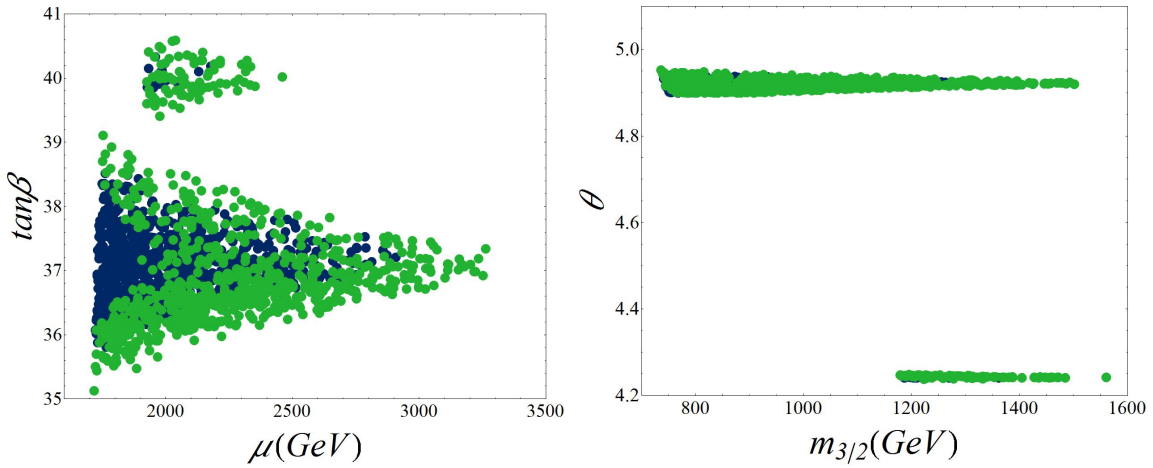

Figure 9.7. *Viable scenarios in the $\mu - \tan\beta$ (left) and $m_{3/2} - \theta$ (right) planes for the OI5d5 model. Blue points represent scenarios with a Dark Matter relic density below 2σ bounds, while green points have the preferred relic density.*

The third generation superpartners mass and Higgs mass planes are shown in Figs. 9.8 and 9.9, where we see no significant differences from the OI4d5 model.

The masses of the gluinos and lightest first and second generation squarks are shown in Fig. 9.10. We see once again the correlation noted in the previous discussion.

The Yukawa coupling ratios observed for the OI4d5 model are reinforced with the results obtained for the OI5d0 case. In particular, we highlight here the nearly exact bottom-tau unification of Yukawa couplings (1% to 6% deviation) as it is shown in Fig. 9.11.

Finally, the LSP mass and LSP-NLSP mass splitting is shown in Fig. 9.12. Without surprise we observe that all solutions consist of bino dominated neutralinos as LSPs, relying on almost degenerate stau NLSPs, in order to favour co-annihilation and produce an acceptable abundance of Dark Matter.

9.3. BIM O-II Orbifold

The final step of this study relies on the analysis of scenarios with moduli dominated supersymmetry breaking, where $\sin\theta$ is rather small. We therefore consider values of the goldstino angle close to zero as well as to π. We are also going to consider two example

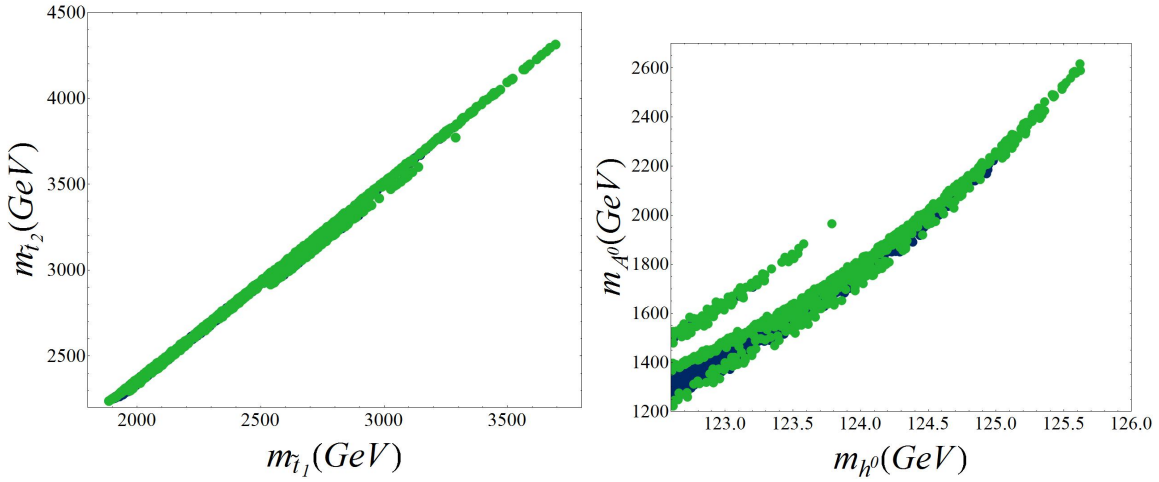

Figure 9.8. *Viable scenarios in the stop mass and lightest scalar - pseudoscalar mass planes for the OI5d5 model, with colours as in Fig. 9.7.*

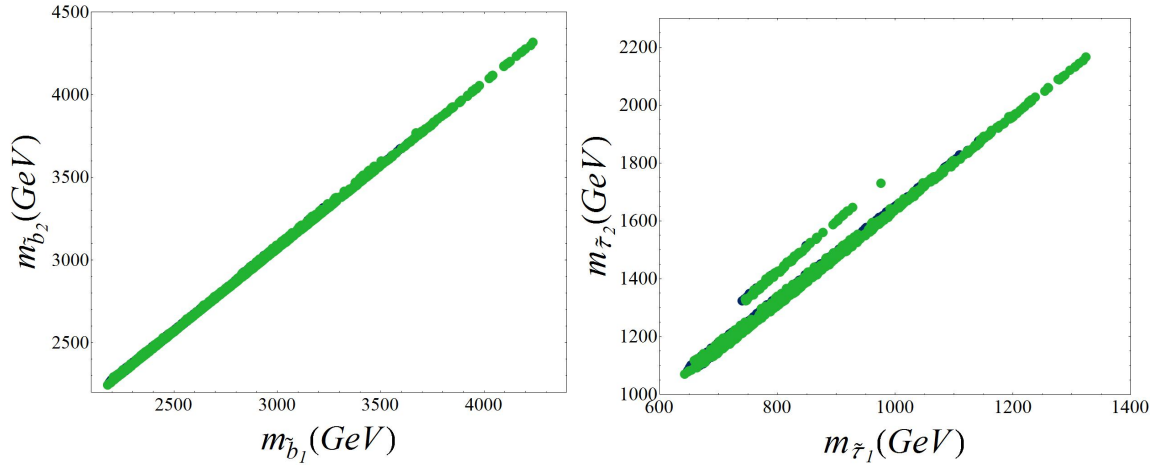

Figure 9.9. *Viable scenarios in the sbottom mass (left) and stau mass (right) planes for the OI5d5 model, with colours as in Fig. 9.7.*

models, one with $\delta_{GS} = -5$, where the gaugino masses reduce to the BIM O-II scenario discussed in chapter 7, and another one with $\delta_{GS} = -6$. We will denote these scenarios as OIId5 and OIId6 model respectively.

From the boundary conditions (9.18 - 9.22) we see that in the moduli dominated region, the gravitino can be significantly larger than the soft parameter. Before moving forward, we need to investigate what is the optimal range of values for θ and for $m_{3/2}$ in order to find physically viable solutions and avoid unnecessary computation. As for the dilaton dominated scenarios, the $m^2_{H_u}$ polynomial at the soft supersymmetry mass scale M_{soft}, is a function of the gravitino mass and the goldstino angle, $m^2_{H_u}(M_{soft}) = a_\theta m^2_{3/2}$. In Fig. 9.13 we show the dependency of $m^2_{H_u}$ in $m_{3/2}$ and θ for $\delta_{GS} = -6$. We varied $m_{3/2}$ between 0

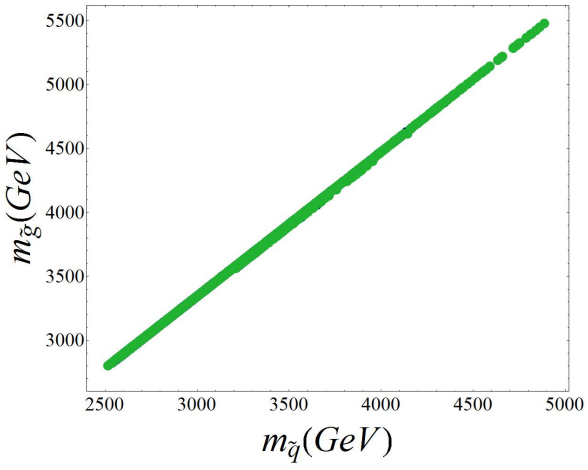

Figure 9.10. *The lightest squark mass and the gluino mass for the OI4d5 model with colours as in Fig. 9.1.*

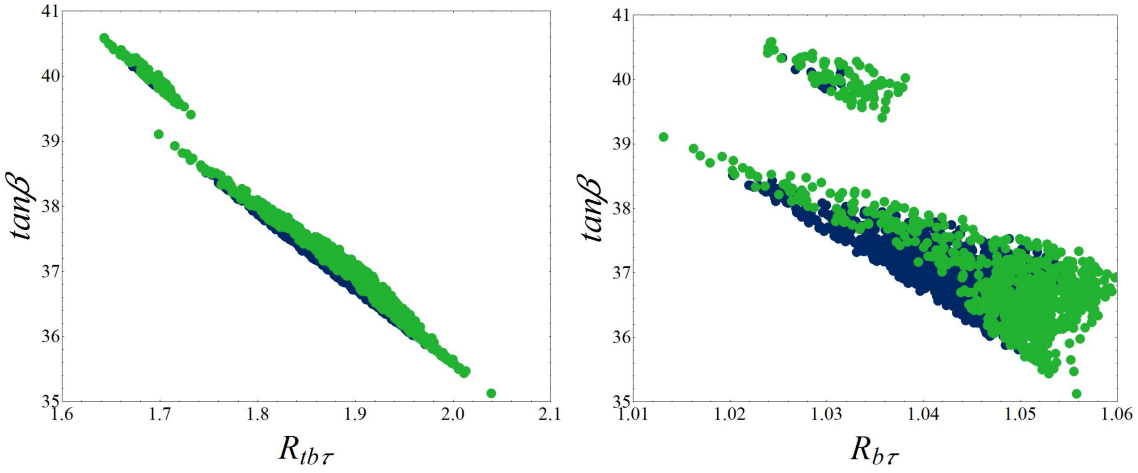

Figure 9.11. *Viable scenarios in the $R_{tb\tau} - \tan\beta$ (left) and $R_{b\tau} - \tan\beta$ (right) planes for the OI5d0 model, with colours as in Fig. 9.1.*

and 80 TeV for four distinct values of the golsdstino angle $\theta = 0$ (top left), $\theta = 0.008$ (top right), $\theta = 0.009$ (bottom left) and $\theta = 0.015$ (bottom right). We see that for the limit $\theta = 0$ the a_θ coefficient quickly becomes positive for $m_{3/2} \approx 7$ TeV with $\left|m_{H_u}\right| \approx 60$ GeV, which is not phenomenologically viable. We have also discussed above that solutions for which the gluino mass is above the LHC limit requires a gravitino mass larger than 126 TeV, which is undoubtedly outside the region of REWSB, with $m^2_{H_u}$ positive and very large. This is unfortunate since the fine-tuning in the goldstino angle is always found to be quite large (as it is for OI scenarios), and we cannot set it to *zero* in order to control Δ_θ, as we did for scalar masses and trilinear couplings in chapters 7 and 8. However, one could argue that increasing the absolute value of δ_{GS}, the difference in the scales of the gravitino and soft masses parameters is attenuated, nevertheless, δ_{GS} is expected be of the same order of the coefficients inside the curved brackets of eqs. (9.20 - 9.22), therefore, natural choices for

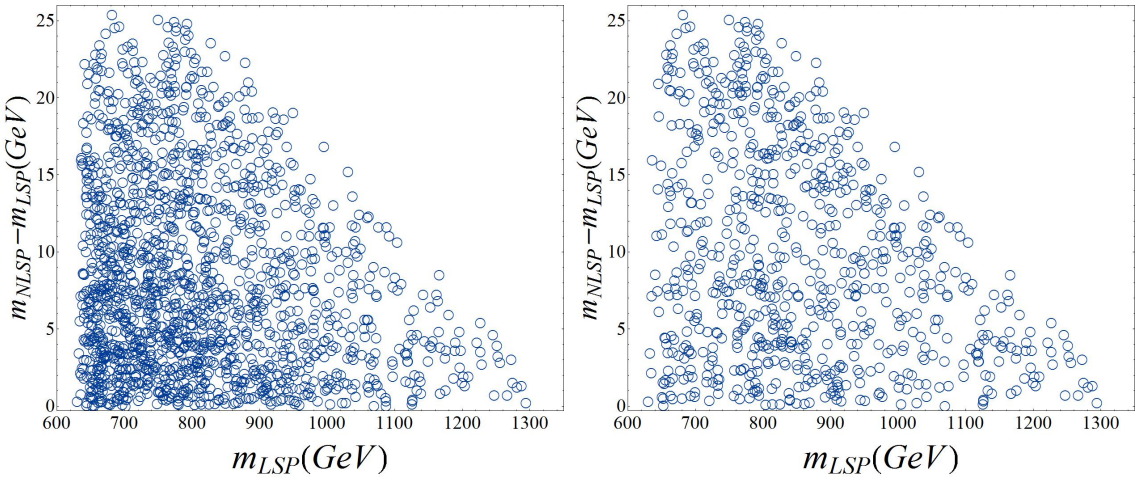

Figure 9.12. *Solutions in the plane of LSP mass vs. the NLSP-LSP mass splitting for the OI5d0 model. All the LSPs are bino dominated neutralinos with stau NLSP. The right panel only shows solutions with the preferred relic density.*

δ_{GS}, are confined approximately to the window $-10 \leq \delta_{GS} \leq 0$. In figure 9.14 we see that for

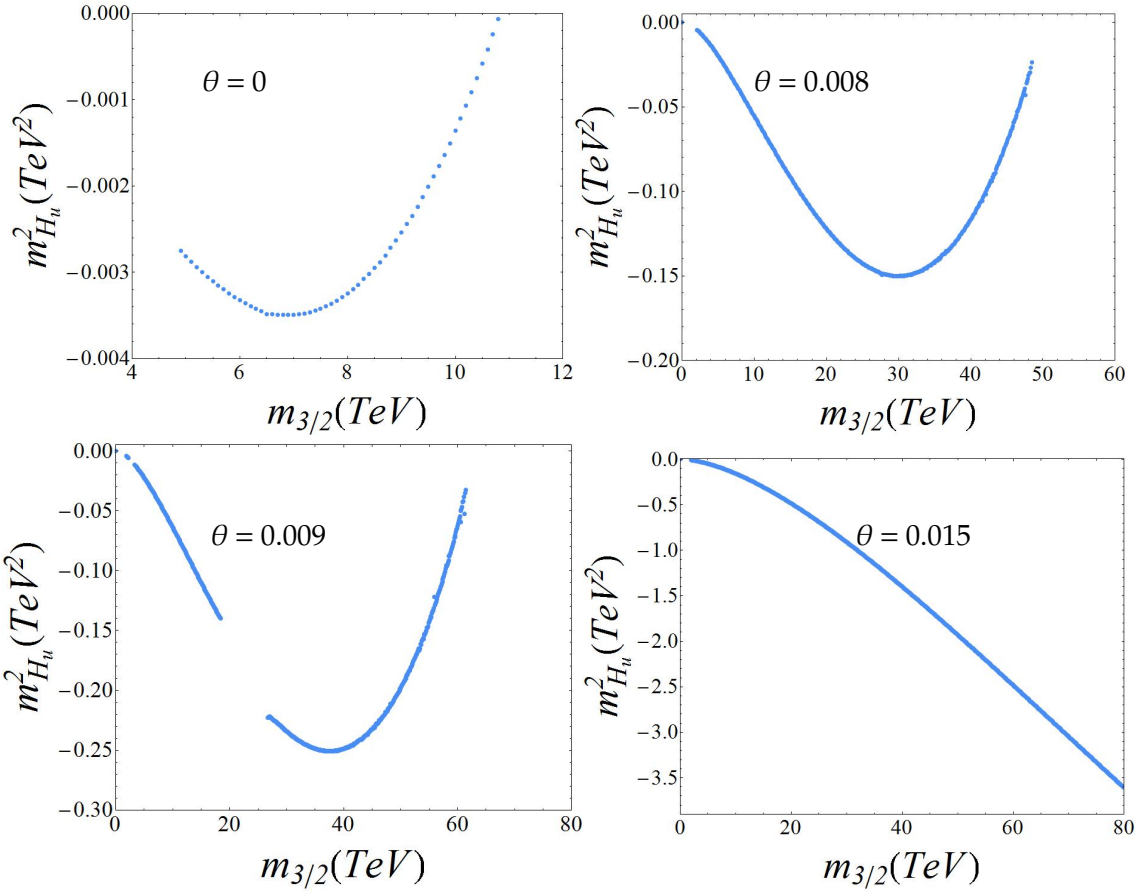

Figure 9.13. *The values of $m^2_{H_u}$ as $m_{3/2}$ and θ are varied for fixed $\delta_{GS} = -6$.*

$\delta_{GS} = -10$, the potentially physically viable solutions are still far away from $m_{3/2} = 126$ TeV, which reinforces the argument that the limit $\sin\theta = 0$ does not produce acceptable solutions. We also note that small variations in the goldstino angle yield largely distinct results, which

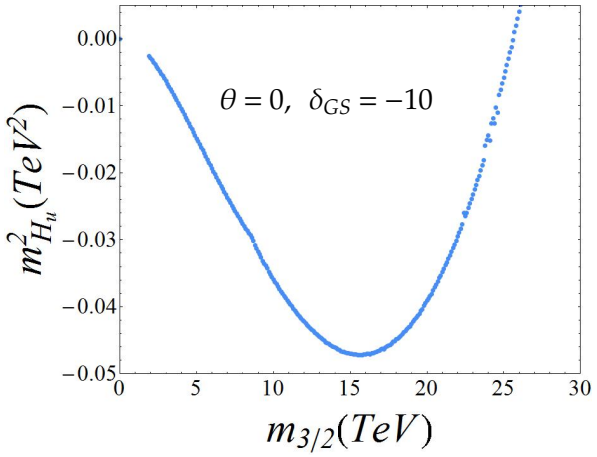

Figure 9.14. *The values of $m^2_{H_u}$ as $m_{3/2}$ is varied for fixed $\delta_{GS} = -10$ and $\theta = 0$.*

implicitly suggests that the fine-tuning in θ is quite severe for the $O-II$ orbifold. Indeed, when we calculate Δ_θ for viable scenarios, we verify that it is of the order of 10^3.

However, we don't really need to consider fine-tuning with respect to θ, since it should be fixed by String Theory. Therefore, we do not consider such scenarios as problematic and do not throw away models with large Δ_θ. The same reasoning can be used for $m_{3/2}$, but here we found that it is possible to find regions in the parameter space where $m^2_{H_u}$ is insensitive to fluctuations in $m_{3/2}$, similarly to what we have observed before for $M_{1/2}$.

We will therefore randomly generate points in two separate regions for the goldstino angle, one with θ between 0.009 and 0.012, and another with $0.009 + \pi < \theta < 0.012 + \pi$. We also allow the gravitino mass to vary in the interval $40 < m_{3/2} < 100$ TeV and, as usual, we let $\tan\beta$ to lie in the range $1 < \tan\beta < 60$. For the O-II orbifold, with one single scalar mass and a universal trilinear coupling, we need to guarantee that $|a_0/m_0| \lesssim 3$. Fortunately this is not an issue for the O-II scenarios that we will consider. Indeed, from the boundary conditions (9.18) and (9.19), we see that

$$\frac{a_0}{m_0} = \frac{-\sqrt{3}\sin\theta}{\sqrt{-\delta_{GS}\times 10^{-3}}}, \tag{9.30}$$

where for $\delta_{GS} = -6, -5$ we have respectively $0.2 \lesssim |a_0/m_0| \lesssim 0.26$ and $0.22 \lesssim |a_0/m_0| \lesssim 0.29$ for the choice of θ above.

9.3.1. OIId6 Model

We first consider a scenario based on the BIM O-II orbifold with $\delta_{GS} = -6$. Out of 531,839 initial scenarios, 5603 ($\sim 1\%$) survived the low scale and stability constraints, and 3162 predict the preferred relic density. All the points generated have $\Delta_{m_{3/2}} < 100$.

We show in Fig. 9.15 (top) the $m_{3/2} - \theta$ plane for the goldstino angle close to zero (left), which generate positive gaugino masses, and close to π (right), where the masses of the gaugino fermions are negative. We see that as we approach the bound $\theta = 0.009$ (and $\theta = 0.009 + \pi$), the density of viable scenarios is greatly reduced. However, the densely populated $\theta \to 0.012$ region, suggests that beyond this bound, further viable scenarios exist. In the $m_h - m_{3/2}$ plane, we see that lower Higgs mass bound forces a lower limit for the gravitino mass of about 54 TeV for the OIId6 model.

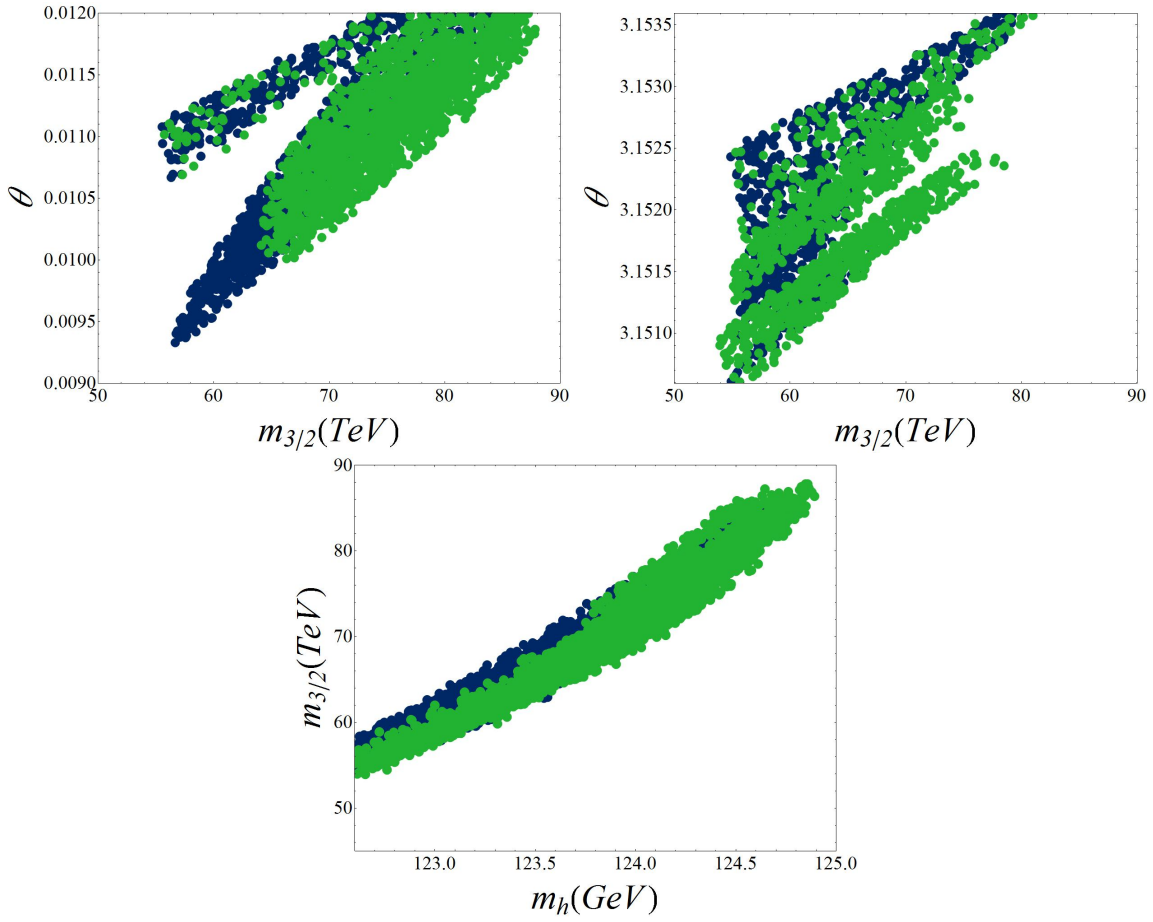

Figure 9.15. *Viable scenarios in the $m_{3/2} - \theta$ (top) and $m_h - m_{3/2}$ (bottom) planes for the OIId6 model. Blue points represent scenarios with a Dark Matter relic density below 2σ bounds, while green points have the preferred relic density.*

In Fig. 9.16 (left) we show the $\mu - \tan\beta$ plane, from where we see a preference for moderate to very large values of $\tan\beta$, in a window that goes from 20 up to 55. The values of μ are now similar to the $SU(5)$ and $SO(10)$ results, lying in the range $650 - 1200$ GeV. We observe however a large distribution of points with the preferred relic density occupying almost the entire range of μ, and a band with $\tan\beta$ roughly between 45 and 55 with $\Delta_{m_{3/2}}$ below 10. The ratio of the gaugino masses obtained in this scenario is shown in the right pane of the same figure, and we see that the preferred region for low-fine tuning (disregarding μ and θ) is below the $SU(5)$ and $SO(10)$ ellipse.

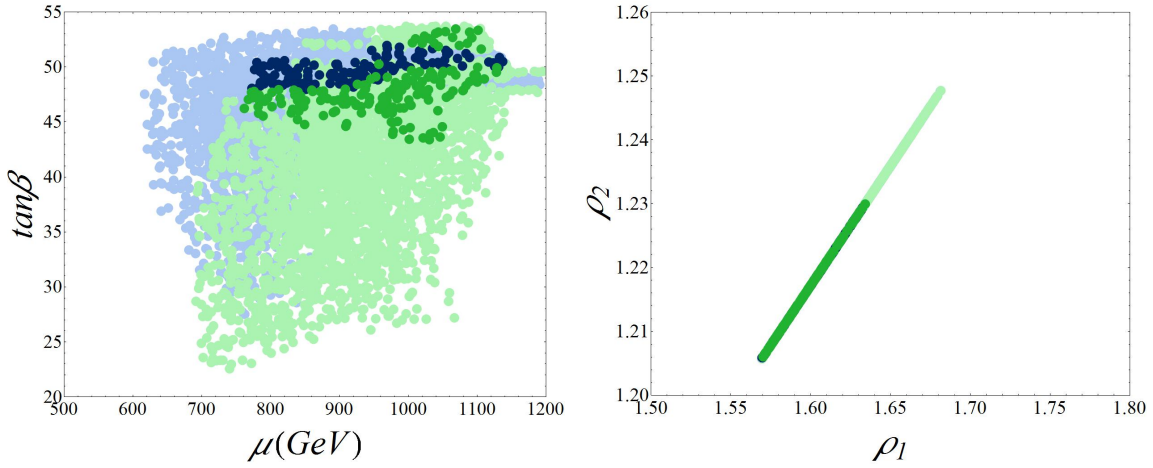

Figure 9.16. *Viable scenarios in the $\mu - \tan\beta$ and $\rho_1 - \rho_2$ planes for the OIId6 model. Points with the preferred Dark Matter relic density are shown in green, while those with a relic density below the bounds are in blue. Darker and lighter shades denote the fine-tuning: darker shades have fine-tuning $\Delta_{m_{3/2}} < 10$ while lighter shades have $10 < \Delta_{m_{3/2}} < 100$.*

We show in Figs. 9.17 and 9.18 the Higgs masses and the third generation sfremion masses. In comparison to the BIM O-I scenarios studied above, we have in general a heavier supersymmetric spectrum and, in particular, significantly heavier staus. However it is interesting to note that if we insist on low fine-tuned gravitino mass, the pseudoscalar Higgs mass is restricted to the band $1 - 3$ TeV, which corresponds approximately to the bottom half of its mass distribution. We also find solutions predicting the preferred Dark Matter abundance with $m_A \approx 800$ GeV, which may be accessible to the 14 TeV LHC (though still challenging). Although the Higgs mass has an upper limit of 124.9 GeV, it is possible to increase its value if we expand our scan range as we will see below.

The gluino and lightest first and second generation squark mass, Fig. 9.19, are no longer correlated as in the scenarios so far analyzed. The horizontal width of the data distribution can be as large as 600 GeV whereas the vertical one is roughly 300 GeV. It is possible to explain this behavior using the previous analytical expressions for $m_{\tilde{d}_R}$, where for the OIId6

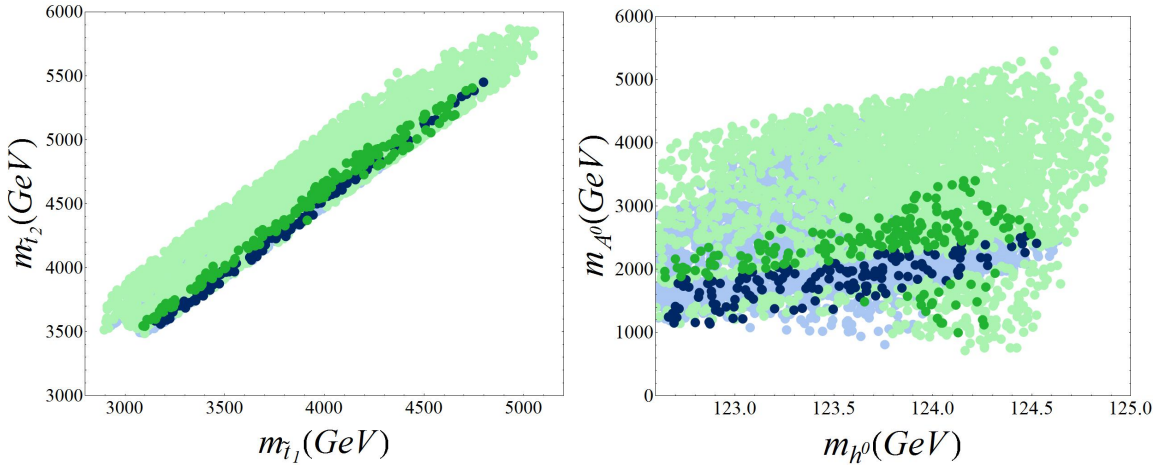

Figure 9.17. *Viable scenarios in the stop mass and lightest scalar - pseudoscalar mass planes for the OIId6 model, with colours as in Fig. 9.16.*

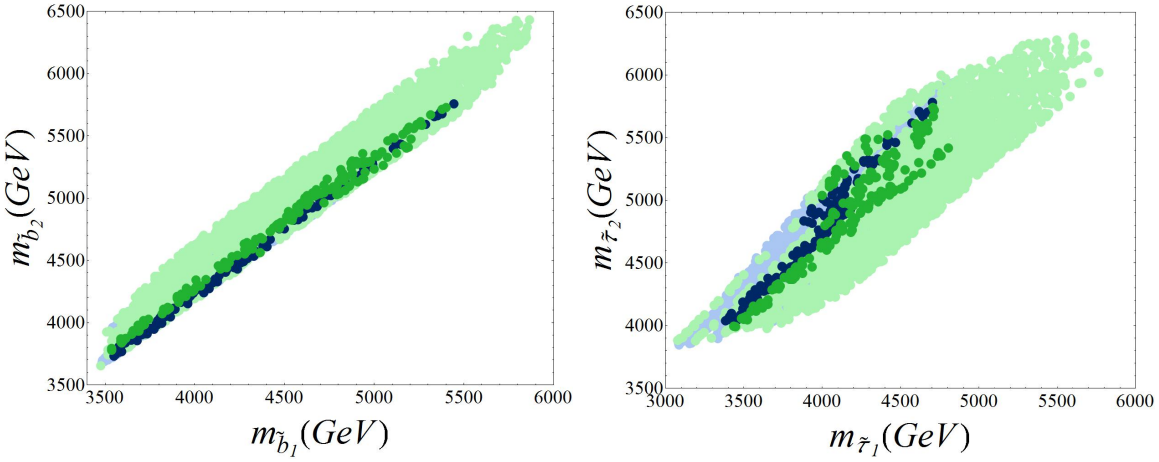

Figure 9.18. *Viable scenarios in the sbottom mass (left) and stau mass (right) planes for the OIId6 model, with colours as in Fig. 9.16.*

model it takes the form

$$m^2_{\tilde{d}_R}(t) = 6\times 10^{-3} m^2_{3/2} + M^2_3(t)\left[0.78 + 0.002\,\rho_1^2\right]. \tag{9.31}$$

Since all values of ρ_1 are rather small, we can neglect the second term inside the square brackets and rewrite eq. (9.31) as

$$m_{\tilde{d}_R}(t_{EW}) \approx 0.08 m_{3/2}\sqrt{1 + 130\frac{m^2_{\tilde{g}}}{m^2_{3/2}}}. \tag{9.32}$$

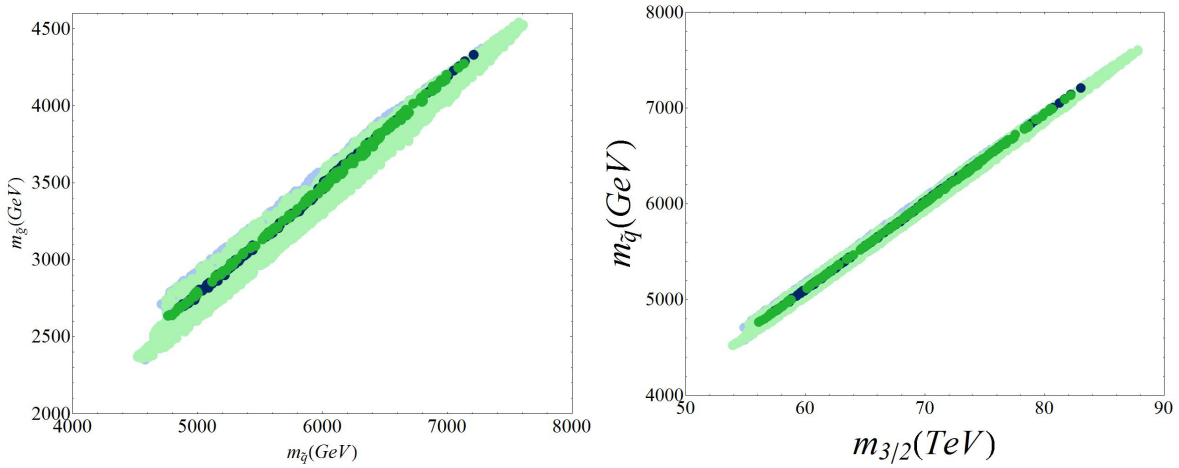

Figure 9.19. *Viable scenarios in the lightest squark - gluino mass plane (left) and gravitino - lightest squark mass plane (rigt) for the OIId6 model, with colours as in Fig. 9.16.*

We know that $m_{\tilde{g}} \ll m_{3/2}$, therefore we can expand eq. (9.32) in powers of $m_{\tilde{g}}^2/m_{3/2}^2$, yielding

$$m_{\tilde{d}_R}(t_{EW}) \approx 0.08 m_{3/2} + 5.2 \frac{m_{\tilde{g}}^2}{m_{3/2}} + O\left(m_{\tilde{g}}^4/m_{3/2}^4\right). \tag{9.33}$$

From eq. (9.33), we see that a relation between the lightest squark and gluino masses is also strongly dependent on the gravitino mass, though a weaker correlation between squark and gluino mass remains. Although we have lost predictive power for this sector, we have gluino masses lighter than any of the sfermions of the three generations, which is a consequence of having gaugino masses lighter than the scalar masses at the GUT scale. We also see that the OIId6 model predicts gluinos as light as 2.5 TeV, which are accessible to the 14 TeV LHC.

We show in Fig. 9.22 the Yukawa unification conditions $R_{tb\tau}$ (left) and $R_{b\tau}$ (right). For the top-bottom-tau Yukawa coupling ratios, we obtain values almost as low as 1.2, which corresponds to a 20% deviation from exact unification. Such results were obtained for those scenarios with goldstino angles close to π (lower branch). For the case of the bottom-tau ratios (right pane) we have two distinct regions, the right branch, where $\theta \sim 0$ and the left branch, for which $\theta \sim \pi$. While for the former case, the bottom-tau Yukawa ratios lie between 1.32 and 1.39, which corresponds to a 12% to 7% deviation from the $y_\tau/y_b = 3/2$ ratio, the latter one predicts ratios as low as 1.16, which are closer to $y_\tau/y_b = 1$.

The identity and masses of the LSP and NLSP are shown in Fig. 9.21. The OIId6 model predicts two possibilities for Dark Matter candidate, either a bino dominated neutralino (blue squares), or a neutralino dominated by its higgsino component (red squares). Furthermore, the NLSP is always a higgsino dominated chargino. We observe a cloud of scattered blue points with an approximately triangular shape with LSP-NLSP mass splittings roughly

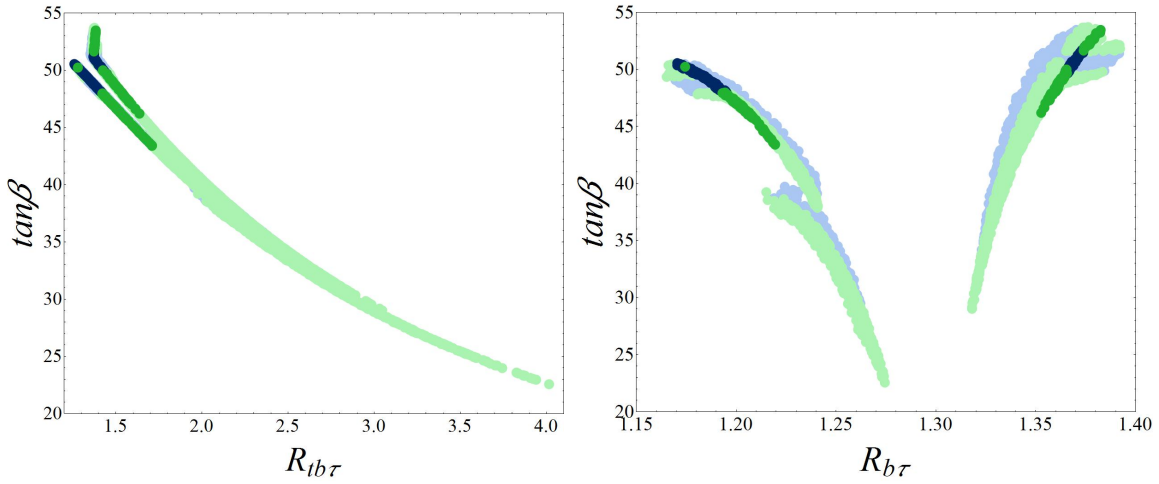

Figure 9.20. *Viable scenarios in the $R_{tb\tau} - \tan\beta$ (left) and $R_{b\tau} - \tan\beta$ (right) planes for the OIId6 model, with colours as in Fig. 9.16.*

between 30 and 110 GeV. For such scenarios, the lightest neutralino is largely bino-like, and relies on a heavy Higgs boson at twice its mass in order to provide resonant decay and reduce the relic density. For the denser region below, we find neutralinos with comparable bino and higgsino components, which favours neutralino-chargino co-annihilation even when the dominant contribution arises from the $U(1)_Y$ gauginos. This is also the reason why we find higgsino neutralinos with the preferred relic density and mass as low as 700 GeV, when before we did not find any of such solutions below 900 GeV. In fact, and as a result of comparable μ and M_1, the comparable bino and higgsino components yield neutralino-chargino pairings not too degenerate as if it was purely higgsino. This favours moderate co-annihilation in order to produce the preferred relic density instead of to little Dark Matter abundance.

As we have pointed out above, if we increase the range of θ and $m_{3/2}$, we may be able to find scenarios with larger Higgs mass. We have therefore performed a scan with θ between 0.012 and 0.013 and $m_{3/2}$ within 80 to 100 TeV. We indeed observe an increase of the Higgs mass up to 125.4 GeV. However, the allowed region tends to get narrower for larger values of $m_{3/2}$, which is due to the reasons discussed in the beginning of the section. The corollary of a heavier Higgs mass is that the supersymmetric spectrum becomes larger. We show the example of the gluino and lightest first and second generation squarks in Fig. 9.23, where we observe masses between 4 and 5.5 TeV for gluinos, and roughly between 7 and 9 TeV for squarks. Such range of masses, and in particular the masses of the squarks, are not expected to be observed at the 14 TeV LHC, and may only be accessible to an energy upgraded super-LHC. The masses of the light components of the third generation sfermions are also within a window that goes from 4 to 7 TeV.

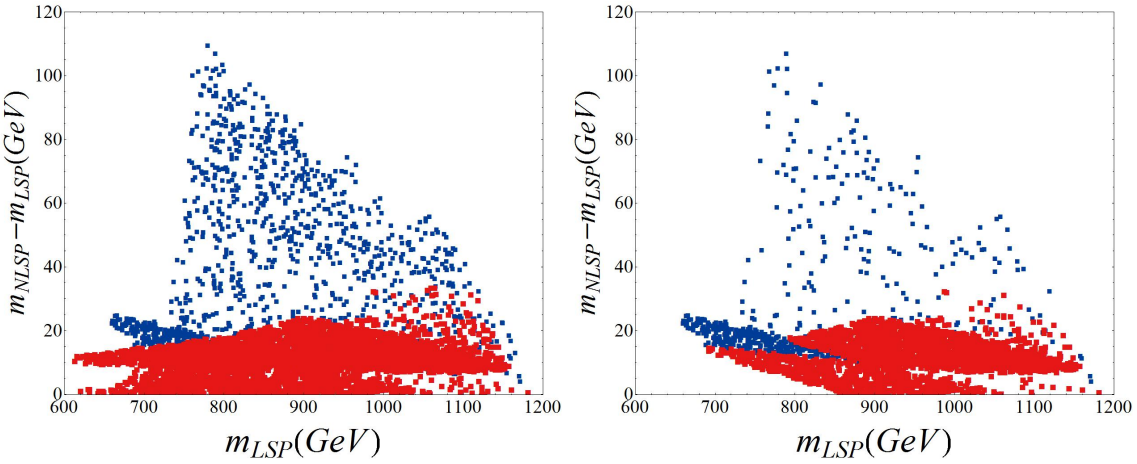

Figure 9.21. *Solutions in the plane of LSP mass vs. the NLSP-LSP mass splitting for the OIId6 model. The colour indicates the flavour of LSP, with red and blue denoting higgsino and bino dominated Dark Matter respectively. The shape indicates the flavour of NLSP with squares denoting chargino NLSP. The right panel only shows solutions with the preferred relic density.*

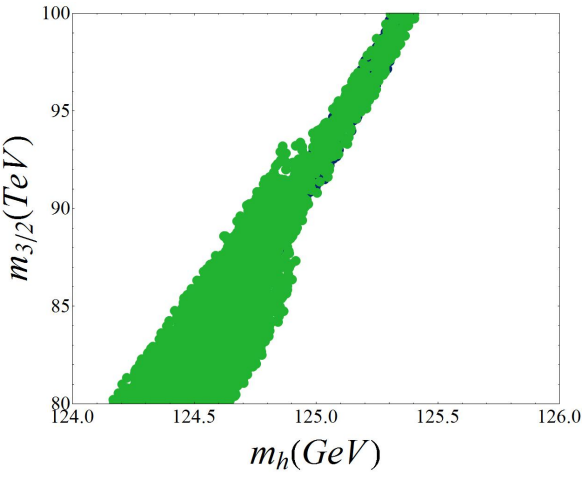

Figure 9.22. *Viable scenarios in the $m_h - m_{3/2}$ plane for the OIId6 model with extend range of θ and $m_{3/2}$, with colours as in Fig. 9.16.*

We show in Fig. 9.24 (top) that as the Higgs mass becomes larger, the distribution of viable scenarios reveals a trend to get confined to a narrow mass band of the heavy Higgs bosons, with $2 \leq m_A \leq 3$ TeV. Equivalently, the corresponding $\tan\beta$ exhibit a preference for very large values around 50. Although the bino component is still important, the LSP is now mostly higgsino accompanied by chargino NLSP, with masses in a window between 1 and 1.5 TeV (Fig. 9.24 bottom).

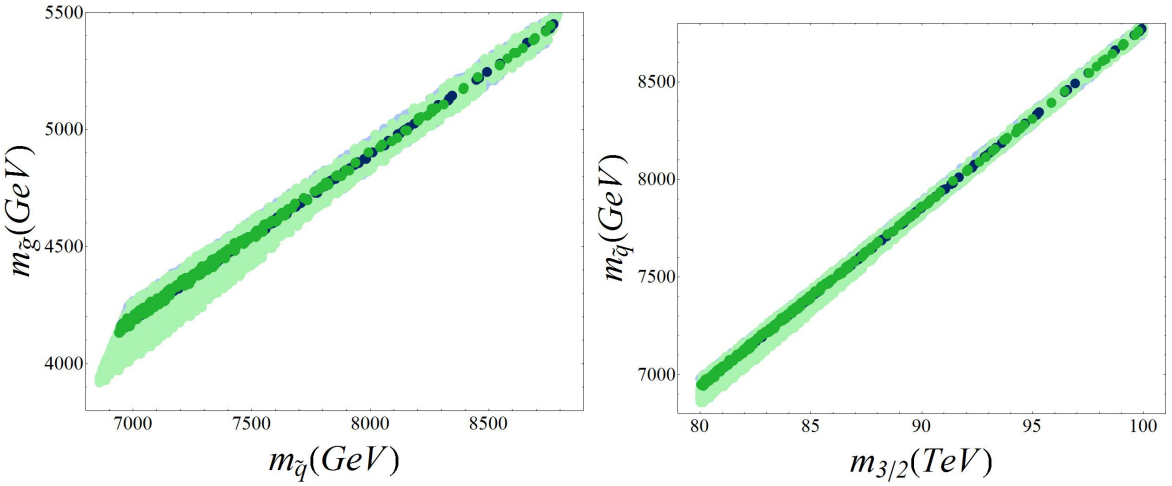

Figure 9.23. *Viable scenarios in the lightest squark - gluino mass plane (left) and gravitino - lightest squark mass plane (right) for the OIId6 model in an extend range of θ and $m_{3/2}$, with colours as in Fig. 9.16.*

9.3.2. OIId5 Model

The last scenario that we study is a BIM O-II orbifold with $\delta_{GS} = -5$. We allow the same range for θ and for $m_{3/2}$ to generate 681,638 initial scenarios. After applying the probability and stability constraints, 5671 ($\sim 0.8\%$) scenarios remained, of which 3383 have the preferred relic density.

We show in Fig. 9.25 (top) the $m_{3/2} - \theta$ plane for goldstino angles close to zero (left pane), and close to π (right pane). The results are very similar to those of the OIId6 model, but now we note that for the same interval of θ, the values of $m_{3/2}$ that generate viable scenarios are larger. The lower Higgs mass bound forces a lower limit for the gravitino mass in the OIId5 model of about 60 TeV.

The allowed scenarios in the $\mu - \tan\beta$ and $\rho_1 - \rho_2$ planes, Fig. 9.26 left and right respectively, are again very similar. The values of μ obtained are identical as for the OIId6 model but now we observe a larger interval of $\tan\beta$, from 38 to 53, where we find solutions with low fine-tuning in $m_{3/2}$.

The supersymmetric spectrum, and in partiular the masses of the squarks of the three generations and of the gluinos, is slightly heavier for its upper bound as it can be attested from Figs. 9.27, 9.28 and 9.29. The reason for this is the larger range of $m_{3/2}$ discussed above, which contributes to scalar and gaugino masses approximately 10% heavier at the GUT sale, when $m_{3/2}$ approaches 100 TeV. The contribution of M_3 makes it more evident for fields which are charged under $SU(3)_C$. The solutions with $\Delta_{m_{3/2}} < 10$ spread over a larger region of the parameter space in comparison to the OIId6 model.

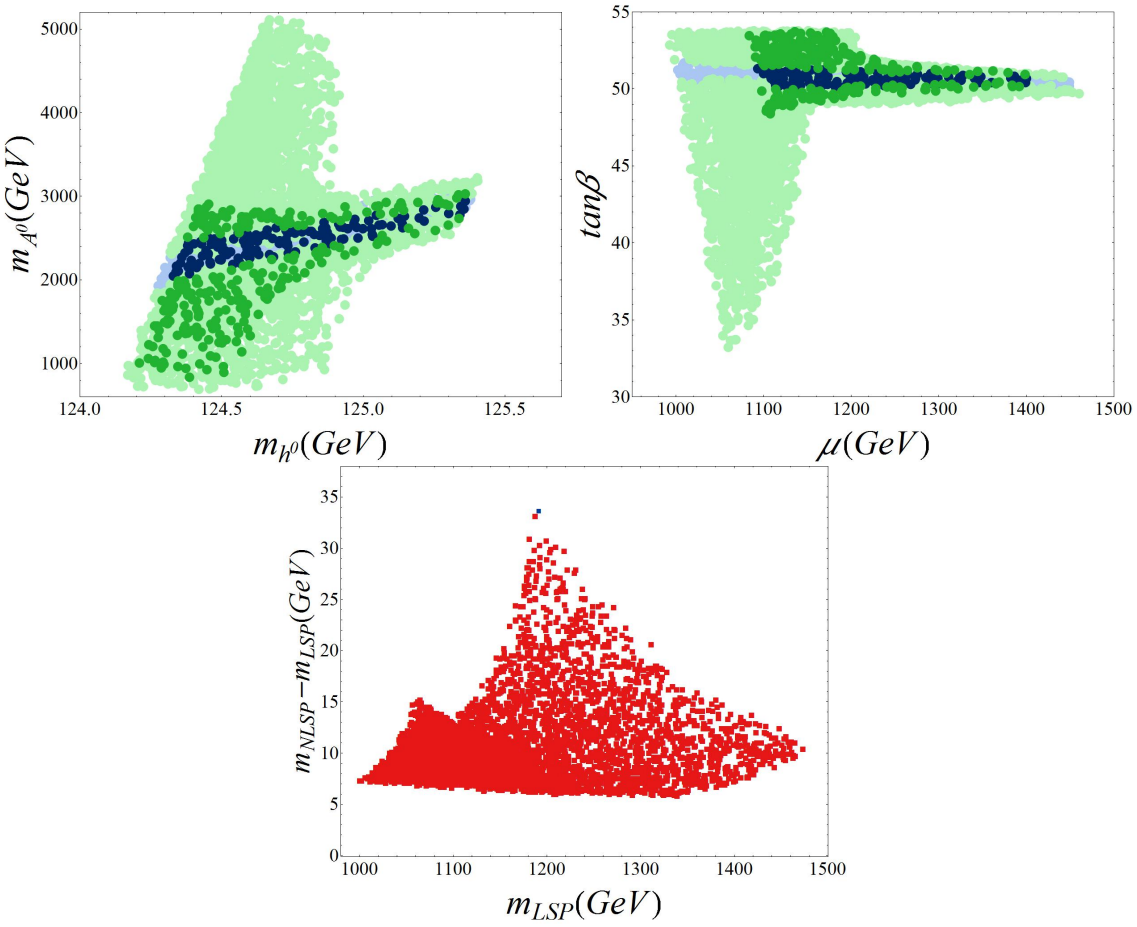

Figure 9.24. *Viable scenarios in the stop mass and lightest scalar - pseudoscalar (top left) mass and $\mu - \tan\beta$ (top right) planes and solutions in the plane of LSP mass vs. the NLSP-LSP mass splitting (bottom) for the OIId6 model. For the top planes, colours are as in Fig. 9.16 whereas for the bottom one it is as in Fig. 9.21.*

The ratios among the Yukawa couplings, Fig. 9.30, do not suffer any perceptible alteration, and the observations of subsec. 9.3.1 remain valid for the OIId5 model.

We show in Fig. 9.31 the identity and masses of the LSP and NLSP. Once again, due to μ and M_1 being comparable, we have neutralinos with comparable bino and higgsino components yielding equivalent results.

We have also not found any solution with a Higgs mass above 125 GeV for the OIId5 model with the initial range that we set for the gravitino mass and the goldstino angle. We will now study the effect of increasing θ to the range 0.012 to 0.013, as well as allowing $m_{3/2}$ to vary between 110 and 130 TeV. The results obtained in $m_h - m_{3/2}$ plane are shown in Fig. 9.32, where we see that a larger gravitino mass significantly helps obtain the correct Higgs mass. However, we note that the viable solutions become a rather sparse. Indeed, out of 426,957

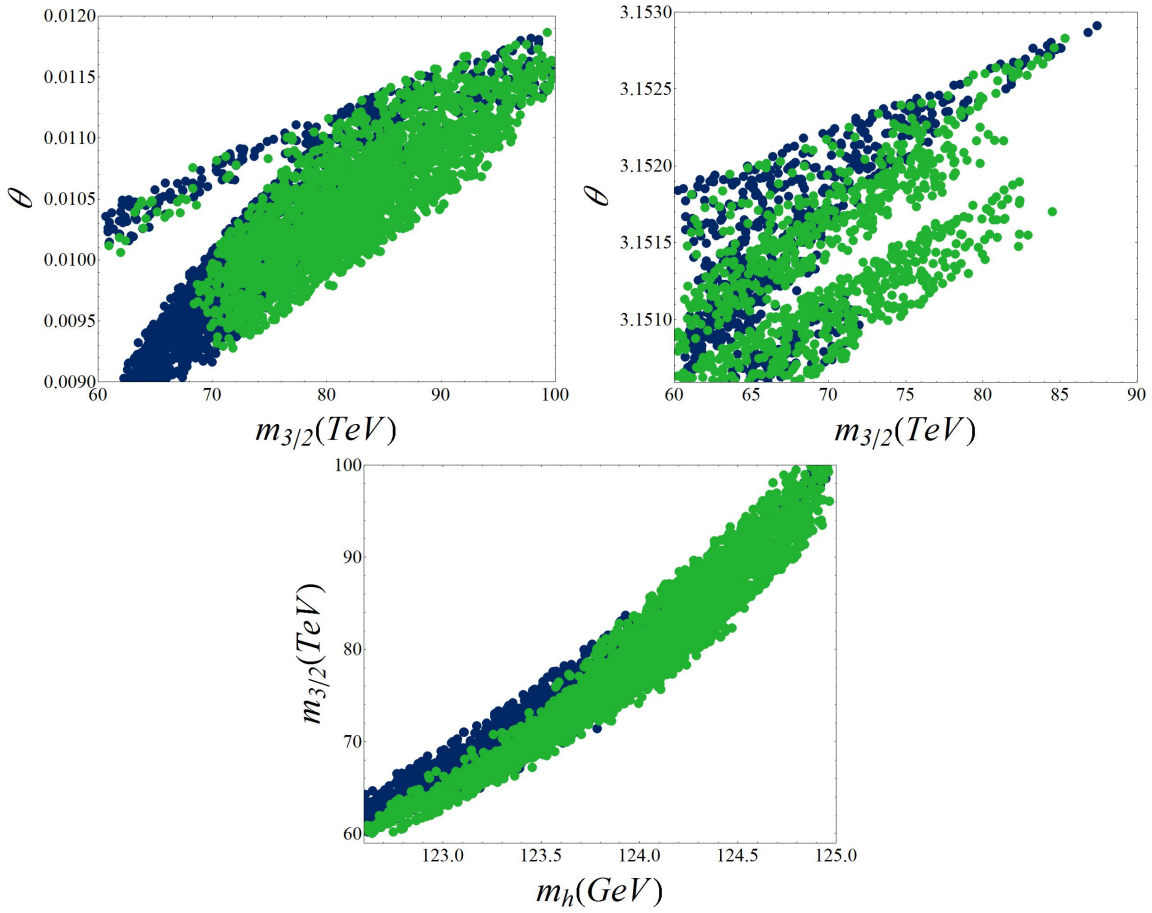

Figure 9.25. *Viable scenarios in the $m_{3/2} - \theta$ (top) and $m_h - m_{3/2}$ (bottom) planes for the OIId5 model. Blue points represent scenarios with a Dark Matter relic density below 2σ bounds, while green points have the preferred relic density.*

initial scenarios only 387 (0.09%) survived the probability and stability constraints.

Although this region is in good agreement with the Higgs mass, the supersymmetric spectrum becomes very heavy with first and second generation squark masses close to 10 TeV and gluinos within 5.4 and 6.7 TeV as in Fig. 9.33. Unfortunately, these scenarios are well beyond the 14 TeV LHC reach. However, in the right panel, we observe a good correlation between the squark mass and the gravitino mass. Indeed, the leading term in eq. (9.33), i.e. $m_{\tilde{q}} \approx 0.08 m_{3/2}$, predicts 125 TeV gravitinos for squarks with a mass of 10 TeV, which agrees with results obtained.

In Fig. 9.34 (top) we show the lightest scalar - pseudoscalar mass (left) and $\mu - \tan\beta$ planes (right) for the 387 solutions generated, and below the same points in the LSP - NLSP mass plane. Despite a very large mass spectrum for the squarks and sleptons, the heavy Higgs partners as well as the lighter neutralinos and charginos have moderately masses.

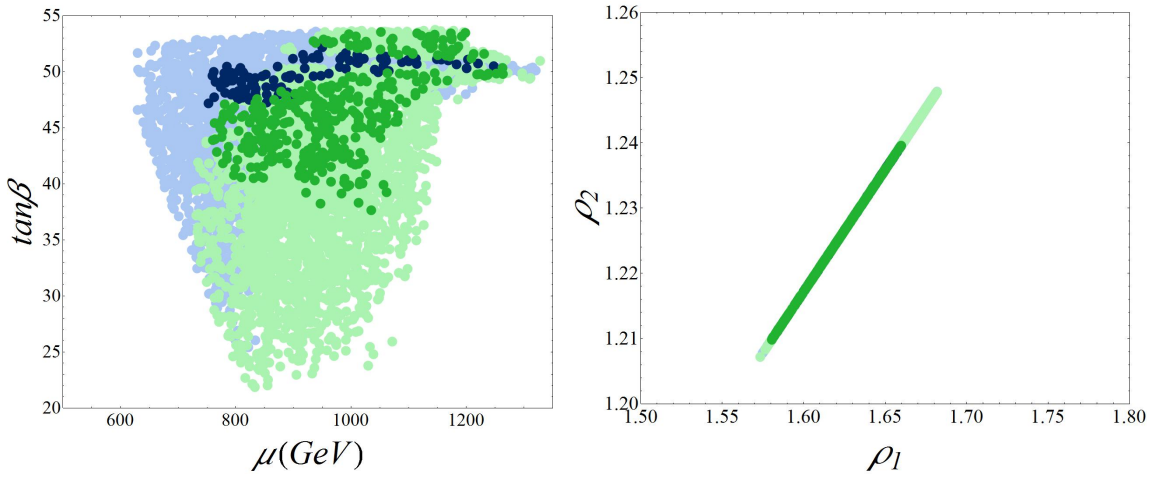

Figure 9.26. *Viable scenarios in the $\mu - \tan\beta$ and $\rho_1 - \rho_2$ planes for the OIId5 model. Points with the preferred Dark Matter relic density are shown in green, while those with a relic density below the bounds are in blue. Darker and lighter shades denote the fine-tuning: darker shades have fine-tuning $\Delta_{m_{3/2}} < 10$ while lighter shades have $10 < \Delta_{m_{3/2}} < 100$.*

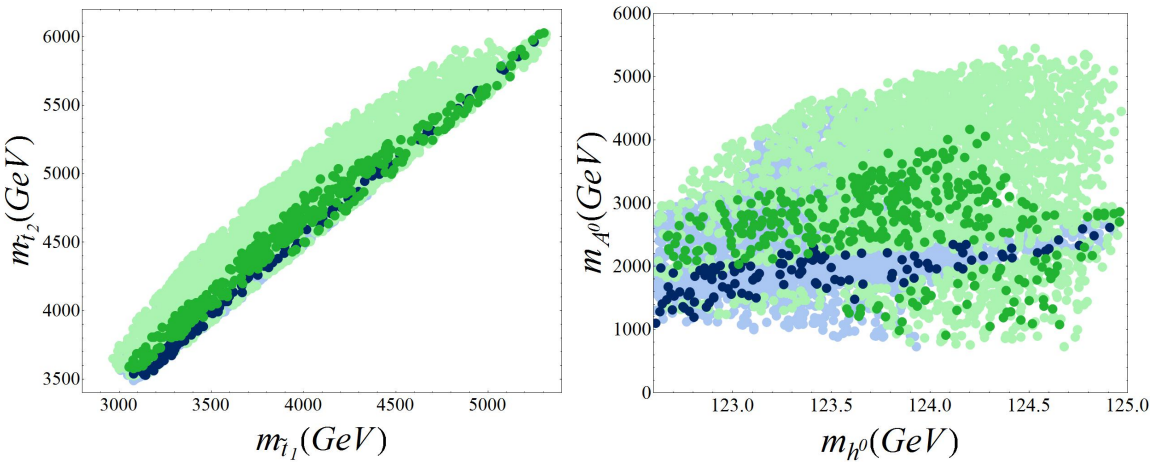

Figure 9.27. *Viable scenarios in the stop mass and lightest scalar - pseudoscalar mass planes for the OIId5 model, with colours as in Fig. 9.26.*

Note that all the solutions are restricted to $\tan\beta \approx 50 - 51$ which predicts $R_{tb\tau} \approx 1.36 - 1.42$ and $R_{b\tau} \approx 1.36 - 1.37$.

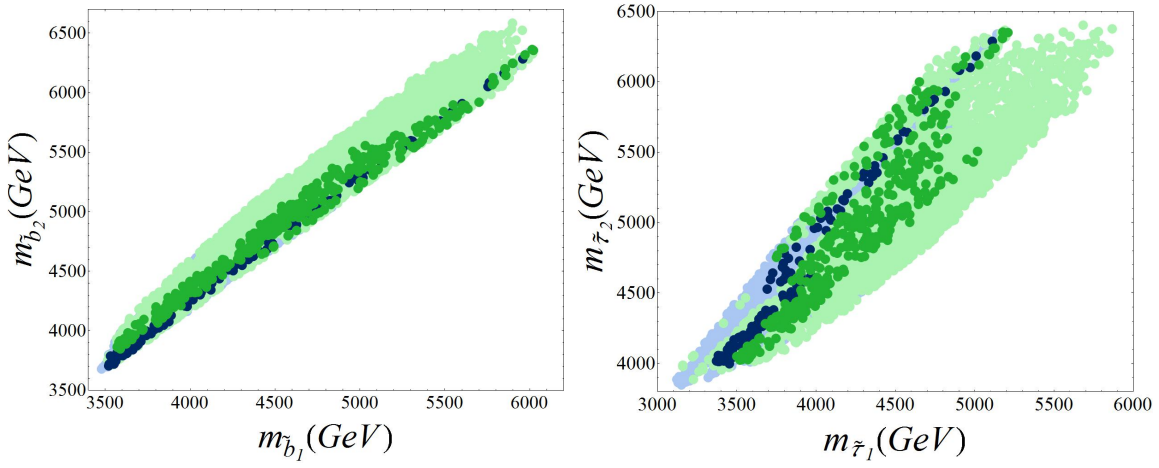

Figure 9.28. *Viable scenarios in the sbottom mass (left) and stau mass (right) planes for the OIId5 model, with colours as in Fig. 9.26.*

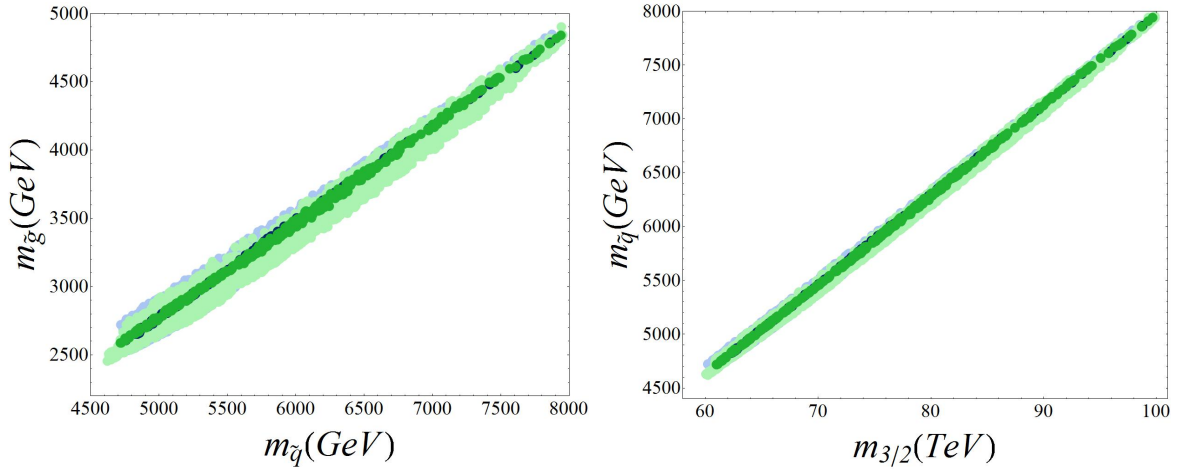

Figure 9.29. *Viable scenarios in the lightest squark - gluino mass plane (left) and gravitino - lightest squark mass plane (rigt) for the OIId5 model, with colours as in Fig. 9.26.*

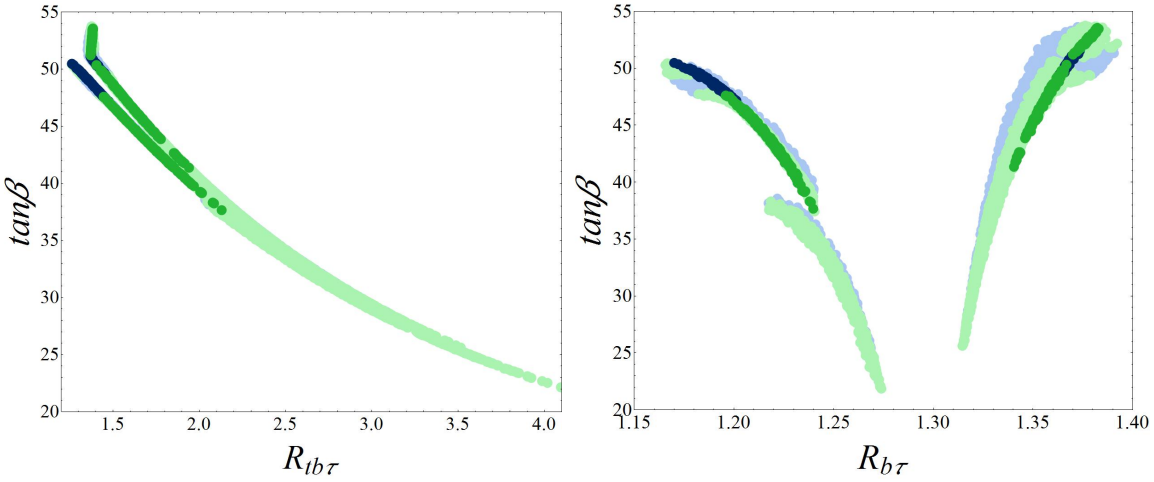

Figure 9.30. *Viable scenarios in the $R_{tb\tau} - \tan\beta$ (left) and $R_{b\tau} - \tan\beta$ (right) planes for the OIId5 model, with colours as in Fig. 9.26.*

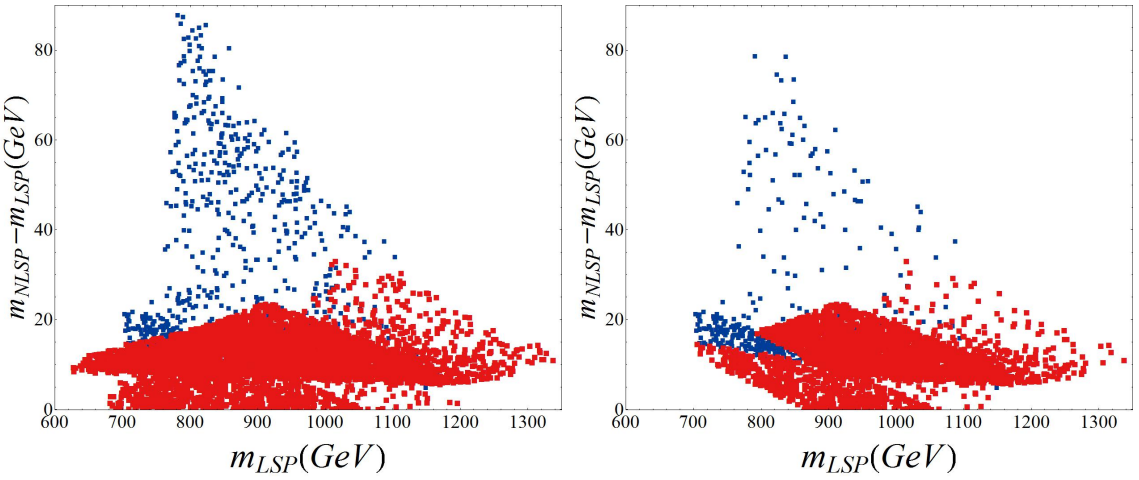

Figure 9.31. *Solutions in the plane of LSP mass vs. the NLSP-LSP mass splitting for the OIId5 model. The colour indicates the flavour of LSP, with red and blue denoting higgsino and bino dominated Dark Matter respectively. The shape indicates the flavour of NLSP with squares denoting chargino NLSP. The right panel only shows solutions with the preferred relic density.*

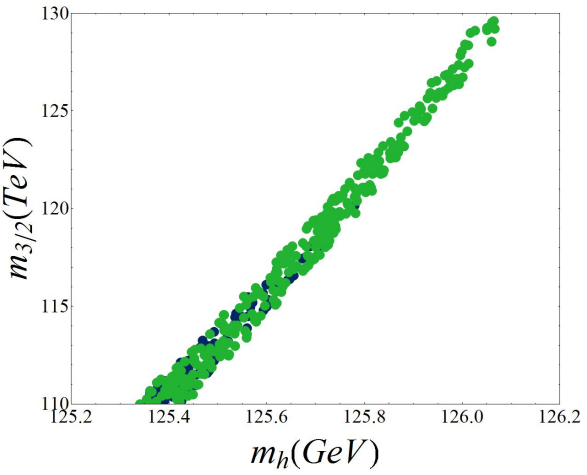

Figure 9.32. *Viable scenarios in the $m_h - m_{3/2}$ plane for the OIId5 model with extend range of θ and $m_{3/2}$, with colours as in Fig. 9.26.*

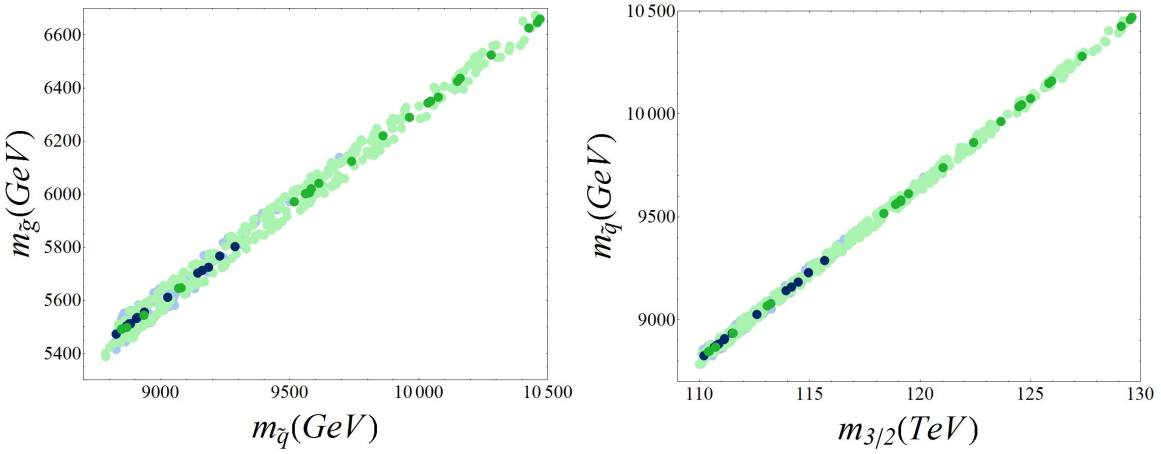

Figure 9.33. *Viable scenarios in the lightest squark - gluino mass plane (left) and gravitino - lightest squark mass plane (right) for the OIId5 model in an extend range of θ and $m_{3/2}$, with colours as in Fig. 9.26.*

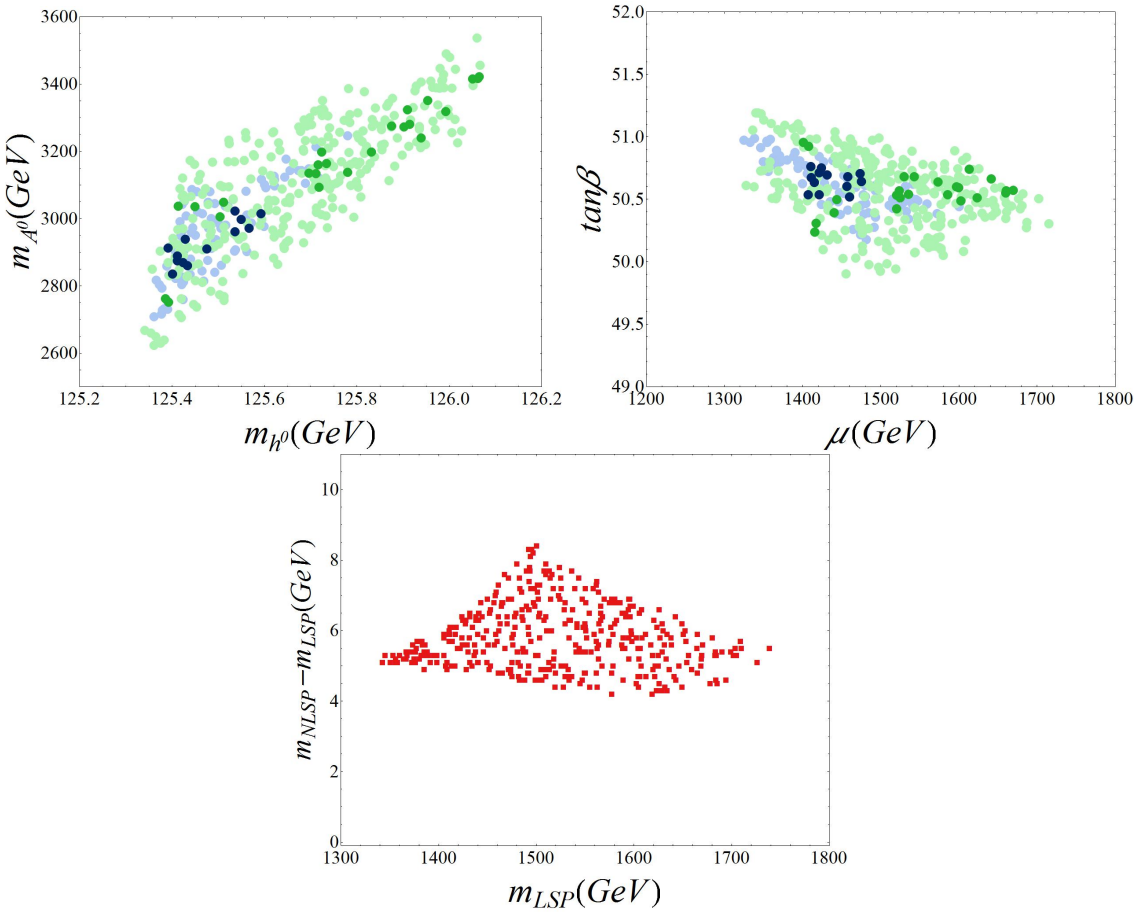

Figure 9.34. *Viable scenarios in the stop mass and lightest scalar - pseudoscalar (top left) mass and* $\mu - \tan\beta$ *(top right) planes and solutions in the plane of LSP mass vs. the NLSP-LSP mass splitting (bottom) for the OIId5 model. For the top planes, colours are as in Fig. 9.26 whereas for the bottom one it is as in Fig. 9.31.*

9.4. Benchmark Points

We present six example points for viable BIM orbifold scenarios that may be interesting to consider at either the 14 TeV LHC or the energy-upgraded Super-LHC with $\sqrt{s} = 28$ TeV. The GUT scale parameters for these scenarios can be found in Tab. 9.1. In Tab. 9.2 we show the masses of the five Higgs bosons. The masses of the first and third generation sfermions are shown in Tab. 9.3 where the second generation sfermions are assumed degenerate with the first. In Tab. 9.4 we show the gaugino masses. Finally in Tab. 9.5 we present μ, $\tan\beta$, the predicted relic density of Dark Matter and the predominant component of the LSP, and, as a point of interest, the fine-tuning from the gravitino mass and from μ alone.

	OI4	OI5	$OII6_1$	$OII6_2$	$OII5_1$	$OII5_2$
$m_{3/2}$	0.8378	0.8539	99.63	61.93	129.1	64.42
θ	4.94	4.90	0.01	3.15	0.01	3.15
δ_{GS}	-5	0	-6	-6	-5	-5

Table 9.1. *GUT scale parameters for our six benchmark scenarios. $m_{3/2}$ in TeV.*

	OI4	OI5	$OII6_1$	$OII6_2$	$OII5_1$	$OII5_2$
m_{h^0}	123.1	123.2	125.4	123.2	126.1	123.0
m_{A^0}	1492	1447	3028	2636	3415	3050
m_{H^0}	1492	1447	3028	2636	3415	3050
$m_{H^\pm}$	1494	1449	3030	2637	3416	3050

Table 9.2. *Higgs masses in GeV for our six benchmark scenarios.*

The first two benchmarks OI4 and OI5, correspond to the BIM OI orbifold model with $n_H + n_{\bar{H}} = -4$ and $\delta_{GS} = -5$, and with $n_H + n_{\bar{H}} = -5$ and $\delta_{GS} = 0$ respectively. Although largely fine-tuned, a string framework as we have been considering in this chapter is a good candidate to solve this problem at once by fixing the parameters of the theory. Furthermore, both points are still consistent with experimental bounds and should not be dismissed out of hand. The supersymmetric spectrum, and in particular all the first and second generation squarks, gluinos, lighest neutralinos, charginos and staus, are within the energy reach of the 14 TeV LHC, which makes these scenarios particularly interesting.

The second and third pairs of benchmarks, $OII6_1$, $OII6_2$, $OII5_1$ and $OII5_2$, correspond to the BIM O-II orbifold with $\delta_{GS} = -6$ and $\delta_{GS} = -5$ respectively. Both models predict

	OI4	OI5	$OII6_1$	$OII6_2$	$OII5_1$	$OII5_2$
$m_{\tilde{t}_1}$	2067	2187	5870	3441	7054	3233
$m_{\tilde{t}_2}$	2443	2554	6669	4012	7990	3876
$m_{\tilde{b}_1}$	2380	2474	6664	4005	7986	3871
$m_{\tilde{b}_2}$	2447	2552	7025	4343	8366	4280
$m_{\tilde{\tau}_1}$	707.9	742.6	5691	3935	6693	3914
$m_{\tilde{\tau}_2}$	1192	1248	6973	4469	8259	4320
$m_{\tilde{\nu}^3}$	1183	1240	6972	4468	8258	4319
$m_{\tilde{u}_L}$	2907	3047	8891	5347	10625	5053
$m_{\tilde{u}_R}$	2779	2914	8770	5293	10467	5003
$m_{\tilde{d}_L}$	2908	3049	8891	5348	10625	5053
$m_{\tilde{d}_R}$	2763	2896	8740	5279	10427	4989
$m_{\tilde{e}_L}$	1281	1344	7940	4898	9425	4649
$m_{\tilde{e}_R}$	999.5	1048	7835	4853	9287	4609
$m_{\tilde{\nu}^1}$	1279	1342	7939	4897	9424	4648

Table 9.3. *First and third generation sfermion masses (we assume the first and second generation sfermions are degenerate) for our six benchmark scenarios. All the masses are in GeV*

	OI4	OI5	$OII6_1$	$OII6_2$	$OII5_1$	$OII5_2$
$M_{\tilde{g}}$	3072	3227	5418	2965	6626	2753
$M_{\tilde{\chi}_1^0}$	696.2	732.9	1410	710.9	1686	784.3
$M_{\tilde{\chi}_2^0}$	1240	1307	1418	809.3	1691	827.6
$M_{\tilde{\chi}_3^0}$	1883	1942	1703	812.1	2145	884.2
$M_{\tilde{\chi}_4^0}$	1886	1946	2485	1323	3105	1242
$M_{\tilde{\chi}_1^\pm}$	1240	1307	1415	783.2	1689	800.8
$M_{\tilde{\chi}_2^\pm}$	1887	1946	2485	1297	3104	1217

Table 9.4. *Gaugino masses in GeV for our six benchmark scenarios.*

very heavy sfremions which would only be accessible to an energy upgraded super-LHC. However, the $OII6_2$ and $OII5_2$ scenarios predict gluinos below 3 TeV and are accessible to

	OI4	OI5	$OII6_1$	$OII6_2$	$OII5_1$	$OII5_2$
μ	1811	1863	1306	805.7	1554	773.2
$\tan\beta$	36.06	37.94	50.17	44.77	50.55	40.58
$R_{tb\tau}$	1.96	1.80	1.41	1.62	1.39	1.91
$R_{b\tau}$	1.05	1.03	1.37	1.21	1.37	1.23
$\Delta_{m_{3/2}}$	1542	1637	2.15	8.44	0.25	9.85
Δ_μ	1739	1851	910.1	355.0	1294	322.4
$\Omega_c h^2$	1.19×10^{-1}	1.25×10^{-1}	1.34×10^{-1}	1.39×10^{-1}	1.40×10^{-1}	1.33×10^{-1}
LSP type	Bino	Bino	Higgsino	Bino/Higgsino	Higgsino	Bino/Higgsino

Table 9.5. *The Higgs parameters μ (in GeV) and $\tan\beta$ for our six benchmark scenarios. Also shown are the individual fine-tuning fromn μ and from $m_{3/2}$ alone, the predicted relic density of Dark Matter, and the predominant component of the LSP.*

the 14 TeV LHC. The six benchmark scenarios considered here provide neutralino Dark Matter with the preferred relic abundance. For the $OII6_2$ and $OII5_2$ cases, the neutralinos are dominated by its $U(1)_Y$ component, but also carry an equivalently measurable contribution from the higgsino fields.

10. Conclusions and Outlook

The discovery of the Higgs boson has provided the last missing block in order to complete the Standard Model puzzle. However, existing issues such as the hierarchy problem and the lack of a Dark Matter candidate, are leading incentives for new physics beyond the SM. Although not the original motivation, the hierarchy problem is one of the strongest motivations for supersymmetry, where the Higgs mass is stabilized against high scale effects. Despite the potential emergence of a little hierarchy problem, particularly if SUSY is observed beyond the LHC energy reach, it is still important since the SM's fine-tuning problem is a lot more severe. Nevertheless, if SUSY remains unbroken at low energies, it predicts equal masses between the known fermions and the new sparticles. Since none of such fields have been observed, if supersymmetry is a true reflection of reality, it has to be an exact symmetry spontaneously broken at the high scale by some unknown mechanism. Various models have been proposed in order to describe the breakdown of supersymmetry and mediation mechanism. One of such examples is gravity mediation, where the information about the breaking is transmitted from a hidden to the visible sector through gravitational interactions. Since this is not a unique possibility, explicit soft SUSY-breaking terms are introduced in order to parametrize our ignorance of this issue, providing model independent couplings of positive mass dimensions.

The minimal supersymmetric extension of the SM, the MSSM, provides a framework with softly broken SUSY, and where the running of the strong and electroweak gauge couplings converge to a common value at a scale of about 10^{16} GeV, suggesting, in the most conventional approach, the existence of a larger gauge structure at the high scale, with a singe unified gauge coupling. Some of the candidates for Grand Unification symmetries are the $SU(5)$, $SO(10)$ and E_6 groups, which we have analyzed in this thesis. Besides the unification of the gauge coupings, these structures also provide constraints for the soft parameters at the GUT scale leaving an imprint on the low scale mass spectrum. Furthermore, as quarks and leptons are embedded in GUT representations of the underlying symmetry, relations among the Yukawa matrices elements emerge, which typically provide predictions for fixed GUT scale ratios upon the Yukawa couplings.

In Grand Unification models, the large adjoint representations foresee the existence of super-heavy gauge fields which mediate baryon and lepton number violating interactions,

predicting proton decay. While this constitutes a strong shortcoming for some non-supersymmetric GUT models, the unification scale of SUSY models is sufficiently large to preserve proton stability, consistent with current experimental bounds. Another source of proton decay arises from coloured fields belonging to complete Higgs representations. In order to evade fast decay rates, the non-singlet $SU(3)_C$ components need to be several orders of magnitude heavier than the electroweak scale doublet counterparts. Such mass splitting is hard to understand for fields that share the same representation, and is a common issue of models with direct breakdown of the GUT gauge group to the SM. However, it is possible to invoke model extensions with extra dimensions such as orbifolds, where odd parities may be attributed to coloured Higgs fields, which naturally split them from the low scale spectrum as they become heavy Kaluza-Klein excitations.

In chapter 6 we have studied the RGEs of the sfermion masses of the first and second generations for $SU(5)$, $SO(10)$ and E_6 boundary conditions. Neglecting Yukawa couplings in the one-loop RGEs for the first two generations allows an analytical analysis. The parameters of the underlying theory were determined as explicit functions of the low scale squark and slepton masses. An $SO(10)$ supersymmetric GUT, with the choice of Higgs fields in a **10** dimensional representation, provides a further constraints on the low scale masses when compared to $SU(5)$. A simplistic E_6 model that breaks to $SO(10)\otimes U(1)$ at the GUT scale, with no extra matter below the GUT scale, presents a similar picture to $SO(10)$ only with $m^2_{\mathbf{16}}$ replaced with the combination $m^2_{\mathbf{27}} + 2g^2_6 D_S$. The same analysis was also done for the E_6SSM, where an extra $U(1)$ and additional matter survive down to the electroweak scale. These new effects alter the RGEs as well as introduce new D-terms, at both the GUT and electroweak scales.

The possibility of preforming an analytical study of the RGEs of the first and second families allowed us to obtain sum rules for the different models, and we observe that the E_6SSM is clearly distinguishable from the other three cases. These sum rules can therefore be used to quickly identify the GUT gauge group from the spectrum of the first two generations.

In chapters 7 and 8 we have investigated Grand Unification with $SU(5)$ and $SO(10)$ boundary conditions. In particular we have relaxed some of the more usual restrictions on the GUT scale masses, allowing scalar masses to vary with generation, and have considered scenarios with non-universal gaugino masses. We have checked that our scenarios are consistent with the new observation of a Higgs boson with mass around 125 GeV, the so far negative direct LHC searches for supersymmetry and the XENON100 direct Dark Matter searches. The scenarios have the correct vacuum structure at low energies and conform with low energy measurements of $b \to s\gamma$, $B_S \to \mu^+\mu^-$ and $B \to \tau\nu_\tau$, $g-2$ of the muon as well as SM. Finally we also insist that the scenarios do not produce a Dark Matter relic density above

the experimental bounds of the WMAP and Planck satellites.

We first studied a model of universal gaugino masses but fail to find any solutions with low fine-tuning. This is not surprising since the fine-tuning from μ alone grows as the square of μ indicating that a small value of μ is required if the model is not to be fine-tuned. Unfortunately this is very difficult to achieve while providing a Higgs boson mass heavy enough for the new resonance and we find no solutions for small μ that do not have to be fine-tuned in one of the other parameters. We therefore take a paradigmatic approach and remove μ from our measure of fine-tuning. However, we do no mean to imply that large fine-tuning in μ is acceptable, but since it is already a parameter that is poorly understood with no justification for its phenomenologically required value, we assume that it is possible that μ has some mechanism of origin that fixes its value in such a way as to avoid the tuning problem. Thus, we consider that it is better keep the fine-tuning in μ and, if possible, remove it from the other fundamental parameters. We therefore attempt instead to minimise only the fine-tuning arising from the soft supersymmetry breaking masses.

However, even with this relaxation, we are still unable to find scenarios with universal gaugino masses that do not have fine-tuning in the soft masses. We therefore turned our attention to the non-universal gaugino masses, initially scanning over all possible ratios. As one might expect we immediately find many more scenarios that conform with the low energy constraints, but although fine-tuning was reduced we still found very few points with acceptable tuning. We examined the cause of this tuning and find that the tunings are greatly reduced for small values of m_{10}, $m_{5'}$ and $a_{5'}$ at the GUT scale. This behaviour does not carry over to the fine-tuning with respect to $M_{1/2}$. We therefore ran an "enhanced" scan over the non-universal gaugino mass scenarios, this time setting the scalar masses and trilinears to small values at the GUT, and allowing them to become sizable due to the large contribution of $M_{1/2}$ in the RGEs. Indeed such scenarios with no fine-tuning were suggested many years ago in Ref. [89], where an R-symmetry was imposed to keep the scalar masses zero. This symmetry is then spontaneously broken in the hidden sector and the breaking is transmitted to the visible sector by supergravity. We note that zero or small GUT scale scalar masses generally predict that the squarks and gluinos be of order the same mass.

Our enhanced scan revealed many scenarios with low (< 10) fine-tuning in the soft parameters, for high scale gaugino masses beyond TeV. The solutions encountered result from regions where $m^2_{H_u}$ and the remaining low scale masses are insensitive to fluctuations in $M_{1/2}$ while still having large (absolute) values. However, one should be careful in the interpretation of such results, and further studies are required. In particular, the impact of different renormalization schemes should be checked. It would also be relevant to perform the same analysis using different software tools in order to validate our results. To achieve

the preferred value for the Dark Matter relic density requires $\mu \sim 1\,\text{TeV}$. Furthermore, we found that all viable scenarios lie on an ellipse in the plane of ρ_1 and ρ_2 where $\rho_i = M_i/M_3$ at the GUT scale. Since various theories of new physics at the GUT scale make predictions for the gaugino mass ratios, it is interesting to ask where these theories lie on this plane, and by comparison to the ellipse examine whether or not they are likely to give low energy predictions compatible with experiment while maintaining minimal fine-tuning. In particular we examined for $SU(5)$ the breaking of supersymmetry using hidden sector fields belonging to the **24**, **75** or **200** representations (the **1** predicts universal gaugino masses), and additionally the Brignole, Ibáñez and Muñoz O-I and O-II orbifold models with various modular weights and Green-Schwarz coefficients. It should be stressed that for the orbifold models we only considered the effect on the gaugino masses and disregarded the constraints on the scalar masses, which was left for chapter 9. We only found three classes of model that provide viable solutions: supersymmetry breaking using hidden sector fields in a **200**; the O-I orbifold with $n_H + n_{\bar{H}} = -4$ and $\delta_{GS} = -5$; and the O-II orbifold with $\delta_{GS} = -6$. For $SO(10)$ we considered hidden sector fields in combinations of two of the **1**, **54**, **210** and **770** irreps, transforming differently under each of the $SO(10)$ maximal subalgebras. This has introduced a representation mixing angle as an extra free parameter, which also required fine-tuning studies, but fortunately, we managed to identify several solutions with low fine-tuning, though less dense than those without mixing. We found three viable models based on hidden sector fields transforming as a $\mathbf{75}+\mathbf{200}$ with Georgi-Glashow embedding; a $\mathbf{75}+\mathbf{1}$ with flipped embedding; and a singlet of $SU(4)\times SU(2)_R$.

Scans particular to the first three models were then performed. All three models turn out to be quite restrictive, predicting particle masses in rather narrow ranges. For example the $SU(5)_{\mathbf{200}}$ model requires a lightest stop in the region 2.25 - 2.43 TeV and the lightest squark in the region 2.74 - 2.89 TeV. Unfortunately the $SU(5)_{\mathbf{200}}$ model is always quite fine-tuned with $\Delta \gtrsim 75$ and always gives a Dark Matter relic density considerably below the preferred range. The O-I orbifold, on the other hand, is nearly perfect allowing scenarios with $\Delta < 10$ and always giving the preferred Dark Matter relic density. Unfortunately it also predicts a rather heavy spectrum which will be beyond the search reach of the 14 TeV LHC. The O-II orbifold is a half-way house, with an accessible spectrum, scenarios that have low fine-tuning and the possibility for the preferred relic density. Unfortunately the latter two properties are not united in a single scenario, so one must chose between low fine-tuning or the correct relic density.

The later three scenarios also proved to be rather restrictive. The $GG75+200$ and $FL75+1$ models have equivalently large spectra beyond the expected 14 TeV LHC reach. Exact top-bottom-tau Yukawa unification is hard to achieve but it is possible to get $R_{tb\tau} < 1.4$, but unfortunately for solutions with too little a Dark Matter density. The bottom-tau unification

provided values between 1.30 and 1.48, which are close to the $y_b/y_\tau = 3/2$ ratio. The $PS1$ model may be accessible to the 14 TeV LHC with squarks lighter than 3 TeV if we do not insist in the preferred relic density and allow $\Delta \sim 100$. This scenario also predicts staus as light as 650 GeV as NLSP. Nevertheless we believe these scenarios are interesting for consideration at future colliders, so we have presented the spectra of some representation benchmark scenarios.

An other possibility for grand unification may arise from a class of orbifold models inspired in four-dimensional strings. This is the case of the O-I and O-II orbifolds which study whether supersymmetry breaking is dilaton or moduli dominated respectively. The unification of the gauge couplings may arise either from special choices of modular weights upon the matter fields, or as a consequence of large loop corrections due to very heavy fields at the string scale. As we have a more definite theoretical background, fine-tuning considerations are relaxed, however, as a point of interest, we consider fine-tuning in $m_{3/2}$ when it is possible to have small values. The two complete O-I scenarios considered provided interesting phenomenology while predicting staus around 700 GeV together with squarks and gluinos close to 3 TeV. Out of all scenarios considered the OI4d5 and OI5d0 models are undoubtedly the major candidates to be probed in earlier runs of the 14 TeV LHC. Furthermore, they predict Yukawa ratios very close to $y_b/y_\tau = 1$. On the other hand, the O-II scenarios contrast with the O-I ones, foreseeing a rather large SUSY spectrum particularly in the scalar sector. However, the OIId5 and OIId6 models are not excluded from being probed at the LHC since we can find gluinos as light as 2.4 TeV. The majority of the solutions nicely predict the preferred relic density relying on contributions from both bino and higgsino components.

Of course this by no means exhausts the possible theories of grand unification. There are plenty more viable points in the ρ_1 - ρ_2 plane that could be explored and should be subject of further studies. It would also be interesting to analyse GUT theories based on other gauge groups (such as E_6 or trinification models $[SU(3)]^3$) with a similar philosophy to see if one can find additional models with desirable properties. We have also highlighted some of the persistent shortcomings of conventional GUT models, such as proton stability, doublet-triplet splitting and the μ-problem. Although we have been invoking string inspired models as possible solutions for these problems, different solutions are also desirable. Therefore, new ideas for Grand Unified Models from less traditional perspectives are required.

The observed Higgs mass at the LHC suggests rather heavy superpartner masses, thus it is not surprising that we have not yet observed any evidence for SUSY. Indeed, the research presented in this thesis has shown that the majority of the supersymmetric spectrum will only be accessible to an energy upgraded super-LHC with center of mass energy $\sqrt{s} = 28$ TeV.

We have also shown that heavy supersymmetry can still be natural, and it will be exciting to see if the scenarios discussed here can be found at the LHC or its successor colliders.

A. Appendix

The discussion that follows is largely based on [124].

A.1. Elements of Representation Theory

It became evident since the first chapter of this thesis, that *Lie Algebras* play an important role in Particle Physics. For example, the $SU(3)_C$ gauge symmetry, which describes quantum chromodynamics, predicts three kinds of fundamental (colour) charges. Each quark (anti-quark) carries one unit of colour (anti-colour) and therefore, is a representation of the symmetry group. It is then important to ask, what are the irreducible representations and how do they correspond to particle states? To answer this, it is relevant to start with the following simplified definitions[1]:

Abelian and nonabelian algebras. *Let $\mathcal{U}$ be some algebra with n elements $u_i, \cdots, u_n$. If all elements commute, i.e. $[u_i, u_j] = 0\ \forall i, j \in \{1, \ldots, n\}$, the algebra is commutative or abelian. Otherwise, the algebra is non-commutative or non-abelian. For example, $U(1)$ is an Abelian whereas $SU(N)$ and $SO(N)$ are not.*

Proper groups. *An group is denoted improper if its subgroups are just itself and the identity. All the other groups are called proper, where G_{SM}, $SU(5)$ and $SO(10)$ are included.*

Ideals. *Consider a subspace $\mathcal{V}$ of a Lie algebra $\mathcal{U}$. If there is any element $u \in \mathcal{U}$ and $v \in \mathcal{V}$ such that $[u, v] \in \mathcal{V}$, then $\mathcal{V}$ is an ideal of $\mathcal{U}$. In Lie algebras, ideals act like subgroups in group theory.*

Simplicity. *A Lie group G is simple if it is non-abelian and if it has no ideal. G is semi-simple if it is non-abelian and does not have an abelian ideal. Clearly, a simple group is also semi-simple. Furthermore, if G is a direct product of n simple and/or semi-simple groups, $G = H_1 \times \cdots \times H_n$, the subgroups $H_1, \ldots, H_n$ are ideals of G. Therefore, G is also semi-simple. Familiar examples of semi-simple groups are the cases of G_{SM} as well as $SU(2)_L \times U(1)_Y$. However, the $SU(3)$ and $SU(2)$ symmetries as well as $SU(5)$ and $SO(10)$, are examples of simple groups.*

Rank. *The rank of a group G, denoted rank(G), is defined as the maximum number of simultaneously diagonalizable or commuting generators. For example, $SU(2)$ is a rank$(SU(2)) = 1$ group since each generator J_i just commutes with itself.*

[1] Many concepts in group theory are formally complicated and rather involved for our purposes in this thesis. We present just some oversimplified definitions/results that are relevant for Physics and in particular for Grand Unification.

Maximal subalgebra. *Let $\mathcal{V}$ be a subalgebra of some closed algebra $\mathcal{U} \supset \mathcal{V}$. We say it is maximal if rank($\mathcal{V}$) = rank($\mathcal{U}$) and there is no other subalgebra $\mathcal{W}$ such that $\mathcal{V} \subset \mathcal{W} \subset \mathcal{U}$. Furthermore, if $\mathcal{V}$ is abelian, it is denominated as Cartan subalgebra.*

A.1.1. Roots and Weights

Suppose that we have the following algebra

$$[H_i, E_\alpha] = \alpha_i E_\alpha, \tag{A.1}$$

with H_i n diagonal elements and α_i structure constants. Here, for each E_α there is a vector $\boldsymbol{\alpha} = (\alpha_1, \ldots, \alpha_n)$ made up by n structure constants. The vector $\boldsymbol{\alpha}$ is denoted as a *root vector* or simply as a *root*. Therefore, the roots can be represented in a n-dimensional Euclidean space. If we now act the elements H_i on a Hilbert space vector $|\lambda\rangle$, we obtain a set of n eigenvalues, $\boldsymbol{\lambda} = (\lambda_1, \ldots, \lambda_n)$, solution of the eigenvalue equations

$$H_i|\lambda\rangle = \lambda_i|\lambda\rangle, \tag{A.2}$$

denoted as *weight of a representation vector*. We have not yet said what the E_α operators are. However, if we note that

$$H_i(E_\alpha|\lambda\rangle) = ([H_i, E_\alpha] + E_\alpha H_i)|\lambda\rangle = (\lambda_i + \alpha_i)E_\alpha|\lambda\rangle, \tag{A.3}$$

therefore

$$E_\alpha|\lambda\rangle \propto |\lambda + \alpha\rangle. \tag{A.4}$$

We find that E_α are *ladder operators* of the group algebra. Furthermore, if $E_\alpha|\lambda\rangle = 0$, then $|\lambda\rangle$ is denoted the state of *highest weight*. Let us now give some illustrative examples. First, consider an $SU(2)$ algebra

$$\left[\mathsf{J}_\alpha, \mathsf{J}_\beta\right] = i\varepsilon_{\alpha\beta\gamma}\mathsf{J}_\gamma, \tag{A.5}$$

where $\mathsf{J}_{1,2,3}$ are the spin generators. For a state with principal spin quantum number s and component along the z-direction m_3, we know that

$$\mathsf{J}_3|s, m_3\rangle = m_3|s, m_3\rangle. \tag{A.6}$$

We understand now that the eigenvalue m_3, which physically represents the projection of the spin angular momentum along the z-axis, is a weight of the $|s, m_3\rangle$ $SU(2)$ representation.

Furthermore, from the commutation relation

$$[\mathsf{J}_3, \mathsf{J}_\pm] = \pm \mathsf{J}_\pm, \tag{A.7}$$

where $\mathsf{J}_\pm$ are the well known $SU(2)$ ladder operators, we have two roots, $\alpha_{1,-1} = \pm 1$, which can be represented in a one dimensional Euclidean space. It is evident from Fig A.1 that it is possible to construct one root with a linear combination of the other one, namely $\alpha_{-1} = -\alpha_1$. We may then introduce the concept of *simple roots*, defined as the positive roots from where it is possible to construct, by linear combinations, all the remaining ones. In $SU(2)$, α_1 is a single simple root. The rank of the group can also be thought of as the dimension of the Euclidean space where the root vectors are defined. In particular for $SU(2)$, this dimension, and accordingly the rank, is *one*.

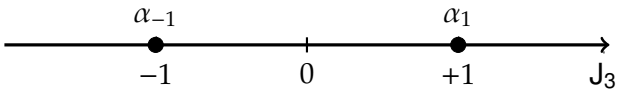

Figure A.1. *Roots of $SU(2)$.*

An other example, which is rather relevant for this chapter, is $SU(3)$, whose algebra is

$$[\Omega_a, \Omega_b] = i f_{abc} \Omega_c, \tag{A.8}$$

with the structure constants

$$\begin{aligned} &f_{123} = 1, \\ &f_{147} = f_{516} = f_{246} = f_{257} = f_{345} = f_{637} = \frac{1}{2} \\ &f_{458} = f_{678} = \frac{\sqrt{3}}{2}, \end{aligned} \tag{A.9}$$

normalized by $f_{acd} f_{bcd} = 3\delta_{ab}$. All the other structure constants not related to those above by permutations of their indices are *zero*. It is possible to choose a basis, called the *Cartan-Weyl* basis[2], with the generators of the Cartan subalgebra

$$\begin{aligned} &H_1 \equiv \Omega_3, \;\; H_2 \equiv \Omega_8 \\ &[H_1, H_2] = i f_{38k} \Omega_k = 0, \end{aligned} \tag{A.10}$$

[2]It is convenient to write the group generators in a Cartan-Weyl basis, since the non-zero roots are non-degenerate. For each ladder operator there is only one root vector.

and the ladder operators

$$I_\pm \equiv \frac{1}{\sqrt{2}}(\Omega_1 \pm i\Omega_2), \;\; U_\pm \equiv \frac{1}{\sqrt{2}}(\Omega_4 \pm \Omega_5), \;\; V_\pm \equiv \frac{1}{\sqrt{2}}(\Omega_6 \pm i\Omega_7). \tag{A.11}$$

We have a maximum of *two* simultaneously diagonalizable generators, thus $SU(3)$ is a *rank* = 2 group and we can represent the roots in a two dimensional euclidean space. The task now is to find the simple roots, which we know *a-priori* that have to be two. From (A.1) and the results above we obtain six roots, $\alpha_I^\pm$,$\alpha_U^\pm$, and, $\alpha_V^\pm$,

$$\begin{aligned}
[H_i, I_\pm] &= \alpha_I^\pm I_\pm \Longrightarrow \alpha_I^\pm = \pm(1,0) \\
[H_i, U_\pm] &= \alpha_U^\pm U_\pm \Longrightarrow \alpha_U^\pm = \pm\left(-\frac{1}{2}, \frac{\sqrt{3}}{2}\right) \\
[H_i, V_\pm] &= \alpha_V^\pm V_\pm \Longrightarrow \alpha_V^\pm = \pm\left(\frac{1}{2}, \frac{\sqrt{3}}{2}\right),
\end{aligned} \tag{A.12}$$

where the positive ones, defined by requiring that the first non-zero component is positive, are α_I^+,α_U^-, and, α_V^+. Taking the positive roots, we see that $\alpha_I^+ = \alpha_U^- + \alpha_V^+$. To find the simple roots, the convention is to choose those that cannot be written as linear combinations of the other positive roots with positive coefficients. Therefore α_V^+ and α_U^- are the linearly independent simple roots and form a basis of the root space. One should note here that different coordinate systems lead to different simple roots, however, their relative lengths and angles are invariant and they always determine the entire algebra. The *Cartan matrix* is then introduced such that any choice of the generators always provides the same result,

$$A_{ij} = 2\frac{\left(\alpha_i, \alpha_j\right)}{\left(\alpha_j, \alpha_j\right)}, \tag{A.13}$$

with $(,)$ the Euclidean inner product. For $SU(3)$ the Cartan matrix takes the form

$$A_{SU(3)} = \begin{pmatrix} 2 & -1 \\ -1 & 2 \end{pmatrix}, \tag{A.14}$$

from where, in the new basis, denoted as *Dynkin basis*, the simple roots can be read off as $\alpha_1 = (2\ -1)$ and $\alpha_2 = (-1\ 2)$. The Cartan matrix is a crucial element in order to work out the entire root system, and the labels $(a_1\ a_2)$ are denoted as *Dynkin labels*.

We could have however chosen a different basis by assigning $I_3 \equiv H_1$ and $Y \equiv \frac{2}{\sqrt{3}}H_2$. The simple roots in the (Y, I_3) coordinate system would be $\alpha_I^+ = (0,1)$ and $\alpha_U^+ = (1, -\frac{1}{2})$, yielding, as expected, the same Cartan matrix (A.14). This choice provides us an intuitive physical

interpretation of the ladder operators as well as the Cartan subalgebra generators. For instance, α_I^+ raises I_3 by one unit; α_U^+ raises Y by one unit and lowers I_3 by 1/2; $\alpha_U^- = (-1, \frac{1}{2})$ lowers Y by 1 and raises I_3 by 1/2 and so on for the remaining operators. The generators of the Cartan subalgebra are actually the $SU(3)$ hypercharge and Isospin generators. There is a theorem of group theory which states that in a Cartan-Weyl basis, the zero root has a degeneracy equal to the rank of the algebra, therefore, we may then represent the complete set of $SU(3)$ roots in the (Y, I_3) plane as in Fig. A.2. Simple Lie algebras are completely characterized by the relative lengths, (α_i, α_i), of their roots as well as the angles among them, which are always the same for any choice of basis. We see that it is indeed true for, (H_1, H_2), (Y, I_3)[3], or the Dynkin basis.

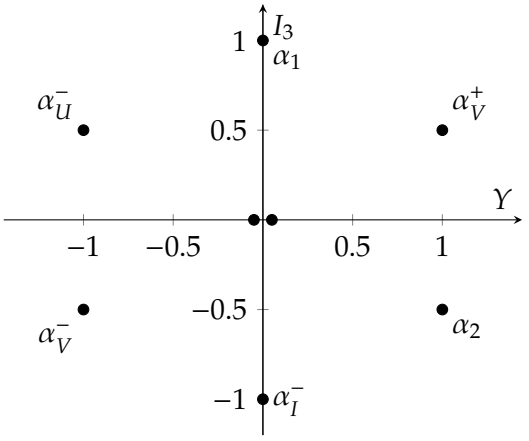

Figure A.2. *Roots of SU(3).*

According to (A.3), if $E_\alpha|\lambda\rangle$ is a non-zero state, its eigenvalues of $H_i(E_\alpha|\lambda\rangle)$ are $\lambda_i + \alpha_i$. This shows that the weight vectors are defined in the same Euclidean space spanned by the simple roots. The points in the root space can be supplemented by points that correspond to weights of a representation, forming a lattice that is denoted as *weight space*. It is then possible to write a generic weight vector Λ as a linear combination of the simple roots,

$$\Lambda = \sum_i \frac{2}{(\alpha_i, \alpha_i)} \overline{\lambda}_i \alpha_i, \tag{A.15}$$

where for $SU(N)$, $SO(2N)$ and exceptional algebras E_N, the only ones we are interested about in this thesis, the length square of the simple roots is normalized to 2, therefore $2/(\alpha_i, \alpha_i) = 1$. The $\overline{\lambda}_i$ coefficients define a weight vector in a basis dual to the Dynkin basis, $\overline{\Lambda} = [\overline{\lambda}_1 \dots \overline{\lambda}_n]$. We introduce now, without demonstration, a crucial theorem of group theory:

[3]Note that here the metric is $diag(\frac{3}{4}\ \ 1)$

Theorem. *For any root or weight written in the Dynkin basis, the Dynkin labels given by*

$$a_i = 2\frac{(\Lambda, \alpha_i)}{(\alpha_i, \alpha_i)}, \tag{A.16}$$

are always integers.

From this theorem and from the expansion of a weight vector in components, eq. (A.15), it becomes clear that any root or weight can be written in term of the integer Dynkin labels $(a_1 \ \ldots \ a_n)$. We can also take from the Fig. A.2, that the root $\alpha_1 = (2 \ -1)$, or a weight with the same Dynkin labels, have $I_3 = +1$ and $Y = 0$; a root or a weight $\lambda = (1\ 1)$, which corresponds to $\alpha_1 + \alpha_2$ and hence α_V^+ in Fig. A.2, have $I_3 = 1/2$ and $Y = 1$; a root or a weight $\lambda = (-1\ 2)$, which corresponds to α_2 in the figure, has $I_3 = -1/2$ and $Y = 1$ and so forth. Analyzing this values, we find that any root or weight, which we may label with Λ, has $SU(3)$ hypercharge and isospin

$$Y(a_1\ a_2) = \frac{a1 + 2a_2}{3}, \tag{A.17}$$

$$I_3(a_1\ a_2) = \frac{a1}{2}, \tag{A.18}$$

respectively. It is then possible to define

$$\frac{a1 + 2a_2}{3} = \overline{Y} \cdot \Lambda, \tag{A.19}$$

$$\frac{a1}{2} = \bar{I}_3 \cdot \Lambda, \tag{A.20}$$

where $\overline{Y}$ and $\bar{I}_3$ are vector of the dual space given by

$$\overline{Y} = \frac{1}{3}[1\ 2], \tag{A.21}$$

$$\bar{I}_3 = \frac{1}{2}[1\ 0]. \tag{A.22}$$

From (A.21) and (A.22) it is possible to determine the electromagnetic charge of any weight by adding up the isospin and hypercharge axis, $Q = I_3 + Y/2$, yielding

$$\overline{Q} = \frac{1}{3}[2\ 1], \ \ Q(a_1\ 1_2) = \overline{Q} \cdot \Lambda. \tag{A.23}$$

The same exercise can be done for any simple Lie algebra and it is convenient to write the hypercharge and isospin generators in the dual basis since the computation of the group charges is reduced to a scalar product. The $SU(3)$ discussion, however, is just a prototype of more complicated simple algebras with multi-dimensional Cartan subalgebras. We are actually interested in embedding the SM into a simple lager group G such that, upon breaking,

we have $G \to G_{SM} \to SU(3)_C \times U(1)_Q$. The axis of the Cartan subalgebra of G, with importance for the Standard Model, are those that generate the weak hypercharge Y^w and weak isospsin I_3^w. For any generic wight of G with $rank(G) = n$, we may write

$$Y^w(a_1 \ \ldots a_n) = \overline{Y}^w \cdot \Lambda \tag{A.24}$$

$$I_3^w(a_1 \ \ldots a_n) = \overline{I}_3^w \cdot \Lambda \tag{A.25}$$

$$Q(a_1 \ \ldots a_n) = \left(\overline{I}_3^w + \frac{1}{2}\overline{Y}^w\right) \cdot \Lambda. \tag{A.26}$$

A.1.2. Representations

In this section, we will show how one may identify all possible physical states in a given representation of simple Lie group. Each weight, which is a vector in a $rank(G)$-dimensional Euclidean space, is used to label a vector in the Hilbert space, therefore, the key ingredient, is to determine the *weight system* of each relevant *irreducible representation* or *irrep*. An irreducible representation $\mathbf{R}$ of a group G, is a representation that cannot be broken up into smaller pieces, i.e., they cannot be decomposed in a direct sum of representations of the same group G, $\mathbf{R}_{reduc} = \mathbf{R}_1 \oplus \cdots \oplus \mathbf{R}_m$.

Let us consider once again the Hilbert space vector $|j,m\rangle$ for the j irrep of $SU(2)$. From (A.15) and (A.16), we take that j has weight m in dual basis or $2m$, always integer, in the Dynkin basis. As we expected, as the rank of $SU(2)$ is one, the weight vector is simply a scalar. It is however a bit more involved for higher rank algebras, and to designate any irrep and its weight system, where we shall use the Dynkin basis, the definitions and theorem that follow are introduced:

Highest root. *The root from which all the remaining ones can be derived by subtraction of simple roots is denoted as highest root.*

Highest weight. *Some vectors in the Hilbert space may be labeled by the same weight Λ, meaning that Λ is degenerate. However, it is always possible to find a non-degenerate weight that uniquely defines the irrep. Such weight is denoted as highest weight.*

Theorem. *The highest weight that defines an irrep, can be selected in such a way that the Dynkin labels $(a_1 \ \ldots \ a_n)$ are non-negative integers.*

Any Lie algebra is allowed to have infinitely many representations for its generators, as long as the commutation relations provided by the Lie brackets are respected. The weight system of an irrep can be entirely determined by subtracting simple roots to the highest weight, however, some rules have to be obeyed, which follow from group theoretical theorems. A useful mnemonic consists in first determining the *level* of a weight. The level tels the number of times that simple roots have to be subtracted from the highest weight in

order to work out the irrep. The level is given by

$$T(\Lambda) = \sum_i \overline{R}_i a_i \tag{A.27}$$

where $\overline{R}$ is the level vector in the dual space, and can be found in table 10 of [124]. If we have n simple roots, we have to subtract each one $T(\Lambda)/n$ times. Suppose now that the highest weight of an irrep of a rank n group is $\Lambda = (a_1 \ \dots \ a_n)$. Recall that from the previous section we know that we have n simple roots $\alpha_1, \dots, \alpha_n$. To obtain the second weight, one subtracts, from the highest weight, the simple roots with the same indices of the non-zero (and positive) entries of the highest weight. For example, if $\Lambda = (0 \ \dots \ a_k \ \dots \ a_m \ 0 \dots \ 0)$, we have to subtract $\Lambda - \alpha_k$ and $\Lambda - \alpha_m$. We are now left with two weights from where we apply the same rules until we reach the lowest weight. This is just a mnemonic, and it may happen, that in some less trivial occasions, we have to subtract roots labeled with indices corresponding to zero or negative entries of the weight vector. A useful theorem for the construction of weight systems is *Dynkin's Theorem*, which says that the weight diagrams have to be *spindle shaped*, or technically, that the the number of weights is the kth level is equal to the number of wights in the $(T(\Lambda) - k)$th level, as well as that the number of weights in the $(k+1)$th level is greater or equal than the number of weights in the kth level, if we are in the first half of the diagram ($k < T(\Lambda)/2$).

We apply now the techniques described above to determine the weight system of the **3**, $\overline{\mathbf{3}}$ and **8** representations of $SU(3)$, with the highest weights (1 0), (0 1) and (1 1) respectively. The level of the fundamental and anti-fundamental irreps is $T(\Lambda) = 2$ where for $SU(3)$ we have used $\overline{R} = [2\ 2]$. This means that we need to subtract two simple roots from the highest weight, and since we have just two of them, we only subtract each one once. For the adjoint representation, its level is $T(\Lambda) = 4$, each root has to be subtracted twice from the state of highest weight. Such diagrams are shown in Fig. A.3. Here, we clearly see that the weight diagram of the **8** is spindle shaped. We had to subtract both simple roots form the (0 0) degenerate weights, since they have to be subtracted twice from the top state. If we are describing QCD, the weights in Fig. A.3 that correspond to the fundamental and anti-fundamental irreps, represent the three colour (anticolour) states of a quark (antiquark) field. For the adjoint irrep, the weights in the weight diagram are actually the roots in A.2, and physically this corresponds to the gluon colour octet.

Although less trivial, these methods can be used for higher rank simple Lie groups such as $SU(5)$, $SO(10)$ and E_6.

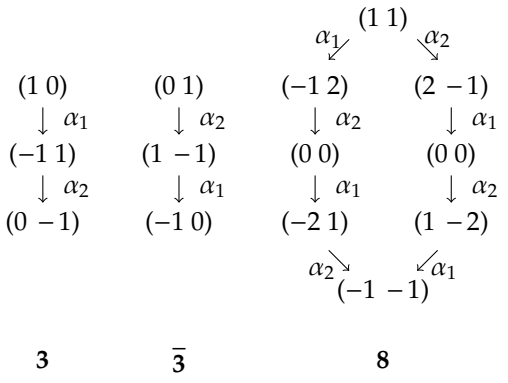

Figure A.3. *Weight diagrams for the fundamental, anti-fundamental and adjoint irreps of SU*(3).

Bibliography

[1] G. Aad *et al.* [ATLAS Collaboration], *Combined search for the Standard Model Higgs boson using up to 4.9 fb^{-1} of pp collision data at $\sqrt{s} = 7$ TeV with the ATLAS detector at the LHC*, Phys. Lett. B **710** (2012) 49 [arXiv:1202.1408 [hep-ex]].

[2] S. Chatrchyan *et al.* [CMS Collaboration], *Combined results of searches for the standard model Higgs boson in pp collisions at $\sqrt{s} = 7$ TeV*, Phys. Lett. B **710** (2012) 26 [arXiv:1202.1488 [hep-ex]].

[3] G. Aad *et al.* [ATLAS Collaboration], *Observation of a new particle in the search for the Standard Model Higgs boson with the ATLAS detector at the LHC*, Phys. Lett. B **716** (2012) 1 [arXiv:1207.7214 [hep-ex]].

[4] S. Chatrchyan *et al.* [CMS Collaboration], *Observation of a new boson at a mass of 125 GeV with the CMS experiment at the LHC*, Phys. Lett. B **716** (2012) 30 [arXiv:1207.7235 [hep-ex]].

[5] Y. Ashie *et al.* [Super-Kamiokande Collaboration], *Evidence for an oscillatory signature in atmospheric neutrino oscillation*, Phys. Rev. Lett. **93** (2004) 101801 [hep-ex/0404034].

[6] T. Araki *et al.* [KamLAND Collaboration], *Measurement of neutrino oscillation with KamLAND: Evidence of spectral distortion*, Phys. Rev. Lett. **94** (2005) 081801 [hep-ex/0406035].

[7] E. Aliu *et al.* [K2K Collaboration], *Evidence for muon neutrino oscillation in an accelerator-based experiment*, Phys. Rev. Lett. **94** (2005) 081802 [hep-ex/0411038].

[8] M. Ambrosio *et al.* [MACRO Collaboration], *Measurements of atmospheric muon neutrino oscillations, global analysis of the data collected with MACRO detector*, Eur. Phys. J. C **36** (2004) 323.

[9] M. C. Sanchez *et al.* [Soudan 2 Collaboration], *Measurement of the L/E distributions of atmospheric neutrinos in Soudan 2 and their interpretation as neutrino oscillations*, Phys. Rev. D **68** (2003) 113004 [hep-ex/0307069].

[10] http://www.u-tokyo.ac.jp/en/todai-research/feature-stories/atlas2012/

[11] C. Amsler et al. (Particle Data Group), Physics Letters B667, 1 (2008)

[12] M. B. Green, J. H. Schwarz and E. Witten, *Superstring Theory. Vol. 1: Introduction*, Cambridge, Uk: Univ. Pr. (1987) 469 P. (Cambridge Monographs On Mathematical Physics)

[13] M. B. Green, J. H. Schwarz and E. Witten, *Superstring Theory. Vol. 2: Loop Amplitudes, Anomalies And Phenomenology*, Cambridge, Uk: Univ. Pr. (1987) 596 P. (Cambridge Monographs On Mathematical Physics)

[14] H. Greaves and T. Thomas, *The CPT theorem*, arXiv:1204.4674 [math-ph].

[15] M. E. Peskin and D. V. Schroeder, *An Introduction to quantum field theory*, Reading, USA: Addison-Wesley (1995) 842 p.

[16] L. Wolfenstein, *Violation of CP Invariance and the Possibility of Very Weak Interactions*, Phys. Rev. Lett. **13** (1964) 562.

[17] V. Fanti *et al.* [NA48 Collaboration], *A New measurement of direct CP violation in two pion decays of the neutral kaon*, Phys. Lett. B **465** (1999) 335 [hep-ex/9909022].

[18] C. -N. Yang and R. L. Mills, *Conservation of Isotopic Spin and Isotopic Gauge Invariance*, Phys. Rev. **96** (1954) 191.

[19] Jorge C. Romão, *O Modelo Standard das Interacções Electrofracas*, IST, 1998.

[20] K. G. Wilson, *Confinement of Quarks*, Phys. Rev. D **10** (1974) 2445.

[21] G. Arnison *et al.* [UA1 Collaboration], *Experimental Observation of Isolated Large Transverse Energy Electrons with Associated Missing Energy at s**(1/2) = 540-GeV*, Phys. Lett. B **122** (1983) 103.

[22] G. Arnison *et al.* [UA1 Collaboration], *Experimental Observation of Lepton Pairs of Invariant Mass Around 95-GeV/c**2 at the CERN SPS Collider*, Phys. Lett. B **126** (1983) 398.

[23] S. L. Glashow, *Partial Symmetries of Weak Interactions*, Nucl. Phys. **22** (1961) 579.

[24] S. Weinberg, *A Model of Leptons*, Phys. Rev. Lett. **19** (1967) 1264.

[25] A. Salam in Elementary Particle Physics (Nobel Symp. N.8), Ed. N.Svartholm, Almquist and Wiksells, Stockholm (1968), p.367.

[26] J. Goldstone, *Field Theories with Superconductor Solutions*, Nuovo Cim. **19** (1961) 154.

[27] J. Goldstone, A. Salam and S. Weinberg, *Broken Symmetries*, Phys. Rev. **127** (1962) 965.

[28] Y. Nambu, *Axial vector current conservation in weak interactions*, Phys. Rev. Lett. **4** (1960) 380.

[29] P. W. Higgs, *Broken symmetries, massless particles and gauge fields*, Phys. Lett. **12** (1964) 132.

[30] P. W. Higgs, *Spontaneous Symmetry Breakdown without Massless Bosons*, Phys. Rev. **145** (1966) 1156.

[31] F. Englert and R. Brout, *Broken Symmetry and the Mass of Gauge Vector Mesons*, Phys. Rev. Lett. **13** (1964) 321.

[32] G. S. Guralnik, C. R. Hagen and T. W. B. Kibble, *Global Conservation Laws and Massless Particles*, Phys. Rev. Lett. **13** (1964) 585.

[33] T. W. B. Kibble, *Symmetry breaking in nonAbelian gauge theories*, Phys. Rev. **155** (1967) 1554.

[34] E. S. Abers and B. W. Lee, *Gauge Theories*, Phys. Rept. **9** (1973) 1.

[35] G. C. Branco, P. M. Ferreira, L. Lavoura, M. N. Rebelo, M. Sher and J. P. Silva, *Theory and phenomenology of two-Higgs-doublet models*, Phys. Rept. **516** (2012) 1 [arXiv:1106.0034 [hep-ph]].

[36] F. J. Dyson, *Divergence of perturbation theory in quantum electrodynamics*, Phys. Rev. **85** (1952) 631.

[37] R. P. Feynman, *Space - time approach to quantum electrodynamics*, Phys. Rev. **76** (1949) 769.

[38] J. S. Schwinger, *On Quantum electrodynamics and the magnetic moment of the electron*, Phys. Rev. **73** (1948) 416.

[39] R. P. Feynman, *Relativistic cutoff for quantum electrodynamics*, Phys. Rev. **74** (1948) 1430.

[40] M. Gell-Mann and F. E. Low, *Quantum electrodynamics at small distances*, Phys. Rev. **95** (1954) 1300.

[41] E. C. G. Stueckelberg and A. Petermann, *The normalization group in quantum theory*, Helv. Phys. Acta **24** (1951) 317.

[42] C. G. Callan, Jr., *Broken scale invariance in scalar field theory*, Phys. Rev. D **2** (1970) 1541.

[43] K. Symanzik, *Small distance behavior in field theory and power counting*, Commun. Math. Phys. **18** (1970) 227.

[44] M. Bohm, A. Denner and H. Joos, *Gauge theories of the strong and electroweak interaction*, Stuttgart, Germany: Teubner (2001) 784 p

[45] P. Langacker and M. -x. Luo, *Implications of precision electroweak experiments for M_t, ρ_0, $\sin^2\theta_W$ and grand unification*, Phys. Rev. D **44** (1991) 817.

[46] J. R. Ellis, S. Kelley and D. V. Nanopoulos, *Probing the desert using gauge coupling unification*, Phys. Lett. B **260** (1991) 131.

[47] U. Amaldi, W. de Boer and H. Furstenau, *Comparison of grand unified theories with electroweak and strong coupling constants measured at LEP*, Phys. Lett. B **260** (1991) 447.

[48] RPP 2008 Particle Data Group Book.

[49] V. Barger, J. Jiang, P. Langacker and T. Li, *Gauge coupling unification in the standard model*, Phys. Lett. B **624** (2005) 233 [hep-ph/0503226].

[50] G. Bertone, D. Hooper and J. Silk, *Particle dark matter: Evidence, candidates and constraints*, Phys. Rept. **405** (2005) 279 [hep-ph/0404175].

[51] A. D. Dolgov, *Cosmology and Neutrino Properties*, Phys. Atom. Nucl. **71** (2008) 2152 [arXiv:0803.3887 [hep-ph]].

[52] G. W. Bennett *et al.* [Muon G-2 Collaboration], *Final Report of the Muon E821 Anomalous Magnetic Moment Measurement at BNL*, Phys. Rev. D **73** (2006) 072003 [hep-ex/0602035].

[53] M. Davier, A. Hoecker, B. Malaescu, C. Z. Yuan and Z. Zhang, *Reevaluation of the hadronic contribution to the muon magnetic anomaly using new $e^+e^- \to \pi^+\pi^-$ cross section data from BABAR*, Eur. Phys. J. C **66** (2010) 1 [arXiv:0908.4300 [hep-ph]].

[54] H. Georgi and S. L. Glashow, *Unity Of All Elementary Particle Forces*, Phys. Rev. Lett. **32**, 438 (1974).

[55] F. Braam, A. Knochel and J. Reuter, *An Exceptional SSM from E6 Orbifold GUTs with intermediate LR symmetry*, JHEP **1006** (2010) 013 [arXiv:1001.4074 [hep-ph]].

[56] F. Wang, *Supersymmetry Breaking Scalar Masses and Trilinear Soft Terms From High-Dimensional Operators in E_6 SUSY GUT*, Nucl. Phys. B **851** (2011) 104 [arXiv:1103.0069 [hep-ph]].

[57] D. Bailin and A. Love, *Supersymmetric gauge field theory and string theory*, Bristol, UK: IOP (1994) 322 p. (Graduate student series in physics)

[58] S. P. Martin, *A Supersymmetry primer*, In *Kane, G.L. (ed.): Perspectives on supersymmetry II* 1-153 [hep-ph/9709356].

[59] I. J. R. Aitchison, *Supersymmetry in Particle Physics. An Elementary Introduction*, Cambridge, UK: Univ. Pr. (2007) 222 p

[60] I. J. R. Aitchison, *Supersymmetry and the MSSM: An Elementary introduction*, hep-ph/0505105.

[61] S. R. Coleman and J. Mandula, *All Possible Symmetries of the S Matrix*, Phys. Rev. **159** (1967) 1251.

[62] R. Haag, J. T. Lopuszanski and M. Sohnius, *All Possible Generators of Supersymmetries of the s Matrix*, Nucl. Phys. B **88** (1975) 257.

[63] M. F. Sohnius, *Introducing Supersymmetry*, Phys. Rept. **128** (1985) 39.

[64] J. Wess and B. Zumino, *A Lagrangian Model Invariant Under Supergauge Transformations*, Phys. Lett. B **49** (1974) 52.

[65] J. Wess and B. Zumino, *Supergauge Transformations in Four-Dimensions*, Nucl. Phys. B **70** (1974) 39.

[66] D. J. H. Chung, L. L. Everett, G. L. Kane, S. F. King, J. D. Lykken and L. -T. Wang, *The Soft supersymmetry breaking Lagrangian: Theory and applications*, Phys. Rept. **407** (2005) 1 [hep-ph/0312378].

[67] L. Girardello and M. T. Grisaru, *Soft Breaking of Supersymmetry*, Nucl. Phys. B **194** (1982) 65.

[68] K. Intriligator and N. Seiberg, *Lectures on supersymmetry breaking*.

[69] M. Dine and J. D. Mason, *Supersymmetry and Its Dynamical Breaking*, Rept. Prog. Phys. **74** (2011) 056201 [arXiv:1012.2836 [hep-th]].

[70] R. Kitano and Y. Ookouchi, *Supersymmetry breaking and gauge mediation in models with a generic superpotential*, Phys. Lett. B **675** (2009) 80 [arXiv:0812.0543 [hep-ph]].

[71] R. Kitano, H. Ooguri and Y. Ookouchi, *Supersymmetry Breaking and Gauge Mediation*, Ann. Rev. Nucl. Part. Sci. **60** (2010) 491 [arXiv:1001.4535 [hep-th]].

[72] Y. Shirman, *TASI 2008 Lectures: Introduction to Supersymmetry and Supersymmetry Breaking*, arXiv:0907.0039 [hep-ph];

[73] S. Ferrara and L. Maiani, *An Introduction To Supersymmetry Breaking In Extended Supergravity*, CERN-TH-4232/85.

[74] L. O'Raifeartaigh, *Spontaneous Symmetry Breaking for Chiral Scalar Superfields*, Nucl. Phys. B **96** (1975) 331.

[75] P. Fayet and J. Iliopoulos, *Spontaneously Broken Supergauge Symmetries and Goldstone Spinors*, Phys. Lett. B **51** (1974) 461.

[76] P. Fayet, *Supergauge Invariant Extension of the Higgs Mechanism and a Model for the electron and Its Neutrino*, Nucl. Phys. B **90** (1975) 104.

[77] M. Dine and W. Fischler, *A Phenomenological Model of Particle Physics Based on Supersymmetry*, Phys. Lett. B **110** (1982) 227.

[78] C. R. Nappi and B. A. Ovrut, *Supersymmetric Extension of the SU(3) x SU(2) x U(1) Model*, Phys. Lett. B **113** (1982) 175.

[79] L. Alvarez-Gaume, M. Claudson and M. B. Wise, *Low-Energy Supersymmetry*, Nucl. Phys. B **207** (1982) 96.

[80] M. Dine and A. E. Nelson, *Dynamical supersymmetry breaking at low-energies*, Phys. Rev. D **48** (1993) 1277 [hep-ph/9303230].

[81] M. Dine, A. E. Nelson and Y. Shirman, *Low-energy dynamical supersymmetry breaking simplified*, Phys. Rev. D **51** (1995) 1362 [hep-ph/9408384].

[82] M. Dine, A. E. Nelson, Y. Nir and Y. Shirman, *New tools for low-energy dynamical supersymmetry breaking*, Phys. Rev. D **53** (1996) 2658 [hep-ph/9507378].

[83] L. Randall and R. Sundrum, *Out of this world supersymmetry breaking*, Nucl. Phys. B **557** (1999) 79 [hep-th/9810155].

[84] G. F. Giudice, M. A. Luty, H. Murayama and R. Rattazzi, *Gaugino mass without singlets*, JHEP **9812** (1998) 027 [hep-ph/9810442].

[85] A. Pomarol and R. Rattazzi, *Sparticle masses from the superconformal anomaly*, JHEP **9905** (1999) 013 [hep-ph/9903448].

[86] A. H. Chamseddine, R. L. Arnowitt and P. Nath, *Locally Supersymmetric Grand Unification*, Phys. Rev. Lett. **49** (1982) 970.

[87] R. Barbieri, S. Ferrara and C. A. Savoy, *Gauge Models with Spontaneously Broken Local Supersymmetry*, Phys. Lett. B **119** (1982) 343.

[88] L. E. Ibanez, *Locally Supersymmetric SU(5) Grand Unification*, Phys. Lett. B **118** (1982) 73.

[89] L. J. Hall, J. D. Lykken and S. Weinberg, *Supergravity as the Messenger of Supersymmetry Breaking*, Phys. Rev. D **27** (1983) 2359.

[90] N. Ohta, *Grand Unified Theories Based On Local Supersymmetry*, Prog. Theor. Phys. **70** (1983) 542.

[91] J. R. Ellis, D. V. Nanopoulos and K. Tamvakis, *Grand Unification in Simple Supergravity*, Phys. Lett. B **121** (1983) 123.

[92] L. Alvarez-Gaume, J. Polchinski and M. B. Wise, *Minimal Low-Energy Supergravity*, Nucl. Phys. B **221** (1983) 495.

[93] E. Cremmer, B. Julia, J. Scherk, P. van Nieuwenhuizen, S. Ferrara and L. Girardello, *SuperHiggs Effect in Supergravity with General Scalar Interactions*, Phys. Lett. B **79** (1978) 231.

[94] E. Cremmer, B. Julia, J. Scherk, S. Ferrara, L. Girardello and P. van Nieuwenhuizen, *Spontaneous Symmetry Breaking and Higgs Effect in Supergravity Without Cosmological Constant*, Nucl. Phys. B **147** (1979) 105.

[95] E. Cremmer, S. Ferrara, L. Girardello and A. Van Proeyen, *Coupling Supersymmetric Yang-Mills Theories to Supergravity*, Phys. Lett. B **116** (1982) 231.

[96] E. Cremmer, S. Ferrara, L. Girardello and A. Van Proeyen, *Yang-Mills Theories with Local Supersymmetry: Lagrangian, Transformation Laws and SuperHiggs Effect*, Nucl. Phys. B **212** (1983) 413.

[97] J. R. Ellis, K. Enqvist, D. V. Nanopoulos and K. Tamvakis, *Gaugino Masses And Grand Unification*, Phys. Lett. B **155** (1985) 381.

[98] M. Drees, *Phenomenological Consequences Of N=1 Supergravity Theories With Nonminimal Kinetic Energy Terms For Vector Superfields*, Phys. Lett. B **158** (1985) 409.

[99] D. G. Cerdeno and C. Munoz, *An introduction to SUGRA*, in proceedings of "Corfu Summer Institute on Elementary Particle Physics" PoS(corfu98)011.

[100] S. Bhattacharya and J. Chakrabortty, *Gaugino mass non-universality in an SO(10) supersymmetric Grand Unified Theory: Low-energy spectra and collider signals*, Phys. Rev. D **81** (2010) 015007 [arXiv:0903.4196 [hep-ph]].

[101] C. T. Hill, *Are There Significant Gravitational Corrections to the Unification Scale?*, Phys. Lett. B **135** (1984) 47.

[102] J. Chakrabortty and A. Raychaudhuri, *A Note on dimension-5 operators in GUTs and their impact*, Phys. Lett. B **673** (2009) 57 [arXiv:0812.2783 [hep-ph]].

[103] J. Chakrabortty and A. Raychaudhuri, *Dimension-5 operators and the unification condition in SO(10) and E(6)*, arXiv:1006.1252 [hep-ph].

[104] S. P. Martin, *Non-universal gaugino masses from non-singlet F-terms in non-minimal unified models*, Phys. Rev. D **79** (2009) 095019 [arXiv:0903.3568 [hep-ph]].

[105] The ATLAS Collaboration, ATLAS-CONF-2012-033; ATLAS-CONF-2012-037; ATLAS-CONF-2012-041

[106] The CMS Collaboration, CMS PAS SUS-11-016 (2011); CMS PAS SUS-12-002 (2012); CMS PAS SUS-12-005 (2012); CMS PAS SUS-12-011 (2012).

[107] E. Witten, *An SU(2) Anomaly*, Phys. Lett. B **117**, 324 (1982).

[108] J. A. Casas, A. Lleyda and C. Munoz, *Strong constraints on the parameter space of the MSSM from charge and color breaking minima*, Nucl. Phys. B **471** (1996) 3 [hep-ph/9507294].

[109] R. P. Feynman and M. Gell-Mann, *Theory of Fermi interaction*, Phys. Rev. **109** (1958) 193.

[110] J. Beringer et al. (Particle Data Group), Phys. Rev. D86, 010001 (2012).

[111] A. Djouadi, *The Higgs particles in the MSSM*, Extended write-up of the Lectures given at the "Ecole de GIF 2001", LAPP Annecy (France), 10-14 Sepember 2001.

[112] J. R. Espinosa and M. Quiros, *Two loop radiative corrections to the mass of the lightest Higgs boson in supersymmetric standard models*, Phys. Lett. B **266** (1991) 389.

[113] J. Kodaira, Y. Yasui and K. Sasaki, *The Mass of the lightest supersymmetric Higgs boson beyond the leading logarithm approximation*, Phys. Rev. D **50** (1994) 7035 [hep-ph/9311366].

[114] M. S. Carena, M. Quiros and C. E. M. Wagner, *Effective potential methods and the Higgs mass spectrum in the MSSM*, Nucl. Phys. B **461** (1996) 407 [hep-ph/9508343].

[115] M. S. Carena, J. R. Espinosa, M. Quiros and C. E. M. Wagner, *Analytical expressions for radiatively corrected Higgs masses and couplings in the MSSM*, Phys. Lett. B **355** (1995) 209 [hep-ph/9504316].

[116] J. A. Casas, J. R. Espinosa, M. Quiros and A. Riotto, *The Lightest Higgs boson mass in the minimal supersymmetric standard model*, Nucl. Phys. B **436** (1995) 3 [Erratum-ibid. B **439** (1995) 466] [hep-ph/9407389].

[117] J. A. Casas, J. R. Espinosa and M. Quiros, *Improved Higgs mass stability bound in the standard model and implications for supersymmetry*, Phys. Lett. B **342** (1995) 171 [hep-ph/9409458].

[118] H. E. Haber, R. Hempfling and A. H. Hoang, *Approximating the radiatively corrected Higgs mass in the minimal supersymmetric model*, Z. Phys. C **75** (1997) 539 [hep-ph/9609331].

[119] S. Heinemeyer, W. Hollik and G. Weiglein, *Precise prediction for the mass of the lightest Higgs boson in the MSSM*, Phys. Lett. B **440** (1998) 296 [hep-ph/9807423]; *QCD corrections to the masses of the neutral CP - even Higgs bosons in the MSSM*, Phys. Rev. D **58** (1998) 091701 [hep-ph/9803277]; *The Masses of the neutral CP - even Higgs bosons in the MSSM: Accurate analysis at the two loop level*, Eur. Phys. J. C **9** (1999) 343 [hep-ph/9812472]; *The Mass of the lightest MSSM Higgs boson: A Compact analytical expression at the two loop level*, Phys. Lett. B **455** (1999) 179 [hep-ph/9903404].

[120] G. Hinshaw, D. Larson, E. Komatsu, D. N. Spergel, C. L. Bennett, J. Dunkley, M. R. Nolta and M. Halpern *et al.*, *Nine-Year Wilkinson Microwave Anisotropy Probe (WMAP) Observations: Cosmological Parameter Results*, arXiv:1212.5226 [astro-ph.CO].

[121] P. A. R. Ade *et al.* [Planck Collaboration], *Planck 2013 results. I. Overview of products and scientific results*, arXiv:1303.5062 [astro-ph.CO].

[122] E. Aprile *et al.* [XENON100 Collaboration], *Dark Matter Results from 225 Live Days of XENON100 Data*, Phys. Rev. Lett. **109** (2012) 181301 [arXiv:1207.5988 [astro-ph.CO]].

[123] P. Ramond, *The Family Group in Grand Unified Theories*, hep-ph/9809459.

[124] R. Slansky, *Group Theory for Unified Model Building*, Phys. Rept. **79** (1981) 1.

[125] H. Nishino *et al.* [Super-Kamiokande Collaboration], *Search for Proton Decay via $p \to e^+\pi^0$ and $p \to \mu + \pi^0$ in a Large Water Cherenkov Detector*, Phys. Rev. Lett. **102** (2009) 141801 [arXiv:0903.0676 [hep-ex]].

[126] S. Dimopoulos and H. Georgi, *Softly Broken Supersymmetry and SU(5)*, Nucl. Phys. B **193**, 150 (1981);

[127] N. Sakai and T. Yanagida, *Proton Decay in a Class of Supersymmetric Grand Unified Models*, Nucl. Phys. B **197**, 533 (1982);

[128] J. R. Ellis, D. V. Nanopoulos and S. Rudaz, *GUTs 3: SUSY GUTs 2*, Nucl. Phys. B **202**, 43 (1982);

[129] S. Dimopoulos, S. Raby and F. Wilczek, *Proton Decay in Supersymmetric Models*, Phys. Lett. B **112**, 133 (1982);

[130] T. Goto and T. Nihei, *Effect of RRRR dimension five operator on the proton decay in the minimal SU(5) SUGRA GUT model*, Phys. Rev. D **59**, 115009 (1999) [hep-ph/9808255];

[131] P. Nath, A. H. Chamseddine and R. L. Arnowitt, *Nucleon Decay in Supergravity Unified Theories*, Phys. Rev. D **32**, 2348 (1985);

[132] P. Nath and R. L. Arnowitt, *Limits On Photino And Squark Masses From Proton Lifetime In Supergravity And Superstring Models*, Phys. Rev. D **38**, 1479 (1988);

[133] J. Hisano, H. Murayama and T. Yanagida, *Nucleon decay in the minimal supersymmetric SU(5) grand unification*, Nucl. Phys. B **402**, 46 (1993) [hep-ph/9207279];

[134] H. Murayama and A. Pierce, *Not even decoupling can save minimal supersymmetric SU(5)*, Phys. Rev. D **65**, 055009 (2002) [hep-ph/0108104].

[135] S. Wiesenfeldt, *Proton decay in supersymmetric GUT models*, Mod. Phys. Lett. A **19** (2004) 2155 [hep-ph/0407173].

[136] Y. Kawamura, *Triplet doublet splitting, proton stability and extra dimension*, Prog. Theor. Phys. **105**, 999 (2001) [hep-ph/0012125].

[137] G. Altarelli and F. Feruglio, *SU(5) grand unification in extra dimensions and proton decay*, Phys. Lett. B **511**, 257 (2001) [hep-ph/0102301];

[138] L. J. Hall and Y. Nomura, *Gauge unification in higher dimensions*, Phys. Rev. D **64**, 055003 (2001) [hep-ph/0103125];

[139] A. Hebecker and J. March-Russell, *A Minimal S**1 / (Z(2) x Z-prime (2)) orbifold GUT*, Nucl. Phys. B **613**, 3 (2001) [hep-ph/0106166];

[140] A. B. Kobakhidze, *Proton stability in TeV scale GUTs*, Phys. Lett. B **514**, 131 (2001) [hep-ph/0102323].

[141] S. Komine and M. Yamaguchi, *Bottom tau unification in SUSY SU(5) GUT and constraints from $b \to s\gamma$ and muon $g-2$*, Phys. Rev. D **65** (2002) 075013 [hep-ph/0110032].

[142] K. S. Babu and S. M. Barr, *Realistic quark and lepton masses through SO(10) symmetry*, Phys. Rev. D **56** (1997) 2614 [hep-ph/9512389].

[143] C. H. Albright and S. M. Barr, *Construction of a minimal Higgs SO(10) SUSY GUT model*, Phys. Rev. D **62** (2000) 093008 [hep-ph/0003251].

[144] P. Minkowski, *$\mu \to e\gamma$ at a Rate of One Out of 1-Billion Muon Decays?*, Phys. Lett. B **67** (1977) 421.

[145] R. N. Mohapatra and G. Senjanovic, *Neutrino Mass and Spontaneous Parity Violation*, Phys. Rev. Lett. **44** (1980) 912.

[146] J. Schechter and J. W. F. Valle, *Neutrino Masses in SU(2) x U(1) Theories*, Phys. Rev. D **22** (1980) 2227.

[147] J. Schechter and J. W. F. Valle, *Neutrino Decay and Spontaneous Violation of Lepton Number*, Phys. Rev. D **25** (1982) 774.

[148] H. Georgi and S. L. Glashow, *Unity of All Elementary Particle Forces*, Phys. Rev. Lett. **32** (1974) 438.

[149] A. De Rujula, H. Georgi and S. L. Glashow, *Flavor Goniometry By Proton Decay* Phys. Rev. Lett. **45** (1980) 413.

[150] S. M. Barr, *SOME COMMENTS ON FLIPPED SU(5) x U(1) AND FLIPPED UNIFICATION IN GENERAL*, Phys. Rev. D **40** (1989) 2457.

[151] S. M. Barr, *A New Symmetry Breaking Pattern for SO(10) and Proton Decay*, Phys. Lett. B **112** (1982) 219.

[152] J. C. Pati and A. Salam, *Lepton Number as the Fourth Color*, Phys. Rev. D **10** (1974) 275 [Erratum-ibid. D **11** (1975) 703].

[153] M. A. Ajaib, I. Gogoladze, Q. Shafi and C. S. Un, *Higgs and Sparticle Masses from Yukawa Unified SO(10): A Snowmass White Paper*, arXiv:1308.4652 [hep-ph].

[154] M. Adeel Ajaib, I. Gogoladze, Q. Shafi and C. S. Un, *A Predictive Yukawa Unified SO(10) Model: Higgs and Sparticle Masses*, arXiv:1303.6964 [hep-ph].

[155] M. Badziak, M. Olechowski and S. Pokorski, *Light staus and enhanced Higgs diphoton rate with non-universal gaugino masses and SO(10) Yukawa unification*, JHEP **10** (2013) 088 [arXiv:1307.7999 [hep-ph]].

[156] Q. Shafi, *Higgs boson mass in Yukawa unified SUSY SO(10)*, J. Phys. Conf. Ser. **384** (2012) 012025.

[157] Q. Shafi, *Higgs boson mass and sparticle spectroscopy in Yukawa unified SUSY SO(10)*, AIP Conf. Proc. **1467** (2012) 101.

[158] K. S. Babu and R. N. Mohapatra, *Predictive neutrino spectrum in minimal SO(10) grand unification*, Phys. Rev. Lett. **70** (1993) 2845 [hep-ph/9209215].

[159] A. S. Joshipura and K. M. Patel, *Yukawa coupling unification in SO(10) with positive μ and a heavier gluino*, Phys. Rev. D **86** (2012) 035019 [arXiv:1206.3910 [hep-ph]].

[160] S. Dar, I. Gogoladze, Q. Shafi and C. S. Un, *Sparticle Spectroscopy with Neutralino Dark matter from t-b-tau Quasi-Yukawa Unification*, Phys. Rev. D **84** (2011) 085015 [arXiv:1105.5122 [hep-ph]].

[161] K. S. Babu, J. C. Pati and F. Wilczek, *Suggested new modes in supersymmetric proton decay*, Phys. Lett. B **423** (1998) 337 [hep-ph/9712307].

[162] P. Nath and R. M. Syed, *Analysis of couplings with large tensor representations in SO(2N) and proton decay*, Phys. Lett. B **506** (2001) 68 [Erratum-ibid. B **508** (2001) 216] [hep-ph/0103165].

[163] T. Asaka, K. Ishiwata and T. Moroi, *Right-handed sneutrino as cold dark matter of the universe*, AIP Conf. Proc. **903** (2007) 16 [J. Phys. Conf. Ser. **120** (2008) 042006];

[164] T. Asaka, K. Ishiwata and T. Moroi, *Right-handed sneutrino as cold dark matter of the universe*, Phys. Rev. D **75** (2007) 065001 [hep-ph/0612211];

[165] T. Asaka, K. Ishiwata and T. Moroi, *Right-handed sneutrino as cold dark matter*, Phys. Rev. D **73** (2006) 051301 [hep-ph/0512118];

[166] K. Ishiwata, M. Kawasaki, K. Kohri and T. Moroi, *Right-handed sneutrino dark matter and big-bang nucleosynthesis*, Phys. Lett. B **689** (2010) 163 [arXiv:0912.0781 [hep-ph]].

[167] S. F. King, S. Moretti and R. Nevzorov, *Theory and phenomenology of an exceptional supersymmetric standard model*, Phys. Rev. D **73**, 035009 (2006) [hep-ph/0510419].

[168] S. F. King, S. Moretti and R. Nevzorov, *Gauge coupling unification in the exceptional supersymmetric standard model*, Phys. Lett. B **650**, 57 (2007) [hep-ph/0701064].

[169] P. Athron, S. F. King, D. J. Miller, S. Moretti and R. Nevzorov, *The Constrained Exceptional Supersymmetric Standard Model*, Phys. Rev. D **80**, 035009 (2009) [arXiv:0904.2169 [hep-ph]];

[170] P. Athron, S. F. King, D. J. Miller, S. Moretti and R. Nevzorov, *Predictions of the Constrained Exceptional Supersymmetric Standard Model*, Phys. Lett. B **681**, 448 (2009) [arXiv:0901.1192 [hep-ph]];

[171] *LHC Signatures of the Constrained Exceptional Supersymmetric Standard Model*, Phys. Rev. D **84**, 055006 (2011) [arXiv:1102.4363 [hep-ph]];

[172] *Constrained Exceptional Supersymmetric Standard Model with a Higgs Near 125 GeV*, arXiv:1206.5028 [hep-ph];

[173] J. L. Hewett and T. G. Rizzo, *Low-Energy Phenomenology of Superstring Inspired E(6) Models*, Phys. Rept. **183**, 193 (1989);

[174] T. G. Rizzo, *Gauge Kinetic Mixing in the E_6SSM*, arXiv:1201.2898 [hep-ph].

[175] G. Aad *et al.* [ATLAS Collaboration], *Search for scalar bottom pair production with the ATLAS detector in pp Collisions at sqrts = 7 TeV*, Phys. Rev. Lett. **108** (2012) 181802 [arXiv:1112.3832 [hep-ex]].

[176] The ATLAS Collaboration, *Search for Scalar Top Quark Pair Production in Natural Gauge Mediated Supersymmetry Models with the ATLAS Detector in pp Collisions at $s\sqrt{}$= 7 TeV*, ATLAS-CONF-2012-036.

[177] *Search for light scalar top quark pair production in final states with two leptons with the ATLAS detector in $\sqrt{s} = 7$ TeV proton–proton collisions*, ATLAS-CONF-2012-059.

[178] H. Baer, V. Barger, P. Huang and X. Tata, *Natural Supersymmetry: LHC, dark matter and ILC searches*, JHEP **1205**, 109 (2012) [arXiv:1203.5539 [hep-ph]].

[179] C. F. Kolda and S. P. Martin, *Low-energy supersymmetry with D term contributions to scalar masses*, Phys. Rev. D **53**, 3871 (1996) [hep-ph/9503445].

[180] D. R. T. Jones and L. Mezincescu, *The Beta Function In Supersymmetric Yang-Mills Theory*, Phys. Lett. B **136**, 242 (1984).

[181] P. C. West, *The Yukawa Beta Function In N=1 Rigid Supersymmetric Theories*, Phys. Lett. B **137**, 371 (1984).

[182] N. K. Falck, *Renormalization Group Equations For Softly Broken Supersymmetry: The Most General Case*, Z. Phys. C **30**, 247 (1986).

[183] S. P. Martin and M. T. Vaughn, *Two loop renormalization group equations for soft supersymmetry breaking couplings*, Phys. Rev. D **50**, 2282 (1994) [Erratum-ibid. D **78**, 039903 (2008)] [hep-ph/9311340].

[184] I. Jack and D. R. T. Jones, *The Gaugino Beta function*, Phys. Lett. B **415**, 383 (1997) [hep-ph/9709364].

[185] P. M. Ferreira, I. Jack and D. R. T. Jones, *The Three loop SSM beta functions*, Phys. Lett. B **387**, 80 (1996) [hep-ph/9605440].

[186] P. M. Ferreira, I. Jack, D. R. T. Jones and C. G. North, *Beta functions in large N(f) supersymmetric gauge theories*, Nucl. Phys. B **504**, 108 (1997) [hep-ph/9705328].

[187] I. Jack, D. R. T. Jones and A. Pickering, *The soft scalar mass beta function*, Phys. Lett. B **432**, 114 (1998) [hep-ph/9803405].

[188] B. Ananthanarayan and P. N. Pandita, *Probing SO(10) symmetry breaking patterns through sfermion mass relations*, Int. J. Mod. Phys. A **20**, 4241 (2005) [hep-ph/0412125].

[189] B. Ananthanarayan and P. N. Pandita, *Sparticle Mass Spectrum in Grand Unified Theories*, Int. J. Mod. Phys. A **22**, 3229 (2007) [arXiv:0706.2560 [hep-ph]].

[190] B. Ananthanarayan and P.N. Pandita, Mod. Phys. Lett. A19, 467 (2004) [hep-ph/0312361].

[191] J. S. Hagelin and S. Kelley, *Sparticle Masses As A Probe Of Gut Physics*, Nucl. Phys. B **342**, 95 (1990).

[192] Y. Kawamura, H. Murayama and M. Yamaguchi, *Probing symmetry breaking pattern using sfermion masses*, Phys. Lett. B **324**, 52 (1994) [hep-ph/9402254].

[193] H. C. Cheng and L. J. Hall, *Squark and slepton mass relations in grand unified theories*, Phys. Rev. D **51**, 5289 (1995) [hep-ph/9411276].

[194] D. Kazakov and G. Moultaka, *Analytical study of nonuniversality of the soft terms in the MSSM*, Nucl. Phys. B **577**, 121 (2000) [hep-ph/9912271].

[195] N. Chamoun, C. -S. Huang, C. Liu and X. -H. Wu, *Nonuniversal gaugino masses in supersymmetric SO(10)*, Nucl. Phys. B **624**, 81 (2002) [hep-ph/0110332].

[196] K. Huitu, J. Laamanen, P. N. Pandita and S. Roy, *Phenomenology of non-universal gaugino masses in supersymmetric grand unified theories*, Phys. Rev. D **72**, 055013 (2005) [hep-ph/0502100].

[197] B. C. Allanach, *SOFTSUSY: a program for calculating supersymmetric spectra*, Comput. Phys. Commun. **143** (2002) 305 [hep-ph/0104145].

[198] H. Baer, A. Belyaev, T. Krupovnickas and A. Mustafayev, *SUSY normal scalar mass hierarchy reconciles* $(g-2)(\mu), b \to s\gamma$ *and relic density*, JHEP **0406** (2004) 044 [hep-ph/0403214].

[199] E. A. Baltz and P. Gondolo, *Markov chain Monte Carlo exploration of minimal supergravity with implications for dark matter*, JHEP **0410** (2004) 052 [hep-ph/0407039].

[200] B. C. Allanach and C. G. Lester, *Multi-dimensional mSUGRA likelihood maps*, Phys. Rev. D **73** (2006) 015013 [hep-ph/0507283].

[201] B. C. Allanach, *Naturalness priors and fits to the constrained minimal supersymmetric standard model*, Phys. Lett. B **635** (2006) 123 [hep-ph/0601089].

[202] R. R. de Austri, R. Trotta and L. Roszkowski, *A Markov chain Monte Carlo analysis of the CMSSM*, JHEP **0605** (2006) 002 [hep-ph/0602028].

[203] B. C. Allanach, C. G. Lester and A. M. Weber, *The Dark side of mSUGRA*, JHEP **0612** (2006) 065 [hep-ph/0609295].

[204] B. C. Allanach, K. Cranmer, C. G. Lester and A. M. Weber, *Natural priors, CMSSM fits and LHC weather forecasts*, JHEP **0708** (2007) 023 [arXiv:0705.0487 [hep-ph]].

[205] L. Roszkowski, R. R. de Austri, J. Silk and R. Trotta, *On prospects for dark matter indirect detection in the Constrained MSSM*, Phys. Lett. B **671** (2009) 10 [arXiv:0707.0622 [astro-ph]].

[206] F. Feroz, B. C. Allanach, M. Hobson, S. S. AbdusSalam, R. Trotta and A. M. Weber, *Bayesian Selection of sign(mu) within mSUGRA in Global Fits Including WMAP5 Results*, JHEP **0810** (2008) 064 [arXiv:0807.4512 [hep-ph]].

[207] M. E. Cabrera, J. A. Casas and R. Ruiz de Austri, *Bayesian approach and Naturalness in MSSM analyses for the LHC*, JHEP **0903** (2009) 075 [arXiv:0812.0536 [hep-ph]].

[208] G. Belanger, F. Boudjema, A. Pukhov and A. Semenov, *micrOMEGAs: Version 1.3*, Comput. Phys. Commun. **174** (2006) 577 [hep-ph/0405253].

[209] A. Djouadi, J. -L. Kneur and G. Moultaka, *SuSpect: A Fortran code for the supersymmetric and Higgs particle spectrum in the MSSM*, Comput. Phys. Commun. **176** (2007) 426 [hep-ph/0211331].

[210] A. Arbey, M. Battaglia, A. Djouadi and F. Mahmoudi, *The Higgs sector of the phenomenological MSSM in the light of the Higgs boson discovery*, JHEP **1209** (2012) 107 [arXiv:1207.1348 [hep-ph]].

[211] Y. Amhis *et al.* [Heavy Flavor Averaging Group Collaboration], *Averages of B-Hadron, C-Hadron, and tau-lepton properties as of early 2012*, arXiv:1207.1158 [hep-ex].

[212] RAaij *et al.* [LHCb Collaboration], *First evidence for the decay $B_s \to \mu^+\mu^-$*, Phys. Rev. Lett. **110** (2013) 021801 [arXiv:1211.2674 [Unknown]].

[213] I. Adachi *et al.* [Belle Collaboration], *Measurement of $B^- \to \tau^- \bar{\nu}_\tau$ with a Hadronic Tagging Method Using the Full Data Sample of Belle*, arXiv:1208.4678 [hep-ex].

[214] J. P. Lees *et al.* [BABAR Collaboration], *Evidence of $B \to \tau\nu$ decays with hadronic B tags*, arXiv:1207.0698 [hep-ex].

[215] P. Biancofiore, P. Colangelo and F. De Fazio, *On the anomalous enhancement observed in $B \to D^{(*)} \tau \bar{\nu}_\tau$ decays*, arXiv:1302.1042 [hep-ph].

[216] P. von Weitershausen, M. Schafer, H. Stockinger-Kim and D. Stockinger, *Photonic SUSY Two-Loop Corrections to the Muon Magnetic Moment*, Phys. Rev. D **81** (2010) 093004 [arXiv:1003.5820 [hep-ph]].

[217] D. Stockinger, *Muon (g-2) and physics beyond the standard model*, (Advanced series on directions in high energy physics. 20);

[218] D. Stockinger, *(g - 2)(mu) and physics beyond the Standard Model*, Nucl. Phys. Proc. Suppl. **181-182** (2008) 32;

[219] D. Stockinger, *The Muon Magnetic Moment and Supersymmetry*, J. Phys. G **34** (2007) R45 [hep-ph/0609168].

[220] R. D. Peccei and H. R. Quinn, *CP Conservation in the Presence of Instantons*, Phys. Rev. Lett. **38** (1977) 1440.

[221] R. D. Peccei and H. R. Quinn, *Constraints Imposed by CP Conservation in the Presence of Instantons*, Phys. Rev. D **16** (1977) 1791.

[222] S. Weinberg, *A New Light Boson?*, Phys. Rev. Lett. **40** (1978) 223.

[223] F. Wilczek, *Problem of Strong p and t Invariance in the Presence of Instantons*, Phys. Rev. Lett. **40** (1978) 279.

[224] J. E. Kim, *Weak Interaction Singlet and Strong CP Invariance*, Phys. Rev. Lett. **43** (1979) 103.

[225] R. Barbieri and G. F. Giudice, *Upper Bounds on Supersymmetric Particle Masses*, Nucl. Phys. B **306** (1988) 63.

[226] P. Athron and D. J. Miller, *A New Measure of Fine Tuning*, Phys. Rev. D **76** (2007) 075010 [arXiv:0705.2241 [hep-ph]].

[227] G. Gamberini, G. Ridolfi and F. Zwirner, *On Radiative Gauge Symmetry Breaking in the Minimal Supersymmetric Model*, Nucl. Phys. B **331** (1990) 331.

[228] R. L. Arnowitt and P. Nath, *Loop corrections to radiative breaking of electroweak symmetry in supersymmetry*, Phys. Rev. D **46** (1992) 3981.

[229] T. Kobayashi and Y. Yamagishi, *QuasiYukawa fixed point due to decoupling of SUSY particles*, Phys. Lett. B **381** (1996) 169 [hep-ph/9601374].

[230] J. A. Casas, J. R. Espinosa and H. E. Haber, *The Higgs mass in the MSSM infrared fixed point scenario*, Nucl. Phys. B **526** (1998) 3 [hep-ph/9801365].

[231] S. Antusch, L. Calibbi, V. Maurer, M. Monaco and M. Spinrath, *Naturalness of the Non-Universal MSSM in the Light of the Recent Higgs Results*, arXiv:1207.7236 [hep-ph].

[232] D. Horton and G. G. Ross, *Naturalness and Focus Points with Non-Universal Gaugino Masses*, Nucl. Phys. B **830** (2010) 221 [arXiv:0908.0857 [hep-ph]].

[233] D. J. Miller, R. Nevzorov and P. M. Zerwas, *The Higgs sector of the next-to-minimal supersymmetric standard model*, Nucl. Phys. B **681** (2004) 3 [hep-ph/0304049].

[234] S. Y. Choi, D. J. Miller and P. M. Zerwas, *The Neutralino sector of the next-to-minimal supersymmetric standard model*, Nucl. Phys. B **711** (2005) 83 [hep-ph/0407209].

[235] S. K. Soni and H. A. Weldon, *Analysis of the Supersymmetry Breaking Induced by N=1 Supergravity Theories*, Phys. Lett. B **126** (1983) 215.

[236] G. F. Giudice and A. Masiero, *A Natural Solution to the mu Problem in Supergravity Theories*, Phys. Lett. B **206** (1988) 480.

[237] F. Brummer, R. Kappl, M. Ratz and K. Schmidt-Hoberg, *Approximate R-symmetries and the mu term*, JHEP **1004** (2010) 006 [arXiv:1003.0084 [hep-th]].

[238] D. Horton and G. G. Ross, *Naturalness and Focus Points with Non-Universal Gaugino Masses*, Nucl. Phys. B **830** (2010) 221 [arXiv:0908.0857 [hep-ph]].

[239] A. Brignole, L. E. Ibanez and C. Munoz, *Towards a theory of soft terms for the supersymmetric Standard Model*, Nucl. Phys. B **422** (1994) 125 [Erratum-ibid. B **436** (1995) 747] [hep-ph/9308271].

[240] H. Baer, V. Barger, P. Huang, D. Mickelson, A. Mustafayev and X. Tata, *Radiative natural supersymmetry: Reconciling electroweak fine-tuning and the Higgs boson massl*, arXiv:1212.2655 [hep-ph].

[241] C. Brenner Mariotto and M. C. Rodriguez, *Investigating gluino production at the LHC*, Braz. J. Phys. **38** (2008) 503 [arXiv:0805.2395 [hep-ph]].

[242] M. R. Kauth, J. H. Kuhn, P. Marquard and M. Steinhauser, *Gluino Pair Production at the LHC: The Threshold*, Nucl. Phys. B **857** (2012) 28 [arXiv:1108.0361 [hep-ph]].

[243] H. Baer, V. Barger, A. Lessa and X. Tata, *Supersymmetry discovery potential of the LHC at s**(1/2) = 10-TeV and 14-TeV without and with missing E(T)*, JHEP **0909** (2009) 063 [arXiv:0907.1922 [hep-ph]].

[244] O. S. Bruning, R. Cappi, R. Garoby, O. Grobner, W. Herr, T. Linnecar, R. Ostojic and K. Potter *et al.*, *LHC luminosity and energy upgrade: A feasibility study*, CERN-LHC-PROJECT-REPORT-626.

[245] C. S. Aulakh, B. Bajc, A. Melfo, G. Senjanovic and F. Vissani, *The Minimal supersymmetric grand unified theory*, Phys. Lett. B **588** (2004) 196 [hep-ph/0306242].

[246] B. Bajc, A. Melfo, G. Senjanovic and F. Vissani, *The Minimal supersymmetric grand unified theory. 1. Symmetry breaking and the particle spectrum*, Phys. Rev. D **70** (2004) 035007 [hep-ph/0402122].

[247] K. S. Babu and S. M. Barr, *Natural suppression of Higgsino mediated proton decay in supersymmetric SO(10)*, Phys. Rev. D **48** (1993) 5354 [hep-ph/9306242].

[248] K. S. Babu and S. M. Barr, *Natural gauge hierarchy in SO(10)*, Phys. Rev. D **50** (1994) 3529 [hep-ph/9402291].

[249] K. S. Babu and S. M. Barr, *Supersymmetric SO(10) simplified*, Phys. Rev. D **51** (1995) 2463 [hep-ph/9409285].

[250] S. Antusch, S. F. King and M. Spinrath, *GUT predictions for quark-lepton Yukawa coupling ratios with messenger masses from non-singlets*, arXiv:1311.0877 [hep-ph].

[251] K. R. Dienes, *String theory and the path to unification: A Review of recent developments*, Phys. Rept. **287** (1997) 447 [hep-th/9602045].

[252] M. B. Green and J. H. Schwarz, *Anomaly Cancellation in Supersymmetric D=10 Gauge Theory and Superstring Theory*, Phys. Lett. B **149** (1984) 117.

[253] L. E. Ibanez and D. Lust, *Duality anomaly cancellation, minimal string unification and the effective low-energy Lagrangian of 4-D strings*, Nucl. Phys. B **382** (1992) 305 [hep-th/9202046].